



Provided by the author(s) and University of Galway in accordance with publisher policies. Please cite the published version when available.

|                  |                                                                                                               |
|------------------|---------------------------------------------------------------------------------------------------------------|
| Title            | Elastin-like polypeptide mediated proangiogenic and anti-inflammatory gene therapy for critical limb ischemia |
| Author(s)        | Dash, Biraja                                                                                                  |
| Publication Date | 2014-12-17                                                                                                    |
| Item record      | <a href="http://hdl.handle.net/10379/4806">http://hdl.handle.net/10379/4806</a>                               |

Downloaded 2024-05-14T06:35:35Z

Some rights reserved. For more information, please see the item record link above.





**Elastin-like Polypeptide Mediated Proangiogenic and Anti-inflammatory Gene Therapy  
for Critical Limb Ischemia**

A thesis submitted to the National University of Ireland for the  
degree of Doctor of Philosophy

by

Biraja Charan Dash

Nov 2014

Network of Excellence for Functional Biomaterials

National University of Ireland, Galway

Research Supervisor: Professor Abhay Pandit

## TABLE OF CONTENTS

|                                                                              |          |
|------------------------------------------------------------------------------|----------|
| TABLE OF CONTENTS.....                                                       | ii       |
| LIST OF FIGURES.....                                                         | ix       |
| LIST OF TABLES.....                                                          | xxiii    |
| ACKNOWLEDGEMENTS.....                                                        | xxv      |
| LIST OF ABBREVIATIONS.....                                                   | xxvii    |
| ABSTRACT.....                                                                | xxx      |
| <br>                                                                         |          |
| <b>1. Introduction.....</b>                                                  | <b>1</b> |
| 1.1 Peripheral Arterial Disease.....                                         | 2        |
| 1.2 Critical Limb Ischemia.....                                              | 2        |
| 1.2.1 Inflammation and Critical Limb Ischemia.....                           | 4        |
| 1.2.2 Markers of Inflammation during PAD .....                               | 4        |
| 1.2.3 Mechanism of Inflammation during Ischemia in the Skeletal Muscle ..... | 5        |
| 1.2.4 IL-0 and its Role in Inflammation .....                                | 7        |
| 1.2.5 IL-10 as a Therapeutic .....                                           | 8        |
| 1.2.6 Angiogenesis in Ischemia.....                                          | 11       |
| 1.2.7 Endothelial Nitric Oxide Synthase and Angiogenesis.....                | 12       |
| 1.2.8 Signalling Pathways for Endothelial NO-mediated Angiogenesis.....      | 12       |
| 1.2.9 eNOS as a Therapeutic .....                                            | 13       |
| 1.3 Elastin as a Biomaterial.....                                            | 13       |
| 1.3.1 Molecular Structure and Synthesis In Vivo.....                         | 15       |
| 1.3.2 Synthesis of Elastin-like Polypeptide.....                             | 15       |
| 1.4 Elastin-like Peptide-based Biomaterials for Drug Delivery.....           | 16       |
| 1.4.1 Nanostructures .....                                                   | 22       |
| 1.4.2 Three Dimensional (3D) Matrices .....                                  | 23       |
| 1.4.3 Films .....                                                            | 24       |
| 1.5 Gene Therapy .....                                                       | 25       |
| 1.5.1 Viral Gene Delivery.....                                               | 25       |
| 1.5.2 Non-viral Gene Delivery .....                                          | 30       |
| 1.5.2.1 Naked Plasmid Delivery .....                                         | 30       |
| 1.5.2.2 Cationic Polymer/Lipid-mediated Delivery.....                        | 30       |
| 1.5.2.3 Biodegradable Reservoir-mediated Delivery.....                       | 31       |

|                                                                                                                     |            |
|---------------------------------------------------------------------------------------------------------------------|------------|
| 1.6 Clinical Trails and Limitations.....                                                                            | 38         |
| 1.7 Hypotheses and Objectives .....                                                                                 | 39         |
| 1.7.1 Phase One (Chapter Two).....                                                                                  | 40         |
| 1.7.2 Phase Two (Chapter Three).....                                                                                | 40         |
| 1.7.3 Phase Three (Chapter Four).....                                                                               | 41         |
| 1.7.4 Phase Four (Chapter Four) .....                                                                               | 42         |
| 1.8 References .....                                                                                                | 43         |
| <b>2. A Hollow Sphere Model System to Study Size and Charge Effect on Cellular Internalization .....</b>            | <b>69</b>  |
| 2.1 Introduction.....                                                                                               | 70         |
| 2.2 Materials and Methods .....                                                                                     | 71         |
| 2.2.1 Materials.....                                                                                                | 71         |
| 2.2.2 Fabrication of Different Sizes of Hollow spheres and FITC Labelling .....                                     | 72         |
| 2.2.3 Alteration of Surface Charge and Function of Hollow Spheres.....                                              | 73         |
| 2.2.4 Cell Maintenance.....                                                                                         | 74         |
| 2.2.5 Cell Metabolic Activity Study.....                                                                            | 74         |
| 2.2.6 Cellular Internalization Behaviour of Hollow Spheres .....                                                    | 74         |
| 2.2.6.1 Characterization by Confocal Imaging.....                                                                   | 74         |
| 2.2.6.2 Characterization by Transmission Electron Microscopy (TEM) .....                                            | 74         |
| 2.2.6.3 Quantification by Flow Cytometry .....                                                                      | 74         |
| 2.2.6.4 Quantification by High Content Analysis (HCA) .....                                                         | 75         |
| 2.2.7 Statistics .....                                                                                              | 75         |
| 2.3 Results .....                                                                                                   | 75         |
| 2.3.1 Size and Surface Charge Analysis .....                                                                        | 75         |
| 2.3.2 Cell Viability .....                                                                                          | 75         |
| 2.3.3 Cellular Internalization Behaviour .....                                                                      | 75         |
| 2.3.3.1 Colocalization .....                                                                                        | 75         |
| 2.3.3.2 Flow Cytometric Analysis of Cellular Internalization .....                                                  | 76         |
| 2.3.3.4 High Content Analysis of Cellular Internalization .....                                                     | 96         |
| 2.4 Discussion .....                                                                                                | 96         |
| 2.5 Conclusions .....                                                                                               | 97         |
| 2.6 References .....                                                                                                | 99         |
| <b>3. Tunable Elastin-like Polypeptide Hollow Spheres as a High Payload and Controlled Delivery Gene Depot.....</b> | <b>101</b> |
| 3.1 Introduction .....                                                                                              | 102        |

|         |                                                      |     |
|---------|------------------------------------------------------|-----|
| 3.2     | Materials and Methods                                | 104 |
| 3.2.1   | Materials.....                                       | 104 |
| 3.2.2   | EP20–24 Polypeptide Expression and Purification..... | 105 |
| 3.2.3   | Purification of mTGase .....                         | 105 |
| 3.2.4   | Fabrication of Hollow Spheres.....                   | 105 |
| 3.2.5   | Size and Zeta Potential Analysis .....               | 105 |
| 3.2.6   | ELP Adsorption Studies .....                         | 106 |
| 3.2.7   | TNBSA Assay for Cross-linking .....                  | 106 |
| 3.2.8   | SDS-PAGE Analysis for Cross-linking .....            | 106 |
| 3.2.9   | Morphological Characterization.....                  | 107 |
| 3.2.9.1 | Surface Morphology Analysis using SEM .....          | 107 |
| 3.2.9.2 | Internal Structure Analysis using TEM .....          | 107 |
| 3.2.10  | Plasmid Propagation and Isolation.....               | 107 |
| 3.2.11  | Polyplex Formulation.....                            | 107 |
| 3.2.12  | Polyplex and Naked <i>p</i> DNA Loading Studies..... | 107 |
| 3.2.13  | <i>In vitro</i> Release Studies.....                 | 108 |
| 3.2.14  | Imaging of Loaded Hollow Spheres by TEM .....        | 108 |
| 3.2.15  | Cell Culture Studies .....                           | 108 |
| 3.2.16  | Cell Viability Studies .....                         | 109 |
| 3.2.17  | Transfection Studies.....                            | 109 |
| 3.2.18  | Cellular Localization of Hollow Spheres .....        | 109 |
| 3.2.19  | Colocalization Studies.....                          | 110 |
| 3.3     | Results                                              | 110 |
| 3.3.1   | Fabrication of Hollow Spheres.....                   | 110 |
| 3.3.2   | Polyplex and <i>p</i> DNA Loading Studies .....      | 111 |
| 3.3.3   | <i>In Vitro</i> Release Studies .....                | 112 |
| 3.3.4   | Transfection and Cellular Viability Studies .....    | 112 |
| 3.3.5   | Cellular Localization Studies .....                  | 113 |
| 3.3.6   | Fluorescence Colocalization Studies.....             | 113 |
| 3.4     | Discussion                                           | 113 |
| 3.5     | Conclusions                                          | 156 |

|            |                                                                                                                                                                                            |            |
|------------|--------------------------------------------------------------------------------------------------------------------------------------------------------------------------------------------|------------|
| 3.6        | References                                                                                                                                                                                 | 157        |
| <b>4.</b>  | <b>Delivery of Therapeutic eNOS and IL-10 genes using an ELP-Based Injectable System to Induce Angiogenesis and Modulate Inflammation Level in the Mouse Hind Limb Ischemic Model.....</b> | <b>161</b> |
| 4.1        | Introduction                                                                                                                                                                               | 162        |
| 4.2        | Materials and Methods                                                                                                                                                                      | 164        |
| 4.2.1      | Materials.....                                                                                                                                                                             | 164        |
| 4.2.2      | EP20-244 Polypeptide Expression and Purification .....                                                                                                                                     | 165        |
| 4.2.3      | Purification of mTGase .....                                                                                                                                                               | 165        |
| 4.2.4      | Fabrication of Hollow Spheres.....                                                                                                                                                         | 165        |
| 4.2.5      | Fabrication of In Situ Injectable Scaffold .....                                                                                                                                           | 165        |
| 4.2.6      | TNBSA Assay for Cross-linking .....                                                                                                                                                        | 167        |
| 4.2.7      | Cell Viability .....                                                                                                                                                                       | 167        |
| 4.2.8      | Propagation of Plasmid and Isolation.....                                                                                                                                                  | 169        |
| 4.2.9      | Formulation of Polyplex.....                                                                                                                                                               | 169        |
| 4.2.10     | <i>In Vitro</i> Internalization Study of ELP Hollow Spheres using Flow Cytometry.....                                                                                                      | 169        |
| 4.2.11     | <i>In Vitro</i> Release Study.....                                                                                                                                                         | 169        |
| 4.2.12     | <i>In Vivo</i> Studies .....                                                                                                                                                               | 170        |
| 4.2.13     | Subcutaneous Dose Response Study.....                                                                                                                                                      | 170        |
| 4.2.14     | Hind Limb Ischemic Study .....                                                                                                                                                             | 171        |
| 4.2.15     | Histology and Immunohistochemistry .....                                                                                                                                                   | 171        |
| 4.2.15.1   | Stereology.....                                                                                                                                                                            | 172        |
| 4.2.15.1.1 | Inflammation.....                                                                                                                                                                          | 172        |
| 4.2.15.1.2 | Angiogenesis.....                                                                                                                                                                          | 173        |
| 4.2.16     | Quantification of heNOS and hIL-10 Level.....                                                                                                                                              | 173        |
| 4.2.17     | Multiplex Cytokine Measurements .....                                                                                                                                                      | 174        |
| 4.2.18     | RT-PCR Analysis.....                                                                                                                                                                       | 174        |
| 4.2.19     | Statistics .....                                                                                                                                                                           | 174        |
| 4.3        | Results                                                                                                                                                                                    | 175        |
| 4.3.1      | Internalization Study of Hollow Spheres .....                                                                                                                                              | 175        |
| 4.3.2      | Fabrication of Injectable Scaffold and its Characterization .....                                                                                                                          | 175        |
| 4.3.3      | <i>In Vitro</i> Release Study.....                                                                                                                                                         | 175        |

|                                                                                     |            |
|-------------------------------------------------------------------------------------|------------|
| 4.3.4 <i>In Vivo</i> Subcutaneous Study.....                                        | 182        |
| 4.3.4.1 Angiogenesis and Inflammation Analysis of Subcutaneous Mouse Model .....    | 182        |
| 4.3.4.2 heNOS and hIL-10 Expression in the Subcutaneous Mouse Model .....           | 183        |
| 4.3.4.3 Inflammatory Markers .....                                                  | 183        |
| 4.3.5 Hind Limb Ischemia Study .....                                                | 196        |
| 4.3.5.1 Angiogenesis and Inflammation Levels in the Ischemic Tissue .....           | 196        |
| 4.3.6 RT-PCR Analysis .....                                                         | 207        |
| 4.3.7 Relation between Angiogenesis and Inflammation in a Subcutaneous Model .....  | 208        |
| 4.4 Discussion .....                                                                | 208        |
| 4.5 Conclusions .....                                                               | 218        |
| 4.6 References.....                                                                 | 219        |
| <b>5. Summary and Future Directions.....</b>                                        | <b>224</b> |
| 5.1 Introduction.....                                                               | 225        |
| 5.2 Summary .....                                                                   | 225        |
| 5.2.1 Phase I – Chitosan Hollow Sphere as a Model System.....                       | 225        |
| 5.2.2 Phase II – Elastin-like Polypeptide Hollow Sphere as Gene Delivery Depot..... | 226        |
| 5.2.3 Phase III – Dual Delivery Release System.....                                 | 227        |
| 5.2.4 Phase IV – <i>In Vivo</i> Animal Study.....                                   | 227        |
| 5.3 Limitations.....                                                                | 228        |
| 5.3.1 Phase I.....                                                                  | 228        |
| 5.3.2 Phase II.....                                                                 | 229        |
| 5.3.3 Phase III.....                                                                | 230        |
| 5.3.4 Phase IV.....                                                                 | 230        |
| 5.4 Conclusions.....                                                                | 231        |
| 5.4.1 Phase I.....                                                                  | 232        |
| 5.4.2 Phase II.....                                                                 | 232        |
| 5.4.3 Phase III.....                                                                | 232        |
| 5.4.4 Phase IV.....                                                                 | 233        |
| 5.5 Future Directions.....                                                          | 233        |
| 5.5.1 Gene and Protein and Cell Screening in an Ischemic Pathophysiology.....       | 235        |

|                                                                                                                  |            |
|------------------------------------------------------------------------------------------------------------------|------------|
| 5.5.1.1 Assessment of mRNA Regulation with Respect to Inflammation, Angiogenesis and Muscle Regeneration.....    | 235        |
| 5.5.1.2 Assessment of Protein Regulation with Respect to Inflammation, Angiogenesis and Muscle Regeneration..... | 235        |
| 5.5.1.3 Assessment of Cell Regulation with Respect to Inflammation, Angiogenesis and Muscle Regeneration.....    | 236        |
| 5.5.2 Cell Therapy for Critical Limb Ischemia.....                                                               | 236        |
| 5.5.3 Hollow Sphere Modifications for Targeting.....                                                             | 241        |
| 5.5.3.1 Evading Immune Barriers for an Efficient Drug Delivery System.....                                       | 241        |
| 5.5.3.2 ELP Hollow Spheres Targeting Ischemic Muscle.....                                                        | 242        |
| 5.5.4. Tissue Engineered Blood Vessel using an ELP Scaffold.....                                                 | 243        |
| 5.5.5 Tumor Xenograft Implantation using an Elastin-based Biomaterial System.....                                | 245        |
| 5.6. Conclusions.....                                                                                            | 248        |
| 5.7. References.....                                                                                             | 249        |
| <b>List of Appendices.....</b>                                                                                   | <b>255</b> |
| A List of reagents / Compounds used.....                                                                         | 256        |
| B. Chitosan/PGA Hollow Spheres.....                                                                              | 258        |
| C. Elastin-like Polypeptide (ELP) Hollow Sphere Fabrication.....                                                 | 259        |
| D. Dual Delivery Injectable ELP-Based System.....                                                                | 260        |
| E. Trinitrobenzene Sulfonic Acid Assay.....                                                                      | 261        |
| F. Bicinchoninic Acid Assay.....                                                                                 | 261        |
| G. Cell Culture.....                                                                                             | 262        |
| H. Cell Viability Assays.....                                                                                    | 265        |
| I. <i>In Vitro</i> Transfection Study.....                                                                       | 266        |
| J. <i>In Vitro</i> Internalization Study.....                                                                    | 267        |
| K. Plasmid DNA Expansion.....                                                                                    | 267        |
| L. Plasmid Labelling.....                                                                                        | 270        |
| M. PicoGreen Assay.....                                                                                          | 271        |
| N. Electrophoresis.....                                                                                          | 273        |
| O. Electron Microscopy.....                                                                                      | 276        |

|                                                    |     |
|----------------------------------------------------|-----|
| P. Fluorescent Microscopy.....                     | 278 |
| Q. Subcutaneous Study Protocol.....                | 279 |
| R. Induction of Unilateral Hind Limb Ischemia..... | 279 |
| S. Immunostaining.....                             | 281 |
| T. Tissue Enzyme Linked Immunosorbent Assay.....   | 281 |
| U. Tissue PCR.....                                 | 282 |
| V. Stereology.....                                 | 283 |
| W. List of Journal Publications.....               | 286 |
| X. Book Chapter.....                               | 286 |
| Y. Conference Presentation (Podium).....           | 286 |
| Z. Conference Presentation (Poster).....           | 288 |

## LIST OF FIGURES

### **Chapter 1**

- Figure 1.1: Elastin-like polypeptide-based physical forms that have been reported in the literature .....17
- Figure 1.2: Gene delivery vehicles used for delivery of therapeutic genes for the treatment of critical limb ischemia in clinical and pre-clinical set ups.....27

### **Chapter 2**

- Figure 2.1: Schematic representation of hollow sphere fabrication and surface modifications....72
- Figure 2.2: Chitosan/PGA hollow spheres observed under TEM (A) 100 nm; (B) 300 nm (C) 500 nm; (D) 1000 nm hollow spheres.....76
- Figure 2.3: Zeta potential analysis of hollow spheres showing net charge after surface modifications of all hollow spheres. Data is represented as the mean  $\pm$  standard deviation ( $n = 3$ ). \* indicates a statistically significant difference between samples with  $p < 0.05$ . .....77
- Figure 2.4: MTT assay showing percentage metabolic index of HUVECs at time points 6, 12, 24 and 48 hr. HUVECs were incubated with 100 nm hollow spheres. Data is represented as the mean  $\pm$  standard deviation ( $n = 3$ ). \* indicates statistical significance ( $p < 0.05$ ) .....78
- Figure 2.5: MTT assay showing percentage metabolic index of HUVECs at time points 6, 12, 24 and 48 hr. HUVECs were incubated with 300 nm hollow spheres. Data is represented as the mean  $\pm$  standard deviation ( $n = 3$ ). \* indicates statistical significance ( $p < 0.05$ ). .....79
- Figure 2.6: MTT assay showing percentage metabolic index of HUVECs at time points 6, 12, 24 and 48 hr. HUVECs were incubated with 500 nm hollow spheres. Data is represented as the mean  $\pm$  standard deviation ( $n = 3$ ). \* indicates statistical significance ( $p < 0.05$ ). .....80
- Figure 2.7: MTT assay showing percentage metabolic index of HUVECs at time points 6, 12, 24 and 48 hr. HUVECs were incubated with 1000 nm hollow spheres. Data is represented as the mean  $\pm$  standard deviation ( $n = 3$ ). \* indicates statistical significance ( $p < 0.05$ ).....81

Figure 2.8: MTT assay showing percentage metabolic index of HUASMCs at time points 6, 12, 24 and 48 hr. HUASMCs were incubated with 100 nm hollow spheres. Data is represented as the mean  $\pm$  standard deviation (n = 3). No statistically significant effect of surface functionalization was observed between hollow spheres.....82

Figure 2.9: MTT assay showing percentage metabolic index of HUASMCs at time points 6, 12, 24 and 48 hr. HUASMCs were incubated with 300 nm hollow spheres. Data is represented as the mean  $\pm$  standard deviation (n = 3). No statistically significant effect of surface functionalization was observed between hollow spheres.....83

Figure 2.10: MTT assay showing percentage metabolic index of HUASMCs at time points 6, 12, 24 and 48 hr. HUASMCs were incubated with 500 nm hollow spheres. Data is represented as the mean  $\pm$  standard deviation (n = 3). No statistically significant effect of surface functionalization was observed between hollow spheres.....84

Figure 2.11: MTT assay showing percentage metabolic index of HUASMCs at time points 6, 12, 24 and 48 hr. HUASMCs were incubated with 1000 nm hollow spheres. Data is represented as the mean  $\pm$  standard deviation (n = 3). No statistically significant effect of surface functionalization was observed between hollow spheres.....85

Figure 2.12: Confocal micrographs of FITC labelled hollow spheres: (A) 100 nm and (B) 300 nm internalized into HUVECs and (C) 100 nm and (D) 300 nm internalized into HUASMCs. All images were taken after 24 hr incubation with cells. ....86

Figure 2.13: TEM images illustrating 100 nm neutrally charged hollow spheres internalized into (A) HUVECs (inset shows the hollow spheres inside lysosome) and (B) HUASMCs (inset shows hollow spheres inside lysosome). (C) Higher magnification image of (A) showing endocytic internalization of hollow spheres from endosome (E) to lysosomes (L) near nucleus (N).....87

Figure 2.14: Flow cytometry data, elucidating the effect of size and surface modifications on the internalization efficiency of hollow spheres into HUVECs at 12 hr incubation.....88

Figure 2.15: Flow cytometry data, elucidating the effect of size and surface modifications on the internalization efficiency of hollow spheres into HUASMCs at 12 hr incubation...89

Figure 2.16: High content analysis showing internalization of PEGylated, neutral and negatively charged hollow spheres of (A) 100 nm and (B) 300 nm with HUVECs over a time course of 6, 12, 24 and 48 hr. Data is represented as the mean  $\pm$  standard deviation ( $n = 3, p < 0.05$ ).....90

Figure 2.17: High content analysis showing internalization of PEGylated, neutral and negatively charged hollow spheres of (A) 500 nm and (B) 1000 nm with HUVECs over a time course of 6, 12, 24 and 48 hr. Data is represented as the mean  $\pm$  standard deviation ( $n = 3, p < 0.05$ ). .....91

Figure 2.18: High content analysis showing internalization of PEGylated, neutral and negatively charged hollow spheres of (A) 100 nm and (B) 300 nm with HUASMCs over a time course of 6, 12, 24 and 48 hr. Data is represented as the mean  $\pm$  standard deviation ( $n = 3, p < 0.05$ ).....92

Figure 2.19: High content analysis showing internalization of PEGylated, neutral and negatively charged hollow spheres of (A) 500 nm and (B) 1000 nm with HUASMCs over a time course of 6, 12, 24 and 48 hr. Data is represented as the mean  $\pm$  standard deviation ( $n = 3, p < 0.05$ ).....93

**Chapter 3**

Figure 3.1: Illustrating ELP20–24<sup>4</sup> structure: (A) ELP20–24<sup>4</sup> polypeptide sequence consisting of domains derived from human exons 20–21–23–24–21–23–24–21–23–24–21–23–24 and (B) showing amino acid sequence present in 20–21–23–24.....113

Figure 3.2: Schematic representation of ELP hollow spheres fabrication using PS beads as a template. The process involves coating of ELP over sulfonated PS beads (Step 1), cross-linking with microbial transglutaminase (Step 2) and removal of PS bead to obtain the hollow spheres (Step 3).....114

Figure 3.3: Schematic representation of (A) polyplex formation using the polymer and naked pDNA, (B) loading of polyplexes inside hollow spheres. ....115

Figure 3.4: Size analysis of coating of ELP over 500 nm PS beads at 37°C with different ratios of ELP to PS beads: statistical significance was determined by one-way ANOVA ( $n = 9, p < 0.05$ ). \* Represents statistical significance between PS beads alone and different ratios of ELP coated PS beads. ....116

Figure 3.5: Size analysis of coating of ELP over 500 nm PS beads at 37°C over different time periods ( $n = 9$ ). No statistical significance was found between different groups. ....117

Figure 3.6: Zeta potential analysis of ELP coating over 500 nm PS beads with different ratios of ELP to PS beads. Statistical significance was determined by one-way ANOVA ( $n = 9$ ,  $p < 0.05$ ). \* represents statistical significance between PS beads alone and different ratios of ELP coated PS beads.....118

Figure 3.7: Zeta potential analysis of ELP coating over 500 nm PS beads over different time periods ( $n = 9$ ). No statistical difference was found between different time points. .119

Figure 3.8: BCA assay for quantification of coating over PS beads with different ratios of ELP to PS beads for 500 nm PS beads. Statistical significance was determined by one-way ANOVA ( $n = 6$ ,  $p < 0.05$ ). \* Represents statistical significance between 50–1 to that of 75–1 and 100–1 groups.....120

Figure 3.9: BCA assay for quantification of coating of ELP on PS beads over different time points at 37°C ( $n = 6$ ). No statistical significance was found between different time points.....121

Figure 3.10: Quantification of ELP required for coating of different sizes of PS beads using BCA assay. Statistical significance was determined by one-way ANOVA ( $n = 6$ ,  $p < 0.05$ ). \* Represents statistical significance between various sizes in terms of their ELP requirement. ....122

Figure 3.11: SEM micrographs of 500 nm (A) uncoated and (B) ELP coated PS beads. The scale bars represent 1  $\mu\text{m}$ .....123

Figure 3.12: TNBSA analysis to characterize the cross-linking of ELP with various amounts of mTGase enzyme. Glutaraldehyde and ELP alone were used as positive and negative controls respectively. Statistical significance was determined by one-way ANOVA ( $n = 9$ ,  $p < 0.05$ ). \* Represents statistical difference between ELP and different ratios of ELP-mTGase along with GTA cross-linked ELP. ....124

Figure 3.13: SDS-PAGE showing the gradual cross-linking of ELP with increase in mTGase amounts. The gel was stained using SimplyBlue™ SafeStain.....125

Figure 3.14: TEM images of hollow spheres fabricated using (A) 100 nm, (B) 300 nm and (C) 1000 nm sizes of PS beads.....126

|                                                                                                                                                                                                                                                                                                                                                                                                                      |     |
|----------------------------------------------------------------------------------------------------------------------------------------------------------------------------------------------------------------------------------------------------------------------------------------------------------------------------------------------------------------------------------------------------------------------|-----|
| Figure 3.15: SEM images of hollow spheres fabricated using (A) 100 nm, (B) 300 nm, (C) 500 nm and (D) 1000 nm sizes of PS beads. ....                                                                                                                                                                                                                                                                                | 127 |
| Figure 3.16: Zeta potential analysis of hollow spheres fabricated using 100, 300, 500 and 1000 nm PS beads ( $n = 9$ ). No statistical significance was found between different groups.....                                                                                                                                                                                                                          | 128 |
| Figure 3.17: Diffraction light scattering particle size analysis data of cross-linked and pre-cross-linked spheres made from 100 nm sulfonated PS beads. (A and B) Size distributions data of pre-cross-linked spheres on days 1 and 15 respectively. (C and D) Size distributions data of cross-linked spheres on days 1 and 15 respectively. PdI, polydispersity index ( $n = 3$ ). ....                           | 129 |
| Figure 3.18: TEM image of self-assembled ELP solid spheres cross-linked with mTGase and 20% THF. The scale bar represents 2 $\mu\text{m}$ .....                                                                                                                                                                                                                                                                      | 130 |
| Figure 3.19: Comparison of <i>p</i> DNA loading efficiency of 300 nm hollow spheres and self-assembled ELP solid spheres of approx. 300 nm size. All the data are represented as mean $\pm$ standard deviation ( $n = 3, p < 0.05$ ). Statistical analysis was performed using Student's <i>t</i> -test. * Represents statistical significance between hollow spheres vs solid spheres.....                          | 131 |
| Figure 3.20: <i>p</i> DNA and polyplex loading behaviour of ELP hollow spheres. <i>p</i> DNA loading efficiency of 500 nm hollow spheres using naked <i>p</i> DNA and polyplex. All the data are represented as mean $\pm$ standard deviation ( $n = 3, p < 0.05$ ). Statistical analysis was performed using Student's <i>t</i> -test. * Represents statistical significance between <i>p</i> DNA vs polyplex. .... | 132 |
| Figure 3.21: Polyplex loading efficiency of 500 nm hollow spheres with varying ratios of polyplex to sphere. All the data are represented as mean $\pm$ standard deviation ( $n = 3, p < 0.05$ ). Statistical analysis was performed using one-way ANOVA. * Represents statistical significance between different ratio of sphere to <i>p</i> DNA. ....                                                              | 133 |
| Figure 3.22: Polyplex loading efficiency of ELP hollow spheres of various sizes: 100 nm, 300 nm, 500 nm and 1000 nm. All the data are represented as mean $\pm$ standard deviation ( $n = 3$ ). No statistical difference was found between different groups. ....                                                                                                                                                   | 134 |

Figure 3.23: Zeta potential analysis of hollow spheres of 500 nm before loading (BL), after loading (AL) and after treatment with PGA to validate PGA method for quantification. All the data are represented as mean  $\pm$  standard deviation ( $n = 3, p < 0.05$ ). Statistical analysis was performed using one-way ANOVA. \* Represents statistical difference between AN vs BL and PGA. .... 135

Figure 3.24: PicoGreen<sup>®</sup> assay showing quantification of polyplex loading outside spheres and inside the hollow spheres after treating the spheres with PGA. All the data are represented as mean  $\pm$  standard deviation ( $n = 3, p < 0.05$ ). Statistical analysis was performed using one-way ANOVA. \* Represents statistical significance between inside vs outside. .... 136

Figure 3.25: TEM images of 500 nm hollow spheres. (A1) Hollow sphere without polyplex, (A2) hollow spheres loaded with polyplex and (A3) hollow spheres after PGA treatment. .... 137

Figure 3.26: TEM images of 500 nm hollow spheres. Hollow spheres loaded with different amounts of polyplex were investigated. (A1) 1:20 ratio shows minimal spheres loaded with polyplex, (A2) 1:40 with comparatively higher number of polyplex loaded spheres and (A3) 1:80 ratio showing almost all the spheres loaded with polyplex. .... 138

Figure 3.27: PicoGreen<sup>®</sup> assay showing release of *pDNA* from the polyplex using polyglutamic acid. The emission values of naked *pDNA*, polyplex and polyplex treated with PGA. Statistical significance in Figure A was determined by one-way ANOVA ( $n = 3, p < 0.05$ ). \* Represents statistical significance between polyplex vs polyplex + PGA. .... 139

Figure 3.28: Agarose gel showing naked *pDNA*, polyplex and polyplex treated with PGA. .... 140

Figure 3.29: Cumulative release profile of *pDNA*/polyplex from all the four different sizes of hollow spheres tested at 37°C. All the data are represented as the mean  $\pm$  standard deviation ( $n = 3, p < 0.05$ ). Statistical analysis was performed using one-way ANOVA. .... 141

Figure 3.30: *In vitro* release study of 1000 nm hollow spheres in the presence of 10 U/g of human leukocyte elastase and protease (pH 7.4) in PBS. All the data are represented as the

|                                                                                                                                                                                                                                                                                                                                                                        |     |
|------------------------------------------------------------------------------------------------------------------------------------------------------------------------------------------------------------------------------------------------------------------------------------------------------------------------------------------------------------------------|-----|
| mean $\pm$ standard deviation ( $n = 3, p < 0.05$ ). Statistical analysis was performed using one-way ANOVA. ....                                                                                                                                                                                                                                                      | 142 |
| Figure 3.31: SEM images of hollow spheres (A) untreated 1000 nm and (B) degrading 1000 nm hollow spheres in the presence of elastase after 72 hr. The scale bar represents 2 $\mu\text{m}$ .....                                                                                                                                                                       | 143 |
| Figure 3.32: Confocal image of ADSCs expressing GFP 48 hr after treatment with polyplexes. The scale bar represents 100 $\mu\text{m}$ .....                                                                                                                                                                                                                            | 144 |
| Figure 3.33: AlamarBlue <sup>®</sup> assays showing the cell viability of loaded hollow spheres of all the four different sizes in ADSCs after 48 hr. All the data are represented as the mean $\pm$ standard deviation ( $n = 3, p < 0.05$ ). Statistical analysis was performed using one-way ANOVA. * Represents polyplex vs other groups. ....                     | 145 |
| Figure 3.34: AlamarBlue <sup>®</sup> assays showing the cell viability of loaded hollow spheres of all the four different sizes in HUVECs after 48 hr. All the data are represented as the mean $\pm$ standard deviation ( $n = 3, p < 0.05$ ). Statistical analysis was performed using one-way ANOVA. * Represents polyplex vs other groups. ....                    | 146 |
| Figure 3.35: Gaussia luciferase assay for investigation of transfection efficiency of all the four different sizes of polyplex loaded hollow spheres in ADSCs. All the data are represented as the mean $\pm$ standard deviation ( $n = 3, p < 0.05$ ). Statistical analysis was performed using one-way ANOVA. * Represents cell and pDNA groups vs other groups..... | 147 |
| Figure 3.36: Gaussia luciferase assay for investigation of transfection efficiency of all the four different sizes polyplex loaded hollow spheres in HUVECs. All the data are represented as the mean $\pm$ standard deviation ( $n = 3, p < 0.05$ ). Statistical analysis was performed using one-way ANOVA. * Represents cell and pDNA groups vs other groups.....   | 148 |
| Figure 3.37: Polyplex loaded hollow spheres versus pDNA loaded hollow spheres using 500 nm hollow spheres. All the data are represented as the mean $\pm$ standard deviation ( $n = 3, p < 0.05$ ). Statistical analysis was performed using one-way ANOVA. * Represents pDNA group vs sphere + pDNA and sphere + polyplex. ....                                       | 149 |

- Figure 3.38: TEM images showing the internalization pathway of 500 nm hollow spheres loaded with polyplexes within ADSCs. Hollow spheres were observed at different locations in the cell: (A) Attachment to cell membrane, (B) cell membrane engulfing a sphere, (C) in early endosomes, (D) lysosome near to nucleus, (E) rupturing the lysosomal membrane and (F) hollow spheres coming out of the lysosome by completely disrupting the lysosomal membrane. Cell membrane, endosomes, lysosome and nucleus are represented as CM, E, L and N respectively in the figures. The arrows point towards the localization of the hollow spheres inside the cell.....150
- Figure 3.39: Fluorescence images showing internalization of *pDNA*- hollow spheres (A1–A3) and polyplex- hollow spheres (B1–B3) by ADSCs. (A1 and B1). The images show fluorescence signal arising from *cy3-pDNA*. (A2 and B2) Lysosomal staining by LysoTracker Blue. (A3 and B3) Merged images of fluorescence signals: *cy3-pDNA* and LysoTracker Blue.....151

#### Chapter 4

- Figure 4.1: A schematic showing the overall goal of this study. The study includes (A) an *in vitro* fabrication of the ELP-in-ELP injectable system and (B) delivery of the therapeutic genes heNOS and hIL-10 in a subcutaneous study to determine a therapeutic dose for heNOS and hIL-10 and a final *in vivo* study in a mouse model of HLI.....166
- Figure 4.2: A schematic representation of injectable elastin-like polypeptide scaffold fabrication method. Elastin-like polypeptide and microbial transglutaminase (mTGase) mixture solution in water forms the scaffold when incubated at 37 °C. The mixture solution of elastin-like polypeptide and mTGase forms aggregated structure rather than a scaffold.....168
- Figure 4.3: Flow cytometry data, elucidating the effect of size on the internalization efficiency of elastin-like polypeptide hollow spheres into activated macrophages THP1 at 24 h incubation. Statistical significance was performed by one-way ANOVA (n=3, p<0.05). \* represents significant difference of 10 µm from rest of the hollow spheres.....176
- Figure 4.4: Flow cytometry data, elucidating the effect of size on the internalization efficiency of elastin-like polypeptide hollow spheres into human umbilical vein endothelial cells at

24 h incubation. Statistical significance was performed by one-way ANOVA (n=3, p<0.05). \* represents significant difference of 1  $\mu\text{m}$  from rest of the hollow spheres.177

Figure 4.5: Photographic image (A) injection of elastin-like polypeptide/mTGase mix solution on a parafilm sheet and (B) solidified elastin-like polypeptide based scaffold after gelation.....178

Figure 4.6:TNBSA analysis to characterize the cross-linking of elastin-like polypeptide scaffold with mTGase enzyme of 100U/g of ELP. Glutaraldehyde and elastin-like polypeptide alone were used as positive and negative controls respectively. Statistical significance was determined by one-way ANOVA (n=3, p<0.05).....179

Figure 4.7:MTT assay was used to characterize the cellular metabolic activity of elastin-like polypeptide scaffold with mTGase enzyme. Glutaraldehyde and elastin-like polypeptide alone were used as negative and positive controls respectively. Statistical significance was determined by one-way ANOVA (n=3, p<0.05).....180

Figure 4.8:Cumulative release profile of pDNA/polyplex from the injectable system: elastin-like polypeptide scaffold/polyplex and elastin-like polypeptide hollow spheres/polyplex at 37 °C and treated with elastase. All the data are represented as the mean  $\pm$  standard deviation (n=3, p<0.05). Statistical significance was performed using t-test.....181

Figure 4.9:H & E staining of subcutaneous implant showing degradation of elastin-like polypeptide scaffold by A) day 7 and B) day 14. Arrows indicate elastin-like polypeptide scaffold at the site of implantation. The scale bar represents 100  $\mu\text{m}$ . ..184

Figure 4.10:Volume fraction of inflammatory cells in the subcutaneous implant area A) day 7 and B) day 14. Nine different doses of eNOS and IL-10 were implanted. Elastin-like polypeptide scaffold was used as a control. Statistical significance by one way ANOVA (n = 6, p < 0.05). \* represents the groups IL-10 treatments groups with statistical difference from ELP and eNOS alone treatment groups on day 7. ¥ represents significant difference between IL-10-10 and 20 treatment groups of day 7 and all the treatment groups of day 14.....186

Figure 4.11: Surface density of blood vessels in the subcutaneous implant area day 7 and day 14. Nine different doses of eNOS and IL-10 were implanted. Elastin-like polypeptide scaffold was used as a control. Statistical significance by one way ANOVA (n = 6, p

< 0.05). \* represents the groups eNOS20 and IL10-10/eNOS20 with statistical difference from ELP alone and IL-10 treatment groups on day 14. ¥ represents significant difference between eNOS20 and IL10-10/eNOS20 groups of day 14 from that of day 7. ....187

Figure 4.12: Length density of blood vessels in the subcutaneous implant area at day 7 and 14. Elastin-like polypeptide scaffold was used as a control. Statistical significance by one way ANOVA (n = 6, p < 0.05). \* represents the groups eNOS20 and IL10-10/eNOS20 with statistical difference from ELP alone and IL10-10 treatment groups on day 14. ¥ represents significant difference between eNOS20 and IL10-10/eNOS20 groups of day 14 from that of day 7.....188

Figure 4.13: CD68 immunostaining for macrophages (stained as green cells) at day 7 and 14 in various treatments in the subcutaneous implant study. (A, B) ELP, (C,D) IL10-10, (E,F) IL10-20 (G,H) eNOS10. The scale bar represents 100 µm. ....189

Figure 4.14: CD68 immunostaining for macrophages (stained as green cells) at day 7 and 14 in various treatments in the subcutaneous implant study. (A,B) eNOS20, (C,D) IL10-10/eNOS10, (E,F) IL10-10/eNOS20 and (G,H) IL10-20/eNOS10 and (I,J) IL10-20/eNOS20. The scale bar represents 100 µm.....190

Figure 4.15: CD31 immunostaining for blood vessels (stained as green cells) at day 7 and 14 in various treatments in the subcutaneous implant study. (A, B) ELP, (C, D) IL10-10, (E, F) eNOS20 and (G, H) IL10-10/eNOS20. The scale bar represents 100 µm.....191

Figure 4.16: Human eNOS expression in the subcutaneous implant for day 7 and 14. Elastin-like polypeptide scaffold only was kept as a control. Statistical significance by one way ANOVA (n = 6, p < 0.05). \* represents significance difference between eNOS containing treatment groups with rest of the groups and ¥ represents significant difference between the day 7 and 14 expression of eNOS. ....192

Figure 4.17: Human IL-10 expression in the subcutaneous implant for day 7 and 14. Elastin-like polypeptide scaffold only was kept as a control. Statistical significance by one way ANOVA (n = 6, p < 0.05). \* represents significance difference between IL-10

|              |                                                                                                                                                                                                                                                                                                                                                                                                                                                                                                                                                             |     |
|--------------|-------------------------------------------------------------------------------------------------------------------------------------------------------------------------------------------------------------------------------------------------------------------------------------------------------------------------------------------------------------------------------------------------------------------------------------------------------------------------------------------------------------------------------------------------------------|-----|
|              | containing treatment groups with rest of the groups and ¥ represents significant difference between the day 7 and 14 expression of IL-10.....                                                                                                                                                                                                                                                                                                                                                                                                               | 193 |
| Figure 4.18: | Screening of inflammatory cytokines expressed in the subcutaneous implant by day 7. Elastin-like polypeptide scaffold only was kept as a control. Statistical significance by one way ANOVA (n = 6, p < 0.05). * represents statistical significance of Interleukin-10 and eNOS only treatment groups from ELP and IL-10/eNOS treatment groups. ** represents statical significance of IL-10 and IL-10/eNOS from rest of the treatment groups. # represents represents statical significance of eNOS treatment group from rest of the treatment groups..... | 194 |
| Figure 4.19  | Screening of inflammatory cytokines expressed in the subcutaneous implant by day 14. Elastin-like polypeptide scaffold only was kept as a control. Statistical significance by one way ANOVA (n = 6, p < 0.05). * represents statistical significance of IL-10/eNOS treatment groups from the rest of the groups.....                                                                                                                                                                                                                                       | 195 |
| Figure 4.20: | Improvement of blood flow recovery at the ischemic site following eNOS treatment. Representative laser doppler perfusion imaging (LDPI) at week 0 (10 min after the ischemic surgery) and week 3 are shown. In these digital color-coded images, maximum perfusion values are in red, medium values in yellow to green and the lowest values in dark blue.....                                                                                                                                                                                              | 197 |
| Figure 4.21: | Blood perfusion measurement of ischemic limb in mouse model. Elastin-like polypeptide scaffold only was kept as a control. Statistical significance by one way ANOVA (n = 7, p < 0.05). * represents statistical significance of eNOS and IL-10/eNOS20 treatment groups from rest of the treatment groups.....                                                                                                                                                                                                                                              | 198 |
| Figure 4.22  | Functional recovery assessment of ischemic mice. Elastin-like polypeptide scaffold only was kept as a control. Measurements were performed by observing parameters such as 1) plantar flexion but mild discoloration, 2) No plantar flexion and mild discoloration, 3) No plantar flexion and moderate to severe discoloration and 4) necrosis. Statistical significance by one way ANOVA (n = 7, p < 0.05). * represents statistical significance IL-10/eNOS20 treatment groups from rest of the treatment groups.....                                     | 199 |

Figure 4.23: Surface density of blood vessels in the ischemic tissue day 7 and 21. Five different doses of eNOS and IL-10 were implanted. Elastin-like polypeptide scaffold was used as a control. Statistical significance by one way ANOVA ( $n = 7, p < 0.05$ ). \* represents statistical significant difference from the rest of the treatment groups at day 21. ¥ represents statistical significant difference between day 7 and 21. ....200

Figure 4.22: Length density of blood vessels in the ischemic tissue at day 7 and 21. Five different doses of eNOS and IL-10 were implanted. Elastin-like polypeptide scaffold was used as a control. Statistical significance by one way ANOVA ( $n = 7, p < 0.05$ ). ¥ represents statistical significant difference between day 7 and 21. ....201

Figure 4.23: Volume fraction of inflammatory cells in the ischemic tissue at day 7 and day 21. Five different doses of eNOS and IL-10 were implanted. Elastin-like polypeptide scaffold was used as a control. Statistical significance by one way ANOVA ( $n = 7, p < 0.05$ ). \* represents statistical significance of IL-10 and IL-10/eNOS20 treatment groups from rest of the treatment groups.....202

Figure 4.24: CD31 staining of blood vessels (stained as green cells) at day 7 and 21 in various treatments in the ischemic study. (A, B) Saline (C, D) ELP, (E, F) IL-10, (G, H) eNOS and (I, J) IL-10/eNOS. The scale bar represents 100  $\mu\text{m}$ . ....203

Figure 4.25: CD68 staining of macrophages (stained as green cells) at day 7 and 14 in various treatments in the ischemic study. (A, B) Saline (C, D) ELP, (E, F) IL-10, (G, H) eNOS and (I, J) IL-10/eNOS. The scale bar represents 100  $\mu\text{m}$ . ....204

Figure 4.26: Human eNOS expression in the ischemic tissue for day 7 and 21. Elastin-like polypeptide scaffold only was kept as a control. Statistical significance by one way ANOVA ( $n = 7, p < 0.05$ ). \* represents statistical significance of eNOS and IL-10/eNOS treatment groups from Scaffold and IL-10 groups and ¥ represents significant difference between the day 7 and 21 expression of eNOS.....205

Figure 4.27: Human IL-10 expression in the ischemic tissue for day 7 and 21. Elastin-like polypeptide scaffold only was kept as a control. Statistical significance by one way ANOVA ( $n = 7, p < 0.05$ ). \* represents significant difference of IL-10 treatment groups than rest of the groups and ¥ represents significant difference between the day 7 and 21 expression of IL-10.....206

Figure 4.28: RT-PCR data showing differential regulation of angiogenic factors with respect to treatment groups ELP, IL-10, eNOS and IL-10/eNOS in the ischemic tissue on day 7 and 21. The differential regulation angiogenic factors studied are: angiopoietin 1 (ANGPT1), serpinF1, fibroblast growth factor 1 (FGF1), platelet derived growth factor B (PDGFB), vascular endothelial cell growth factors A and B (VEGFA and VEGFB), leptin and matrix metalloproteinase protein 9 (MMP-9). Statistical significance was determined by one way ANOVA (n = 3, p < 0.05).\* represents a significant difference in the upregulation of a factor on day 21 compared to its early time point day 7. ¥ represents a significant difference in the upregulation of a factor on day 21 compared rest of the treatment groups. ....210

Figure 4.29: RT-PCR data showing differential regulation of inflammatory factors with respect to treatment groups ELP, IL-10, eNOS and IL-10/eNOS in the ischemic tissue on day 7 and 21. The differential regulation inflammatory factors studied are: Interleukin-1 , -2, -4, -6 and -10 (IL-1 , IL-2, IL-4, IL-6 and IL-10), tissue necrosis factor (TNF ) and interferon (IFN ). Statistical significance was determined by one way ANOVA (n = 3, p < 0.05). \* represents a significant difference in the upregulation of a factor on day 21 compared to its early time point day 7. ¥ represents a significant difference in the upregulation of a factor on day 21 compared rest of the treatment groups. .211

Figure 4.30: The schematic summarizes (A) dose response study to determine therapeutic doses of eNOS and IL-10 to enhance angiogenesis and modulate inflammation and (B) the therapeutic goal (in terms of changes in the angiogenesis and inflammation level in the ischemic tissue) achieved by the treatment group eNOS and IL-10/eNOS and the key factors associated with these changes at a molecular level.....214

**Chapter 5**

Figure 5.1: A schematic showing an overview of future applications stemming from the current study. The future studies both aim for understanding the pathophysiology of the CLI with respect to its cellular, molecular and biochemical aspects and also treating the condition via targeted delivery of drugs, cell therapy and engineered blood vessel. 234

Figure 5.2: A schematic elucidating the future studies which aim at understanding the pathophysiology of the CLI with respect to its cellular, molecular and biochemical aspects. ....237

Figure 5.3: A schematic showing the future study which aims at using cell therapy to treat the ischemic condition. The engineered endothelial cells and pericytes will be implanted in subcutaneously in mice and finally in an ischemic mouse model. ....240

Figure 5.4: A schematic presenting ways in which ELP hollow spheres can be engineered further to evade the immune system and surface functionalized to target the ischemic area. ....244

Figure 5.5: A schematic showing the fabrication of an ELP-based tissue engineered blood vessel. SMCs will be embedded while fabricating the ELP scaffold and then cultured in a bioreactor for 4-5 weeks. The blood vessels will be harvested and characterised for their mechanical strength before the implantation.....246

Figure 5.6: A schematic showing encapsulation of tumor within the ELP scaffold for xenograft studies and anti-cancer drug screening. ....247

**Appendices**

Figure A.1: Gridlines on hemocytometer. ....264

## LIST OF TABLES

### **Chapter 1**

|                                                                                                         |    |
|---------------------------------------------------------------------------------------------------------|----|
| Table 1.1: Fontaine classification of chronic leg ischemic.....                                         | 3  |
| Table 1.2: Summary of preclinical studies of IL-10 based gene therapy in various diseases. ....         | 9  |
| Table 1.3: Summary of preclinical in vivo studies utilising eNOS gene therapy for various diseases..... | 14 |
| Table 1.4: Summary of ELP based biomaterials for drug delivery application.....                         | 18 |
| Table 1.5: Summary of ELP based biomaterials for tissue engineering application.....                    | 20 |
| Table 1.6: Summary of in vivo viral based gene delivery for angiogenesis in various CLI models.....     | 28 |
| Table 1.7: Summary of in vivo non-viral based gene therapy for angiogenesis in various CLI models.....  | 32 |
| Table 1.8: Summary of clinical studies of angiogenic gene therapy in human CLI patients.....            | 36 |

### **Chapter 2**

|                                                                                                   |    |
|---------------------------------------------------------------------------------------------------|----|
| Table 2.1: Summary of effect of size (nm) and surface charge on all parameters investigated. .... | 94 |
|---------------------------------------------------------------------------------------------------|----|

### **Chapter 4**

|                                                                                                                                                                                                                                                                                                                                                                                                       |     |
|-------------------------------------------------------------------------------------------------------------------------------------------------------------------------------------------------------------------------------------------------------------------------------------------------------------------------------------------------------------------------------------------------------|-----|
| Table 4.1: The table contains nine different treatment groups used for the subcutaneous dose study.....                                                                                                                                                                                                                                                                                               | 185 |
| Table 4.2: Pearson's correlations' values between angiogenic and inflammatory parameters as a function of time in the subcutaneous implant study. I=change in inflammatory cells, L= change in length density of vessels, eNOS= change in eNOS expression, SD= change in surface density, IL-10= change in IL-10 expression, all between 7 and 14 days. * indicates significance ( $P < 0.05$ ). .... | 212 |
| Table 4.3: Pearson's correlations' values between angiogenic and inflammatory parameters as a function of time in the hind limb ischemic tissue study. I=change in inflammatory cells, L= change in length density of vessels, eNOS= change in eNOS expression, SD=                                                                                                                                   |     |

change in surface density, IL-10= change in IL-10 expression, all between 7 and 21 days. \* indicates significance ( $P < 0.05$ ).....213

## **Appendices**

|                                                                            |     |
|----------------------------------------------------------------------------|-----|
| Table A.1: List of compounds and reagents used in this study .....         | 256 |
| Table A.2: Protocol for preparation of DNA labelling reaction mixture..... | 270 |
| Table A.3: Protocol for the preparation of high range standard curve.....  | 273 |
| Table A.4: Protocol for preparing low range standard curve.....            | 273 |
| Table A.5: Master mix.....                                                 | 283 |
| Table A.6: Machine protocol.....                                           | 283 |

## Acknowledgements

I would like to sincerely thank Professor Abhay Pandit for his valuable guidance and constant support throughout this project. He has helped me immensely to develop my research skills in the field of biomaterials and has always encouraged me to think independently and work hard to achieve the goal. I would also like to thank Science Foundation Ireland, for providing funds for this project and Elastin Specialties, Canada for kindly providing elastin-like polypeptide.

I would like to thank all the former and current members of Network of Excellence for Functional Biomaterials. A special thanks to Dr. Gildas Rethore for mentoring me in the early months of my PhD and teaching me the hollow sphere fabrication technique. I would also like to thank Dr. Kathleen Fitzgerald for high content imaging analysis; Dr. Michael Monaghan for his help in RT-PCR analysis; Mr. Dilip Thomas for his help during my animal studies; Dr. Asha Mathew and Dr. Wenxin Wang for providing polymer; Dr. Mangesh Kulkarni for teaching me stereology techniques; Dr. Sunil Mahor for his valuable suggestions during elastin hollow sphere fabrication, Dr. Christophe Helary for his help in macrophage culture; Dr. Carolyn Holladay for the help during *in vivo* studies and Mr. Joshua Chao for helping in performing ELISA in my absence. I would also like to specifically thank Dr. Oliver Carroll for his assistance in day-to-day laboratory issues, help in plasmid expansion and mTGase enzyme purification; Mr. Anthony Sloan for his language editing; Mr. Keith Feerick, Mrs. Tara Cosgrave and Mr. Vidoja Kovacevic for their extraordinary support in administrative matters.

I highly appreciate the guidance I received from Professors William Gallagher, Timothy O'Brien and Kimberly Woodhouse while designing my experiments. I would like to thank Dr. Xizhe Chen for teaching me mouse hind limb ischemic surgery; Dr. Yolanda Garcia, Mr. Charles McHale, and Gerry Mchale for their crucial help in the *in vivo* studies. I would like to extend my gratitude to David Connolly for assistance with microscopes, Enda O'Connell for assistance with RT-PCR. Eadaoin Timmins for assistance with SEM and Pierce Lalor for assistance with TEM.

I would also like to extend thanks to some of the NFB members with whom I was socializing and hence alleviated my home sickness. Specially, I would like to thank Dr. Estelle Collin, Mr. Shane Brown, Mr. Gianluca Fontana, Dr. Akshaya Srivastava, Mr. Abhigyan Satyam, Mr. Pramod Kumar, Dr. Ahmed Aeid. Very special thanks to Mr. Max Adam, my housemate and everyone from Galway Hare Krishna group. I highly appreciate the support and encouragement I received at Yale University from Dr. Yibing Qyang.

My final acknowledgements are to the closest ones. I would like thank my parents, although I understand any amount of gratitude shown to them is insufficient. My mother's unconditional support is largely the reason that this PhD is completed in Ireland. No words are adequate to describe my late father's contribution to my life. I owe every bit of existence to him. This thesis is dedicated to his memory. I have been lucky to receive tremendous affection and support from several members in my extended family, which has been instrumental in overcoming several ups and downs in life. I am particularly grateful to my elder brothers Bhutesh and Girija for their love and care. Last but never least, I am grateful to my wife Reena, who has kept exemplary patience while I completed my PhD thesis. She has supported me emotionally and encouraged me to finish. I am indeed blessed to have her in my life.

## LIST OF ABBREVIATIONS

|         |                                                                                              |
|---------|----------------------------------------------------------------------------------------------|
| AAV     | Adeno-associated Virus                                                                       |
| ADSC    | Adipose Derived Stem Cell                                                                    |
| ANG-1   | Angiopoietin-1                                                                               |
| BCA     | Bicinchoninic Acid                                                                           |
| bFGF    | Basic Fibroblast Growth Factor                                                               |
| CD      | Cluster of Differentiation                                                                   |
| CLI     | Critical Limb Ischemia                                                                       |
| DC      | Dendritic Cell                                                                               |
| DOTMA   | N-[1-(2, 3-dioleoyloxy) propyl]-n, n, n-trimethyl ammonium chloride                          |
| EC      | Endothelial Cell                                                                             |
| ECM     | Extracellular Matrix                                                                         |
| EDC/NHS | <i>N</i> -Ethyl- <i>N</i> -(3-Diethylaminopropyl)-Carbodiimide/ <i>N</i> -Hydroxysuccinimide |
| EDGMA   | Ethylene Dimethacrylate                                                                      |
| EGM     | Endothelial Cell Growth Medium                                                               |
| ELP     | Elastin-like Polypeptide                                                                     |
| ELISA   | Enzyme Linked Immunosorbent Assay                                                            |
| eNOS    | Endothelial NOS                                                                              |
| EPC     | Endothelial Progenitor Cell                                                                  |
| FGF     | Fibroblast Growth Factor                                                                     |
| FITC    | Fluorescein Isothiocyanate                                                                   |
| GFP     | Green Fluorescent Protein                                                                    |
| GLuc    | Gaussia Luciferase                                                                           |
| GM-CSF  | Granulocyte Macrophage Colony Stimulating Factor                                             |
| GTA     | Glutaraldehyde                                                                               |
| HGF     | Hepatocyte Growth Factor                                                                     |
| HIF     | Hypoxia Inducible Factor                                                                     |
| HLI     | Hind Limb Ischemia                                                                           |
| HS      | Hollow Sphere                                                                                |

|         |                                                |
|---------|------------------------------------------------|
| HSP     | Heat Shock Protein                             |
| HUASMC  | Human Umbilical Artery Smooth Muscle Cell      |
| HUVEC   | Human Umbilical Vein Endothelial Cell          |
| IFN-    | Interferon-                                    |
| IGF     | Insulin-like Growth Factor                     |
| IL      | Interleukin                                    |
| IGF     | Insulin-like Growth Factor                     |
| iNOS    | Inducible NOS                                  |
| LCST    | Lower Critical Solution Temperature            |
| LDPI    | Laser Doppler Perfusion Imaging                |
| Lv      | Length Density                                 |
| MEA     | Methoxy Ethanol Amine                          |
| MHC     | Major Histocompatibility Complex               |
| MMPs    | Matrix Metalloproteinases                      |
| MSCs    | Mesenchymal Stem Cells                         |
| mTGase  | Microbial Transglutaminase                     |
| NF- B   | Nuclear Factor B                               |
| nNOS    | Neuronal NOS                                   |
| NO      | Nitric Oxide                                   |
| NOS     | Nitric Oxide Synthase                          |
| PA      | Propyl Amine                                   |
| PAD     | Peripheral Arterial Disease                    |
| pDNA    | Plasmid DNA                                    |
| PDGF    | Platelet Derived Growth Factor                 |
| PDMAEMA | Poly (2-dimethyl-aminoethylmethacrylate)       |
| PEG     | Polyethylene Glycol                            |
| PEGMEMA | Poly Ethylene Glycol Methyl Ether Methacrylate |
| PEI     | Polyethylenimine                               |
| PGA     | Polyglutamic Acid                              |
| PLA     | Polylactic Acid                                |

|                |                                         |
|----------------|-----------------------------------------|
| PLGA           | Poly (Lactic- <i>Co</i> -Glycolic Acid) |
| PS             | Polystyrene                             |
| ROS            | Reactive Oxygen Species                 |
| SCID           | Severe Combined Immune Deficient        |
| SDF-1          | Stromal-Derived Growth Factor-1 SEM     |
| Shh            | Sonic Hedgehog                          |
| SMC            | Smooth Muscle Cell                      |
| SMGM           | Smooth Muscle Cell Growth Medium        |
| S <sub>v</sub> | Surface Density                         |
| TEM            | Transmission Electron Microscopy        |
| TGF-           | Transforming Growth Factor-             |
| THF            | Tetrahydrofuran                         |
| TLR            | Toll-like Receptor                      |
| TNBSA          | Trinitrobenzene Sulfonic Acid Assay     |
| TNF-           | Tumor Necrosis Factor-                  |
| VEGF           | Vascular Endothelial Growth Factor      |
| V <sub>v</sub> | Volume Fraction                         |

## **Abstract**

Critical limb ischemia is a major clinical problem. Despite rigorous treatment regimes, there has been modest success in reducing the rate of amputations in these patients. Reduced level of blood flow and enhanced inflammation are the two major pathophysiological changes that occur in the ischemic tissue. The objective of this thesis was to develop a controlled delivery system capable of delivering multiple therapeutic genes in an extended manner. Initially, a Chitosan/Polyglutamic acid hollow sphere system was tested *in vitro* as a model system to elucidate the combinatorial effects of physicochemical properties such as size and surface charge on cell viability and, most importantly, on cellular internalization. In order to deliver multiple therapeutic genes, an elastin-like polypeptide (ELP) based injectable system was designed. The injectable system was comprised of hollow spheres and *in situ* scaffold of elastin-like polypeptide. The hollow spheres and *in situ* scaffold were independently capable of carrying gene complexes and released the gene complexes in an extended manner. Furthermore, the ELP based injectable system was used to deliver human eNOS and IL-10 therapeutic genes *in vivo*. Initially, a subcutaneous dose study was performed in the mouse model to determine a therapeutic dose of hIL-10 and heNOS. In the injectable ELP system, hIL-10 was loaded inside the scaffold and heNOS inside the ELP hollow spheres. Human eNOS(20 µg) and hIL-10(10 µg)/heNOS(20 µg) showed comparatively more blood vessel density than other groups and hIL-10(10 µg) showed comparatively reduced the amount of inflammatory cells. These groups were then selected for the hind limb ischemic study including control groups: saline, injectable system only. The treatment groups that showed higher blood perfusion measured using laser doppler perfusion imaging were the groups with heNOS treatment groups. Saline group showed signs of sever necrosis. Human IL-10 treatment groups showed reduction in the level of inflammatory cells. Furthermore, a mechanistic study showed proangiogenic activity of eNOS by up-regulating major proangiogenic growth factors such as vascular endothelial growth factors, platelet derived growth factor B and fibroblast growth factor 1. These factors help in formation of a stable vascular network. Thus, ELP injectable system mediated non-viral delivery of IL10-eNOS is a promising therapy towards treating limb ischemia.

## **Chapter 1**

### **Introduction**

Contents of this chapter are currently under preparation for manuscript submission:

1. Dash BC, Pandit A. “Recent Advances in Gene Delivery for Critical Limb Ischemia”.
2. Dash BC, Pandit A. “Elastin-like Polypeptide Based Biomaterials for Drug Delivery and Tissue Engineering Applications”.

### **1.1 Peripheral Arterial Disease**

Peripheral artery disease (PAD) is caused by the obstruction of blood flow in the arteries and is a manifestation of atherosclerosis, embolism, thrombus formation or arterial stenosis [1]. PAD related vascular diseases are a major healthcare issue worldwide, affecting 27 million individuals in Europe and North America alone [2-7]. Patients with PAD have an increased risk of mortality with vascular diseases such as coronary arterial (CAD), cerebro-vascular and renal disease.

The histo-pathological basis of peripheral atherosclerosis is identical with that seen in the coronary vasculature and other vascular beds. The atherosclerosis has three stages i) initial lesion formation, ii) progression of the lesion, and iii) plaque complications [8]. The initial lesion formation starts with the deposition of the mononuclear leucocytes into the intimal layer of the vessel wall. The leucocytes in the intima accumulate lipids and form a fatty streak. The fatty streak becomes an advanced plaque because of a further build-up of foam cells. The plaque becomes a fibrous matrix with the accumulation of smooth muscle cells (SMCs) and extracellular macromolecules. Once the lesion ulcerates, the underlying plaque is exposed to the bloodstream, and the potential for thrombotic occlusion or embolization increases [1, 9-11].

The risk factors associated with peripheral arterial disease are: age, gender, diabetes, tobacco abuse, hypertension, and hyperlipidaemia. The most important non-modifiable factors are age and gender, and these factors increase the risk of peripheral arterial disease two to threefold. The most important modifiable risk is smoking, which increases the risk of PAD threefold [11].

### **1.2 Critical Limb Ischemia**

Critical limb ischemia (CLI) is the end result of PAD, leading to insufficient blood flow to the muscles and other tissues. The factors associated with CLI are: diabetes, smoking, and age and lipid abnormalities. CLI patients suffer from ischemic rest pain, non-healing ulcers and tissue loss. The Fontaine score helps in classifying the severity of CLI and is useful while treating the condition. The Fontaine classification broadly classifies the severity of CLI as asymptomatic stage, intermittent claudication stage and the final stage: pain at rest, ulceration and gangrene (Table 1.1). It is estimated there are roughly 220 new cases of CLI per million people every year in Europe and North America and 500–1000 people per million of the population are diagnosed with CLI. Thus, it is considered as a critical public health issue.

**Table 1.1: Fontaine classification of chronic leg ischemic.**

|           |                                                                                         |
|-----------|-----------------------------------------------------------------------------------------|
| Stage I   | No symptoms                                                                             |
| Stage II  | Intermittent claudication                                                               |
| Stage IIa | Without pain on resting, but with claudication at a distance of greater than 200 metres |
| Stage IIb | Without pain on resting, but with a claudication distance of less than 200 metres       |
| Stage III | Nocturnal and / or resting pain                                                         |
| Stage IV  | Necrosis (death of tissue) and/ or gangrene in the limb                                 |

The pathophysiology of limb ischemia involves progressive changes that take place in the ischemic tissue, such as skeletal muscle, skin, bone and nerve. The skeletal muscle, being the major mass of tissue in the limb, is most vulnerable to ischemia and tolerant up to 4 hr [11]. Also, changes in the microcirculation, which develop progressively during the ischemic period have been reported. The other major pathophysiological change involves triggering of inflammatory response at the interface between dead and damaged muscle. The breakdown products of the muscle trigger the inflammatory response. This inflammatory response is multifactorial and is required to clean and dispose of the damaged tissue and to initiate a healing cascade.

### *1.2.1 Inflammation and Critical Limb Ischemia*

Inflammation has been implicated in the pathogenesis of PAD including both atherosclerosis and limb ischemia [12]. This is a fundamental pathological process consisting of a complex and highly dynamic sequence of reactions that occurs in affected blood vessels and adjacent tissues in response to an injury or abnormal stimulation caused by a physical, chemical, or biologic agent [13]. The trigger for the inflammatory response is tissue damage, most likely the breakdown products of muscle [14].

### *1.2.2 Markers of Inflammation during PAD*

Both limb ischemia and ischemic reperfusion are associated with an increased level of inflammatory markers such as pro-inflammatory cytokines: interleukin-1 (IL-1), tumor necrosis factor- (TNF- ), IL-6, C-reactive protein (CRP), cellular adhesion molecules (CAMs). Among others, white blood cell (WBC) count is assessed as a cellular response to inflammation [15].

IL-1 family contains 11 members out of which IL-1 , IL-1 , IL-1 receptor antagonist and IL-18 are well known and have been thoroughly investigated *in vitro* and *in vivo* in disease models and in humans [16, 17]. This cytokine family is closely linked to the innate immune response. Fundamental inflammatory responses induced by IL-1 include induction of cyclooxygenase type 2, increased expression of adhesion molecules, or synthesis of nitric oxide synthase (NOS). The cytokine IL-1 specifically is the most studied member of the family and is pro-inflammatory in nature and induces local and systemic inflammation. IL-1 has the ability to up-regulate expression of endothelial cell adhesion molecules and thus increases accumulation of neutrophils and, as a result, increases inflammation. Reports show an increase in IL-1 during ischemia and ischemic reperfusion. In humans, therapeutic approaches involving blocking of IL-1 has entered clinical medicine [16-22].

TNF- $\alpha$  has been most extensively characterized for its proinflammatory nature in animal models of disease and *in vitro* models of inflammatory tissue injury. It is a key multifunctional cytokine which mediates key roles in acute and chronic inflammation. The role of TNF- $\alpha$  has been documented in myocardial and limb ischemic tissue. Tissue and serum levels of TNF- $\alpha$  have been shown to be elevated globally during ischemic conditions. TNF- $\alpha$  mediates increases in vascular permeability through both neutrophil dependent and neutrophil independent mechanisms. Oxygen radicals have also been demonstrated to be involved in TNF- $\alpha$  mediated injury [23-31].

CRP is an acute phase reactant and increases in response to inflammatory processes. It is a pentameric protein mainly produced in the liver in response to IL-6 and other inflammatory cytokines. Inflammation also appears to be associated with a decline in function and physical activity often seen in patients with PAD and results in a significant impact on quality of life. Higher levels of CRP were correlated with impaired functional capacity, decreased physical activity, and future functional decline in several cohort studies [15, 32, 33].

IL-6 is an inflammatory cytokine produced by hepatocytes, lymphocytes, and endothelial cells [34]. IL-6 is the stimulus for CRP production in the liver, and is more upstream in the inflammatory cascade. The findings of several studies suggest that IL-6 levels may be regulated by physical activity. Although IL-6 levels are significantly increased after exercise in PAD patients [35], a higher IL-6 level has been associated with lower functional capacity in such patients [36]. CAMs are expressed on the vascular endothelium and circulating leukocytes. CAMs mediate recruitment of leukocytes to the vascular wall and into sub-endothelial spaces and help in all stages of atherogenesis [37]. Khaleghi et al. have reported that soluble ICAM-1 and VCAM-1 are associated with the presence of PAD in African Americans, but not in non-Hispanic whites [38].

WBCs are associated with PAD as a result of inflammation induced by several cytokines such as IL-1, IL-6 and TNF- $\alpha$ . Monocytes are the only subtypes which are significantly and independently associated with PAD [39]. According to Haumer et al., patients with more neutrophil counts are at a higher risk of major adverse cardiovascular events such as: myocardial infarction, limb ischemia and death [40]. The mechanisms by which an elevated WBC count is related to adverse outcomes might be because of increased inflammation, endothelial damage, pro-coagulant effects and microvascular damage [41, 42].

### *1.2.3 Mechanism of Inflammation during Ischemia in the Skeletal Muscle*

Numerous studies have been carried out on the pathophysiology of PAD while its downstream effects on skeletal muscle are yet to be understood. A better understanding of the

pathophysiological processes occurring within the skeletal muscle due to hypoxic/ischemic injury may enable us to identify potential therapeutic targets [43].

The inflammation during ischemia is closely associated with a raised level of proinflammatory cytokines such as TNF- $\alpha$  and IL-6. TNF- $\alpha$  and IL-6 have been shown to induce muscle proteolysis, and this in turn has been associated with reduced muscle mass and strength [44-46]. In addition, TNF- $\alpha$  has also been reported to induce apoptosis in skeletal myoblasts [47]. It is therefore possible that the elevated levels of TNF- $\alpha$  and IL-6 play a role in skeletal muscle damage in CLI.

Toll-like receptors (TLR) also have a role in the pathophysiology of limb ischemia. TLRs 1–9 are expressed in skeletal muscle [43, 48-50]. They are either activated by pathogen-associated molecular patterns or by endogenous ligands. Activation of TLRs culminates in the release of proinflammatory cytokines: TNF- $\alpha$ , IL-6, and IL-1 $\beta$ , chemokines. Endogenous ligands such as high mobility group proteins (HMGB-1) and heat shock proteins (HSPs) have been shown to be expressed in skeletal muscle [51, 52]. TLRs 2, 4, 6, 8, and 9 are up-regulated following freeze-induced skeletal muscle damage and Warren et al. have recently found up-regulation of TLRs 2, 4, and 6 protein expression in muscle biopsies obtained from patients with CLI [48]. There is ample evidence that TLRs of both immune and non-immune cells are up-regulated and activated in ischemia leading to the production of various proinflammatory cytokines and chemokines. TLRs through both MyD88-dependent and MyD88-independent signalling pathways are involved in mediating the ischemic tissue damage, and the dominant signalling cascade [43]. TLRs have also been implicated in apoptotic cell death, and play a large part in ischemia-induced cell damage. Thus TLR contributes to the tissue damage that occurs, and this provides the rationale to further elucidate the role of TLRs in the pathogenesis of skeletal muscle damage in CLI. A better understanding of the pathophysiology of CLI with the concomitant development of TLR antagonists may identify treatment modalities that can be translated into clinical benefit for patients with CLI [43].

Another mechanism behind skeletal muscle damage is the presence of reactive oxygen species (ROS) that is generated during ischemic reperfusion [53-55]. ROS can induce TNF- $\alpha$  by an activation of p38 mitogen activated kinase (MAPK) [56, 57]. Additionally, an increase in the intracellular Ca<sup>+2</sup>-concentration with generation of calcium pyrophosphate complexes and the formation of uric acid can act as danger signals and help in DNA fragmentation, cell membrane fragmentation and can also bind to intracellular protein complexes referred to as inflammasomes [58, 59]. The inflammasomes mediate an increase in the production and secretion of IL-1 $\beta$ . Furthermore, an increased Ca<sup>+2</sup>-concentration activates TLRs, eventually

stimulating the secretion of further proinflammatory cytokines/chemokines through an activation of nuclear factor kappa B (NF- $\kappa$ B) [60, 61]. The transcription factor NF- $\kappa$ B plays a central role in the generation of an inflammatory response and helps in activation and the formation of other proinflammatory factors such as IL-1, TNF- $\alpha$ , or interferon (IFN)- $\gamma$  and chemokines such as IL-8, monocyte chemo-attractant protein (MCP)-1, or RANTES (Regulated on Activation, Normal T cell Expressed and Secreted) potentiating the inflammatory response [55]. The inflammatory response is followed by an infiltration of lymphocytes, mononuclear cells/macrophages, and granulocytes into the injured tissue. Adhesion molecules like the leukocyte function associated antigen-1 (LFA-1) or the intercellular adhesion molecule (ICAM)-1 play an important role [55]. The cellular infiltrate together with the expression of cytokines/chemokines aggravates the interstitial edema of the inflamed tissue [54, 55].

#### *1.2.4 IL-10 and its Role in Inflammation*

IL-10 is an anti-inflammatory cytokine and was originally identified by Mosmann. IL-10 is known to be produced by macrophages, dendritic cells (DC), B cells, and various subsets of CD4- and CD8-T cells [62-64]. IL-10 achieves the anti-inflammatory activity by modulating the expression of cytokines, chemokines, soluble mediators and cell surface molecules by cells of myeloid origin: DCs, macrophages and monocytes [63, 65-70].

IL-10 potently inhibits production of IL-1, IL-6, IL-10 itself, IL-12, IL-18, granulocyte macrophage colony-stimulating factor (GM-CSF), granulocyte colony-stimulating factor (G-CSF), macrophage colony-stimulating factor (M-CSF), TNF- $\alpha$ , leukaemia inhibitory factor (LIF) and platelet activation factor (PAF) produced by activated monocytes/macrophages [71-75]. The inhibitory effects of IL-10 on IL-1 and TNF- $\alpha$  production especially are crucial to its anti-inflammatory activities. These cytokines (IL-1 and TNF- $\alpha$ ) often have synergistic activities on inflammatory pathways and processes. IL-10 also inhibits production of chemokines: IL-8, IFN- $\gamma$  induced protein 10 (IP-10), macrophage inflammatory protein 2 (MIP-2) [69, 76-78]. These chemokines activate inflammation by recruiting monocytes, dendritic cells, neutrophils, and T cells.

IL-10, has been reported to enhance production of interleukin-1 receptor antagonist (IL-1RA) and soluble factors p55 and p75 TNFR [79-82]. The IL-1RA inhibits the expression of IL-1RI and IL-1RII [71, 83, 84] produced by activated monocytes. This specific activity shows that IL-10 not only deactivates monocytes but also induces production of anti-inflammatory molecules. Furthermore, IL-10 is an inhibitor of antigen presentation. It inhibits major histocompatibility complex class II expression as well as the up-regulation of co-stimulatory

molecules CD80 and CD86. IL-10 inhibits the differentiation and maturation of DCs [85, 86]. Collectively, these observations indicate that IL-10 induces differentiation of a macrophage-like cell that limits ongoing immune responses and inflammation, and contributes to clearance of the infection via enhanced phagocytosis [63].

#### *1.2.5 IL-10 as a Therapeutic*

Preclinical and human clinical trials on the use of IL-10 to treat inflammatory diseases began more than a decade ago (Table 1.2). Some of the earliest trials were done in patients with psoriasis, immune and inflammatory bowel diseases [87], and the initial results of trials performed on small numbers of patients were quite encouraging. However, these trials did not include CLI patients [87-90].

One potentially interesting new approach included the delivery of therapeutic molecules to specific areas of the gastrointestinal tract via the oral administration of gelatin nanoparticles. The IL-10 gene has been delivered to the gastrointestinal tract using this technique. These nanoparticles preferentially accumulate in the large intestine where the IL-10 gene expression could be detected by reverse transcriptase polymerase chain reaction. In a murine acute colitis model, this approach resulted in the restoration of colon length, suppression of inflammatory responses, and increased body weight [91].

Even though the clinical effects of IL-10 must be considered modest, there remain reasons to be optimistic about the prospects for IL-10 therapy. The local delivery of IL-10 is an area that continues to be of interest to several researchers, and the use of IL-10 in combination with other cytokines, growth factors, or therapeutics continues to hold potential. Finally, our understanding of IL-10 gene expression may allow us to manipulate specific immune cells to 'program' them to home to lesions and preferentially produce IL-10 rather than inflammatory cytokines.

#### **1.2.5 Angiogenesis and Limb Ischemia**

Functional recovery of ischemic tissues is dependent on re-establishing the blood supply by collateral networks [92]. During ischemic insults, most tissues in the body try to compensate for low levels of blood supply by mechanisms of angiogenesis, arteriogenesis, vascular remodelling, and haematopoiesis. One of the molecular mechanisms underlying re-supply of blood oxygen involves up-regulation of hypoxia inducible factors 1 and 2 (HIF-1 and HIF-2). These induce the expression of several targeted genes, including vascular endothelial growth factors A (VEGFA), nitric oxide (NO), and erythropoietin (EPO), which in turn induce angiogenesis, arteriogenesis, vasodilation, and haematopoiesis [93-97].

**Table 1.2: Summary of preclinical studies of IL-10 based gene therapy in various diseases.**

| <b>Delivery Method</b>               | <b>Disease</b>             | <b>Preclinical Model</b> | <b>Observation</b>                                                                                                                                                                                                                                                                                                                                                | <b>Reference</b> |
|--------------------------------------|----------------------------|--------------------------|-------------------------------------------------------------------------------------------------------------------------------------------------------------------------------------------------------------------------------------------------------------------------------------------------------------------------------------------------------------------|------------------|
| Cationic liposome                    | Severe acute pancreatitis  | Rat                      | <ul style="list-style-type: none"> <li>• Reduced serum amylase, tissue TNF-</li> <li>• Reduced severity and mortality</li> </ul>                                                                                                                                                                                                                                  | [100]            |
| Plasmid                              | Liver fibrosis             | Mouse                    | <ul style="list-style-type: none"> <li>• Reduced TGF- <math>\beta</math>1, TNF- <math>\alpha</math>, collagen 1, VCAM-1, ICAM-1 and TIMPs</li> <li>• Attenuation of <math>\alpha</math>-smooth muscle actin and cyclooxygenase-2</li> </ul>                                                                                                                       | [101]            |
| Plasmid                              | Rheumatoid arthritis       | Mouse                    | <ul style="list-style-type: none"> <li>• Less synovitis</li> <li>• Decreased proteoglycan depletion</li> <li>• Reduced severity</li> </ul>                                                                                                                                                                                                                        | [102]            |
| Polyplexes (SuperFect <sup>®</sup> ) | Myocardial infarction      | Rat                      | <ul style="list-style-type: none"> <li>• Increased MSC survival in the scaffold</li> <li>• Improved overall cardiac function</li> </ul>                                                                                                                                                                                                                           | [103]            |
| Gelatin nanoparticle                 | Inflammatory bowel disease | Mouse                    | <ul style="list-style-type: none"> <li>• Suppression of proinflammatory cytokines, such as IFN- <math>\gamma</math>, TNF- <math>\alpha</math>, IL-1 <math>\beta</math>, IL-1 <math>\alpha</math> and IL-12, as well as certain chemokines.</li> <li>• Increased weight and restoration of colon length and weight</li> <li>• Reduced clinical severity</li> </ul> | [91]             |
| GAP:DLRIE Liposome                   | Heart transplantation      | Rabbit                   | <ul style="list-style-type: none"> <li>• Reduced lymphocytes infiltration</li> <li>• Decreased CD4+ and CD8+ responsiveness</li> <li>• Reduced expression of IL-2, IFN- <math>\gamma</math> and TNF- <math>\alpha</math></li> <li>• Localised immunosuppression</li> </ul>                                                                                        | [104]            |
| AAV                                  | Kidney transplantation     | Rat                      | <ul style="list-style-type: none"> <li>• Increased allograft survival rates from 22% to 90%</li> <li>• Reduced creatinine level</li> <li>• Decreased allograft histological abnormalities</li> </ul>                                                                                                                                                              | [105]            |

**Table 1.2 (continued): Summary of preclinical studies of IL-10 based gene therapy in various diseases.**

| <b>Delivery Method</b>                         | <b>Disease</b>            | <b>Preclinical Model</b> | <b>Observation</b>                                                                                                                                                                                                    | <b>Reference</b> |
|------------------------------------------------|---------------------------|--------------------------|-----------------------------------------------------------------------------------------------------------------------------------------------------------------------------------------------------------------------|------------------|
| AAV                                            | Atherosclerosis           | Mouse                    | <ul style="list-style-type: none"> <li>• Reduced serum cholesterol level</li> <li>• 31% reduction in plaque surface area</li> <li>• Reduced inflammation</li> </ul>                                                   | [106]            |
| Retroviral                                     | Osteoarthritis            | Rabbit                   | <ul style="list-style-type: none"> <li>• Reduced cartilage breakdown</li> </ul>                                                                                                                                       | [107]            |
| Ad-virus                                       | Periprosthetic osteolysis | Mouse                    | <ul style="list-style-type: none"> <li>• Reduced cyclooxygenase 2 and TNF- expression</li> <li>• Inhibition of wear debris–induced proinflammatory cytokine production, osteoclastogenesis, and osteolysis</li> </ul> | [108]            |
| Ad-virus                                       | Brain ischemia            | Rat                      | <ul style="list-style-type: none"> <li>• Significantly smaller brain infarction</li> <li>• Reduced infiltrations of leukocytes and macrophages</li> <li>• Reduced IL-1 and TNF- level</li> </ul>                      | [109]            |
| Hemagglutinating virus of Japan (HVJ)-liposome | Atherosclerosis           | Mouse                    | <ul style="list-style-type: none"> <li>• Increased IL-10 plasma level</li> <li>• Reduced Th1 response by inhibiting IL-12 and IFN-</li> <li>• Suppression of atherosclerotic lesion formation</li> </ul>              | [110]            |

However, it has been seen that VEGFA induced by HIF-1 during the hypoxic conditions of the tissue causes vascular permeability, which results in edema in ischemic tissues [98, 99]. For therapeutic angiogenesis, it is essential to understand the molecular mechanisms of angiogenesis and arteriogenesis in tissue hypoxia conditions [92].

#### *1.2.6 Angiogenesis in Ischemia*

Angiogenesis, a process of formation of new capillaries from existing blood vessels, and arteriogenesis, which involves remodelling of pre-existing arteries and arterioles by the process of vasodilation and allowing of perfusion through anastomosis [94, 111, 112] are tightly regulated by a distinct set of vascular modulators during ischemia [92].

During the initial stage of angiogenesis, the dormant endothelial cells (ECs) get interconnected by VE-cadherin and form a monolayer [113] and later on this layer becomes covered by pericytes. The role of pericytes is to restrict the growth of endothelial cells from by not allowing growth factors such as VEGFA, fibroblast growth factors (FGFs): FGF1 and FGF2, angiopoietin (ANG)-1 [114, 115] to be in contact with ECs. During hypoxic or inflammatory conditions, the pericytes detach by the influence of ANG-2 and matrix metalloproteinase (MMPs); especially MMP9 and makes ECs prone to a signal from VEGFA. This phenomenon increases the permeability of the EC layer [116-18]. This EC layer with the help of plasma proteins build an extracellular matrix (ECM)-based scaffold. Moreover, the ECM scaffold releases VEGFA and FGFs (FGF1 and FGF-2) and also attracts ECs by integrin signalling. During the process of capillary formation, one EC acts as a tip cell and the neighbours of the tip cell behave as stalk cells. The tip cell is tightly regulated in the presence of factors such as VEGF receptors, neuropilins (NRPs) and the NOTCH ligands DLL4 and JAGGED. Moreover, the stalk cells divide and elongate by the influence of NOTCH, NOTCH-regulated ankyrin repeat protein (NRARP), WNTs, placental growth factor (PIGF) and FGFs (FGF1 and 2). The stalk cells form a lumen mediated by VE-cadherin, CD34, sialomucins, VEGFA and sonic hedgehog [119-21]. During hypoxia, HIF-1 makes endothelial cells responsive to angiogenic signals by up-regulating angiogenic factors such as VEGFA. Myeloid bridge cells help in fusion of one vessel with another vessel branch, allowing the initiation of blood flow. Platelet-derived growth factor B (PDGF-B), ANG-1, transforming growth factor- (TGF- ), ephrin-B2 and NOTCH help in the maturation of the blood vessel by recruiting pericytes. This is followed by the secretion of factors such as protease inhibitors known as tissue inhibitors of metalloproteinase (TIMPs) and plasminogen activator inhibitor-1 (PAI-1) that help in the deposition of a basement membrane, and junctions are re-established to ensure optimal flow distribution [114, 122].

During ischemia, switching of angiogenesis and arteriogenesis by hypoxia occurs simultaneously in order to compensate for the insufficient blood supply and maintain tissue functions. This is controlled via a regulatory mechanism by different vascular modulators of angiogenesis and arteriogenesis. HIF-1 expression represents a molecular switch that initiates the angiogenic cascade in response to hypoxia/ischemia. Oxygen works as a regulator for HIF-1 via prolyl hydroxylase enzymes (PHDs). Under a normoxic condition, HIFs get hydroxylated by PHDs. The hydroxylated HIFs then become a target of proteosomal degradation. While, under hypoxic condition, PHDs become inactive because of no oxygen supply. The unhydroxylated HIFs then initiate their broad transcriptional responses to trigger angiogenesis through the up-regulation of angiogenic factors such as VEGFA. In general, HIF-1 promotes vessel sprouting, whereas HIF-2 mediates vascular maintenance [116, 123].

#### *1.2.7 Endothelial Nitric Oxide Synthase and Angiogenesis*

NO is a gaseous molecule with an astonishingly wide range of physiological and pathophysiological activities. These include the regulation of vessel tone and angiogenesis in wound healing, inflammation, ischemic cardiovascular diseases and malignant diseases. NOS, producing NO has three isoforms: endothelial NOS (eNOS), inducible NOS (iNOS) and neuronal NOS (nNOS). eNOS and nNOS are constitutively expressed predominantly in vascular endothelial cells and neuronal cells respectively and termed as cNOS. cNOS activity is dependent on the concentration of cytosolic  $Ca^{+2}$ . The NO produced from eNOS helps in neovascularisation, vascular permeability and regulation of blood vessel tone during inflammation, wound healing and tumor growth. iNOS is calcium independent and transcriptionally regulated by inflammatory cytokines, endotoxins, hypoxia and oxidative stress. The NO produced from nNOS mediates transmission of neuronal signal. All these isoforms of NOS catalyse the oxidation of L-arginine to L-citrulline to produce NO [124-26].

#### *1.2.8 Signalling Pathways for Endothelial NO-mediated Angiogenesis*

Angiogenic stimuli of major angiogenic factors such as VEGFA induce NO production by eNOS in endothelial cells. In endothelial cells, VEGFA activates eNOS by the induction of calcium flux, the recruitment of HSP90 and the phosphorylation of NOS via the phosphatidylinositol-3-OH-kinase [PtdIns(3)K]–Akt pathway [127]. The endogenous and/or exogenous NO acts through multiple signalling pathways either through S-nitrosylation and/or cGMP. S-nitrosylation of Cys163 of caspase 3 results in reduced activity of caspase-3 and in turn decreases apoptosis and, in the same way, S-nitrosylation of Ras activation results in increased proliferation and migration of endothelial cells [128-31]. Activation of protein kinase C (PKC) and inhibition of PKC results in increased endothelial cell proliferation and

migration [129, 132, 133]. NO triggered signalling through soluble guanylyl cyclase (sGC)–cGMP pathway induces increased angiogenesis. NO binding to sGC induces an increased synthesis of cGMP and this NO-induced cGMP activates Ras and cGMP-dependent protein kinase (PKG). PKG interacts with Raf. The Ras–Raf–MEK (MAPK (mitogen-activated protein kinase) or ERK kinase)–ERK (extracellular signal-regulated protein kinase) pathway then increases the DNA binding of activator protein 1 (AP1), which results in increased cell proliferation [134] and migration [128, 129, 135]. MMP13 and ERK mediate NO-induced endothelial-cell migration by PKG and by Akt activation through phosphoinositide 3-kinase (PI3K) [134, 136, 137].

### *1.2.9 eNOS as a Therapeutic*

Reduced NO bioavailability and dysfunction in the eNOS enzymes has been associated with a wide variety of vascular disease states. This includes atherosclerosis, coronary artery disease, diabetes mellitus, hypercholesterolemia, hypertension, immune reactions, inflammation, migraine, peripheral vascular disease, post subarachnoid hemorrhage vasospasm and vascular restenosis, thus making it an attractive target for both pharmacological and gene therapies [138, 139]. Pharmacological therapies target increased NO bioavailability by influencing the activity of endogenous eNOS. The focus of gene therapy has been to deliver the eNOS gene directly to the site of injury resulting in a local increase of NO without any systemic NO toxicity [138, 139]. Accordingly, gene transfer of NOS may provide a pleiotropic therapeutic strategy for suppression or modification of the response to cardiovascular injury. Specifically, enhanced NO production from recombinant NOS expression may provide a continuous NO supply to inhibit platelet activation, leukocyte infiltration, platelet-leukocyte interaction, migration of SMCs and adventitial fibroblasts, endothelial cell apoptosis and matrix synthesis, while stimulating beneficial responses such as re-endothelialization and increased blood flow.

eNOS gene therapy in particular has the potential to induce angiogenesis and is likely to be an effective treatment in ischemic diseases. NO has been shown to be pro-angiogenic and thus local delivery of NOS to the ischemic area may have therapeutic potential (Table 1.3).

### **1.3 Elastin as a Biomaterial**

Elastin is a versatile elastic protein and essential component of the ECM in various tissues that require elasticity as part of their function. These include arteries, skin, lungs, ligament, cartilage and tendons [140, 141]. Elastin comprises of almost 90% of the elastic fibre and is an extremely durable protein with a mean residence time of 74 years [141]. In terms of its mechanical properties, the young's modulus of elastic fibres typically ranges from 300 - 600 kPa [142].

**Table 1.3: Summary of preclinical in vivo studies utilising eNOS gene therapy for various diseases.**

| <b>Delivery Method</b>         | <b>Disease</b>           | <b>Preclinical Model</b> | <b>Observation</b>                                                                                                                                                                         | <b>Reference</b> |
|--------------------------------|--------------------------|--------------------------|--------------------------------------------------------------------------------------------------------------------------------------------------------------------------------------------|------------------|
| Plasmid                        | Limb ischemia            | Rat                      | <ul style="list-style-type: none"> <li>• Enhanced eNOS expression</li> <li>• Increased peripheral blood flow</li> <li>• Increased capillary density after 4 weeks</li> </ul>               | [147]            |
| Cationic liposome              | Cardiac ischemia         | Rabbit                   | <ul style="list-style-type: none"> <li>• Increased eNOS production</li> <li>• Reduced neutrophil and T-lymphocytes population</li> <li>• Reduced VCAM-1 and ICAM-1 expression</li> </ul>   | [148]            |
| Fibrin scaffold/microparticles | Wound healing            | Rabbit                   | <ul style="list-style-type: none"> <li>• Increased eNOS production</li> <li>• Increased angiogenesis</li> <li>• Enhanced wound healing</li> </ul>                                          | [149]            |
| Ad-virus                       | Limb ischemia            | Rat                      | <ul style="list-style-type: none"> <li>• Enhanced NO level</li> <li>• Increased blood perfusion and flow</li> <li>• Increased cGMP level</li> <li>• Increased capillary density</li> </ul> | [150]            |
| Ad-virus                       | Limb ischemia            | Rat                      | <ul style="list-style-type: none"> <li>• Enhanced eNOS</li> <li>• Increased blood flow and perfusion</li> <li>• Increased number of arteries</li> </ul>                                    | [151]            |
| Ad-virus                       | Diabetic wound           | Mouse                    | <ul style="list-style-type: none"> <li>• Increased level of No</li> <li>• Reduced level of O<sub>2</sub></li> <li>• Restored wound healing in a diabetic mouse</li> </ul>                  | [152]            |
| Ad-virus                       | Diabetic wound           | Rabbit                   | <ul style="list-style-type: none"> <li>• Increased eNOS synthesis</li> <li>• Enhanced reepithelialisation</li> <li>• Reduced inflammatory response</li> </ul>                              | [153]            |
| Ad-virus                       | Erectile dysfunction     | Rat                      | <ul style="list-style-type: none"> <li>• Stimulates erection in aged rats</li> <li>• Enhanced blood perfusion and increased capillary density</li> </ul>                                   | [154]            |
| Ad-virus                       | Subarachnoid haemorrhage | Dog                      | <ul style="list-style-type: none"> <li>• Enhanced eNOS expression</li> <li>• Restored the impaired nitric oxide-mediated relaxation</li> </ul>                                             | [155]            |
| Ad-virus                       | Stent thrombosis         | Rabbit                   | <ul style="list-style-type: none"> <li>• Enhanced eNOS</li> <li>• Enhanced endothelialisation</li> <li>• Reduction in neointimal formation</li> </ul>                                      | [156]            |
| Ad-virus                       | Renal failure            | Rat                      | <ul style="list-style-type: none"> <li>• Reduced blood pressure</li> <li>• Reduced level of serum creatinine</li> <li>• Reduced renal vascular, glomerular and tubular injury</li> </ul>   | [157]            |

Another important role of elastin *in vivo* is that it helps in cell proliferation, migration and maintaining cell morphology of various cardiovascular cell types such as: SMCs and ECs, through a receptor mediated pathway [143-46].

### *1.3.1 Molecular Structure and Synthesis In Vivo*

Human tropoelastin is encoded by a single gene that possesses 34 exons and gives rise to multiple isoforms via splicing. A high level of homology exists between the genes that encode human, chicken, rat and cattle tropoelastin. The mRNA encodes a mature tropoelastin with a molecular weight of at least 60 kDa. The tropoelastin amino acid sequence is divided into two major domain types: hydrophilic and hydrophobic domains. The hydrophobic domains are rich in the non-polar residues Val, Pro, Ala and Gly (Valine-Val, Proline-Pro, Alanine-Ala, Glycine-Gly), typically occurring in repeating motifs of tetra-, penta- and hexarepeats, such as Val-Pro-Gly-Gly, Val-Pro-Gly-Val-Gly and Ala-Pro-Gly-Val-Gly-Val. Alternating with these domains are hydrophilic regions characterized by their high lysine and alanine content and their involvement in cross-linking [142, 146, 158].

The mature tropoelastin monomers, through an elastogenesis process, assemble and crosslink to form elastin. The tropoelastin monomer is produced from the expression of the elastin gene by cells such as SMCs, endothelial cells, fibroblasts and chondroblasts. The first step in the process is the transport of mature tropoelastin to the cell surface with the help of the elastin binding protein. Tropoelastin is then released from the cell surface as a result of competition of galactosides. Released tropoelastin on the cell surface subsequently aggregates by coacervation. The coacervated tropoelastin is deposited onto microfibrils which serve as a scaffold to direct tropoelastin cross-linking by lysyl oxidase and consequential elastic fibre formation. Multiple cross-links result in the mature insoluble elastic fibre [142, 146, 158].

### *1.3.2 Synthesis of Elastin-like Polypeptide*

Recombinant elastin-like polypeptide (ELP) based on human tropoelastin sequences have been generated using genetic engineering tools [159]. ELP has pentapeptide repeats of [Val-Pro-X-Y-Gly]<sub>n</sub>. The X in the ELP sequence can be Glycine or Alanine and Y can be any amino acid besides proline. The ELP with pentapeptide repeats undergo a hydrophobic self-assembly process in an aqueous p. The self-assembly occurs above a lower critical solution temperature (LCST) and is reversible and temperature dependent. During the self-assembly, ELP undergoes a conformational change in its local secondary structure from a random coil to  $\alpha$ -turns. The fourth amino group is crucial for the self-assembly process, as any modification of the fourth amino acid changes the temperature dependent phase behaviour of the ELP. ELP, with such tuneable properties [158-62].

The simplest ELP sequence engineered to date is poly [Val-Pro-(Gly)-(Val)-Gly] based on the pentapeptide sequence [Val-Pro-(X)-(Y)-Gly]. The side aliphatic chains of valine and proline in this ELP sequence induce the thermal transition. Incorporation of glutamic acid at the fourth residue instead of Valine significantly increases the value of transition temperature ( $T_t$ ) to 75 °C in aqueous solutions [160-62].

Furthermore, ELP-based amphiphilic block copolymers have been generated. The amphiphilic block copolymer contains (VPGEG), a hydrophilic sequence, flanked on both sides by hydrophobic sequences of (VPGAG). The hydrophilicity of the sequence (VPGEG) is due to the presence of glutamic acid (E). The triblock copolymers show phase separation behaviour due to solubility differences in aqueous solution [163-165] and also display plasticity in their mechanical responses [166-68]. ELP with a similar sequence [(VPGVG)<sub>2</sub>-VPGEG-(VPGVG)<sub>2</sub>]<sub>n</sub> responds to a change in pH in the aqueous solution. The -carboxylic group of the glutamic acid (E) exhibits strong polarity changes between its protonated and deprotonated states as a consequence of pH changes around its effective  $pK_a$ . The  $T_t$  changes from 28 °C at a lower pH=2.5 to above 85 °C at pH=8.0 [162, 169].

ELPs with alternating hydrophobic and hydrophilic domains have the capacity to form physical crosslinks through microphase separation [170]. Further modifications on ELP have been performed to facilitate chemical cross-linking. Introduction of lysine residues into elastin-mimetic protein polymers provide free reactive amines for crosslinking using a variety of approaches. This mimics the native tropoelastin, where lysine residues present in the tropoelastin help in an enzymatic cross-linking to form the elastic fibres [166, 168, 171, 172]. Crosslinking of elastin-based biomaterials has been investigated using  $\gamma$ -irradiation, microbial transglutaminase and chemical cross-linkers: isocyanates, glutaraldehyde, hydroxymethylphosphine and genipin [161, 164, 173-77].

#### **1.4 Elastin-like Peptide-based Biomaterials for Drug Delivery**

ELP of various sizes, and composition can self-assemble into a range of supramolecular structure with a subtle change in the temperature and pH of the aqueous solution. Amphiphilic ELP copolymers, especially, hold significant promise as drug delivery vehicles (Table 1.4) as well as for tissue engineering applications (Table 1.5) [158, 178]. So far ELPs have been used to fabricate a variety of drug delivery platforms such as micelles, nano/microparticles, hydrogels and films (Figure 1.1) [158, 160, 161, 179-81].

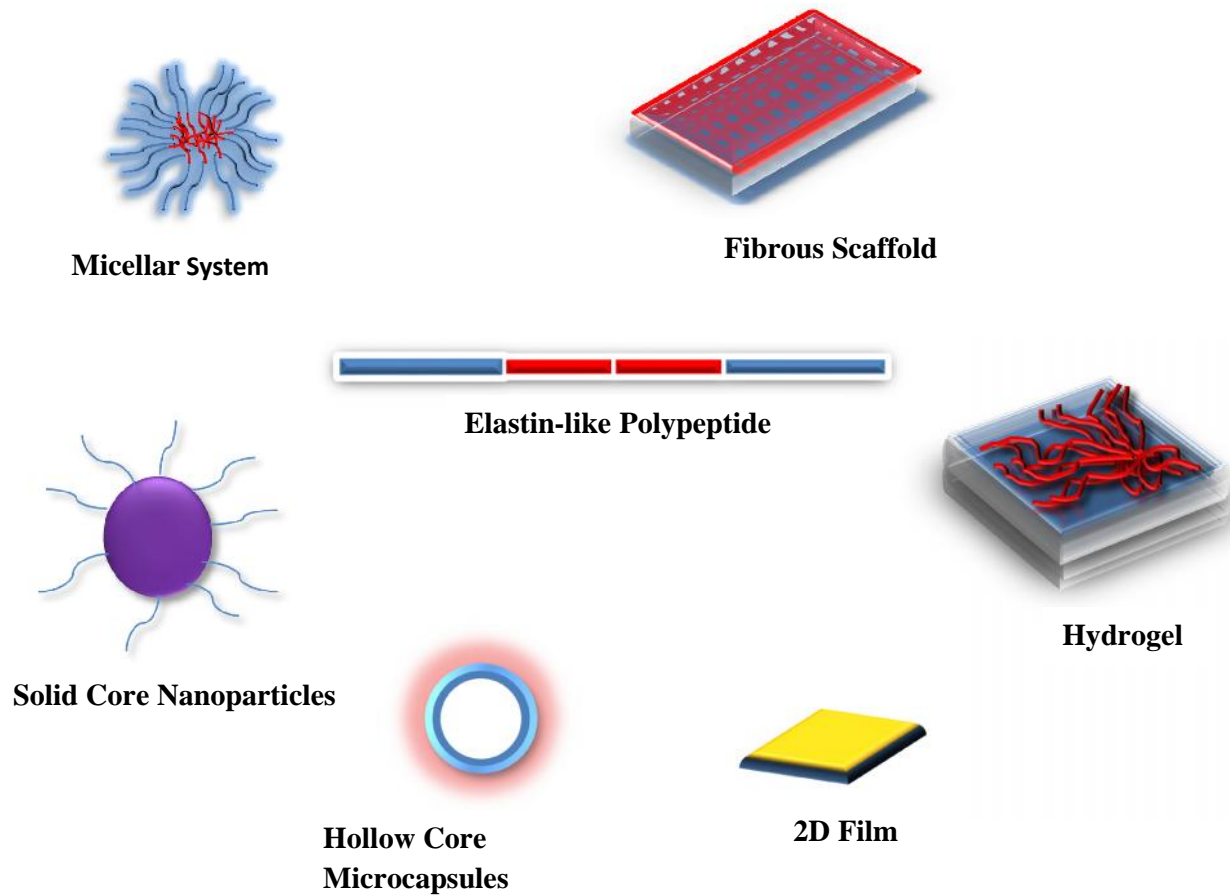


**Figure 1.1** Elastin-like polypeptide-based physical forms that have been reported in the literature.

**Table 1.4: Summary of ELP based biomaterials for drug delivery application.**

| Platform             | Drug/Gene                        | Methods                                                                                                                                                                                                     | Results                                                                                                                                                                                                                                                                    | Reference |
|----------------------|----------------------------------|-------------------------------------------------------------------------------------------------------------------------------------------------------------------------------------------------------------|----------------------------------------------------------------------------------------------------------------------------------------------------------------------------------------------------------------------------------------------------------------------------|-----------|
| Polymer              | GLUC                             | <ul style="list-style-type: none"> <li>• A hybrid polymer with ELP and DET modified aspartic was generated</li> <li>• Polyplexes were formed by using the hybrid copolymer and pGL4 plasmid</li> </ul>      | <ul style="list-style-type: none"> <li>• Polyplexes showed significant transfection efficiency with low cytotoxicity</li> </ul>                                                                                                                                            | [182]     |
| Polymer              | GFP                              | <ul style="list-style-type: none"> <li>• A hybrid polymer (K8-ELP [1-60]) of ELP and cationic oligolysine was synthesised</li> <li>• Polyplexes were formed by using K8-ELP (1-60) and EGFP</li> </ul>      | <ul style="list-style-type: none"> <li>• Polyplexes successfully transfected MCF-7 cells and with reduced toxicity</li> </ul>                                                                                                                                              | [183]     |
| Nanofibrous scaffold | GFP                              | <ul style="list-style-type: none"> <li>• Electrospun scaffold of ELP and poly (-caprolactone) (PCL) were fabricated</li> </ul>                                                                              | <ul style="list-style-type: none"> <li>• AAV-GFP gene delivery complexes encapsulated within the scaffold showed a controlled release</li> <li>• NIH 3T3 cells were efficiently transduced</li> </ul>                                                                      | [184]     |
| Film                 | GFP                              | <ul style="list-style-type: none"> <li>• ELP was adsorbed as a thin film on a tissue culture wells</li> <li>• AAV-GP gene complexes were efficiently adsorbed on the ELP films</li> </ul>                   | <ul style="list-style-type: none"> <li>• High transduction of human neural stem cells and NIH 3T3 cells were observed</li> </ul>                                                                                                                                           | [185]     |
| Hollow sphere        | GLUC, GFP                        | <ul style="list-style-type: none"> <li>• ELP hollow spheres of various sizes were fabricated</li> <li>• Polyplexes of GFP and GLUC plasmid were efficiently loaded inside the ELP hollow spheres</li> </ul> | <ul style="list-style-type: none"> <li>• The polyplexes loaded ELP hollow spheres efficiently transfected adipose derived stem cells and HIUVECs</li> </ul>                                                                                                                | [177]     |
| Particles            | Hydrophobic drug                 | <ul style="list-style-type: none"> <li>• ELP and Doxorubicin drug microparticles were fabricated using an electro-spraying method</li> </ul>                                                                | <ul style="list-style-type: none"> <li>• The particles were of sizes between 300-400 nm.</li> <li>• Drug release was pH dependent</li> </ul>                                                                                                                               | [186]     |
| Micelles             | Hydrophobic fluorescent molecule | <ul style="list-style-type: none"> <li>• Amphiphilic diblock ELP mimetic polymer were generated</li> </ul>                                                                                                  | <ul style="list-style-type: none"> <li>• Particles were formed from these polymers with a spherical core shell structure</li> <li>• Hydrophobic fluorescent molecules were efficiently encapsulated with a potential to encapsulate hydrophobic drugs in future</li> </ul> | [187]     |

**Table 1.4 (continued): Summary of ELP based biomaterials for drug delivery application.**

| <b>Platform</b>     | <b>Drug/Gene</b>                    | <b>Methods</b>                                                                                                                                                                                                                                                           | <b>Results</b>                                                                                                                                                                                                                                                                            | <b>Reference</b> |
|---------------------|-------------------------------------|--------------------------------------------------------------------------------------------------------------------------------------------------------------------------------------------------------------------------------------------------------------------------|-------------------------------------------------------------------------------------------------------------------------------------------------------------------------------------------------------------------------------------------------------------------------------------------|------------------|
| Particle            | Dexamethasone phosphate             | <ul style="list-style-type: none"> <li>• Poly(VPAVG) elastin-like polymer were used to develop micro- and nanoparticles</li> <li>•</li> </ul>                                                                                                                            | <ul style="list-style-type: none"> <li>• Significant amount of dexamethasone phosphate was encapsulated within these microparticles</li> <li>• Showed a sustained release of DMP for 30 days</li> <li>• Particles formed were below 3µm and stable at room or body temperature</li> </ul> | [188]            |
| Nanoparticle        | BMP protein                         | <ul style="list-style-type: none"> <li>• Poly(VPAVG) elastin-like polymer self-assembled to form nanoparticles of size 240 nm.</li> <li>• Bone Morphogenetic Protein-2 (BMP-2) at high concentrations were encapsulated and released over a period of 14 days</li> </ul> | <ul style="list-style-type: none"> <li>• Bioactivity of BMP-2 was retained as shown by the induction of ALP activity and osteogenic mineralization in C2C12 cells</li> </ul>                                                                                                              | [189]<br>[190]   |
| ELP coated nanorod  | Heat shock protein inhibitor 17-AAG | <ul style="list-style-type: none"> <li>• Gold nanorod ELP matrices were fabricated</li> <li>• Loaded efficiently with the heat-shock protein (HSP)90 inhibitor 17-(allylamino)-17-demethoxygeldanamycin (17-AAG)</li> </ul>                                              | <ul style="list-style-type: none"> <li>• Combination of hyperthermic temperatures and the release of 17-AAG from the matrix, both induced by laser irradiation, resulted in significant (&gt;90%) death of cancer cells</li> </ul>                                                        | [191, 192]       |
| Nanoparticle        | Hydrophobic fluorescent molecule    | <ul style="list-style-type: none"> <li>• Engineered a fusion proteins of ELP and a polyaspartic acid chain</li> <li>• Monodisperse particles of 100 nm were developed</li> </ul>                                                                                         | <ul style="list-style-type: none"> <li>• 1-anilino-8-naphthalene-sulfonic acid was encapsulated with high efficiency</li> </ul>                                                                                                                                                           | [193]            |
| Hydrogel            | BSA-FITC                            | <ul style="list-style-type: none"> <li>• Cystein modified ELP polymer were synthesized to fabricate a hydrogel</li> <li>• BSA-FITC was successfully incorporated inside the hydrogel</li> </ul>                                                                          | <ul style="list-style-type: none"> <li>• Showed a sustained release of BSA-FITC from the hydrogel</li> </ul>                                                                                                                                                                              | [194, 195]       |
| Hydrogel            | BSA and doxycycline                 | <ul style="list-style-type: none"> <li>• ELP hydrogel scaffolds using a novel ultrasonication method</li> <li>• BSA and doxycycline were loaded in the ELP hydrogel</li> </ul>                                                                                           | <ul style="list-style-type: none"> <li>• BSA and doxycycline showed a gradual time dependent release</li> </ul>                                                                                                                                                                           | [196]            |
| Injectable hydrogel | Cefazolin and vancomycin            | <ul style="list-style-type: none"> <li>• In situ ELP hydrogel was fabricated</li> <li>• Cefazolin and Vancomycin were loaded inside the hydrogel</li> </ul>                                                                                                              | <ul style="list-style-type: none"> <li>• Cefazolin was released for 25 hr and Vancomycin for 500 hr</li> </ul>                                                                                                                                                                            | [197]            |

**Table 1.5: Summary of ELP based biomaterials for tissue engineering application.**

| <b>Platform</b> | <b>Tissue Engineering Application</b> | <b>Observation</b>                                                                                                                                                                                                                                                                                                                                                                                                                                                                                                                         | <b>Reference</b> |
|-----------------|---------------------------------------|--------------------------------------------------------------------------------------------------------------------------------------------------------------------------------------------------------------------------------------------------------------------------------------------------------------------------------------------------------------------------------------------------------------------------------------------------------------------------------------------------------------------------------------------|------------------|
| Hydrogel        | Bone<br>Cartilage                     | <ul style="list-style-type: none"> <li>• ELP with tissue transglutaminase was used to fabricate an injectable scaffold</li> <li>• Chondrocytes were used to encapsulate within the <i>in situ</i> hydrogel</li> <li>• Increased deposition of sulfated glycosaminoglycans and type II collagen was seen with enhanced mechanical strength</li> <li>• Applied for cartilage matrix repair in critically sized defects in goat knees.</li> <li>• At three months, ELP treated defects scored significantly higher for integration</li> </ul> | [198, 199]       |
| Hydrogel        | Bone<br>Cartilage                     | <ul style="list-style-type: none"> <li>• Human ADSCs were encapsulated within the ELP hydrogel</li> <li>• By two weeks, ELP hydrogel in chondrogenic differentiation medium exhibited significant increases in sulfated glycosaminoglycan and collagen type II contents</li> </ul>                                                                                                                                                                                                                                                         | [200]            |
| Hydrogel        | Spinal disc                           | <ul style="list-style-type: none"> <li>• A thiol-modified hyaluronan ELP injectable hydrogel was used to restore the mechanical properties of spinal motion segments with early stage disc degeneration</li> <li>• The injectable ELP hydrogel was able to restore initial mechanical behaviour in early-stage disc degeneration</li> </ul>                                                                                                                                                                                                | [201]            |
| Porous Scaffold | Bone                                  | <ul style="list-style-type: none"> <li>• A composite ELP-collagen scaffold was fabricated</li> <li>• ELP-collagen scaffold helped MC3T3-E1 pre-osteoblast cell attachment, differentiation, and subsequent mineralization over a period of three weeks.</li> </ul>                                                                                                                                                                                                                                                                         | [202]            |

**Table 1.5 (continued): Summary of ELP based biomaterials for tissue engineering application.**

| <b>Platform</b>  | <b>Tissue Engineering</b> | <b>Observation</b>                                                                                                                                                                                                                                                                                                                                                                                                                                                                                                                                                                                 | <b>Reference</b> |
|------------------|---------------------------|----------------------------------------------------------------------------------------------------------------------------------------------------------------------------------------------------------------------------------------------------------------------------------------------------------------------------------------------------------------------------------------------------------------------------------------------------------------------------------------------------------------------------------------------------------------------------------------------------|------------------|
| Hydrogel         | Cartilage                 | <ul style="list-style-type: none"> <li>• Chondrocytes were cultured on ELP scaffolds</li> <li>• Enhanced collagen type II and sulfated glycosaminoglycans were deposited by 28 days</li> </ul>                                                                                                                                                                                                                                                                                                                                                                                                     | [203]            |
| Porous Scaffold  | Knee                      | <ul style="list-style-type: none"> <li>• ELP hydrogel with an elastic modulus of 470kPa were developed using genipin as a cross-linker and were used as acellular plug for the treatment of osteochondral defect in the rabbit knee</li> <li>• ELP hydrogels were tightly integrated with host tissue and have no cytotoxicity and show no evidence of inflammatory response</li> <li>• Regeneration of subchondral bone was seen at the periphery of the implanted ELP hydrogel, with hyaline-like overgrowth across the apical surface in 11/16 cases</li> </ul>                                 | [204]            |
| Film             | Vascular tissue           | <ul style="list-style-type: none"> <li>• ELP coated surfaces showed better SMC attachment and spreading</li> <li>• Enhanced cell proliferation was seen compared to control group</li> <li>• Promising as surface modifiers for candidate scaffolds for vascular tissue engineering</li> </ul>                                                                                                                                                                                                                                                                                                     | [205]            |
| Fibrous scaffold | Hernia                    | <ul style="list-style-type: none"> <li>• ELP based thin lamellae with continuous collagen microfiber embedded at controlled orientations and densities were developed</li> <li>• The Sheets showed mechanical strength of 13-fold in elongation to break (23-314%), six-fold in Young's modulus (5.3-33.1 MPa), and more than two-fold in tensile strength (1.85-4.08 MPa)</li> <li>• Sheets, when used as a fascial substitute for ventral hernia repair, prevent hernia recurrence in Wistar rats over an 8-week period with new tissue formation and sustained structural integrity.</li> </ul> | [206]            |

#### 1.4.1 Nanostructures

Self-assembly of amphiphilic block co-polymers has been shown to form micellar micro and nano-particles with a solid core for drug delivery applications [160, 161, 181]. Most of the elastin-mimetic micelles reported so far are based on amphiphilic di-block copolymer systems comprised of hydrophilic blocks flanked by hydrophobic blocks to form spherical nanoparticles [161, 207]. An ELP amphiphilic di-block copolymer has been synthesized with a core of cysteine residues and N and C terminal containing glutamic acid and tyrosine residues respectively. The cysteine residues help in cross-linking. The micelles formed from this di-block polymer are monodisperse and have the ability to encapsulate hydrophobic drugs and imaging agents [187]. Furthermore, an *in vivo* study was performed to characterize the efficacy of the micellar system as an imaging agent [208]. The micelles were conjugated with a fluorescent molecule on their surface and used to image the balloon injured aorta in a rat model. A selective uptake of micelles was seen at the site of the injured vessel wall [208]. A range of micelles to target tumors with anticancer drugs has been developed [209-12]. A novel pH sensitive di-block ELP based peptide has been reported for tumor targeting. The ELP peptide self-assembles at a pH of 7.4 and disassembles at around pH of 6.4. This narrow range of pH resembles the pH difference between normal tissue (7.2–7.4) and many solid tumors (pH 6.2–6.9) resulting from hypoxia [209]. In another strategy to target the tumor vasculature, ELP micelles were tagged with NGR (CD 13) peptide. The *in vivo* studies showed a greater accumulation of micelles in tumor tissue than in normal tissue [210]. The stimuli responsive, biocompatible and biodegradable ELP copolymer thus can be used as targeted drug delivery systems for pharmacological and cosmetic applications.

In one of the studies, the geometry and size of a thermo responsive micelles made from three-armed star elastin-like polypeptides were investigated as a function of temperature, pH, and salt concentration. The micelles can only form in the solutions above pH 9.6, and they were shown to reach to a constant, minimum size at pH greater than 10.2. The effect of salt on the size of the micelles was also investigated. The micelles in the low-salt regime (below 15 mM) were shown to be spherical and consisted of only 35 unimers, while micelles in the high-salt regime (above 30 mM) were found to be very elongated cylindrical particles with high molecular weights [213].

Furthermore, nanoparticles of 55 nm sizes have been developed using genetically engineered elastin-like block recombinamer (ELbcR) containing a major membrane protein sequence from mycobacterium tuberculosis. An initial pro-chemotactic cytokine response IL-1 followed by a pro-Th2/IL-5 response was observed in mouse plasma following subcutaneous administration

of the antigen-loaded nano vesicles in mice. This biphasic model of cytokine production was coupled with humoral isotype switching from IgM- to IgG-specific antibodies against the antigen, which was only observed in the presence of both the antigen and the polymer in the same construct and in the absence of additional adjuvant [214].

Recently, Costa et al., developed a composite microcapsule consisting of chitosan and ELP. A sacrificial CaCO<sub>3</sub> template was used to fabricate the microcapsules. Briefly, they coated CaCO<sub>3</sub> alternately with chitosan and ELP until they made 3-5 layers and then CaCO<sub>3</sub> was dissolved using ethylenediaminetetraacetic acid (EDTA). Bovine serum albumin (BSA) -FITC was used to study the release profile. The release profile of BSA, which was studied at 25 and 37 °C, shows higher retention and Fickian diffusion at physiological temperature. The self-assembled multilayers act as a barrier and allow for sustained release over 14 days. The capsules studied are non-cytotoxic towards L929 cells [215].

Moreover, stable nanoparticles from ELP have been developed using several methods. In one of the works, ELP containing both hydrophobic and cross-linking domains was used. The particles were formed using a self-assembly method. Addition of PEG in a high concentration helped reduce the coalescence of the particles and increased their stability by coating the particles. Particle stabilization was also achieved through covalent cross-linking using glutaraldehyde. This study laid the foundation for optimization of particle size and stability through modification of the solvent system and has shown that this family of elastin-based polypeptides holds potential for use as particulate drug carriers [216]. In another such study, fusion proteins of low ELP and a poly aspartic acid chain were used to fabricate monodisperse particles. The particles of less than 100nm in diameter were formed around 37 °C. The ELP particles have a more hydrophobic or rigid region and could hold hydrophobic drugs [193].

#### *1.4.2 Three Dimensional (3D) Matrices*

Three dimensional matrices such as scaffolds, hydrogels, nanofibres and injectable hydrogels have been fabricated using ELP for drug delivery applications. Injectable ELP gels have been developed for sustained delivery of antibiotics such as cefazolin and vancomycin and immunomodulators [197, 217]. The injectable ELP gel showed a sustained-release of the immunomodulators to the dorsal root ganglion [217]. Furthermore, an ELP triblock polymer was used to fabricate a scaffold to study the release pattern of model compounds, such as theophylline, vitamin B12 and ovalbumin [218]. Also, it has been demonstrated that elastin-mimetic triblock copolymers undergo reversible gelation in order to form a viscoelastic hydrogel [167, 168].

Hydrogels from ELP have been developed by using both chemical and enzymatic cross-linker by introducing lysine in the ELP sequence. Tris-succinimidyl amino triacetate was used to

facilitate the cross-linking to produce hydrogels [194]. These hydrogels displayed a change in the stiffness with respect to a change in temperature: the stiffness of the hydrogel was 0.24 to 3.7 kPa at 7 °C, while at 37 °C the stiffness increased from 1.6 to 15 kPa. Additionally, ELP containing glutamine and lysine residues were treated with an enzymatic cross-linker, transglutaminase to fabricate hydrogels [199]. Moreover, genipin, a natural cross-linker, has been used to fabricate ELP hydrogels with possible drug delivery applications [204]. The ELP was designed to have a cross-linking domain with lysine and glutamic acid. Furthermore, an ultra-sonication method was used to develop an ELP hydrogel. Model drug molecules such as BSA and doxycycline were used to characterize the release behaviour of the hydrogels. Both the drug molecules were released in a time dependent pattern [196].

Furthermore, ELP-collagen composites were used to fabricate a hydrogel with tuneable release of model drugs. The composite hydrogels were prepared by incubation at 37, 45, or 55 °C, and finally air-drying at 37 °C. BSA and antibiotic doxycycline were used as a model drug to characterize their release profile. A gradual time dependent BSA release that followed the power law and a burst release of doxycycline followed by a linear zero-order release were observed. Importantly, it was observed that BSA and doxycycline releases were dependent on the ELP micro-aggregate size which was governed by the processing temperatures. This study laid the foundation to achieve optimized composite microstructures by controlling processing conditions for drug delivery applications [219]. Furthermore, nanofibrous scaffolds were fabricated using a combination of ELP and poly ( $\epsilon$ -caprolactone). The ELP/PCL composite scaffolds showed a controlled release of adeno associated virus (AAV)-mediated gene delivery and efficiently transfected fibroblast cells [184].

#### *1.4.3 Films*

ELP Films have been fabricated using a solvent casting evaporation process [220]. The films with Young's modulus of 0.03-0.05 MPa and ultimate tensile strength of 0.78-0.96 MPa have been reported. These films are specifically used in a site specific application with a sustained release property of the drug [221, 222]. Furthermore, ELP microstructure can be modified to achieve films with tuneable mechanical strength and release rates. ELP with pentapeptide repeats of [Val-Pro-Gly-Val-Gly] was used to develop films on tissue culture plates. The films delivered AAV based gene delivery systems to transduce fibroblasts and human neural stem cells (hNSCs) [185]. The sustained release of AAV/genes from ELP films transfected cells with a higher efficiency than that with bolus delivery [185]. This ELP/AAV gene delivery systems, thus, have potential to be used in tissue engineering applications as well as in neurodegenerative disorder treatments.

## 1.5 Gene Therapy

Gene therapy involves the delivery of genes for the treatment of a genetical defect. It is also considered as a substitute for protein therapy to overcome the problems inherent in protein therapy: bioavailability of protein drugs in terms of administration, systemic toxicity, *in vivo* clearance rate and manufacturing cost [223]. The concept of gene therapy started during the 1960s and has drawn a lot of attention since then in the field of medical and pharmaceutical science [224]. In the last 15 years, more than 400 clinical cases have been carried out but have yielded little success. Thus there is a need for further optimization of gene delivery systems, one of the key components of gene therapy, to protect the genetic materials from premature degradation in the systemic blood stream and to efficiently transfer the therapeutic genes to target cells [223, 225].

Therapeutic angiogenesis is one of the hotspots which has been discussed over the past few decades. Among several approaches, gene therapy is evolving as a novel and promising angiogenic therapy for those patients who cannot undergo surgical intervention or angioplasty for revascularization. Undeniably, gene delivery of VEGF, especially its isoform VEGF<sub>165</sub>, FGF-1, hepatocyte growth factor (HGF) and HIF-1 has resulted in improved angiogenesis and functional recovery of ischemic tissues in an animal model of myocardial or hind limb ischemia. And, thus, the use of these growth factor in gene therapy has shown therapeutic potential for patients with severe myocardial ischemia or critical limb ischemia [226-28]. The main angiogenic therapeutic genes that have been used so far in clinical trials are VEGF<sub>165</sub> and FGF-1. The delivery of these genes has been shown to induce collateral vessel formation, to improve blood supply and the clinical state of patients in both preclinical and clinical studies [229].

The delivery methods used so far in angiogenic gene therapy are i) naked plasmid DNA ii) viral gene delivery and iii) non-viral gene delivery system (Figure 1.2).

### 1.5.1 Viral Gene Delivery

Recombinant adenovirus (Ad) and AAV are the two most extensively used delivery system for proangiogenic gene therapy (Table 1.6). Additionally, these two vectors have the ability to transduce a variety of quiescent cell types after *in vivo* injection, including skeletal muscle cells [230-232].

Ad-vectors have so far been widely used as a gene delivery vehicle for the cardiovascular system. These vectors have some of the remarkable properties of a gene delivery system such as: they can accommodate large inserts, mediate transient but high levels of protein expression, and can be easily produced at high titers [233, 234]. A modified version of the Ad-vectors

consists of helper-dependent vectors, which contain the therapeutic gene along with two repeated regulatory regions at the 3' and 5' of the wild type genome and also the signals required for packaging the genome into viral particles [230, 233]. Preclinical and clinical studies have been performed using adenovirus [230, 235]. The major angiogenic growth factors used were VEGF<sub>165</sub>, FGF-1, HGF [236]. Ad-*p*VEGF treatment showed an increased level of neovascularisation in the case of diabetic mice [237], while, Ad-*p*HIF-1 along with HIF-1 activated cells, improved the blood perfusion, motor function, and limb salvage in old mice subjected to femoral artery ligation [238].

AAV, unlike Ad, is a small non-enveloped, single-stranded (ss) DNA virus. AAV has recently been widely exploited for gene therapy due to several favourable characteristics: the high efficiency of transduction in muscle, heart, brain and retina and the long-term persistence of transgene expression [230, 239]. VEGF<sub>165</sub>, FGF-1, HGF and ANG-1 are the major growth factors so far used in various preclinical and clinical set ups of limb ischemia.

Chen et al. injected AAV-*p*VEGF<sub>165</sub>/Angpt1 for induction of angiogenesis in a rabbit model of limb ischemia [240]. The treatment group with AAV-*p*VEGF<sub>165</sub>/Angpt1 showed a significantly increased blood-flow recovery in ischemic hind limbs when compared to the other groups. VEGF<sub>165</sub> and Angpt1 were detected by RT-PCR, Western blotting and histochemical staining. The result further suggested that AAV vectors can simultaneously encode two proteins which can be efficiently and stably co-expressed in transduced tissues. A very similar study was performed on a rabbit model of limb ischemia by Zheng et al. They used AAV vector to deliver human VEGF<sub>165</sub> and bone morphogenetic protein (BMP). Eight weeks after gene transfer, there was an increased blood flow in the AAV-*p*VEGF<sub>165</sub>/BMP group [241]. In another such study, extracellular superoxide dismutase (EcSOD) was used in a 12-week-old mouse [242]. The EcSOD is a major scavenger of superoxide and regulates nitric oxide bioavailability and thus helps in protecting against vascular dysfunction. AAV-*p*EcSOD, when injected intramuscularly into the hind-limb muscles of Ischemia, resulted in an increase in blood perfusion compared to control mice [242]. Furthermore, CD151 gene was delivered in the skeletal muscle of the rat hind-limb ischemia model. AAV-*p*CD151 treatment group induced neovascularization, especially arteriogenesis [243]. The gene transfer using AAV into rat skeletal muscles was found to be efficient, stable, and had no ectopic expression.

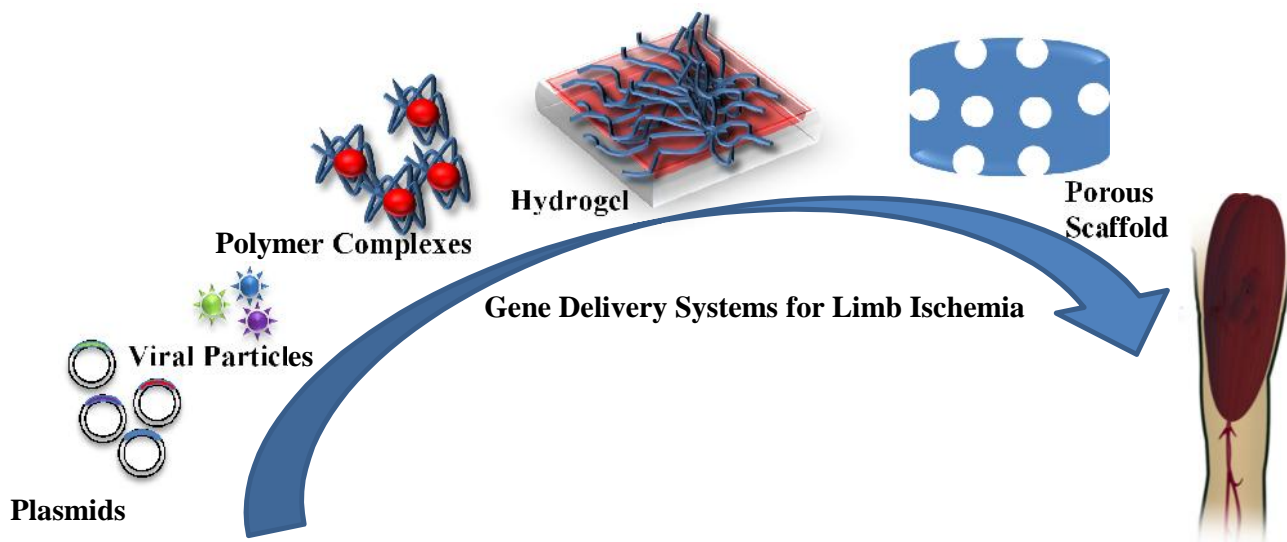


**Figure 1.2 Gene delivery vehicles used for delivery of therapeutic genes for the treatment of critical limb ischemia in clinical and pre-clinical set ups.**

**Table 1.6: Summary of in vivo viral based gene delivery for angiogenesis in various CLI models.**

| <b>Delivery Method</b> | <b>Target Gene</b>                                     | <b>Methods</b>                                                                                                                                                                                                                                                                                              | <b>Results</b>                                                                                                                                                                                                                             | <b>Reference</b> |
|------------------------|--------------------------------------------------------|-------------------------------------------------------------------------------------------------------------------------------------------------------------------------------------------------------------------------------------------------------------------------------------------------------------|--------------------------------------------------------------------------------------------------------------------------------------------------------------------------------------------------------------------------------------------|------------------|
| rAAV                   | Antimicrobial peptide cathelicidin                     | <ul style="list-style-type: none"> <li>Human antimicrobial peptide cathelicidin (LL-37/hCAP-18) was transduced using recombinant adeno-associated viruses (rAAV) into the anterior tibial vein of ischemic rabbits</li> </ul>                                                                               | <ul style="list-style-type: none"> <li>Induced functionally relevant neovascularization by day 35</li> </ul>                                                                                                                               | [244]            |
| AAV                    | VEGF <sub>165</sub> and ANG-1                          | <ul style="list-style-type: none"> <li>AAV vector was constructed simultaneously encoding human VEGF<sub>165</sub> and ANG-1</li> </ul>                                                                                                                                                                     | <ul style="list-style-type: none"> <li>Enhanced neovascularization, no capillary leakage, and improved blood perfusion were seen in the rabbit hind-limb ischemic model treated with AAV-VEGF<sub>165</sub>/Ang1 by eight weeks</li> </ul> | [240]            |
| Sendai virus           | FGF-2                                                  | <ul style="list-style-type: none"> <li>Sendai virus vector was constructed to encode FGF-2</li> <li>Effect of FGF-2 on neointimal hyperplasia of VGs was examined in a rabbit model of poor-runoff limbs</li> </ul>                                                                                         | <ul style="list-style-type: none"> <li>Showed significantly increased blood flow</li> <li>Collateral flow was significantly restored in the thigh muscles</li> </ul>                                                                       | [245]            |
| Ad-virus               | bFGF                                                   | <ul style="list-style-type: none"> <li>Adenovirus-mediated ex vivo gene transfer of basic fibroblast growth factor (bFGF) was performed in a rabbit hind limb ischemic model</li> <li>Fibroblast cells were transduced with Ad-bFGF and then administered through the left internal iliac artery</li> </ul> | <ul style="list-style-type: none"> <li>Showed significantly greater development of collateral vessels</li> </ul>                                                                                                                           | [246]            |
| Ad-virus               | Zinc-finger DNA-binding transcription factor (ZFP-32E) | <ul style="list-style-type: none"> <li>Adenoviral vectors encoding a ZFP-32E were designed to increase the expression of all VEGF isoforms</li> <li>Higher VEGF protein and mRNA were observed</li> </ul>                                                                                                   | <ul style="list-style-type: none"> <li>Enhanced capillary density and blood perfusion were achieved in a mice model of limb ischemia by day 21</li> </ul>                                                                                  | [247]            |
| Ad-virus               | HIF-1                                                  | <ul style="list-style-type: none"> <li>HIF-1 was injected intramuscularly with adenovirus as the vector, along with intravenous administration of bone-marrow-derived angiogenic cells</li> </ul>                                                                                                           | <ul style="list-style-type: none"> <li>Enhanced blood perfusion, motor function, and limb salvage in old mice were observed</li> </ul>                                                                                                     | [248]            |

**Table 1.6 (continued): Summary of in vivo viral based gene delivery for angiogenesis in various CLI models.**

| <b>Delivery Method</b> | <b>Target Gene</b> | <b>Methods</b>                                                                                                                                       | <b>Results</b>                                                                                                                                                                                                                                                                                                                           | <b>Reference</b> |
|------------------------|--------------------|------------------------------------------------------------------------------------------------------------------------------------------------------|------------------------------------------------------------------------------------------------------------------------------------------------------------------------------------------------------------------------------------------------------------------------------------------------------------------------------------------|------------------|
| Ad-virus               | HIF-1              | <ul style="list-style-type: none"> <li>Ad-HIF-1 was injected intramuscularly in a diabetic hind limb ischemic model</li> </ul>                       | <ul style="list-style-type: none"> <li>Helped in the recovery of limb perfusion and function, reduced tissue necrosis, rescued the diabetes-associated impairment of circulating angiogenic cells, enhanced endothelial nitric oxide synthase activation, and increased vessel density and luminal area in the ischemic limb.</li> </ul> | [249]            |
| Ad-virus               | HIF-1              | <ul style="list-style-type: none"> <li>Ad-HIF-1 improved the recovery of perfusion in older mice to levels similar to those in young mice</li> </ul> | <ul style="list-style-type: none"> <li>Enhanced the number of circulating angiogenic cells when injected in the non-ischemic limb</li> </ul>                                                                                                                                                                                             | [250]            |
| Ad-virus               | HIF-1              | <ul style="list-style-type: none"> <li>Ad-HIF-1 was injected in a rabbit model of hind limb ischemia</li> </ul>                                      | <ul style="list-style-type: none"> <li>Improved perfusion</li> <li>Enhanced HIF-1, MCP-1, placental growth factor, PDGFB, SDF-1, and VEGF mRNA levels were seen</li> <li>Enhanced blood perfusion level was seen</li> </ul>                                                                                                              | [251]            |
| Ad-virus               | Neurotrophin-3     | <ul style="list-style-type: none"> <li>Ad-NT3 was constructed and injected intramuscularly</li> </ul>                                                | <ul style="list-style-type: none"> <li>NT-3 overexpression increased muscular capillary and arteriolar densities in either the absence or the presence of ischemia and improved post-ischemic blood flow recovery in mouse hind limbs</li> </ul>                                                                                         | [254]            |
| Lenti virus            | eNOS               | <ul style="list-style-type: none"> <li>eNOS was injected in the ischemic hind limb</li> </ul>                                                        | <ul style="list-style-type: none"> <li>eNOS transduction helped in enhanced neovascularization and improved ischemic hind limb perfusion via circulating angiogenic cells</li> </ul>                                                                                                                                                     | [255]            |
| Ad-virus               | Extracellular SOD  | <ul style="list-style-type: none"> <li>AAV-EcSOD was constructed and injected into a hind limb muscle of mouse</li> </ul>                            | <ul style="list-style-type: none"> <li>Upregulated twice within 14 days in the mice muscle</li> <li>Enhanced blood perfusion, capillary density and limb salvage and reduced apoptosis were observed</li> </ul>                                                                                                                          | [242]            |

### *1.5.2 Non-viral Gene Delivery*

Although viral vectors are efficient gene delivery systems, they are immunogenic and hence not always suitable for clinical applications [256]. Also, they can pack comparatively less *pDNA* compared to some non-viral vectors [256]. Several methods of non-viral gene transfer have been explored to deliver genes of interest to ischemic tissues for therapeutic angiogenesis (Table 1.7). The genes that can stimulate angiogenic signal transduction have been administered either by cationic polymers, lipid, or 3D scaffolds. Genetically engineered stem or progenitor cells have been transplanted into ischemic tissues as an indirect gene delivery strategy to secrete angiogenic factors [227].

#### *1.5.2.1 Naked Plasmid Delivery*

Gene therapy for angiogenesis started with introduction of naked plasmid DNA to achieve therapeutic benefit. The genes encoding angiogenic growth factors have been applied for therapeutic angiogenesis in ischemic animal models such as intramuscular administration of naked plasmids expressing growth factors such as VEGF<sub>165</sub>, FGF-1 and -2, HGF, insulin-like growth factor-1 (IGF-1), ANG-1 and eNOS in the case of limb ischemia. This treatment not only enhanced collateral vessel formation in ischemic muscle, but also improved limb blood perfusion [226, 227, 257-61].

Netrins and nerve growth factors are a class of proteins involved in axon guidance, and were recently reported to control angiogenesis [262, 263]. Intramuscular local delivery of *pNetrin-1* or *pNetrin-4* enhanced neovascularization in a model of hind limb ischemia and also reversed neuropathy and vasculopathy in a diabetic model [262]. This study proposes that the vascular and neural guidance functions of Netrins can offer a potential for therapeutic angiogenesis.

Stromal cell-derived factor-1 (SDF-1) and sonic hedgehog (Shh) based gene therapy have been found to induce angiogenesis in various studies. The role of SDF-1 is to help in homing of stem cells, which in turn facilitates angiogenesis by triggering endogenous endothelial progenitor cell (EPC) mobilization [264]. The study showed that bSDF-1 gene therapy enhances EPC mobilization and neovascularization through the VEGF/eNOS signalling pathway [264]. Shh, in a similar way, up-regulates the expression of SDF-1 and enhances recruitment and incorporation of bone marrow-derived EPCs into the ischemic tissues [265, 266].

#### *1.5.2.2 Cationic Polymer/Lipid-mediated Delivery*

Naked plasmid, because of its negative charge, does not easily penetrate the cell membrane and has a higher chance of degradation. Therefore, non-viral cationic polymers, lipids, and liposomes are the most widely used systems for non-viral gene transfer [267]. The cationic polymer helps in reducing the size of the plasmid by a tight condensation of the complex and, in addition, protects the plasmid DNA against extracellular degradation and increases the cellular uptake of plasmid DNA via charge

interactions. Thus, the use of cationic substances improves gene delivery efficiency compared with the delivery of naked plasmid [227, 257].

Cationic polymers such as linear or branched polyethylenimine (PEI) of various molecular weights, polyamidoamine dendrimer, poly-(l-lysine), and poly ( -amino esters) (PBAEs) have been tested for gene transfection into vascular or cardiac cells (ECs, SMCs, or cardiomyocytes) [268-272]. The positively charged polymer helps the DNA escape the endosomal compartment during endocytosis via the proton-sponge effect [227]. PEI, being cationic, shows toxicity but have been modified to reduce this toxicity with an improved transfection. One of the modifications include conjugation of PEI with heparin. The PEI/heparin hybrid polymers have been shown to enhance the blood compatibility of the polymer [273]. *p*VEGF<sub>165</sub> delivered using heparin-conjugated PEI has increased angiogenesis in mouse ischemic limbs, compared with VEGF<sub>165</sub> gene delivery using unmodified PEI or a commercial reagent (Lipofectamine<sup>®</sup>) [274]. Water soluble cholesterol has been used to modify PEI, which helps in increased uptake of the polyplex and hence increased transfection with less toxicity in vascular or cardiac cells (SMCs and cardiomyocytes) [275, 276]. The delivery of *p*VEGF<sub>165</sub> using this lipopolymer has resulted in an increase in angiogenesis in a myocardial infarction model [276, 277]. This lipopolymer is nontoxic as it is eliminated from the body by macrophages [278].

Cationic lipids have been explored for gene delivery to cardiovascular cells because of their serum resistance and stability and nuclease protection abilities [133]. Cationic lipids such as N-[1-(2, 3-dioleoyloxy)propyl]-N,N,N-trimethylammonium chloride (DOTMA), and 1,3-dioleoyloxy-2-(6-carboxyspermyl)-propyl amide (DOSPER) have been used for gene transfer to vascular cells (ECs and SMCs) in the form of complex and/or by encapsulation as a liposome [279-82]. Cationic lipids condense negatively charged *p*DNA through electrostatic interactions. Ultrasound-mediated destruction of lipid microbubbles has been used to deliver plasmid DNA for cardiac or skeletal muscle [283, 284]. Also, it has been seen that an intravenous infusion of cationic lipid microbubbles carrying VEGF<sub>165</sub> markedly enhances blood vessel formation and perfusion in ischemic limbs [283]. Modification of liposomes with cell-penetrating trans-activating transcriptional activator (TAT) improved gene transfection efficiency in cardiomyocytes. Additional modification with the anti-cardiac myosin antibody further improved the transfection efficiency of TAT-modified liposomes. Such modified liposomes increasingly accumulated in ischemic myocardium, demonstrating their targeted gene delivery to ischemic myocardium [227, 285].

#### *1.5.2.3 Biodegradable Reservoir-mediated Delivery*

Biodegradable reservoirs such as micro-/nanoparticles, sponges, or hydrogels have recently been used to facilitate the sustained release of the therapeutic genes, to protect against denaturation or degradation by nucleases and to prolong gene expression on the specific sites [227, 318].

**Table 1.7: Summary of in vivo non-viral based gene therapy for angiogenesis in various CLI models.**

| <b>Delivery Method</b> | <b>Target Genes</b>                   | <b>Methods</b>                                                                                                                          | <b>Results</b>                                                                                                                                                                                                                                                                                 | <b>Reference</b> |
|------------------------|---------------------------------------|-----------------------------------------------------------------------------------------------------------------------------------------|------------------------------------------------------------------------------------------------------------------------------------------------------------------------------------------------------------------------------------------------------------------------------------------------|------------------|
| Plasmid                | VEGF <sub>165</sub>                   | <ul style="list-style-type: none"> <li>A plasmid vector with VEGF and a hypoxia-responsive element sequence was constructed</li> </ul>  | <ul style="list-style-type: none"> <li>Enhanced gastrocnemius mass and force recovery and ameliorated limb necrosis was observed in the ischemic limb of mice</li> <li>Increased capillary density, matured vessels and reduced number of necrotic cells and fibrosis were observed</li> </ul> | [286]<br>[287]   |
| Plasmid                | VEGF <sub>165</sub>                   | <ul style="list-style-type: none"> <li>A plasmid vector with VEGF and an engineered transcription factor was constructed</li> </ul>     | <ul style="list-style-type: none"> <li>Enhanced blood perfusion and capillary density were observed in the treated ischemic mice with diabetes</li> </ul>                                                                                                                                      | [288]            |
| Plasmid                | VEGF <sub>165</sub> and bFGF          | <ul style="list-style-type: none"> <li>A plasmid vector with VEGF and bFGF was constructed</li> </ul>                                   | <ul style="list-style-type: none"> <li>Enhanced angiogenesis, arteriogenesis and limb salvage in the ischemic mice</li> <li>Increased upregulation of genes associated with arteriogenesis</li> </ul>                                                                                          | [289]            |
| Plasmid                | VEGF <sub>165</sub>                   | <ul style="list-style-type: none"> <li>A plasmid vector with VEGF and integrase was constructed to treat mouse ischemic limb</li> </ul> | <ul style="list-style-type: none"> <li>Enhanced VEGF and blood perfusion level in the ischemic limb</li> </ul>                                                                                                                                                                                 | [290]            |
| Plasmid                | Urokinase plasminogen activator (UPA) | <ul style="list-style-type: none"> <li>A plasmid vector with UPA was constructed to treat mouse ischemic limb</li> </ul>                | <ul style="list-style-type: none"> <li>Enhanced blood perfusion was observed</li> </ul>                                                                                                                                                                                                        | [291]            |
| Plasmid                | ANG-1 and VEGF <sub>165</sub>         | <ul style="list-style-type: none"> <li>Intramuscular injection of ANG-1 was followed by VEGF administration</li> </ul>                  | <ul style="list-style-type: none"> <li>Increased blood pressure and blood perfusion were observed in the ischemic rabbit limb</li> <li>No edema was seen</li> </ul>                                                                                                                            | [292]            |
| Plasmid                | ANG-1 and VEGF <sub>165</sub>         | <ul style="list-style-type: none"> <li>ANG-1 and VEGF were injected in a rabbit limb ischemia model</li> </ul>                          | <ul style="list-style-type: none"> <li>Enhanced blood perfusion and capillary density in the combined treatment group</li> </ul>                                                                                                                                                               | [293]            |

**Table 1.7 (continued): Summary of *in vivo* non-viral based gene therapy for angiogenesis in various CLI models.**

| <b>Delivery Method</b>     | <b>Target Gene</b>  | <b>Methods</b>                                                                                                                                                                                        | <b>Results</b>                                                                                                                                                                                                                                                                                                                                                                           | <b>Reference</b> |
|----------------------------|---------------------|-------------------------------------------------------------------------------------------------------------------------------------------------------------------------------------------------------|------------------------------------------------------------------------------------------------------------------------------------------------------------------------------------------------------------------------------------------------------------------------------------------------------------------------------------------------------------------------------------------|------------------|
| Plasmid + Cell             | Shh and BM-EPCs     | <ul style="list-style-type: none"> <li>Sonic hedgehog (Shh) in combination with bone marrow (BM)-derived endothelial progenitor cells (EPCs) were injected into the ischemic limb of mouse</li> </ul> | <ul style="list-style-type: none"> <li>Shh helped in survival of the transplanted BM-EPCs</li> <li>Increased number of regenerating myofibres and enhanced capillary density were observed</li> <li>Shh and BM-EPCs help in angiogenesis and muscle regeneration</li> </ul>                                                                                                              | [294]            |
| Plasmid                    | IGF-1               | <ul style="list-style-type: none"> <li>IGF-1 was injected intramuscularly followed by electroporation in mouse model of ischemic limb</li> </ul>                                                      | <ul style="list-style-type: none"> <li>Enhanced the expression of VEGF, VEGF receptors fetal liver kinase-1 and FmS-like tyrosine kinase receptor-1, as well as platelet endothelial cell adhesion molecule-1, on endothelial cells</li> <li>Reversed diabetic microangiopathy by increased angiogenesis and arterial flow</li> </ul>                                                    | [259]            |
| PLGA nanoparticle (260 nm) | VEGF <sub>165</sub> | <ul style="list-style-type: none"> <li>PLGA nanoparticle were loaded with <i>pDNA</i></li> </ul>                                                                                                      | <ul style="list-style-type: none"> <li>PLGA loaded <i>pDNA</i> with 87% efficiency and showed a sustained release of <i>pDNA</i> for 11 days</li> <li>Released <i>pDNA</i> retain their structural and functional integrity</li> <li>PLGA/VEGF showed enhanced VEGF expression compared to PEI/VEGF with lower cytotoxicity</li> <li>Enhanced neovascularization was observed</li> </ul> | [295]            |
| Syndecan-4 proteoliposome  | FGF-2               | <ul style="list-style-type: none"> <li>FGF-2 was co-delivered with a liposomally embedded co-receptor, syndecan-4 in a ischemic limb of rat</li> </ul>                                                | <ul style="list-style-type: none"> <li>Enhanced endothelial proliferation, migration, and angiogenic tube formation in response to FGF-2 were observed in an <i>in vitro</i> set up</li> <li>Increased neovascularisation and blood perfusion were reported in the rat ischemic limb</li> </ul>                                                                                          | [296]            |

**Table 1.7 (continued): Summary of *in vivo* non-viral based gene therapy for angiogenesis in various CLI models.**

| <b>Delivery Method</b> | <b>Target Gene</b>            | <b>Methods</b>                                                                                                                                                                                                                                                                                                          | <b>Results</b>                                                                                                                                                                                                  | <b>Reference</b> |
|------------------------|-------------------------------|-------------------------------------------------------------------------------------------------------------------------------------------------------------------------------------------------------------------------------------------------------------------------------------------------------------------------|-----------------------------------------------------------------------------------------------------------------------------------------------------------------------------------------------------------------|------------------|
| Bubble liposome        | bFGF                          | <ul style="list-style-type: none"> <li>• Mouse ischemic hind limb was delivered with bubble liposomes and ultrasound-mediated intramuscular gene transfer of bFGF</li> </ul>                                                                                                                                            | <ul style="list-style-type: none"> <li>• Enhanced capillary density and blood perfusion were seen in the treatment group</li> </ul>                                                                             | [297]            |
| HVJ liposome           | HGF                           | <ul style="list-style-type: none"> <li>• Hemagglutinating virus of Japan (HVJ)-liposome method was used to deliver HGF in an ischemic limb of rat</li> </ul>                                                                                                                                                            | <ul style="list-style-type: none"> <li>• Significant increase in blood perfusion and capillary density was reported even in the case of diabetic rat limb ischemia model</li> </ul>                             | [298]            |
| Plasmid                | eNOS                          | <ul style="list-style-type: none"> <li>• Mutant mice deficient in eNOS (ecNOS-KO) were generated</li> <li>• phosphomimetic mutant of eNOS gene was delivered along with electroporation into the ischemic mice ecNOS-KO and balb/c mice</li> </ul>                                                                      | <ul style="list-style-type: none"> <li>• Enhanced blood perfusion was observed in both cases</li> </ul>                                                                                                         | [258]            |
| Plasmid                | HIF-1                         | <ul style="list-style-type: none"> <li>• A plasmid was constructed using protein consisting of DNA-binding and dimerization domains from the HIF-1 subunit and the transactivation domain from herpes simplex virus VP16 protein</li> <li>• HIF-1 /VP16 was injected in a rabbit model of hind limb ischemia</li> </ul> | <ul style="list-style-type: none"> <li>• Significant improvements in calf blood pressure ratio, angiographic score, resting and maximal regional blood flow, and capillary density were reported</li> </ul>     | [299]            |
| Plasmid                | PD-ECGF                       | <ul style="list-style-type: none"> <li>• Platelet-derived endothelial cell growth factor (PD-ECGF) and TP were combined in a plasmid construct and injected in the ischemic limb of rabbit</li> </ul>                                                                                                                   | <ul style="list-style-type: none"> <li>• Increased blood perfusion, capillary density and arteriogenesis</li> </ul>                                                                                             | [300]            |
| Plasmid                | HO-1                          | <ul style="list-style-type: none"> <li>• A plasmid construct carrying human HO-1 driven by three hypoxia response elements (HREs) was generated</li> </ul>                                                                                                                                                              | <ul style="list-style-type: none"> <li>• An increased blood flow was observed associated with reduced IL-6 and CXCL1</li> <li>• Influenced the regenerative ability of myocytes in the ischemic limb</li> </ul> | [301]            |
| Plasmid                | ANG-1 and VEGF <sub>165</sub> | <ul style="list-style-type: none"> <li>• Rat model of hind limb ischemia was treated using combination of ANG-1 and VEGF</li> </ul>                                                                                                                                                                                     | <ul style="list-style-type: none"> <li>• Increased capillary density and blood perfusion were observed</li> <li>• No leaky vessels were seen</li> </ul>                                                         | [287]            |

**Table 1.7 (continued): Summary of *in vivo* non-viral based gene therapy for angiogenesis in various CLI models.**

| <b>Delivery Method</b> | <b>Target Gene</b> | <b>Methods</b>                                                                                                                                     | <b>Results</b>                                                                                                                                                                                                                                                               | <b>Reference</b> |
|------------------------|--------------------|----------------------------------------------------------------------------------------------------------------------------------------------------|------------------------------------------------------------------------------------------------------------------------------------------------------------------------------------------------------------------------------------------------------------------------------|------------------|
| Plasmid + cell         | ANG-1 and BM-MNC   | <ul style="list-style-type: none"> <li>• ANG-1 and BM-MNC were delivered in rabbit model of limb ischemia</li> </ul>                               | <ul style="list-style-type: none"> <li>• Improved angiographic score and capillary density and transcutaneous oxygen pressure were observed</li> </ul>                                                                                                                       | 210              |
| Plasmid                | FGF-2 and Cyr61    | <ul style="list-style-type: none"> <li>• FGF-2 and Cyr61 bicistronic vector was injected using electroporation into mouse ischemic limb</li> </ul> | <ul style="list-style-type: none"> <li>• Enhanced blood perfusion was observed with active incorporation of FGF-2 and Cyr61 in therapeutic angiogenesis of hind limb ischemia</li> </ul>                                                                                     | [289, 302]       |
| Plasmid                | FGF-2              | <ul style="list-style-type: none"> <li>• Intradermal injection of FGF-2 was delivered in a rat model of limb ischemia</li> </ul>                   | <ul style="list-style-type: none"> <li>• Enhanced blood perfusion and capillary density were observed</li> </ul>                                                                                                                                                             | [303]            |
| Plasmid                | bFGF               | <ul style="list-style-type: none"> <li>• bFGF was delivered using electroporation into the ischemic limb of rabbit</li> </ul>                      | <ul style="list-style-type: none"> <li>• With increased voltage gene transfection efficiency increased</li> <li>• Angiogenic responses, calf blood pressure ratio, <i>in vivo</i> blood flow, and capillary density were higher than that of control LacZ plasmid</li> </ul> | [304]            |
| Plasmid                | HGF                | <ul style="list-style-type: none"> <li>• HGF gene with the prostacyclin synthase gene were injected into mouse and rabbit ischemic limb</li> </ul> | <ul style="list-style-type: none"> <li>• Increased blood perfusion and capillary density were observed in both the cases</li> <li>• Diabetic neuropathy was reversed with the use of HGF and prostacyclin synthase</li> </ul>                                                | [305]            |
| Plasmid                | HGF                | <ul style="list-style-type: none"> <li>• HGF was injected intramuscularly in a rat and rabbit ischemic limbs</li> </ul>                            | <ul style="list-style-type: none"> <li>• Increased blood perfusion and enhanced capillary density were reported</li> </ul>                                                                                                                                                   | [306]            |

**Table 1.8: Summary of clinical studies of angiogenic gene therapy in human CLI patients.**

| <b>Delivery</b> | <b>Target Genes</b>         | <b>Methods</b>                                                                                                                                                                                                                                                                                       | <b>Results</b>                                                                                                                                                                                                       | <b>Reference</b> |
|-----------------|-----------------------------|------------------------------------------------------------------------------------------------------------------------------------------------------------------------------------------------------------------------------------------------------------------------------------------------------|----------------------------------------------------------------------------------------------------------------------------------------------------------------------------------------------------------------------|------------------|
| Ad-virus        | HIF-1                       | <ul style="list-style-type: none"> <li>34 no-option patients with CLI were injected with HIF-1 at doses of <math>1 \times 10^8</math> to <math>2 \times 10^{11}</math> viral particles in a phase I dose response study</li> </ul>                                                                   | <ul style="list-style-type: none"> <li>HIF-1 treatment was well tolerated by all the patients with no serious adverse events</li> </ul>                                                                              | [307]            |
| Ad-virus        | HIF-                        | <ul style="list-style-type: none"> <li>281 patients were randomized in a double-blind manner to various doses of HIF-1</li> </ul>                                                                                                                                                                    | <ul style="list-style-type: none"> <li>HIF-1 treatment was not effective for patients with intermittent claudication</li> </ul>                                                                                      | [308]            |
| Plasmid         | VEGF <sub>165</sub>         | <ul style="list-style-type: none"> <li>54 adult diabetic patients with CLI underwent a double-blind, placebo-controlled study and VEGF was administered intramuscularly</li> </ul>                                                                                                                   | <ul style="list-style-type: none"> <li>Significant improvement was found in patients treated with a VEGF<sub>165</sub>-containing plasmid with no substantial adverse events</li> </ul>                              | [309]            |
| Plasmid         | VEGF <sub>165</sub>         | <ul style="list-style-type: none"> <li>17 diabetic CLI patients were randomized to receive phVEGF<sub>165</sub> gene product (n = 11) or placebo (n = 6)</li> </ul>                                                                                                                                  | <ul style="list-style-type: none"> <li>No increase in capillary leakage in diabetic CLI patients was found with VEGF treatment</li> </ul>                                                                            | [310]            |
| Plasmid         | HGF                         | <ul style="list-style-type: none"> <li>21 patients with CLI were consecutively assigned to receive increasing doses of HGF gene, and were administered into the ischemic calf</li> <li>No serious adverse events were observed in any of the 21 patients for the 3-month follow-up period</li> </ul> | <ul style="list-style-type: none"> <li>A significant reduction in pain and improvement in wound healing were observed</li> </ul>                                                                                     | [311]            |
| Plasmid         | VEGF <sub>165</sub> and HGF | <ul style="list-style-type: none"> <li>43 patients were assigned with 29 in the treatment group and 14 allocated to the placebo group</li> <li>An increased limb salvage was observed for the treatment group</li> </ul>                                                                             | <ul style="list-style-type: none"> <li>Pain at rest was improved in 65% of patients in the treatment group compared to placebo</li> <li>No significant adverse effects were found for the treatment group</li> </ul> | [312]            |

**Table 1.8 (continued): Summary of clinical studies of angiogenic gene therapy in human CLI patients.**

| <b>Delivery Method</b> | <b>Target Gene</b> | <b>Methods</b>                                                                                                                                                                                    | <b>Results</b>                                                                                                                                                                                                                                                                                                                                   | <b>Reference</b> |
|------------------------|--------------------|---------------------------------------------------------------------------------------------------------------------------------------------------------------------------------------------------|--------------------------------------------------------------------------------------------------------------------------------------------------------------------------------------------------------------------------------------------------------------------------------------------------------------------------------------------------|------------------|
| Plasmid                | HGF                | <ul style="list-style-type: none"> <li>10 patients with Buerger's disease and with ischemic ulcers were enrolled in Japan for an open-label clinical study from May 2004 to April 2008</li> </ul> | <ul style="list-style-type: none"> <li>Decrease in size of the ulcer was reported in 6/9 (66.7%) patients and the ulcers healed completely in 5/9 (55.6%) patients after gene therapy</li> <li>No major amputation, deaths occurred or major safety concerns were observed</li> </ul>                                                            | [313]            |
| Plasmid                | HGF                | <ul style="list-style-type: none"> <li>22 patients with critical limb ischemia were administered with HGF by intramuscular injection</li> </ul>                                                   | <ul style="list-style-type: none"> <li>No serious adverse event especially no peripheral edema was observed by gene transfer over a follow-up of 6 months</li> <li>Increased ankle-brachial index was observed in 11/17 (64.7%) patients,</li> <li>Decreased ulcer size was observed in 18/25 (72%) ulcers</li> </ul>                            | [314]            |
| Plasmid                | HGF                | <ul style="list-style-type: none"> <li>Efficacy and safety of intramuscular injection of a naked HGF plasmid gene was investigated in patients with CLI</li> </ul>                                | <ul style="list-style-type: none"> <li>The overall improvement rate of the primary end point was 70.4% (19/27) in HGF group and 30.8% (4/13) in placebo group with no major safety problems</li> </ul>                                                                                                                                           | [315]            |
| Plasmid                | FGF-1              | <ul style="list-style-type: none"> <li>A three-year follow-up in patients suffering from CLI or intermittent claudication was performed with 93 evaluable patients</li> </ul>                     | <ul style="list-style-type: none"> <li>At three years, no increase in retinopathy or renal dysfunction associated with delivery of this angiogenic factor was seen</li> <li>No difference in the number of strokes, MI or deaths, respectively, for FGF-1 versus placebo</li> </ul>                                                              | [316]            |
| Plasmid                | FGF-1              | <ul style="list-style-type: none"> <li>A phase III trial was conducted with 525 CLI patients enrolled from 171 sites in 30 countries</li> </ul>                                                   | <ul style="list-style-type: none"> <li>Major amputation or death in 86 patients (33%) in the placebo group, and 96 (36%) in the active group were reported</li> <li>No significant safety issues were recorded</li> <li>TAMARIS provided no evidence that FGF-1 is effective in reduction of amputation or death in patients with CLI</li> </ul> | [317]            |

This sustained delivery of therapeutic genes is required to maintain this vasculature. VEGF<sub>165</sub> *pDNA* was encapsulated in poly (lactic-co-glycolic acid) PLGA nanoparticles and these particles displayed a sustained release of VEGF *pDNA*. Moreover, the released *pDNA* showed structural and functional integrity for more than 10 days [295]. When the PLGA particles along with VEGF<sub>165</sub> were injected in the ischemic limbs, an increased expression of VEGF<sub>165</sub> was seen along with an increase in blood perfusion. Porous PLGA and collagen scaffolds have been used to deliver *pVEGF*<sub>165</sub>, *pPDGF*-B and *pFGF*-1. The release of all these therapeutic genes was seen to be in a sustained manner and induced angiogenesis in subcutaneous mouse models [319-322]. Injectable gelatin hydrogel was fabricated to deliver *pFGF*-4 in the ischemic limb of mouse model. The treatment groups induced blood perfusion in the ischemic limb muscle more effectively than naked *pFGF*-4 did [323]. Alginate hydrogels loaded with PEI-*pVEGF*<sub>165</sub> complexes were implanted in the ischemic limb of the mice. The PEI-*pVEGF* complexes when released enhanced the recovery of blood perfusion in an ischemic hind limb mouse model [324].

### 1.6 Clinical Trials and Limitations

Numerous clinical trials have been performed using proangiogenic genes: VEGF<sub>165</sub>, FGF-1, and HGF-1 . The gene delivery was achieved either by intramuscular injection or by using a catheter [227]. The clinical trials of viral and non-viral gene delivery for therapeutic angiogenesis are summarized in the table (Table 1.8).

The first clinical trial was reported by Isner et al. using naked *pVEGF*<sub>165</sub> delivery for patients with critical limb ischemia. *pVEGF*<sub>165</sub> were delivered both via a catheter and through intramuscular injection in the ischemic limb and this resulted in an increased collateral blood vessel improvement and enhanced distal blood perfusion in ischemic regions [325-27]. The VEGF<sub>165</sub> gene therapy also resulted in improved ischemic ulcer healing and limb salvage in some patients. Additionally, very similar results were obtained in the case of patients with Buerger's disease with CLI, when treated with naked *pVEGF*<sub>165</sub> [328]. The patients with Buerger's disease tolerated the injection procedure and the treatment resulted in collateral vessel formation around the injection sites. Furthermore, ischemic pain was relieved in a significant number of patients along with improved ulcer healing.

Factors used in clinical trials other than VEGF<sub>165</sub> are FGF-1, HGF and HIF-1 . Naked *pFGF*-1 delivered by intramuscular injection was well tolerated by CLI patients and had reduced mortality and limb amputations compared to placebo [226]. Another clinical trial performed by Baumgartner et al. on patients waiting for limb amputations showed expression of FGF-1 on the site of injections. The histological and RTPCR data proved expression of FGF-1 in muscles retrieved from the patients [329]. Likewise, intramuscular injection of *pHGF* showed reductions of ischemic pain and size of ischemic ulcers in a majority of patients [330].

Viral vectors are immunogenic and thus a non-viral gene delivery option should be considered. VEGF<sub>165</sub>, HGF-1 and FGF-1 naked *pDNA* gene therapy was well tolerated by patients with no adverse effect. Reduction in pain and increased limb salvage were reported in the patients. However, several double-blind, placebo-controlled clinical studies have reported controversial clinical outcomes. There was no difference in pain relief, wound healing or limb salvage with compared to the placebo control group. This makes it problematic to draw conclusions regarding the efficacy of these gene therapy [309, 331, 332].

Therefore, non-viral gene delivery must be developed into a more clinically relevant therapy to enable its application for therapeutic angiogenesis. As described earlier, naked *pDNA* gene therapy may not be efficient for clinical applications due to its instability inside the cytoplasm and also because they lack a well-organized mechanism to facilitate their transport into the cytoplasm and nucleus [227]. Cationic polymers and lipid-based delivery vectors have been developed to facilitate gene transfer and also to protect the *pDNA* from enzymatic degradation. However, the efficacy of these delivery vectors decrease in the presence of serum and these systems have been reported to have very low *in vivo* gene transfer efficiency [333]. Moreover, cardiovascular cells such as ECs, SMCs, cardiomyocytes, and skeletal myoblasts have an intrinsic mechanism to resist the gene transfer [334] and are surrounded by ECM barriers that may hinder efficient gene transfer [335]. Thus, unique approaches are required for the development of functional delivery vectors with low cytotoxicity and high efficiency of *in vivo* gene transfer. Again, a functional gene delivery vector with ligand-based targeting strategy for vascular cells can improve the *in vivo* performance of non-viral gene delivery vectors by increasing specificity to target tissues and minimizing toxic side effects. High-throughput screening approaches can help in mining functional ligands for delivery vehicles with high efficiency and ensured safety [227].

### **1.7 Hypotheses and Objectives**

The ultimate aim of this project was to develop a therapy for CLI using a non-viral gene delivery system. It was hypothesized that an injectable ELP system encoding eNOS and IL-10 genes will enhance angiogenesis and reduce inflammation in a CLI induced mouse model. The therapeutic effects of eNOS and IL-10 will lead to functional angiogenesis and reduction in inflammation respectively.

The research project had two strands. The first was the development of a suitable gene delivery system for controlled delivery of multiple genes, and the other was to investigate at a molecular level the cross-talk between eNOS and IL-10 in an *in vivo* study. The overall study was divided into four phases, each with specific objectives and hypotheses.

### 1.7.1 Phase One (Chapter Two)

**Overall aim:** To assess the cellular uptake behaviour and cell viability of hollow spheres with respect to various size and charge using chitosan/polyglutamic acid (PGA) hollow spheres as a model system.

**Hypotheses:**

- Chitosan hollow spheres of various size and surface charges can be developed by manipulating the size of the template and surface functionalities of the chitosan/PGA hollow spheres.
- Chitosan/PGA hollow spheres with various size and surface charges will show different pattern in their cell viability with respect to different cell lines.
- Chitosan/PGA hollow spheres with various size and surface charges will show a different pattern in their cellular internalization with respect to different cell lines.

**Objectives:**

- To fabricate chitosan/PGA hollow spheres of various sizes and surface charge using various sizes of polystyrene beads as template and chemically modifying the surface of hollow spheres with methoxyethanol amine and linear PEG molecule.
- To measure *in vitro* cellular viability of different combinations of size and charge of chitosan/PGA hollow spheres with HUVECs and HUASMCs by performing cellular metabolic assays.
- To perform *in vitro* cellular uptake studies using different combinations of size and charge of hollow spheres with HUVECs and HUASMCs by performing flow cytometry and high content imaging analysis.

### 1.7.2 Phase Two (Chapter Three)

**Overall aim:** To fabricate tuneable and non-toxic ELP hollow spheres of various size and use them as a gene delivery depot.

**Hypotheses:**

- Stable, non-toxic ELP hollow spheres of various size can be fabricated using a template-based method and mTGase as a cross-linker.
- The ELP hollow spheres can be used as a high payload gene delivery depot.
- The hollow spheres loaded with polyplexes will show a sustained release of *pDNA* due to an electrostatic interaction between polyplexes and hollow spheres.
- The polyplexes loaded hollow spheres will show better cell viability than polyplexes only.
- The polyplexes loaded hollow spheres and released polyplexes from the hollow spheres will transfect cells.
- The polyplex loaded hollow spheres will be internalised in the cells through a lysosome mediated pathway.

**Objectives:**

- To fabricate ELP hollow spheres of various sizes using sulfonated PS beads of defined sizes.
- To load naked plasmid and polymer/plasmid complexes (polyplexes) into the ELP hollow spheres of various sizes and characterize these spheres for loading efficiency in various sizes of ELP hollow spheres by performing PicoGreen® based DNA quantification and TEM analysis.
- To perform *in vitro* release studies of *pDNA* (green fluorescent protein) loaded hollow spheres under the treatment of enzymes such as elastase and protease and characterize the bioactivity of the released *pDNA* by performing fluorescence imaging of the green fluorescent protein transfected cells.
- To perform cell viability of ELP hollow spheres on HUVECs and adipose derived stem cells (ADSCs) by performing alamarBlue® assay.
- To perform *in vitro* transfection studies using ELP hollow spheres loaded with polyplex of *pGLUC* and characterise using GLUC assay.
- To perform *in vitro* cellular uptake studies of ELP hollow spheres loaded with polyplexes by TEM imaging and LysoTracker® fluorescence imaging.

*1.7.3 Phase Three (Chapter Four)*

**Overall aim:** To design and fabricate a dual gene delivery ELP based injectable system for eNOS and IL-10.

**Hypotheses:**

- An injectable ELP scaffold can be fabricated using mTGase as a cross-linker.
- 1000 nm hollow spheres can be used as a reservoir system.
- A combination of injectable ELP scaffold and 1000 nm ELP hollow spheres can be used as dual gene delivery depot.

**Objectives:**

- To fabricate an injectable ELP scaffold using microbial transglutaminase as a cross-linker.
- To assess the cross-linking of ELP scaffold by carrying out trinitrobenzene sulfonic acid assay.
- To assess the cytotoxicity of the mTGase cross-linked scaffold by performing cellular metabolic assay.
- To screen various sizes of ELP hollow spheres for their cellular uptake behaviour in HUVECs and activated and non-activated macrophages (THP1 cells) by FACS analysis.
- To perform *in vitro* release study of ELP based injectable systems i) ELP scaffold-*pGLUC*/hollow spheres and ii) ELP scaffold/hollow spheres-*pGLUC* under the treatment of elastase.

#### *1.7.4 Phase Four (Chapter Four)*

**Overall aim:** To decide a therapeutic dose for eNOS and IL-10 using a subcutaneous mouse model and to deliver therapeutic doses of eNOS and IL-10 intramuscularly using an injectable ELP system to treat limb ischemia in a mouse model of CLI.

**Hypotheses:**

- The ELP based injectable system containing eNOS and IL-10 will contribute towards increasing angiogenesis and reduced inflammation.
- A combination of therapeutic doses of heNOS and hIL-10 dose will enhance angiogenesis and reduce inflammation.
- heNOS and hIL-10 will be expressed in a spatio-temporal manner.
- Specific therapeutic doses of heNOS and hIL-10 will enhance blood perfusion level in the ischemic limb as well as reduce the inflammation level significantly.
- heNOS and hIL-10 delivery in the ischemic tissue will show an effect on the expression of various angiogenic and inflammatory markers at a molecular level.

**Objectives:**

- To carry out a subcutaneous dose response study in a mouse model using different combinations of doses of eNOS and IL-10.
- To assess the angiogenesis and inflammation level in subcutaneous tissue by performing stereological analysis (surface and length density of blood vessels and volume fraction of inflammatory cells), followed by immunofluorescence staining with CD31 for endothelial cells and CD68 for inflammatory cells.
- To assess the level of human eNOS and IL-10 expression level in subcutaneous and ischemic tissue by performing ELISA.
- To perform a gene therapy study using heNOS and hIL-10 in a mouse model of CLI using selected doses of heNOS and hIL-10 and combination of them with saline as a control.
- To assess the blood perfusion level of the treated ischemic limbs by performing laser doppler perfusion imaging.
- To assess recovery of blood perfusion by characterizing angiogenesis and inflammation with stereological analysis.
- To evaluate the expression levels of selected angiogenic and inflammatory markers in the heNOS and hIL-10 treated ischemic tissue by carrying out RT-PCR analysis.

## 1.8 References

- [1] Ouriel K. Peripheral arterial disease. *Lancet*. 2001;358:1257-64.
- [2] Harris K. The worldwide burden of peripheral artery disease. 2012.
- [3] Belch JJ, Topol EJ, Agnelli G, Bertrand M, Califf RM, Clement DL. Critical issues in peripheral arterial disease detection and management: a call to action. *Arch Intern Med*. 2003;163:884-92.
- [4] Golomb BA, Dang TT, Criqui MH. Peripheral arterial disease: morbidity and mortality implications. *Circulation*. 2006;114:688-99.
- [5] Hirsch AT, Haskal ZJ, Hertzner NR, Bakal CW, Creager MA, Halperin JL. ACC/AHA guidelines for the management of patients with peripheral arterial disease (lower extremity, renal, mesenteric, and abdominal aortic). *J Vasc Interv Radiol*. 2006;17:1383-98.
- [6] Norgren L, Hiatt WR, Dormandy JA, Nehler MR, Harris KA, Fowkes FGR. Inter-society consensus for the management of peripheral arterial disease (TASC II). *Eur J Vasc Endovasc*. 2007;33:S5-S75.
- [7] Selvin E, Erlinger TP. Prevalence of and risk factors for peripheral arterial disease in the United States. *Circulation*. 2004;110:738-43.
- [8] Vink A, Schoneveld AH, Borst C, Pasterkamp G. The contribution of plaque and arterial remodeling to de novo atherosclerotic luminal narrowing in the femoral artery. *J Vasc Surg*. 2002;36:1194-7.
- [9] Libby P, Theroux P. Pathophysiology of coronary artery disease. *Circulation*. 2005;111:3481-8.
- [10] Libby P. Changing concepts of atherogenesis. *J Intern Med*. 2000;247:349-58.
- [11] Garcia LA. Epidemiology and pathophysiology of lower extremity peripheral arterial disease. *J Endovasc Ther*. 2006;13:3-9.
- [12] McDermott MM, Guralnik JM, Corsi A, Albay M, Macchi C, Bandinelli S. Patterns of inflammation associated with peripheral arterial disease: the InCHIANTI study. *Am Heart J*. 2005;150:276-81.
- [13] Gute DC, Ishida T, Yarimizu K, Korthuis RJ. Inflammatory responses to ischemia and reperfusion in skeletal muscle. *Mol Cell Biochem*. 1998;179:169-87.
- [14] Blaisdell FW. The pathophysiology of skeletal muscle ischemia and the reperfusion syndrome: a review. *Cardiovasc Surg*. 2002;10:620-30.
- [15] Khawaja FJ, Kullo IJ. Novel markers of peripheral arterial disease. *Vasc Med*. 2009;14:381-92.
- [16] Mills KH, Dunne A. Immune modulation: IL-1, master mediator or initiator of inflammation. *Nat Med*. 2009;15:1363-4.
- [17] Gabay C, Lamacchia C, Palmer G. IL-1 pathways in inflammation and human diseases. *Nat Rev Rheumatol*. 2010;6:232-41.

- [18] Guilloteau K, Paris I, Pedretti N, Boniface K, Juchaux F, Huguier V. Skin inflammation induced by the synergistic action of IL-17A, IL-22, oncostatin M, IL-1 , and TNF- recapitulates some features of psoriasis. *J Immunol.* 2010.
- [19] Joosten LA, Helsen MM, Saxne T, van De Loo FA, Heinegard D, van Den Berg WB. IL-1 blockade prevents cartilage and bone destruction in murine type II collagen-induced arthritis, whereas TNF- blockade only ameliorates joint inflammation. *J Immunol.* 1999;163:5049-55.
- [20] Seki M, Kohno S, Newstead MW, Zeng X, Bhan U, Lukacs NW. Critical role of IL-1 receptor-associated kinase-M in regulating chemokine-dependent deleterious inflammation in murine influenza pneumonia. *J Immunol.* 2010;184:1410-8.
- [21] Besnard AG, Togbe D, Couillin I, Tan Z, Zheng SG, Erard F. Inflammasome-IL-1-Th17 response in allergic lung inflammation. *J Mol Cell Biol.* 2012;4:3-10.
- [22] Maloff BL, Shaw JE, Di Meo TM. IL-1 dependent model of inflammation mediated by neutrophils. *J Pharmacol Methods.* 1989;22:133-40.
- [23] Whitehouse MW. Anti-TNF- therapy for chronic inflammation: reconsidering pentoxifylline as an alternative to therapeutic protein drugs. *Inflammopharmacology.* 2004;12:223-7.
- [24] Kitagaki M, Isoda K, Kamada H, Kobayashi T, Tsunoda S, Tsutsumi Y. Novel TNF- receptor 1 antagonist treatment attenuates arterial inflammation and intimal hyperplasia in mice. *J Atheroscler Thromb.* 2012;19:36-46.
- [25] Swain MG, Appleyard CB, Wallace JL, Maric M. TNF- facilitates inflammation-induced glucocorticoid secretion in rats with biliary obstruction. *J Hepatol.* 1997;26:361-8.
- [26] Finotto S, Ohno I, Marshall JS, Gauldie J, Denburg JA, Dolovich J. TNF- production by eosinophils in upper airways inflammation (nasal polyposis). *J Immunol.* 1994;153:2278-89.
- [27] Hui-Yuen JS, Duong TT, Yeung RS. TNF- is necessary for induction of coronary artery inflammation and aneurysm formation in an animal model of Kawasaki disease. *J Immunol.* 2006;176:6294-301.
- [28] Lukacs NW, Strieter RM, Chensue SW, Widmer M, Kunkel SL. TNF- mediates recruitment of neutrophils and eosinophils during airway inflammation. *J Immunol.* 1995;154:5411-7.
- [29] Wolfs TG, Buurman WA, van Schadewijk A, de Vries B, Daemen MA, Hiemstra PS. In vivo expression of Toll-like receptor 2 and 4 by renal epithelial cells: IFN- and TNF- mediated up-regulation during inflammation. *J Immunol.* 2002;168:1286-93.
- [30] Graziewicz MA, Tarrant TK, Buckley B, Roberts J, Fulton L, Hansen H. An endogenous TNF- antagonist induced by splice-switching oligonucleotides reduces inflammation in hepatitis and arthritis mouse models. *Mol Ther.* 2008;16:1316-22.

- [31] Wilderman MJ, Kim S, Gillespie CT, Sun J, Kapoor V, Vachani A. Blockade of TNF- decreases both inflammation and efficacy of intrapulmonary Ad.IFN immunotherapy in an orthotopic model of bronchogenic lung cancer. *Mol Ther.* 2006;13:910-7.
- [32] McDermott MM, Liu K, Guralnik JM, Ferrucci L, Green D, Greenland P. Functional decline in patients with and without peripheral arterial disease: predictive value of annual changes in levels of C-reactive protein and D-dimer. *J Gerontol A Biol Sci Med Sci.* 2006;61:374-9.
- [33] McDermott MM, Guralnik JM, Greenland P, Green D, Liu K, Ridker PM. Inflammatory and thrombotic blood markers and walking-related disability in men and women with and without peripheral arterial disease. *J Am Geriatr Soc.* 2004;52:1888-94.
- [34] Nishimoto N, Kishimoto T. Interleukin 6: from bench to bedside. *Nat Clin Pract Rheumatol.* 2006;2:619-26.
- [35] Signorelli SS, Mazzarino MC, Di Pino L, Malaponte G, Porto C, Pennisi G. High circulating levels of cytokines (IL-6 and TNF ), adhesion molecules (VCAM-1 and ICAM-1) and selectins in patients with peripheral arterial disease at rest and after a treadmill test. *Vasc Med.* 2003;8:15-9.
- [36] Nylaende M, Kroese A, Strandén E, Morken B, Sandbaek G, Lindahl AK. Markers of vascular inflammation are associated with the extent of atherosclerosis assessed as angiographic score and treadmill walking distances in patients with peripheral arterial occlusive disease. *Vasc Med.* 2006;11:21-8.
- [37] Brevetti G, Schiano V, Chiariello M. Cellular adhesion molecules and peripheral arterial disease. *Vasc Med.* 2006;11:39-47.
- [38] Khaleghi M, Ali Z, Mosley TH, Jr., Turner ST, Kullo IJ. Association of soluble cell adhesion molecules with ankle-brachial index in a biethnic cohort of predominantly hypertensive individuals. *Clin Chem.* 2008;54:1788-95.
- [39] Nasir K, Guallar E, Navas-Acien A, Criqui MH, Lima JA. Relationship of monocyte count and peripheral arterial disease: results from the National Health and Nutrition Examination Survey 1999-2002. *Arterioscler Thromb Vasc Biol.* 2005;25:1966-71.
- [40] Haumer M, Amighi J, Exner M, Mlekusch W, Sabeti S, Schlager O. Association of neutrophils and future cardiovascular events in patients with peripheral artery disease. *J Vasc Surg.* 2005;41:610-7.
- [41] Collier BS. Leukocytosis and ischemic vascular disease morbidity and mortality: is it time to intervene? *Arterioscler Thromb Vasc Biol.* 2005;25:658-70.
- [42] Madjid M, Awan I, Willerson JT, Casscells SW. Leukocyte count and coronary heart disease: implications for risk assessment. *J Am Coll Cardiol.* 2004;44:1945-56.

- [43] Patel H, Shaw SG, Shi-Wen X, Abraham D, Baker DM, Tsui JC. Toll-like receptors in ischemia and its potential role in the pathophysiology of muscle damage in critical limb ischemia. *Cardiol Res Pract.* 2012;2012:121237.
- [44] Goodman MN. Tumor necrosis factor induces skeletal muscle protein breakdown in rats. *Am J Physiol.* 1991;260:E727-30.
- [45] Goodman MN. Interleukin-6 induces skeletal muscle protein breakdown in rats. *Proc Soc Exp Biol Med.* 1994;205:182-5.
- [46] Visser M, Pahor M, Taaffe DR, Goodpaster BH, Simonsick EM, Newman AB. Relationship of interleukin-6 and tumor necrosis factor- with muscle mass and muscle strength in elderly men and women: the Health ABC Study. *J Gerontol A Biol Sci Med Sci.* 2002;57:M326-32.
- [47] Meadows KA, Holly JM, Stewart CE. Tumor necrosis factor- induced apoptosis is associated with suppression of insulin-like growth factor binding protein-5 secretion in differentiating murine skeletal myoblasts. *J Cell Physiol.* 2000;183:330-7.
- [48] Warren GL, Hulderman T, Liston A, Simeonova PP. Toll-like and adenosine receptor expression in injured skeletal muscle. *Muscle Nerve.* 2011;44:85-92.
- [49] Frost RA, Nystrom GJ, Lang CH. Multiple Toll-like receptor ligands induce an IL-6 transcriptional response in skeletal myocytes. *Am J Physiol Regul Integr Comp Physiol.* 2006;290:R773-84.
- [50] Lang CH, Silvis C, Deshpande N, Nystrom G, Frost RA. Endotoxin stimulates in vivo expression of inflammatory cytokines tumor necrosis factor , interleukin-1 , -6, and high-mobility-group protein-1 in skeletal muscle. *Shock.* 2003;19:538-46.
- [51] Grundtman C, Bruton J, Yamada T, Ostberg T, Pisetsky DS, Harris HE. Effects of HMGB1 on in vitro responses of isolated muscle fibers and functional aspects in skeletal muscles of idiopathic inflammatory myopathies. *FASEB J.* 2010;24:570-8.
- [52] Liu Y, Steinacker JM. Changes in skeletal muscle heat shock proteins: pathological significance. *Front Biosci.* 2001;6:D12-25.
- [53] Gillani S, Cao J, Suzuki T, Hak DJ. The effect of ischemia reperfusion injury on skeletal muscle. *Injury.* 2012;43:670-5.
- [54] Eliason JL, Wakefield TW. Metabolic consequences of acute limb ischemia and their clinical implications. *Semin Vasc Surg.* 2009;22:29-33.
- [55] Lutz J, Thurmel K, Heemann U. Anti-inflammatory treatment strategies for ischemia/reperfusion injury in transplantation. *J Inflamm (Lond).* 2010;7:27.

- [56] Nakao N, Kurokawa T, Nonami T, Tumurkhuu G, Koide N, Yokochi T. Hydrogen peroxide induces the production of tumor necrosis factor- $\alpha$  in RAW 264.7 macrophage cells via activation of p38 and stress-activated protein kinase. *Innate Immun.* 2008;14:190-6.
- [57] Meldrum DR, Dinarello CA, Cleveland JC, Jr., Cain BS, Shames BD, Meng X. Hydrogen peroxide induces tumor necrosis factor  $\alpha$ -mediated cardiac injury by a P38 mitogen-activated protein kinase-dependent mechanism. *Surgery.* 1998;124:291-6; discussion 7.
- [58] Maslanik T, Mahaffey L, Tannura K, Beninson L, Greenwood BN, Fleshner M. The inflammasome and danger associated molecular patterns (DAMPs) are implicated in cytokine and chemokine responses following stressor exposure. *Brain Behav Immun.* 2012.
- [59] Bryant C, Fitzgerald KA. Molecular mechanisms involved in inflammasome activation. *Trends Cell Biol.* 2009;19:455-64.
- [60] Gomariz RP, Gutierrez-Canas I, Arranz A, Carrion M, Juarranz Y, Leceta J. Peptides targeting Toll-like receptor signalling pathways for novel immune therapeutics. *Curr Pharm Des.* 2010;16:1063-80.
- [61] Moynagh PN. Toll-like receptor signalling pathways as key targets for mediating the anti-inflammatory and immunosuppressive effects of glucocorticoids. *J Endocrinol.* 2003;179:139-44.
- [62] Couper KN, Blount DG, Riley EM. IL-10: the master regulator of immunity to infection. *J Immunol.* 2008;180:5771-7.
- [63] Moore KW, de Waal Malefyt R, Coffman RL, O'Garra A. Interleukin-10 and the interleukin-10 receptor. *Annu Rev Immunol.* 2001;19:683-765.
- [64] Fiorentino DF, Bond MW, Mosmann TR. Two types of mouse T helper cell. IV. Th2 clones secrete a factor that inhibits cytokine production by Th1 clones. *J Exp Med.* 1989;170:2081-95.
- [65] Armstrong L, Jordan N, Millar A. Interleukin 10 (IL-10) regulation of tumour necrosis factor (TNF- $\alpha$ ) from human alveolar macrophages and peripheral blood monocytes. *Thorax.* 1996;51:143-9.
- [66] Park DR, Skerrett SJ. IL-10 enhances the growth of *Legionella pneumophila* in human mononuclear phagocytes and reverses the protective effect of IFN- $\gamma$ : differential responses of blood monocytes and alveolar macrophages. *J Immunol.* 1996;157:2528-38.
- [67] Thomassen MJ, Divis LT, Fisher CJ. Regulation of human alveolar macrophage inflammatory cytokine production by interleukin-10. *Clin Immunol Immunopathol.* 1996;80:321-4.
- [68] Zissel G, Schlaak J, Schlaak M, Muller-Quernheim J. Regulation of cytokine release by alveolar macrophages treated with interleukin-4, interleukin-10, or transforming growth factor  $\beta$ . *Eur Cytokine Netw.* 1996;7:59-66.

- [69] Berkman N, John M, Roesems G, Jose PJ, Barnes PJ, Chung KF. Inhibition of macrophage inflammatory protein-1 expression by IL-10. Differential sensitivities in human blood monocytes and alveolar macrophages. *J Immunol.* 1995;155:4412-8.
- [70] Nicod LP, el Habre F, Dayer JM, Boehringer N. Interleukin-10 decreases tumor necrosis factor and in alloreactions induced by human lung dendritic cells and macrophages. *Am J Respir Cell Mol Biol.* 1995;13:83-90.
- [71] de Waal Malefyt R, Abrams J, Bennett B, Figdor CG, de Vries JE. Interleukin 10(IL-10) inhibits cytokine synthesis by human monocytes: an autoregulatory role of IL-10 produced by monocytes. *J Exp Med.* 1991;174:1209-20.
- [72] Fiorentino DF, Zlotnik A, Mosmann TR, Howard M, O'Garra A. IL-10 inhibits cytokine production by activated macrophages. *J Immunol.* 1991;147:3815-22.
- [73] de Waal Malefyt R, Figdor CG, Huijbens R, Mohan-Peterson S, Bennett B, Culpepper J. Effects of IL-13 on phenotype, cytokine production, and cytotoxic function of human monocytes. Comparison with IL-4 and modulation by IFN- or IL-10. *J Immunol.* 1993;151:6370-81.
- [74] D'Andrea A, Aste-Amezaga M, Valiante NM, Ma X, Kubin M, Trinchieri G. Interleukin 10 (IL-10) inhibits human lymphocyte interferon -production by suppressing natural killer cell stimulatory factor/IL-12 synthesis in accessory cells. *J Exp Med.* 1993;178:1041-8.
- [75] Gruber MF, Williams CC, Gerrard TL. Macrophage-colony-stimulating factor expression by anti-CD45 stimulated human monocytes is transcriptionally up-regulated by IL-1 and inhibited by IL-4 and IL-10. *J Immunol.* 1994;152:1354-61.
- [76] Rossi DL, Vicari AP, Franz-Bacon K, McClanahan TK, Zlotnik A. Identification through bioinformatics of two new macrophage proinflammatory human chemokines: MIP-3 and MIP-3 . *J Immunol.* 1997;158:1033-6.
- [77] Marfaing-Koka A, Maravic M, Humbert M, Galanaud P, Emilie D. Contrasting effects of IL-4, IL-10 and corticosteroids on RANTES production by human monocytes. *Int Immunol.* 1996;8:1587-94.
- [78] Kopydlowski KM, Salkowski CA, Cody MJ, van Rooijen N, Major J, Hamilton TA. Regulation of macrophage chemokine expression by lipopolysaccharide in vitro and in vivo. *J Immunol.* 1999;163:1537-44.
- [79] Hart PH, Hunt EK, Bonder CS, Watson CJ, Finlay-Jones JJ. Regulation of surface and soluble TNF receptor expression on human monocytes and synovial fluid macrophages by IL-4 and IL-10. *J Immunol.* 1996;157:3672-80.

- [80] Joyce DA, Steer JH. IL-4, IL-10 and IFN- have distinct, but interacting, effects on differentiation-induced changes in TNF- and TNF receptor release by cultured human monocytes. *Cytokine*. 1996;8:49-57.
- [81] Zhao SP, Zeng LH. Elevated plasma levels of tumor necrosis factor in chronic heart failure with cachexia. *Int J Cardiol*. 1997;58:257-61.
- [82] Dickensheets HL, Freeman SL, Smith MF, Donnelly RP. Interleukin-10 upregulates tumor necrosis factor receptor type-II (p75) gene expression in endotoxin-stimulated human monocytes. *Blood*. 1997;90:4162-71.
- [83] Jenkins JK, Malyak M, Arend WP. The effects of interleukin-10 on interleukin-1 receptor antagonist and interleukin-1 production in human monocytes and neutrophils. *Lymphokine Cytokine Res*. 1994;13:47-54.
- [84] Dickensheets HL, Donnelly RP. IFN- and IL-10 inhibit induction of IL-1 receptor type I and type II gene expression by IL-4 and IL-13 in human monocytes. *J Immunol*. 1997;159:6226-33.
- [85] Mosser DM, Zhang X. Interleukin-10: new perspectives on an old cytokine. *Immunol Rev*. 2008;226:205-18.
- [86] Akdis CA, Blaser K. Mechanisms of interleukin-10-mediated immune suppression. *Immunology*. 2001;103:131-6.
- [87] Zhang YC, Pileggi A, Agarwal A, Molano RD, Powers M, Brusko T. Adeno-associated virus-mediated IL-10 gene therapy inhibits diabetes recurrence in syngeneic islet cell transplantation of NOD mice. *Diabetes*. 2003;52:708-16.
- [88] Al-Robaee AA, Al-Zolibani AA, Al-Shobili HA, Kazamel A, Settin A. IL-10 implications in psoriasis. *Int J Health Sci (Qassim)*. 2008;2:53-8.
- [89] Asadullah K, Sterry W, Volk HD. Interleukin-10 therapy--review of a new approach. *Pharmacol Rev*. 2003;55:241-69.
- [90] Ruan S, Tate C, Lee JJ, Ritter T, Kolls JK, Shellito JE. Local delivery of the viral interleukin-10 gene suppresses tissue inflammation in murine *Pneumocystis carinii* infection. *Infect Immun*. 2002;70:6107-13.
- [91] Bhavsar MD, Amiji MM. Oral IL-10 gene delivery in a microsphere-based formulation for local transfection and therapeutic efficacy in inflammatory bowel disease. *Gene Ther*. 2008;15:1200-9.
- [92] Cao Y. Therapeutic angiogenesis for ischemic disorders: what is missing for clinical benefits? *Discov Med*. 2010;9:179-84.
- [93] Boutin AT, Weidemann A, Fu Z, Mesropian L, Gradin K, Jamora C. Epidermal sensing of oxygen is essential for systemic hypoxic response. *Cell*. 2008;133:223-34.

- [94] Cao Y. Monotherapy versus combination therapy of angiogenic and arteriogenic factors for the treatment of ischemic disorders. *Curr Mol Med.* 2009;9:967-72.
- [95] Cao Y, Hong A, Schulten H, Post MJ. Update on therapeutic neovascularization. *Cardiovasc Res.* 2005;65:639-48.
- [96] Makino Y, Cao R, Svensson K, Bertilsson G, Asman M, Tanaka H. Inhibitory PAS domain protein is a negative regulator of hypoxia-inducible gene expression. *Nature.* 2001;414:550-4.
- [97] Lendahl U, Lee KL, Yang H, Poellinger L. Generating specificity and diversity in the transcriptional response to hypoxia. *Nat Rev Genet.* 2009;10:821-32.
- [98] Eriksson A, Cao R, Pawliuk R, Berg SM, Tsang M, Zhou D. Placenta growth factor-1 antagonizes VEGF-induced angiogenesis and tumor growth by the formation of functionally inactive PlGF-1/VEGF heterodimers. *Cancer Cell.* 2002;1:99-108.
- [99] Senger DR, Galli SJ, Dvorak AM, Perruzzi CA, Harvey VS, Dvorak HF. Tumor cells secrete a vascular permeability factor that promotes accumulation of ascites fluid. *Science.* 1983;219:983-5.
- [100] Zou WG, Wang DS, Lang MF, Jin DY, Xu DH, Zheng ZC. Human interleukin 10 gene therapy decreases the severity and mortality of lethal pancreatitis in rats. *J Surg Res.* 2002;103:121-6.
- [101] Hung KS, Lee TH, Chou WY, Wu CL, Cho CL, Lu CN. Interleukin-10 gene therapy reverses thioacetamide-induced liver fibrosis in mice. *Biochem Biophys Res Commun.* 2005;336:324-31.
- [102] Bessis N, Doucet C, Cottard V, Douar AM, Firat H, Jorgensen C. Gene therapy for rheumatoid arthritis. *J Gene Med.* 2002;4:581-91.
- [103] Holladay CA, Duffy AM, Chen X, Sefton MV, O'Brien TD, Pandit AS. Recovery of cardiac function mediated by MSC and interleukin-10 plasmid functionalised scaffold. *Biomaterials.* 2012;33:1303-14.
- [104] Hong YS, Laks H, Cui G, Chong T, Sen L. Localized immunosuppression in the cardiac allograft induced by a new liposome-mediated IL-10 gene therapy. *J Heart Lung Transplant.* 2002;21:1188-200.
- [105] Chen B, Kapturczak MH, Joseph R, George JF, Campbell-Thompson M, Wasserfall CH. Adeno-associated viral vector-mediated interleukin-10 prolongs allograft survival in a rat kidney transplantation model. *Am J Transplant.* 2007;7:1112-20.
- [106] Yoshioka T, Okada T, Maeda Y, Ikeda U, Shimpo M, Nomoto T. Adeno-associated virus vector-mediated interleukin-10 gene transfer inhibits atherosclerosis in apolipoprotein E-deficient mice. *Gene Ther.* 2004;11:1772-9.
- [107] Zhang X, Mao Z, Yu C. Suppression of early experimental osteoarthritis by gene transfer of interleukin-1 receptor antagonist and interleukin-10. *J Orthop Res.* 2004;22:742-50.

- [108] Carmody EE, Schwarz EM, Puzas JE, Rosier RN, O'Keefe RJ. Viral interleukin-10 gene inhibition of inflammation, osteoclastogenesis, and bone resorption in response to titanium particles. *Arthritis Rheum*. 2002;46:1298-308.
- [109] Ooboshi H, Ibayashi S, Shichita T, Kumai Y, Takada J, Ago T. Postischemic gene transfer of interleukin-10 protects against both focal and global brain ischemia. *Circulation*. 2005;111:913-9.
- [110] Namiki M, Kawashima S, Yamashita T, Ozaki M, Sakoda T, Inoue N. Intramuscular gene transfer of interleukin-10 cDNA reduces atherosclerosis in apolipoprotein E-knockout mice. *Atherosclerosis*. 2004;172:21-9.
- [111] Folkman J. Angiogenesis in cancer, vascular, rheumatoid and other disease. *Nat Med*. 1995;1:27-31.
- [112] Cao R, Brakenhielm E, Pawliuk R, Wariaro D, Post MJ, Wahlberg E. Angiogenic synergism, vascular stability and improvement of hind-limb ischemia by a combination of PDGF-BB and FGF-2. *Nat Med*. 2003;9:604-13.
- [113] Wallez Y, Vilgrain I, Huber P. Angiogenesis: the VE-cadherin switch. *Trends Cardiovasc Med*. 2006;16:55-9.
- [114] Carmeliet P, Jain RK. Molecular mechanisms and clinical applications of angiogenesis. *Nature*. 2011;473:298-307.
- [115] van Weel V, van Tongeren RB, van Hinsbergh VW, van Bockel JH, Quax PH. Vascular growth in ischemic limbs: a review of mechanisms and possible therapeutic stimulation. *Ann Vasc Surg*. 2008;22:582-97.
- [116] Pugh CW, Ratcliffe PJ. Regulation of angiogenesis by hypoxia: role of the HIF system. *Nat Med*. 2003;9:677-84.
- [117] Chen L, Endler A, Shibasaki F. Hypoxia and angiogenesis: regulation of hypoxia-inducible factors via novel binding factors. *Exp Mol Med*. 2009;41:849-57.
- [118] Hickey MM, Simon MC. Regulation of angiogenesis by hypoxia and hypoxia-inducible factors. *Curr Top Dev Biol*. 2006;76:217-57.
- [119] Tung JJ, Tattersall IW, Kitajewski J. Tips, Stalks, Tubes: Notch-mediated cell fate determination and mechanisms of tubulogenesis during angiogenesis. *Cold Spring Harb Perspect Med*. 2012;2.
- [120] Lamallice L, Le Boeuf F, Huot J. Endothelial cell migration during angiogenesis. *Circ Res*. 2007;100:782-94.
- [121] Hellstrom M, Phng LK, Gerhardt H. VEGF and Notch signaling: the yin and yang of angiogenic sprouting. *Cell Adh Migr*. 2007;1:133-6.
- [122] Papetti M, Herman IM. Mechanisms of normal and tumor-derived angiogenesis. *Am J Physiol Cell Physiol*. 2002;282:C947-70.

- [123] Arany Z, Foo SY, Ma Y, Ruas JL, Bommi-Reddy A, Girnun G. HIF-independent regulation of VEGF and angiogenesis by the transcriptional coactivator PGC-1. *Nature*. 2008;451:1008-12.
- [124] Duda DG, Fukumura D, Jain RK. Role of eNOS in neovascularization: NO for endothelial progenitor cells. *Trends Mol Med*. 2004;10:143-5.
- [125] Moncada S, Higgs A. The L-arginine-nitric oxide pathway. *N Engl J Med*. 1993;329:2002-12.
- [126] Fukumura D, Xavier R, Sugiura T, Chen Y, Park EC, Lu N. Tumor induction of VEGF promoter activity in stromal cells. *Cell*. 1998;94:715-25.
- [127] Lala PK, Chakraborty C. Role of nitric oxide in carcinogenesis and tumour progression. *Lancet Oncol*. 2001;2:149-56.
- [128] Oliveira CJ, Schindler F, Ventura AM, Morais MS, Arai RJ, Debbas V. Nitric oxide and cGMP activate the Ras-MAP kinase pathway-stimulating protein tyrosine phosphorylation in rabbit aortic endothelial cells. *Free Radic Biol Med*. 2003;35:381-96.
- [129] Jones MK, Tsugawa K, Tarnawski AS, Baatar D. Dual actions of nitric oxide on angiogenesis: possible roles of PKC, ERK, and AP-1. *Biochem Biophys Res Commun*. 2004;318:520-8.
- [130] Rossig L, Fichtlscherer B, Breitschopf K, Haendeler J, Zeiher AM, Mulsch A. Nitric oxide inhibits caspase-3 by S-nitrosation in vivo. *The Journal of biological chemistry*. 1999;274:6823-6.
- [131] Kim YM, Talanian RV, Billiar TR. Nitric oxide inhibits apoptosis by preventing increases in caspase-3-like activity via two distinct mechanisms. *J Biol Chem*. 1997;272:31138-48.
- [132] Shizukuda Y, Tang S, Yokota R, Ware JA. Vascular endothelial growth factor-induced endothelial cell migration and proliferation depend on a nitric oxide-mediated decrease in protein kinase C $\delta$  activity. *Circ Res*. 1999;85:247-56.
- [133] Faneca H, Simoes S, de Lima MC. Evaluation of lipid-based reagents to mediate intracellular gene delivery. *Biochim Biophys Acta*. 2002;1567:23-33.
- [134] Kawasaki K, Smith RS, Jr., Hsieh CM, Sun J, Chao J, Liao JK. Activation of the phosphatidylinositol 3-kinase/protein kinase Akt pathway mediates nitric oxide-induced endothelial cell migration and angiogenesis. *Mol Cell Biol*. 2003;23:5726-37.
- [135] Ridnour LA, Isenberg JS, Espey MG, Thomas DD, Roberts DD, Wink DA. Nitric oxide regulates angiogenesis through a functional switch involving thrombospondin-1. *Proc Natl Acad Sci U S A*. 2005;102:13147-52.
- [136] Lopez-Rivera E, Lizarbe TR, Martinez-Moreno M, Lopez-Novoa JM, Rodriguez-Barbero A, Rodrigo J. Matrix metalloproteinase 13 mediates nitric oxide activation of endothelial cell migration. *Proc Natl Acad Sci U S A*. 2005;102:3685-90.
- [137] Fukumura D, Kashiwagi S, Jain RK. The role of nitric oxide in tumour progression. *Nat Rev Cancer*. 2006;6:521-34.

- [138] Chen AF, Ren J, Miao CY. Nitric oxide synthase gene therapy for cardiovascular disease. *Jpn J Pharmacol.* 2002;89:327-36.
- [139] O'Connor DM, O'Brien T. Nitric oxide synthase gene therapy: progress and prospects. *Expert Opin Biol Ther.* 2009;9:867-78.
- [140] Heise RL, Ivanova J, Parekh A, Sacks MS. Generating elastin-rich small intestinal submucosa-based smooth muscle constructs utilizing exogenous growth factors and cyclic mechanical stimulation. *Tissue Eng Part A.* 2009;15:3951-60.
- [141] Shapiro SD, Endicott SK, Province MA, Pierce JA, Campbell EJ. Marked longevity of human lung parenchymal elastic fibers deduced from prevalence of D-aspartate and nuclear weapons-related radiocarbon. *J Clin Invest.* 1991;87:1828-34.
- [142] Mithieux SM, Weiss AS. Elastin. *Adv Protein Chem.* 2005;70:437-61.
- [143] Jung S, Rutka JT, Hinek A. Tropoelastin and elastin degradation products promote proliferation of human astrocytoma cell lines. *J Neuropathol Exp Neurol.* 1998;57:439-48.
- [144] Faury G, Garnier S, Weiss AS, Wallach J, Fulop T, Jr., Jacob MP. Action of tropoelastin and synthetic elastin sequences on vascular tone and on free Ca<sup>2+</sup> level in human vascular endothelial cells. *Circ Res.* 1998;82:328-36.
- [145] Mochizuki S, Brassart B, Hinek A. Signaling pathways transduced through the elastin receptor facilitate proliferation of arterial smooth muscle cells. *J Biol Chem.* 2002;277:44854-63.
- [146] Lisa NS, Weiss A. Elastin based constructs. *Regen Med Tissue Eng Biomater.* 2011:323-40.
- [147] Namba T, Koike H, Murakami K, Aoki M, Makino H, Hashiya N. Angiogenesis induced by endothelial nitric oxide synthase gene through vascular endothelial growth factor expression in a rat hindlimb ischemia model. *Circulation.* 2003;108:2250-7.
- [148] Iwata A, Sai S, Nitta Y, Chen M, de Fries-Hallstrand R, Dalesandro J. Liposome-mediated gene transfection of endothelial nitric oxide synthase reduces endothelial activation and leukocyte infiltration in transplanted hearts. *Circulation.* 2001;103:2753-9.
- [149] Kulkarni M, O'Loughlin A, Vazquez R, Mashayekhi K, Rooney P, Greiser U, O'Toole E, O'Brien T, Malagon M.M, Pandit A. Use of a fibrin-based system for enhancing angiogenesis and modulating inflammation in the treatment of hyperglycemic wounds. *Biomaterials.* 2014;35:2001-10.
- [150] Smith RS, Jr., Lin KF, Agata J, Chao L, Chao J. Human endothelial nitric oxide synthase gene delivery promotes angiogenesis in a rat model of hindlimb ischemia. *Arterioscler Thromb Vasc Biol.* 2002;22:1279-85.
- [151] Brevetti LS, Chang DS, Tang GL, Sarkar R, Messina LM. Overexpression of endothelial nitric oxide synthase increases skeletal muscle blood flow and oxygenation in severe rat hind limb ischemia. *J Vasc Surg.* 2003;38:820-6.

- [152] Luo JD, Wang YY, Fu WL, Wu J, Chen AF. Gene therapy of endothelial nitric oxide synthase and manganese superoxide dismutase restores delayed wound healing in type 1 diabetic mice. *Circulation*. 2004;110:2484-93.
- [153] Breen AM, Dockery P, O'Brien T, Pandit AS. The use of therapeutic gene eNOS delivered via a fibrin scaffold enhances wound healing in a compromised wound model. *Biomaterials*. 2008;29:3143-51.
- [154] Magee TR, Ferrini M, Garban HJ, Vernet D, Mitani K, Rajfer J. Gene therapy of erectile dysfunction in the rat with penile neuronal nitric oxide synthase. *Biol Reprod*. 2002;67:1033-41.
- [155] Onoue H, Tsutsui M, Smith L, Stelter A, O'Brien T, Katusic ZS. Expression and function of recombinant endothelial nitric oxide synthase gene in canine basilar artery after experimental subarachnoid hemorrhage. *Stroke*. 1998;29:1959-65.
- [156] Sharif F, Hynes SO, Cooney R, Howard L, McMahon J, Daly K. Gene-eluting stents: adenovirus-mediated delivery of eNOS to the blood vessel wall accelerates re-endothelialization and inhibits restenosis. *Mol Ther*. 2008;16:1674-80.
- [157] Savard S, Lavoie P, Villeneuve C, Agharazii M, Lebel M, Lariviere R. eNOS gene delivery prevents hypertension and reduces renal failure and injury in rats with reduced renal mass. *Nephrol Dial Transplant*. 2012;27:2182-90.
- [158] Almine JF, Bax DV, Mithieux SM, Nivison-Smith L, Rnjak J, Waterhouse A. Elastin-based materials. *Chem Soc Rev*. 2010;39:3371-9.
- [159] Floss DM, Schallau K, Rose-John S, Conrad U, Scheller J. Elastin-like polypeptides revolutionize recombinant protein expression and their biomedical application. *Trends Biotechnol*. 2010;28:37-45.
- [160] Chilkoti A, Christensen T, MacKay JA. Stimulus responsive elastin biopolymers: Applications in medicine and biotechnology. *Curr Opin Chem Biol*. 2006;10:652-7.
- [161] Kim W, Chaikof EL. Recombinant elastin-mimetic biomaterials: Emerging applications in medicine. *Adv Drug Delivery Rev*. 2010;62:1468-78.
- [162] Rodriguez-Cabello JC, Javier Reguera, Alessandra Girotti, Matilde Alonso, Testera AM. Developing functionality in elastin-like polymers by increasing their molecular complexity: the power of the genetic engineering approach. *Prog. Polym Sci*. 2005:1119-45.
- [163] van Hest JC, Tirrell DA. Protein-based materials, toward a new level of structural control. *Chem Commun (Camb)*. 2001:1897-904.
- [164] Urry DW, Shaw RG, Prasad KU. Polypentapeptide of elastin: temperature dependence of ellipticity and correlation with elastomeric force. *Biochem Biophys Res Commun*. 1985;130:50-7.

- [165] Urry DW, Hugel T, Seitz M, Gaub HE, Sheiba L, Dea J. Elastin: a representative ideal protein elastomer. *Philos Trans R Soc Lond B Biol Sci.* 2002;357:169-84.
- [166] Wu X, Sallach R, Haller CA, Caves JA, Nagapudi K, Conticello VP. Alterations in physical cross-linking modulate mechanical properties of two-phase protein polymer networks. *Biomacromolecules.* 2005;6:3037-44.
- [167] Nagapudi K, Brinkman WT, Thomas BS, Park JO, Srinivasarao M, Wright E. Viscoelastic and mechanical behavior of recombinant protein elastomers. *Biomaterials.* 2005;26:4695-706.
- [168] Wu X, Sallach RE, Caves JM, Conticello VP, Chaikof EL. Deformation responses of a physically cross-linked high molecular weight elastin-like protein polymer. *Biomacromolecules.* 2008;9:1787-94.
- [169] Rodríguez-Cabello, M. Alonso, L. Guiscardo, V. Rebotto, Girotti A. Amplified photoresponse of a p-phenylazobenzene derivative of an elastin-like polymer by  $\alpha$ -cyclodextrin: the amplified Tt mechanism. *Adv Mater.* 2002;14:1151-4.
- [170] Wright ER, Conticello VP. Self-assembly of block copolymers derived from elastin-mimetic polypeptide sequences. *Adv Drug Delivery Rev.* 2002;54:1057-73.
- [171] Urry DW, Parker TM. Mechanics of elastin: molecular mechanism of biological elasticity and its relationship to contraction. *J Muscle Res Cell Motil.* 2002;23:543-59.
- [172] Vrhovski B, Weiss AS. Biochemistry of tropoelastin. *Eur J Biochem.* 1998;258:1-18.
- [173] Lee J, Macosko CW, Urry DW. Elastomeric polypentapeptides cross-linked into matrixes and fibers. *Biomacromolecules.* 2001;2:170-9.
- [174] Kagan HM, Tseng L, Trackman PC, Okamoto K, Rapaka RS, Urry DW. Repeat polypeptide models of elastin as substrates for lysyl oxidase. *J Biol Chem.* 1980;255:3656-9.
- [175] Bellingham CM, Lillie MA, Gosline JM, Wright GM, Starcher BC, Bailey AJ. Recombinant human elastin polypeptides self-assemble into biomaterials with elastin-like properties. *Biopolymers.* 2003;70:445-55.
- [176] Lim DW, Nettles DL, Setton LA, Chilkoti A. In situ cross-linking of elastin-like polypeptide block copolymers for tissue repair. *Biomacromolecules.* 2008;9:222-30.
- [177] Dash BC, Mahor S, Carroll O, Mathew A, Wang W, Woodhouse KA, Pandit A. Tunable elastin-like polypeptide hollow sphere as a high payload and controlled delivery gene depot. *J Control Release.* 2011;152:382-92.
- [178] Kataoka K, Harada A, Nagasaki Y. Block copolymer micelles for drug delivery: design, characterization and biological significance. *Adv Drug Delivery Rev.* 2001;47:113-31.
- [179] Chiellini F, Piras AM, Errico C, Chiellini E. Micro/nanostructured polymeric systems for biomedical and pharmaceutical applications. *Nanomedicine (Lond).* 2008;3:367-93.

- [180] Kwon GS, Okano T. Soluble self-assembled block copolymers for drug delivery. *Pharm Res.* 1999;16:597-600.
- [181] Nettles DL, Chilkoti A, Setton LA. Applications of elastin-like polypeptides in tissue engineering. *Adv Drug Delivery Rev.* 2010;62:1479-85.
- [182] Chen TH, Bae Y, Furgeson DY, Kwon GS. Biodegradable hybrid recombinant block copolymers for non-viral gene transfection. *Int J Pharm.* 2012;427:105-12.
- [183] Chen TH, Bae Y, Furgeson DY. Intelligent biosynthetic nanobiomaterials (IBNs) for hyperthermic gene delivery. *Pharm Res.* 2008;25:683-91.
- [184] Lee S, Kim JS, Chu HS, Kim GW, Won JI, Jang JH. Electrospun nanofibrous scaffolds for controlled release of adeno-associated viral vectors. *Acta Biomater.* 2011;7:3868-76.
- [185] Kim JS, Chu HS, Park KI, Won JI, Jang JH. Elastin-like polypeptide matrices for enhancing adeno-associated virus-mediated gene delivery to human neural stem cells. *Gene Ther.* 2012;19:329-37.
- [186] Wu Y, MacKay JA, McDaniel JR, Chilkoti A, Clark RL. Fabrication of elastin-like polypeptide nanoparticles for drug delivery by electrospraying. *Biomacromolecules.* 2009;10:19-24.
- [187] Kim W, Thevenot J, Ibarboure E, Lecommandoux S, Chaikof EL. Self-assembly of thermally responsive amphiphilic diblock copolypeptides into spherical micellar nanoparticles. *Angew Chem Int Ed Engl.* 2010;49:4257-60.
- [188] Herrero-Vanrell R, Rincon AC, Alonso M, Reboto V, Molina-Martinez IT, Rodriguez-Cabello JC. Self-assembled particles of an elastin-like polymer as vehicles for controlled drug release. *J Control Release.* 2005;102:113-22.
- [189] Machado R, Bessa PC, Reis RL, Rodriguez-Cabello JC, Casal M. Elastin-based nanoparticles for delivery of bone morphogenetic proteins. *Methods Mol Biol.* 2012;906:353-63.
- [190] Bessa PC, Machado R, Nurnberger S, Dopler D, Banerjee A, Cunha AM. Thermoresponsive self-assembled elastin-based nanoparticles for delivery of BMPs. *J Control Release.* 2010;142:312-8.
- [191] Huang HC, Yang Y, Nanda A, Koria P, Rege K. Synergistic administration of photothermal therapy and chemotherapy to cancer cells using polypeptide-based degradable plasmonic matrices. *Nanomedicine (Lond).* 2011;6:459-73.
- [192] Huang HC, Koria P, Parker SM, Selby L, Megeed Z, Rege K. Optically responsive gold nanorod-polypeptide assemblies. *Langmuir.* 2008;24:14139-44.
- [193] Fujita Y, Mie M, Kobatake E. Construction of nanoscale protein particle using temperature-sensitive elastin-like peptide and polyaspartic acid chain. *Biomaterials.* 2009;30:3450-7.
- [194] Trabbic-Carlson K, Setton LA, Chilkoti A. Swelling and mechanical behaviors of chemically cross-linked hydrogels of elastin-like polypeptides. *Biomacromolecules.* 2003;4:572-80.

- [195] Asai D, Xu D, Liu W, Garcia Quiroz F, Callahan DJ, Zalutsky MR. Protein polymer hydrogels by in situ, rapid and reversible self-gelation. *Biomaterials*. 2012;33:5451-8.
- [196] Amruthwar SS, Janorkar AV. Preparation and characterization of elastin-like polypeptide scaffolds for local delivery of antibiotics and proteins. *J Mater Sci Mater Med*. 2012;23:2903-12.
- [197] Adams SB, Jr., Shamji MF, Nettles DL, Hwang P, Setton LA. Sustained release of antibiotics from injectable and thermally responsive polypeptide depots. *J Biomed Mater Res B Appl Biomater*. 2009;90:67-74.
- [198] Nettles DL, Kitaoka K, Hanson NA, Flahiff CM, Mata BA, Hsu EW. In situ crosslinking elastin-like polypeptide gels for application to articular cartilage repair in a goat osteochondral defect model. *Tissue Eng Part A*. 2008;14:1133-40.
- [199] McHale MK, Setton LA, Chilkoti A. Synthesis and in vitro evaluation of enzymatically cross-linked elastin-like polypeptide gels for cartilaginous tissue repair. *Tissue Eng*. 2005;11:1768-79.
- [200] Betre H, Ong SR, Guilak F, Chilkoti A, Fermor B, Setton LA. Chondrocytic differentiation of human adipose-derived adult stem cells in elastin-like polypeptide. *Biomaterials*. 2006;27:91-9.
- [201] Leckie AE, Akens MK, Woodhouse KA, Yee AJ, Whyne CM. Evaluation of thiol-modified hyaluronan and elastin-like polypeptide composite augmentation in early-stage disc degeneration: comparing 2 minimally invasive techniques. *Spine*. 2012;37:E1296-303.
- [202] Amruthwar SS, Janorkar AV. In vitro evaluation of elastin-like polypeptide-collagen composite scaffold for bone tissue engineering. *Dent Mater*. 2012.
- [203] Nettles DL, Chilkoti A, Setton LA. Early metabolite levels predict long-term matrix accumulation for chondrocytes in elastin-like polypeptide biopolymer scaffolds. *Tissue Eng Part A*. 2009;15:2113-21.
- [204] Hrabchak C, Rouleau J, Moss I, Woodhouse K, Akens M, Bellingham C. Assessment of biocompatibility and initial evaluation of genipin cross-linked elastin-like polypeptides in the treatment of an osteochondral knee defect in rabbits. *Acta Biomater*. 2010;6:2108-15.
- [205] Blit PH, Battiston KG, Yang M, Paul Santerre J, Woodhouse KA. Electrospun elastin-like polypeptide enriched polyurethanes and their interactions with vascular smooth muscle cells. *Acta Biomater*. 2012;8:2493-503.
- [206] Caves JM, Cui W, Wen J, Kumar VA, Haller CA, Chaikof EL. Elastin-like protein matrix reinforced with collagen microfibers for soft tissue repair. *Biomaterials*. 2011;32:5371-9.
- [207] McDaniel JR, Callahan DJ, Chilkoti A. Drug delivery to solid tumors by elastin-like polypeptides. *Adv Drug Delivery Rev*. 2010;62:1456-67.
- [208] Kim W, Brady C, Chaikof EL. Amphiphilic protein micelles for targeted in vivo imaging. *Acta Biomater*. 2012;8:2476-82.

- [209] Callahan DJ, Liu W, Li X, Dreher MR, Hassouneh W, Kim M. Triple stimulus-responsive polypeptide nanoparticles that enhance intratumoral spatial distribution. *Nano Lett.* 2012;12:2165-70.
- [210] Simnick AJ, Amiram M, Liu W, Hanna G, Dewhirst MW, Kontos CD. In vivo tumor targeting by a NGR-decorated micelle of a recombinant diblock copolypeptide. *J Control Release.* 2011;155:144-51.
- [211] McDaniel JR, Macewan SR, Dewhirst M, Chilkoti A. Doxorubicin-conjugated chimeric polypeptide nanoparticles that respond to mild hyperthermia. *J Control Release.* 2012;159:362-7.
- [212] Simnick AJ, Valencia CA, Liu R, Chilkoti A. Morphing low-affinity ligands into high-avidity nanoparticles by thermally triggered self-assembly of a genetically encoded polymer. *ACS Nano.* 2010;4:2217-27.
- [213] Ghoorchian A, Vandemark K, Freeman K, Kambow S, Holland NB, Strelitzky KA. Size and shape characterization of thermoreversible micelles of three-armed star elastin-like polypeptides. *J Phys Chem B.* 2013;117:8865-74.
- [214] Garcia-Arevalo C, Bermejo-Martin JF, Rico L, Iglesias V, Martin L, Rodriguez-Cabello JC. Immunomodulatory nanoparticles from elastin-like recombinamers: single-molecules for tuberculosis vaccine development. *Mol Pharm.* 2013;10:586-97.
- [215] Costa RR, Custodio CA, Arias FJ, Rodriguez-Cabello JC, Mano JF. Nanostructured and thermoresponsive recombinant biopolymer-based microcapsules for the delivery of active molecules. *Nanomedicine.* 2013;9:895-902.
- [216] Osborne JL, Farmer R, Woodhouse KA. Self-assembled elastin-like polypeptide particles. *Acta Biomater.* 2008;4:49-57.
- [217] Shamji MF, Whitlatch L, Friedman AH, Richardson WJ, Chilkoti A, Setton LA. An injectable and in situ-gelling biopolymer for sustained drug release following perineural administration. *Spine.* 2008;33:748-54.
- [218] Hart DS, Gehrke SH. Thermally associating polypeptides designed for drug delivery produced by genetically engineered cells. *J Pharm Sci.* 2007;96:484-516.
- [219] Patel NU, Purser CA, Baker RC, Janorkar AV. Effect of processing temperature on the morphology and drug-release characteristics of elastin-like polypeptide-collagen composite coatings. *Biomacromolecules.* 2013;14:2891-9.
- [220] Krishna UM, Martinez AW, Caves JM, Chaikof EL. Hydrazone self-crosslinking of multiphase elastin-like block copolymer networks. *Acta Biomater.* 2012;8:988-97.
- [221] Zilberman M, Shifrovitch Y, Aviv M, Hershkovitz M. Structured drug-eluting bioresorbable films: microstructure and release profile. *J Biomater Appl.* 2009;23:385-406.

- [222] Kawatsu S, Oda K, Saiki Y, Tabata Y, Tabayashi K. External application of rapamycin-eluting film at anastomotic sites inhibits neointimal hyperplasia in a canine model. *Ann Thorac Surg.* 2007;84:560-7; discussion 7.
- [223] Park TG, Jeong JH, Kim SW. Current status of polymeric gene delivery systems. *Adv Drug Delivery Rev.* 2006;58:467-86.
- [224] Friedmann T. A brief history of gene therapy. *Nat Genet.* 1992;2:93-8.
- [225] Blau H, Khavari P. Gene therapy: progress, problems, prospects. *Nat Med.* 1997;3:612-3.
- [226] Khan TA, Sellke FW, Laham RJ. Gene therapy progress and prospects: therapeutic angiogenesis for limb and myocardial ischemia. *Gene Ther.* 2003;10:285-91.
- [227] Park HJ, Yang F, Cho SW. Nonviral delivery of genetic medicine for therapeutic angiogenesis. *Adv Drug Delivery Rev.* 2012;64:40-52.
- [228] Hedman M, Hartikainen J, Yla-Herttuala S. Progress and prospects: hurdles to cardiovascular gene therapy clinical trials. *Gene Ther.* 2011;18:743-9.
- [229] Malecki M, Kolsut P, Proczka R. Angiogenic and antiangiogenic gene therapy. *Gene Ther.* 2005;12 Suppl 1:S159-69.
- [230] Giacca M. Virus-mediated gene transfer to induce therapeutic angiogenesis: where do we stand? *Int J Nanomedicine.* 2007;2:527-40.
- [231] Guzman RJ, Lemarchand P, Crystal RG, Epstein SE, Finkel T. Efficient gene transfer into myocardium by direct injection of adenovirus vectors. *Circ Res.* 1993;73:1202-7.
- [232] Fisher KJ, Jooss K, Alston J, Yang Y, Haecker SE, High K. Recombinant adeno-associated virus for muscle directed gene therapy. *Nat Med.* 1997;3:306-12.
- [233] Brunetti-Pierri N, Ng P. Progress and prospects: gene therapy for genetic diseases with helper-dependent adenoviral vectors. *Gene Ther.* 2008;15:553-60.
- [234] St George JA. Gene therapy progress and prospects: adenoviral vectors. *Gene Ther.* 2003;10:1135-41.
- [235] Tafuro S, Ayuso E, Zacchigna S, Zentilin L, Moimas S, Dore F. Inducible adeno-associated virus vectors promote functional angiogenesis in adult organisms via regulated vascular endothelial growth factor expression. *Cardiovasc Res.* 2009;83:663-71.
- [236] Madonna R, Rokosh G. Insights into gene therapy for critical limb ischemia: the devil is in the details. *Vasc Pharmacol.* 2012;57:10-4.
- [237] Rivard A, Silver M, Chen D, Kearney M, Magner M, Annex B, et al. Rescue of diabetes-related impairment of angiogenesis by intramuscular gene therapy with adeno-VEGF. *Am J Pathol.* 1999;154:355-63.

- [238] Rey S, Lee K, Wang CJ, Gupta K, Chen S, McMillan A. Synergistic effect of HIF-1 gene therapy and HIF-1-activated bone marrow-derived angiogenic cells in a mouse model of limb ischemia. *Proc Natl Acad Sci U S A*. 2009;106:20399-404.
- [239] Favre D, Provost N, Blouin V, Blancho G, Cherel Y, Salvetti A. Immediate and long-term safety of recombinant adeno-associated virus injection into the nonhuman primate muscle. *Mol Ther*. 2001;4:559-66.
- [240] Chen F, Tan Z, Dong CY, Chen X, Guo SF. Adeno-associated virus vectors simultaneously encoding VEGF and angiopoietin-1 enhances neovascularization in ischemic rabbit hind-limbs. *Acta Pharmacol Sin*. 2007;28:493-502.
- [241] Zhang C, Wang KZ, Qiang H, Tang YL, Li Q, Li M. Angiopoiesis and bone regeneration via co-expression of the hVEGF and hBMP genes from an adeno-associated viral vector in vitro and in vivo. *Acta Pharmacol Sin*. 2010;31:821-30.
- [242] Saqib A, Prasad KM, Katwal AB, Sanders JM, Lye RJ, French BA. Adeno-associated virus serotype 9-mediated overexpression of extracellular superoxide dismutase improves recovery from surgical hind-limb ischemia in BALB/c mice. *J Vasc Surg*. 2011;54:810-8.
- [243] Lan RF, Liu ZX, Liu XC, Song YE, Wang DW. CD151 promotes neovascularization and improves blood perfusion in a rat hind-limb ischemia model. *J Endovasc Ther*. 2005;12:469-78.
- [244] Pinkenburg O, Pfosser A, Hinkel R, Bottcher M, Dinges C, Lebherz C. Recombinant adeno-associated virus-based gene transfer of cathelicidin induces therapeutic neovascularization preferentially via potent collateral growth. *Hum Gene Ther*. 2009;20:159-67.
- [245] Shoji T, Yonemitsu Y, Komori K, Tanii M, Itoh H, Sata S. Intramuscular gene transfer of FGF-2 attenuates endothelial dysfunction and inhibits intimal hyperplasia of vein grafts in poor-runoff limbs of rabbit. *Am J Physiol Heart Circ Physiol*. 2003;285:H173-82.
- [246] Ohara N, Koyama H, Miyata T, Hamada H, Miyatake SI, Akimoto M. Adenovirus-mediated ex vivo gene transfer of basic fibroblast growth factor promotes collateral development in a rabbit model of hind limb ischemia. *Gene Ther*. 2001;8:837-45.
- [247] Xie D, Li Y, Reed EA, Odronic SI, Kontos CD, Annex BH. An engineered vascular endothelial growth factor-activating transcription factor induces therapeutic angiogenesis in ApoE knockout mice with hindlimb ischemia. *J Vasc Surg*. 2006;44:166-75.
- [248] Rey S, Luo W, Shimoda LA, Semenza GL. Metabolic reprogramming by HIF-1 promotes the survival of bone marrow-derived angiogenic cells in ischemic tissue. *Blood*. 2011;117:4988-98.
- [249] Sarkar K, Fox-Talbot K, Steenbergen C, Bosch-Marce M, Semenza GL. Adenoviral transfer of HIF-1 enhances vascular responses to critical limb ischemia in diabetic mice. *Proc Natl Acad Sci U S A*. 2009;106:18769-74.

- [250] Bosch-Marce M, Okuyama H, Wesley JB, Sarkar K, Kimura H, Liu YV. Effects of aging and hypoxia-inducible factor-1 activity on angiogenic cell mobilization and recovery of perfusion after limb ischemia. *Circ Res.* 2007;101:1310-8.
- [251] Patel TH, Kimura H, Weiss CR, Semenza GL, Hofmann LV. Constitutively active HIF-1 improves perfusion and arterial remodeling in an endovascular model of limb ischemia. *Cardiovasc Res.* 2005;68:144-54.
- [252] Levanon K, Varda-Bloom N, Greenberger S, Barshack I, Goldberg I, Orenstein A. Vascular wall maturation and prolonged angiogenic effect by endothelial-specific platelet-derived growth factor expression. *Pathobiology.* 2006;73:149-58.
- [253] Huang J, Inoue M, Hasegawa M, Tomihara K, Tanaka T, Chen J. Sendai viral vector mediated angiopoietin-1 gene transfer for experimental ischemic limb disease. *Angiogenesis.* 2009;12:243-9.
- [254] Cristofaro B, Stone OA, Caporali A, Dawbarn D, Ieronimakis N, Reyes M. Neurotrophin-3 is a novel angiogenic factor capable of therapeutic neovascularization in a mouse model of limb ischemia. *Arterioscler Thromb Vasc Biol.* 2010;30:1143-50.
- [255] Ward MR, Thompson KA, Isaac K, Vecchiarelli J, Zhang Q, Stewart DJ. Nitric oxide synthase gene transfer restores activity of circulating angiogenic cells from patients with coronary artery disease. *Mol Ther.* 2011;19:1323-30.
- [256] Islam MA, Park TE, Singh B, Maharjan S, Firdous J, Cho MH. Major degradable polycations as carriers for DNA and siRNA. *J Control Release.* 2014.
- [257] Deveza L, Choi J, Yang F. Therapeutic angiogenesis for treating cardiovascular diseases. *Theranostics.* 2012;2:801-14.
- [258] Qian HS, Liu P, Huw LY, Orme A, Halks-Miller M, Hill SM. Effective treatment of vascular endothelial growth factor refractory hindlimb ischemia by a mutant endothelial nitric oxide synthase gene. *Gene Ther.* 2006;13:1342-50.
- [259] Rabinovsky ED, Draghia-Akli R. Insulin-like growth factor I plasmid therapy promotes in vivo angiogenesis. *Mol Ther.* 2004;9:46-55.
- [260] Kobayashi K, Kondo T, Inoue N, Aoki M, Mizuno M, Komori K. Combination of in vivo angiopoietin-1 gene transfer and autologous bone marrow cell implantation for functional therapeutic angiogenesis. *Arterioscler Thromb Vasc Biol.* 2006;26:1465-72.
- [261] Herweijer H, Wolff JA. Progress and prospects: naked DNA gene transfer and therapy. *Gene Ther.* 2003;10:453-8.
- [262] Wilson BD, Ii M, Park KW, Suli A, Sorensen LK, Larrieu-Lahargue F. Netrins promote developmental and therapeutic angiogenesis. *Science.* 2006;313:640-4.

- [263] Emanuelli C, Salis MB, Pinna A, Graiani G, Manni L, Madeddu P. Nerve growth factor promotes angiogenesis and arteriogenesis in ischemic hindlimbs. *Circulation*. 2002;106:2257-62.
- [264] Hiasa K, Ishibashi M, Ohtani K, Inoue S, Zhao Q, Kitamoto S. Gene transfer of stromal cell-derived factor-1 enhances ischemic vasculogenesis and angiogenesis via vascular endothelial growth factor/endothelial nitric oxide synthase-related pathway: next-generation chemokine therapy for therapeutic neovascularization. *Circulation*. 2004;109:2454-61.
- [265] Kusano KF, Pola R, Murayama T, Curry C, Kawamoto A, Iwakura A. Sonic hedgehog myocardial gene therapy: tissue repair through transient reconstitution of embryonic signaling. *Nat Med*. 2005;11:1197-204.
- [266] Palladino M, Gatto I, Neri V, Straino S, Silver M, Tritarelli A. Pleiotropic beneficial effects of sonic hedgehog gene therapy in an experimental model of peripheral limb ischemia. *Mol Ther*. 2011;19:658-66.
- [267] Green JJ, Langer R, Anderson DG. A combinatorial polymer library approach yields insight into nonviral gene delivery. *Acc Chem Res*. 2008;41:749-59.
- [268] Bechler SL, Lynn DM. Characterization of degradable polyelectrolyte multilayers fabricated using DNA and a fluorescently-labeled poly( -amino ester): shedding light on the role of the cationic polymer in promoting surface-mediated gene delivery. *Biomacromolecules*. 2012;13:542-52.
- [269] Brito L, Little S, Langer R, Amiji M. Poly( -amino ester) and cationic phospholipid-based lipopolyplexes for gene delivery and transfection in human aortic endothelial and smooth muscle cells. *Biomacromolecules*. 2008;9:1179-87.
- [270] Xu P, Li SY, Li Q, Ren J, Van Kirk EA, Murdoch WJ. Biodegradable cationic polyester as an efficient carrier for gene delivery to neonatal cardiomyocytes. *Biotechnol Bioeng*. 2006;95:893-903.
- [271] Nam HY, Nam K, Hahn HJ, Kim BH, Lim HJ, Kim HJ. Biodegradable PAMAM ester for enhanced transfection efficiency with low cytotoxicity. *Biomaterials*. 2009;30:665-73.
- [272] Zaric V, Weltin D, Erbacher P, Remy JS, Behr JP, Stephan D. Effective polyethylenimine-mediated gene transfer into human endothelial cells. *J Gene Med*. 2004;6:176-84.
- [273] Han DK, Jeong SY, Kim YH. Evaluation of blood compatibility of PEO grafted and heparin immobilized polyurethanes. *J Biomed Mater Res*. 1989;23:211-28.
- [274] Jeon O, Yang HS, Lee TJ, Kim BS. Heparin-conjugated polyethylenimine for gene delivery. *J Control Release*. 2008;132:236-42.
- [275] Lee M, Choi D, Choi MJ, Jeong JH, Kim WJ, Oh S. Hypoxia-inducible gene expression system using the erythropoietin enhancer and 3'-untranslated region for the VEGF gene therapy. *J Control Release*. 2006;115:113-9.

- [276] Yockman JW, Choi D, Whitten MG, Chang CW, Kastenmeier A, Erickson H. Polymeric gene delivery of ischemia-inducible VEGF significantly attenuates infarct size and apoptosis following myocardial infarct. *Gene Ther.* 2009;16:127-35.
- [277] Lee M, Rentz J, Bikram M, Han S, Bull DA, Kim SW. Hypoxia-inducible VEGF gene delivery to ischemic myocardium using water-soluble lipopolymer. *Gene Ther.* 2003;10:1535-42.
- [278] Zhang JX, Zalipsky S, Mullah N, Pechar M, Allen TM. Pharmacologic attributes of dioleoylphosphatidylethanolamine/cholesterylhemisuccinate liposomes containing different types of cleavable lipopolymers. *Pharmacol Res.* 2004;49:185-98.
- [279] Zelphati O, Szoka FC, Jr. Mechanism of oligonucleotide release from cationic liposomes. *Proc Natl Acad Sci U S A.* 1996;93:11493-8.
- [280] Anwer K, Kao G, Rolland A, Driessen WH, Sullivan SM. Peptide-mediated gene transfer of cationic lipid/plasmid DNA complexes to endothelial cells. *J Drug Target.* 2004;12:215-21.
- [281] Golda A, Pelisek J, Klocke R, Engelmann MG, Rolland PH, Mekkaoui C. Small poly-L-lysines improve cationic lipid-mediated gene transfer in vascular cells in vitro and in vivo. *J Vasc Res.* 2007;44:273-82.
- [282] Eastman SJ, Siegel C, Tousignant J, Smith AE, Cheng SH, Scheule RK. Biophysical characterization of cationic lipid: DNA complexes. *Biochim Biophys Acta.* 1997;1325:41-62.
- [283] Leong-Poi H, Kuliszewski MA, Lekas M, Sibbald M, Teichert-Kuliszewska K, Klibanov AL. Therapeutic arteriogenesis by ultrasound-mediated VEGF<sub>165</sub> plasmid gene delivery to chronically ischemic skeletal muscle. *Circ Res.* 2007;101:295-303.
- [284] Bekeredjian R, Chen S, Frenkel PA, Grayburn PA, Shohet RV. Ultrasound-targeted microbubble destruction can repeatedly direct highly specific plasmid expression to the heart. *Circulation.* 2003;108:1022-6.
- [285] Torchilin VP, Levchenko TS, Rammohan R, Volodina N, Papahadjopoulos-Sternberg B, D'Souza GG. Cell transfection in vitro and in vivo with nontoxic TAT peptide-liposome-DNA complexes. *Proc Natl Acad Sci U S A.* 2003;100:1972-7.
- [286] Yasumura EG, Stilhano RS, Samoto VY, Matsumoto PK, de Carvalho LP, Valero Lapchik VB. Treatment of mouse limb ischemia with an integrative hypoxia-responsive vector expressing the vascular endothelial growth factor gene. *PloS One.* 2012;7:e33944.
- [287] Jiang J, Jiang N, Gao W, Zhu J, Guo Y, Shen D. Augmentation of revascularization and prevention of plasma leakage by angiopoietin-1 and vascular endothelial growth factor co-transfection in rats with experimental limb ischaemia. *Acta Cardiol.* 2006;61:145-53.

- [288] Li Y, Hazarika S, Xie D, Phippen AM, Kontos CD, Annex BH. In mice with type 2 diabetes, a vascular endothelial growth factor (VEGF)-activating transcription factor modulates VEGF signaling and induces therapeutic angiogenesis after hindlimb ischemia. *Diabetes*. 2007;56:656-65.
- [289] Lee JS, Kim JM, Kim KL, Jang HS, Shin IS, Jeon ES. Combined administration of naked DNA vectors encoding VEGF and bFGF enhances tissue perfusion and arteriogenesis in ischemic hindlimb. *Biochem Biophys Res Commun*. 2007;360:752-8.
- [290] Portlock JL, Keravala A, Bertoni C, Lee S, Rando TA, Calos MP. Long-term increase in mVEGF164 in mouse hindlimb muscle mediated by phage phiC31 integrase after nonviral DNA delivery. *Hum Gene Ther*. 2006;17:871-6.
- [291] Traktuev DO, Tsokolaeva ZI, Shevelev AA, Talitskiy KA, Stepanova VV, Johnstone BH. Urokinase gene transfer augments angiogenesis in ischemic skeletal and myocardial muscle. *Mol Ther*. 2007;15:1939-46.
- [292] Yamauchi A, Ito Y, Morikawa M, Kobune M, Huang J, Sasaki K. Pre-administration of angiopoietin-1 followed by VEGF induces functional and mature vascular formation in a rabbit ischemic model. *J Gene Med*. 2003;5:994-1004.
- [293] Shyu KG, Chang H, Isner JM. Synergistic effect of angiopoietin-1 and vascular endothelial growth factor on neoangiogenesis in hypercholesterolemic rabbit model with acute hindlimb ischemia. *Life Sci*. 2003;73:563-79.
- [294] Palladino M, Gatto I, Neri V, Stigliano E, Smith RC, Pola E. Combined therapy with sonic hedgehog gene transfer and bone marrow-derived endothelial progenitor cells enhances angiogenesis and myogenesis in the ischemic skeletal muscle. *J Vasc Res*. 2012;49:425-31.
- [295] Kang SW, Lim HW, Seo SW, Jeon O, Lee M, Kim BS. Nanosphere-mediated delivery of vascular endothelial growth factor gene for therapeutic angiogenesis in mouse ischemic limbs. *Biomaterials*. 2008;29:1109-17.
- [296] Jang E, Albadawi H, Watkins MT, Edelman ER, Baker AB. Syndecan-4 proteoliposomes enhance fibroblast growth factor-2 (FGF-2)-induced proliferation, migration, and neovascularization of ischemic muscle. *Proc Natl Acad Sci U S A*. 2012;109:1679-84.
- [297] Negishi Y, Matsuo K, Endo-Takahashi Y, Suzuki K, Matsuki Y, Takagi N. Delivery of an angiogenic gene into ischemic muscle by novel bubble liposomes followed by ultrasound exposure. *Pharm Res*. 2011;28:712-9.
- [298] Taniyama Y, Morishita R, Hiraoka K, Aoki M, Nakagami H, Yamasaki K. Therapeutic angiogenesis induced by human hepatocyte growth factor gene in rat diabetic hind limb ischemia model: molecular mechanisms of delayed angiogenesis in diabetes. *Circulation*. 2001;104:2344-50.

- [299] Vincent KA, Shyu KG, Luo Y, Magner M, Tio RA, Jiang C. Angiogenesis is induced in a rabbit model of hindlimb ischemia by naked DNA encoding an HIF-1 /VP16 hybrid transcription factor. *Circulation*. 2000;102:2255-61.
- [300] Yamada N, Li W, Ihaya A, Kimura T, Morioka K, Uesaka T. Platelet-derived endothelial cell growth factor gene therapy for limb ischemia. *J Vasc Surg*. 2006;44:1322-8.
- [301] Jazwa A, Stepniewski J, Zamykal M, Jagodzinska J, Meloni M, Emanuelli C. Pre-emptive hypoxia-regulated HO-1 gene therapy improves post-ischaemic limb perfusion and tissue regeneration in mice. *Cardiovasc Res*. 2012.
- [302] Rayssac A, Neveu C, Pucelle M, Van den Berghe L, Prado-Lourenco L, Arnal JF. IRES-based vector coexpressing FGF2 and Cyr61 provides synergistic and safe therapeutics of lower limb ischemia. *Mol Ther*. 2009;17:2010-9.
- [303] Ferraro B, Cruz YL, Baldwin M, Coppola D, Heller R. Increased perfusion and angiogenesis in a hindlimb ischemia model with plasmid FGF-2 delivered by noninvasive electroporation. *Gene Ther*. 2010;17:763-9.
- [304] Nishikage S, Koyama H, Miyata T, Ishii S, Hamada H, Shigematsu H. In vivo electroporation enhances plasmid-based gene transfer of basic fibroblast growth factor for the treatment of ischemic limb. *J Surg Res*. 2004;120:37-46.
- [305] Koike H, Morishita R, Iguchi S, Aoki M, Matsumoto K, Nakamura T. Enhanced angiogenesis and improvement of neuropathy by cotransfection of human hepatocyte growth factor and prostacyclin synthase gene. *FASEB J*. 2003;17:779-81.
- [306] Taniyama Y, Morishita R, Aoki M, Nakagami H, Yamamoto K, Yamazaki K. Therapeutic angiogenesis induced by human hepatocyte growth factor gene in rat and rabbit hindlimb ischemia models: preclinical study for treatment of peripheral arterial disease. *Gene Ther*. 2001;8:181-9.
- [307] Rajagopalan S, Olin J, Deitcher S, Pieczek A, Laird J, Grossman PM. Use of a constitutively active hypoxia-inducible factor-1 transgene as a therapeutic strategy in no-option critical limb ischemia patients: phase I dose-escalation experience. *Circulation*. 2007;115:1234-43.
- [308] Creager MA, Olin JW, Belch JJ, Moneta GL, Henry TD, Rajagopalan S. Effect of hypoxia-inducible factor-1 gene therapy on walking performance in patients with intermittent claudication. *Circulation*. 2011;124:1765-73.
- [309] Kusumanto YH, van Weel V, Mulder NH, Smit AJ, van den Dungen JJ, Hooymans JM. Treatment with intramuscular vascular endothelial growth factor gene compared with placebo for patients with diabetes mellitus and critical limb ischemia: a double-blind randomized trial. *Hum Gene Ther*. 2006;17:683-91.

- [310] de Leeuw K, Kusumanto Y, Smit AJ, Oomen P, van der Hoeven JH, Mulder NH. Skin capillary permeability in the diabetic foot with critical limb ischaemia: the effects of a phVEGF<sub>165</sub> gene product. *Diabet Med.* 2008;25:1241-4.
- [311] Gu Y, Zhang J, Guo L, Cui S, Li X, Ding D. A phase I clinical study of naked DNA expressing two isoforms of hepatocyte growth factor to treat patients with critical limb ischemia. *J Gene Med.* 2011;13:602-10.
- [312] Anghel A, Taranu G, Seclaman E, Rata A, Tamas L, Moldovan H. Safety of vascular endothelial and hepatocyte growth factor gene therapy in patients with critical limb ischemia. *Curr Neurovasc Res.* 2011;8:183-9.
- [313] Shigematsu H, Yasuda K, Sasajima T, Takano T, Miyata T, Ohta T. Transfection of human HGF plasmid DNA improves limb salvage in Buerger's disease patients with critical limb ischemia. *Int Angiol.* 2011;30:140-9.
- [314] Morishita R, Makino H, Aoki M, Hashiya N, Yamasaki K, Azuma J. Phase I/IIa clinical trial of therapeutic angiogenesis using hepatocyte growth factor gene transfer to treat critical limb ischemia. *Arterioscler Thromb Vasc Biol.* 2011;31:713-20.
- [315] Shigematsu H, Yasuda K, Iwai T, Sasajima T, Ishimaru S, Ohashi Y. Randomized, double-blind, placebo-controlled clinical trial of hepatocyte growth factor plasmid for critical limb ischemia. *Gene Ther.* 2010;17:1152-61.
- [316] Niebuhr A, Henry T, Goldman J, Baumgartner I, van Belle E, Gerss J. Long-term safety of intramuscular gene transfer of non-viral FGF1 for peripheral artery disease. *Gene Ther.* 2012;19:264-70.
- [317] Belch J, Hiatt WR, Baumgartner I, Driver IV, Nikol S, Norgren L. Effect of fibroblast growth factor NV1FGF on amputation and death: a randomised placebo-controlled trial of gene therapy in critical limb ischaemia. *Lancet.* 2011;377:1929-37.
- [318] Storrie H, Mooney DJ. Sustained delivery of plasmid DNA from polymeric scaffolds for tissue engineering. *Adv Drug Delivery Rev.* 2006;58:500-14.
- [319] Jang JH, Rives CB, Shea LD. Plasmid delivery in vivo from porous tissue-engineering scaffolds: transgene expression and cellular transfection. *Mol Ther.* 2005;12:475-83.
- [320] Mao Z, Shi H, Guo R, Ma L, Gao C, Han C. Enhanced angiogenesis of porous collagen scaffolds by incorporation of TMC/DNA complexes encoding vascular endothelial growth factor. *Acta Biomater.* 2009;5:2983-94.
- [321] Doukas J, Blease K, Craig D, Ma C, Chandler LA, Sosnowski BA. Delivery of FGF genes to wound repair cells enhances arteriogenesis and myogenesis in skeletal muscle. *Mol Ther.* 2002;5:517-27.

- [322] Shea LD, Smiley E, Bonadio J, Mooney DJ. DNA delivery from polymer matrices for tissue engineering. *Nat Biotechnol.* 1999;17:551-4.
- [323] Kasahara H, Tanaka E, Fukuyama N, Sato E, Sakamoto H, Tabata Y. Biodegradable gelatin hydrogel potentiates the angiogenic effect of fibroblast growth factor 4 plasmid in rabbit hindlimb ischemia. *J Am Coll Cardiol.* 2003;41:1056-62.
- [324] Kong HJ, Kim ES, Huang YC, Mooney DJ. Design of biodegradable hydrogel for the local and sustained delivery of angiogenic plasmid DNA. *Pharm Res.* 2008;25:1230-8.
- [325] Isner JM, Pieczek A, Schainfeld R, Blair R, Haley L, Asahara T. Clinical evidence of angiogenesis after arterial gene transfer of phVEGF<sub>165</sub> in patient with ischaemic limb. *Lancet.* 1996;348:370-4.
- [326] Arveschoug A, Christensen KS. Constitutive expression of phVEGF<sub>165</sub> after intramuscular gene transfer promotes collateral vessel development in patients with critical limb ischemia. *Circulation.* 1999;99:2967-8.
- [327] Baumgartner I, Pieczek A, Manor O, Blair R, Kearney M, Walsh K. Constitutive expression of phVEGF<sub>165</sub> after intramuscular gene transfer promotes collateral vessel development in patients with critical limb ischemia. *Circulation.* 1998;97:1114-23.
- [328] Kim HJ, Jang SY, Park JI, Byun J, Kim DI, Do YS. Vascular endothelial growth factor-induced angiogenic gene therapy in patients with peripheral artery disease. *Exp Mol Med.* 2004;36:336-44.
- [329] Baumgartner I, Chronos N, Comerota A, Henry T, Pasquet JP, Finiels F. Local gene transfer and expression following intramuscular administration of FGF-1 plasmid DNA in patients with critical limb ischemia. *Mol Ther.* 2009;17:914-21.
- [330] Morishita R, Aoki M, Hashiya N, Makino H, Yamasaki K, Azuma J. Safety evaluation of clinical gene therapy using hepatocyte growth factor to treat peripheral arterial disease. *Hypertension.* 2004;44:203-9.
- [331] Gaffney MM, Hynes SO, Barry F, O'Brien T. Cardiovascular gene therapy: current status and therapeutic potential. *Br J Pharmacol.* 2007;152:175-88.
- [332] Powell RJ, Simons M, Mendelsohn FO, Daniel G, Henry TD, Koga M. Results of a double-blind, placebo-controlled study to assess the safety of intramuscular injection of hepatocyte growth factor plasmid to improve limb perfusion in patients with critical limb ischemia. *Circulation.* 2008;118:58-65.
- [333] Merdan T, Kopecek J, Kissel T. Prospects for cationic polymers in gene and oligonucleotide therapy against cancer. *Adv Drug Delivery Rev.* 2002;54:715-58.
- [334] Suh W, Han SO, Yu L, Kim SW. An angiogenic, endothelial-cell-targeted polymeric gene carrier. *Mol Ther.* 2002;6:664-72.

[335] Lu QL, Bou-Gharios G, Partridge TA. Non-viral gene delivery in skeletal muscle: a protein factory. *Gene Ther.* 2003;10:131-42.

## Chapter 2

### **A Hollow Sphere Model System to Study Size and Charge Effect on Cellular Internalization**

Sections of this chapter have been previously published in:

Dash BC, Rethore G, Monaghan M, Fitzgerald K, Gallagher W, Pandit, A. The Influence of Size and Charge of Chitosan/Polyglutamic Acid Hollow Spheres on Cellular Internalization, Viability and Blood Compatibility. *Biomaterials* 2010; 31: 8188–97.

## 2.1 Introduction

Nanoscale technology, an emerging field in biomaterials, offers the opportunity of developing and optimizing biomaterials in a clinically translational form such as synthetic capsules or hollow spheres to deliver therapeutics [1]. In the past few decades interest has grown in the design of biomaterial-based delivery vehicles to use as a depot for various therapeutic molecules, e.g. genes and growth factors [1–6]. Among several methods for the fabrication of hollow spherical structures from synthetic or natural polymer, the template-based method is an attractive one in creating monodisperse nanometre to micron-sized hollow spheres [7]. The template method employs either coating of a single polymer or layer-by-layer coating of multiple polymers on a sacrificial template [4, 8]. Hollow spheres thus fabricated can be designed with various structural characteristics such as surface charge, size, shell thickness, pore size and mechanical strength. These modifications allow for efficient loading and sustained release of various therapeutics, e.g. genes, peptides and drugs, for the desired clinical targets [7].

However, therapeutic efficacy of any micrometre or nanometre size delivery vehicle depends on its cellular internalization behavior and cell viability. It is now an established fact that small physicochemical differences have significant biological implications in the cellular internalization and other biological processes of solid spheres [9]. Size and surface charge can affect the efficiency and pathway of cellular internalization for liposomes [10], quantum dots [11], polymeric spheres [12, 13], gold spheres [14, 15], silver [15] and silica spheres [16] by influencing the adhesion of the particles and their interaction with cells [17]. Also, for *in vitro* cytotoxicity and haemotoxicity studies, the careful and accurate characterization of particle size and surface charge is a crucial issue [18–24]. Thus *in vitro* experimental studies with consistency of sphere size and surface charge are desired for elucidating the effects of these properties on cellular internalization and viability.

Previous investigations on the effects of sphere size and surface charge offered modest consideration to independently altering one variable at a time while monitoring the effect of each variable [16, 24, 25]. Although commercially available fluorescent polystyrene (PS) beads have been used as a model and extensively applied in evaluating the effect of particle size on cellular internalization and blood compatibility behavior [12, 13, 24, 26–8], the difficulties in controlling the surface charge during the size control processes and the lack of surface functionality impaired the precise evaluation of the relationship between physicochemical properties of polymeric spheres and their biological process [12, 27]. No study to date has reported on the combinatorial effect of size and charge.

Herein, it is hypothesized that polymeric hollow spheres prepared using a template-based method can be used as a model system to study combinatorial effect of surface charge and size on cell viability and cellular uptake. The specific objectives of this study were to fabricate monodisperse chitosan/polyglutamic acid (PGA) hollow spheres of various sizes along with a range of surface charges, and to evaluate the effect of both size and surface charge on the cellular viability, blood compatibility and cellular internalization behaviour of these hollow spheres. The influence of size was determined by fabricating four different sizes of hollow spheres – 100, 300, 500 and 1000 nm (Figure 2.1) – while the effect of surface charge was investigated by creating negative, neutral and PEGylated surface modified hollow spheres. Human umbilical vein endothelial cells (HUVECs) and human umbilical artery smooth muscle cells (HUASMCs) were chosen for this experiment as model cell types.

### **2.2 Materials and Methods**

#### **2.2.1 Materials**

All reagents were purchased from Sigma-Aldrich (Dublin, Ireland) unless otherwise noted: PS beads 100 and 300 nm, sulfuric acid, chitosan (low molecular weight, 90% of deacetylation), ethanol, acetic acid, tetrahydrofuran (THF), PGA, phosphate buffered saline (PBS), 2-(*N*-morpholino)ethanesulfonic acid (MES), *N*-hydroxysuccinimide (NHS) and trypsin-EDTA, methylthiazolyldiphenyl-tetrazolium bromide (MTT), 1-ethyl-3-(3-dimethylaminopropyl) carbodiimide (EDC) and 2-methoxy ethylamine (MEA); PS beads 510 and 1000nm (Gentaur, UK); propyl amine (PA) series polyethylene glycol (PEG) 3400 Da (Sunbright, Japan), agar low viscosity resin kit (Agar Scientific Ltd., UK); fluorescein isothiocyanate (FITC), TO-PRO-3 iodide and bovine serum albumin (BSA) (Invitrogen, Ireland); endothelial cell growth medium-2 (EGM-2) and smooth muscle cell growth media (SmGM-2) bullet kits (Lonza, France).

#### **2.2.2 Fabrication of Different Sizes of Hollow spheres and FITC Labelling**

Chitosan/PGA hollow spheres were fabricated as described in the protocol [4]. Briefly, a 0.5wt% solution of chitosan in 1% (v/v) acetic acid was added to a colloidal solution of sulfonated PS beads of various sizes (100, 300, 500 and 1000 nm) and the mixture was then shaken for 24 hr at 4°C. PGA (1.7 equivalent) in MES (0.05M, pH 5.5) was mixed for five minutes with NHS (0.8eq.) and EDC (0.8eq.). This was then added to the chitosan/PS solution and the solution was stirred for 24 hr. Cross-linking reaction occurred over 24 hr. To obtain a surface negative charge on the native hollow spheres an additional 0.7 equivalent PGA was added to chitosan during the fabrication process.

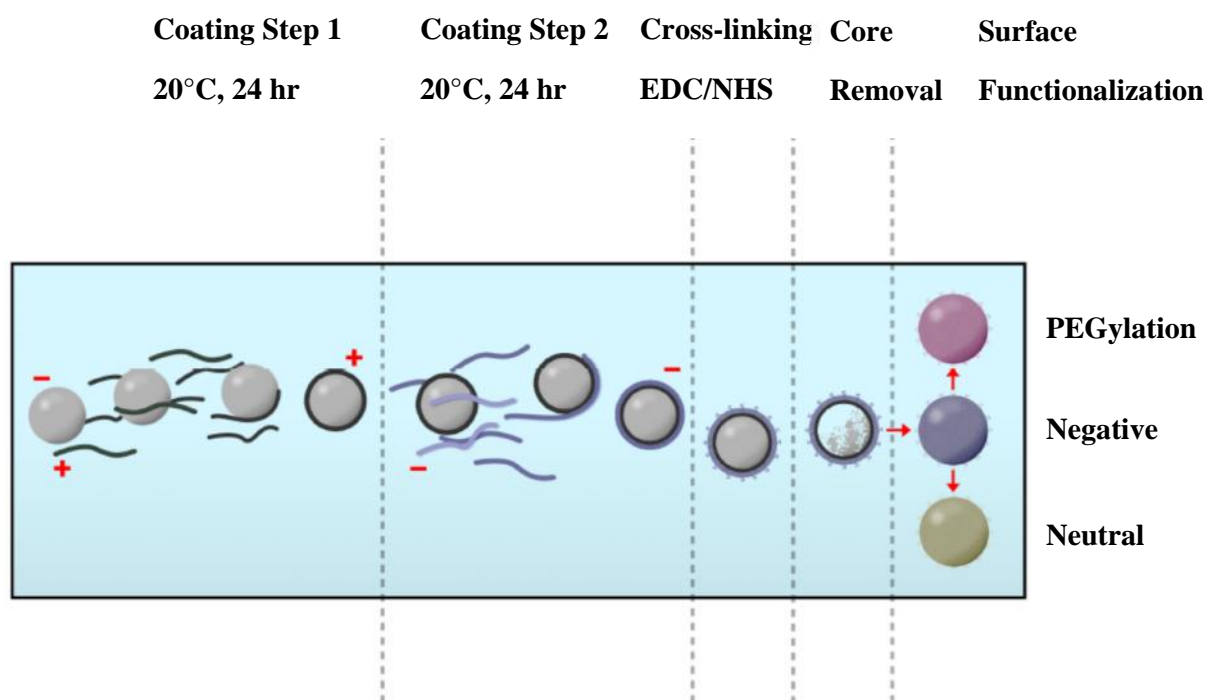


Figure 2.1: Schematic representation of hollow sphere fabrication and surface modifications.

Finally, to obtain hollow spheres, PS cores were dissolved with THF and dried under vacuum to evaporate excessive solvent. To analyse their internal structure and size, hollow spheres were observed under transmission electron microscopy (TEM). FITC labelling was performed as described in previous study [4]. PGA was labelled with FITC prior to the cross-linking step during the hollow spheres fabrication process. A weight ratio of 1:40 of FITC to PGA was used. FITC labelled PGA was then used to fabricate the hollow spheres.

### **2.2.3 Alteration of Surface Charge and Function of Hollow Spheres**

Hollow spheres of all the four sizes were used for surface modifications. For neutralization, native hollow spheres were covalently cross-linked with MEA. Briefly, 50 mg of chitosan/PGA hollow spheres (0.086 mmol of carboxylic group) was dispersed in MES buffer (2–3 ml, pH 5.5) in a round bottom flask and 22.24  $\mu$ l of MEA (0.258 mmol of amino group), EDC (0.172 mmol) and NHS (0.172 mmol) was then added. The mixture was stirred overnight at room temperature and dialysed to remove the unreacted chemicals. Surface PEGylation of these hollow spheres was performed using PA-functionalized amino-terminated PEG. 0.043 mmol of PEG was mixed with 0.086 mmol hollow spheres with EDC (0.086 mmol) and NHS (0.086 mmol) in MES buffer (pH 5.5). The mixture was then stirred overnight and dialysed to remove unreacted chemicals. Surface charge was analysed in mV using zeta sizer (NanoZS, Malvern, UK) after surface modifications of all the hollow spheres.

### **2.2.4 Cell Maintenance**

HUVECs and HUASMCs were grown in T75 flasks using EGM-2 and SmGM-2 media respectively and incubated at 37°C in an atmosphere of 5% CO<sub>2</sub>. The culture medium was changed every 36 hr. The cells were harvested and sub-cultured when >80% confluency was observed.

### **2.2.5 Cell Metabolic Activity Study**

Cells were seeded in 96 well plates. Hollow spheres of various sizes and surface charges were added to each cell type (HUVEC and HUASMC) and incubated for different time points at 6, 12, 24 and 48 hr. 50  $\mu$ l of (3-(4,5-dimethylthiazol-2-yl)-2,5-diphenyltetrazolium bromide (MTT) was added to each sample 3 hr prior to completion of time course (e.g. for 12 hr time point, MTT was added at 9 hr for 3 hr incubation). Finally, 100  $\mu$ l dimethyl sulfoxide (DMSO) was added, and read at 570 nm. Results were expressed as a percentage of metabolic activity of treated samples compared to non-treated cells (100%) over the specified time course.

## **2.2.6 Cellular Internalization Behaviour of Hollow Spheres**

### *2.2.6.1 Characterization by Confocal Imaging*

In order to visualize the hollow spheres within HUVECs and HUASMCs, confocal microscopy was performed. Cells were incubated with FITC labelled hollow spheres for the desired time point at 37 °C and then fixed with paraformaldehyde (4%) and stained for cytoskeleton using rhodamine phalloidin.

### *2.2.6.2 Characterization by Transmission Electron Microscopy (TEM)*

Internalization and colocalization of hollow spheres were characterized by TEM. Cells were incubated with 50 µg of hollow spheres for 24 hr. After incubation, cells were washed and fixed with paraformaldehyde, dehydrated by using a gradient of ethanol and then embedded into resin. After polymerization of the resin (3 days at 60°C), cut sections of 90 nm thickness were done using an ultramicrotome and samples were then analysed using TEM.

### *2.2.6.3 Quantification by Flow Cytometry*

Cells were grown in T25 tissue culture flasks and hollow spheres at a concentration of 50 µg/ml were added. After the desired incubation time, cells were trypsinized and resuspended in a buffer (1% BSA in PBS). Cells were then analysed using flow cytometry for internalization efficiency.

### *2.2.6.4 Quantification by High Content Analysis (HCA)*

HUVECs and HUASMCs were seeded on 96 well plates. FITC-hollow spheres were seeded and incubated for different time points: 6, 12, 24 and 48 hr. After the desired incubation times, cells were fixed and stained for nucleus using TO-PRO-3 iodide. Finally, the plates were read using In Cell Analyzer 1000 (GE Healthcare) for 420 nm (FITC) and 620 nm (TO-PRO-3 iodide).

## **2.2.7 Statistics**

Results are expressed as mean ± standard deviation. Statistical significance was assessed using the analysis of variance (ANOVA). *P* values of <0.05 were considered significant. In all studies, the minimum sample size was three.

## **2.3 Results**

### **2.3.1 Size and Surface Charge Analysis**

Size analysis of hollow spheres was carried out using TEM. Monodispersed hollow spheres were obtained for all the sizes (Figure 2.2). The size of hollow spheres was  $110 \pm 7.8$  nm,  $315 \pm 10.4$  nm,  $508 \pm 7.6$  nm and  $990 \pm 70$  nm for 100, 300, 500 and 1000 nm polystyrene beads respectively. Zeta potential analysis was used to characterize the surface modification. Native hollow spheres characterized previously [4] had a resultant negative potential of between –35

and  $-40$  mV over all sizes. Neutralization of the negatively charged hollow spheres using MEA was achieved, with an approximately neutral value of zeta potential of  $-4$  mV. PEG engraftment on the surfaces was also verified; as the quantity of PEG was less than that of MEA, an adjustment of the zeta potential to  $-20$  mV was observed, indicating that half of the carboxyl groups on the surface of the native hollow spheres were used to link the PEG moiety (Figure 2.3). No significant difference in size was found after surface modifications of hollow spheres.

### **2.3.2 Cell Viability**

The data suggests good cell viability following exposure to all the hollow spheres in both HUVECs and HUASMCs (Figures 2.4–2.11). A brief discussion about their size, surface charge and cell type effect appears in the discussion section.

### **2.3.3 Cellular Internalization Behaviour**

#### *2.3.3.1 Co-localization*

Confocal micrographs show localization of the negatively charged FITC labelled spheres (green) within HUVECs and HUASMCs after 24 hr incubation (Figure 2.12). Confocal micrographs of 1000 nm hollow spheres are not shown in this report as there was negligible internalization of this size of hollow spheres. 100 nm and 300 nm hollow spheres can be seen in the perinuclear region of the cells. Flow cytometry and fluorescence microscopy only detect gross fluorescence that emits from cells; highly dispersed hollow spheres, such as single sphere, might not therefore be detectable using either technique. The cell uptake of single hollow spheres must be investigated by other methods, such as TEM. Cells incubated with 100 nm neutral hollow spheres for 24 hr were observed under TEM (Figure 2.13). TEM micrographs show hollow spheres inside lysosomes of both the cell types (Figure 2.13A and B). Figure 2.13C illustrates the endocytic pathway of hollow spheres from early endosome to lysosome in HUVEC.

#### *2.3.3.2 Flow Cytometric Analysis of Cellular Internalization*

The impact of size and surface charge on cellular internalization was quantified after 12 hr of incubation using flow cytometry. Figure 2.14 and 2.15 show internalization efficiency of spheres within HUVECs and HUASMCs respectively. 100 nm neutral hollow spheres showed increased internalization compared all other sizes and surface charge of hollow spheres in both cell types with 76% and 56% of uptake in HUVECs and HUASMCs respectively. HUASMCs had lower sphere uptake than HUVECs in all the sizes and surface modifications investigated. 300 and 500 nm hollow spheres show similar internalization efficiency in both HUVECs and HUASMCs.

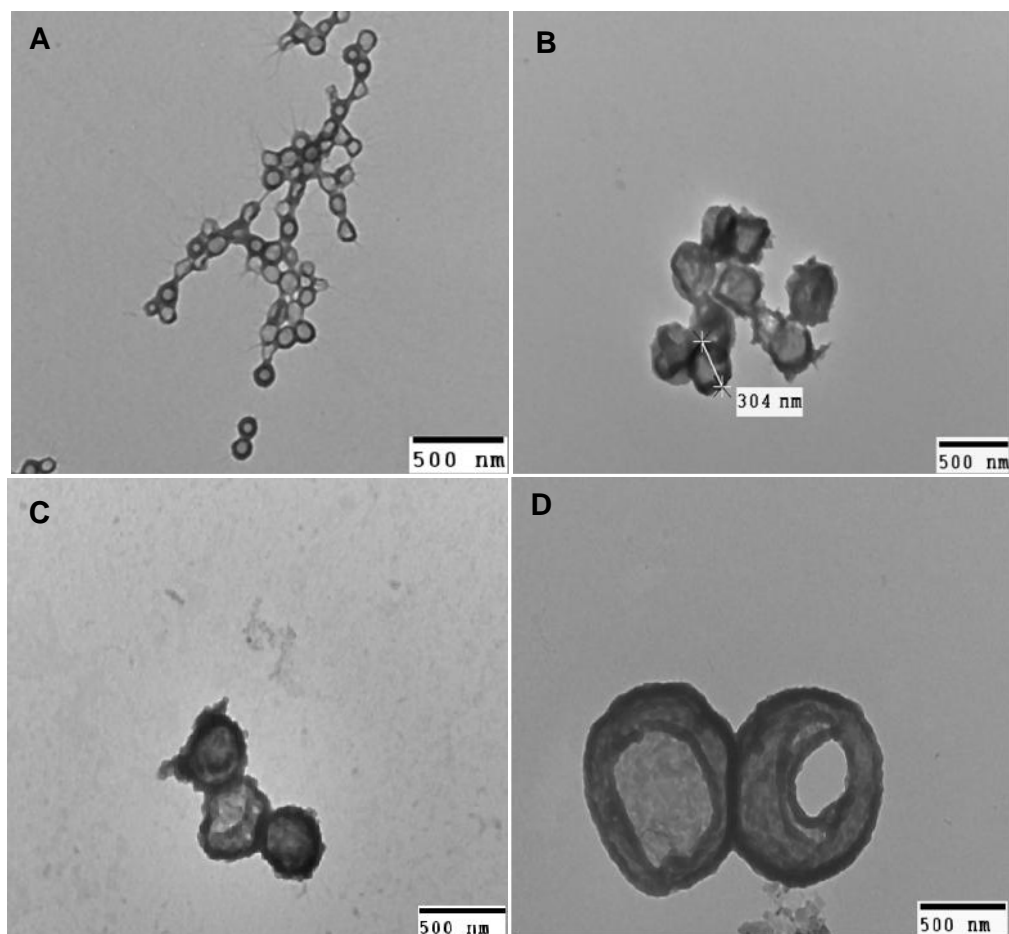


**Figure 2.2: Chitosan/PGA hollow spheres observed under TEM. (A) 100 nm; (B) 300 nm; (C) 500 nm; (D) 1000 nm hollow spheres.**

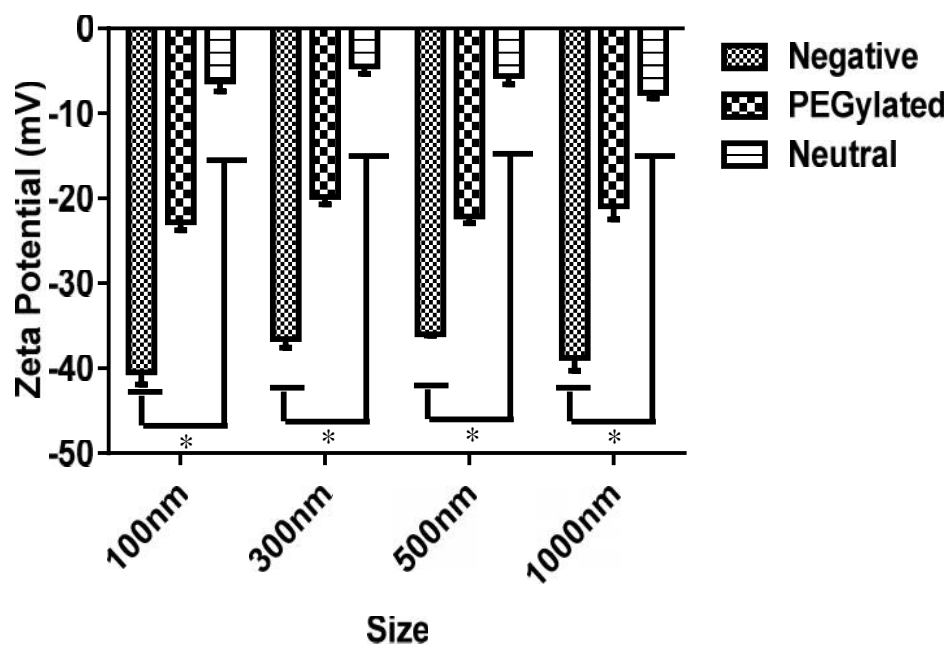


**Figure 2.3: Zeta potential analysis of hollow spheres showing net charge after surface modifications of all hollow spheres. Data is represented as the mean  $\pm$  standard deviation ( $n = 3$ ). \* indicates a statistically significant difference between samples with  $p < 0.05$ .**

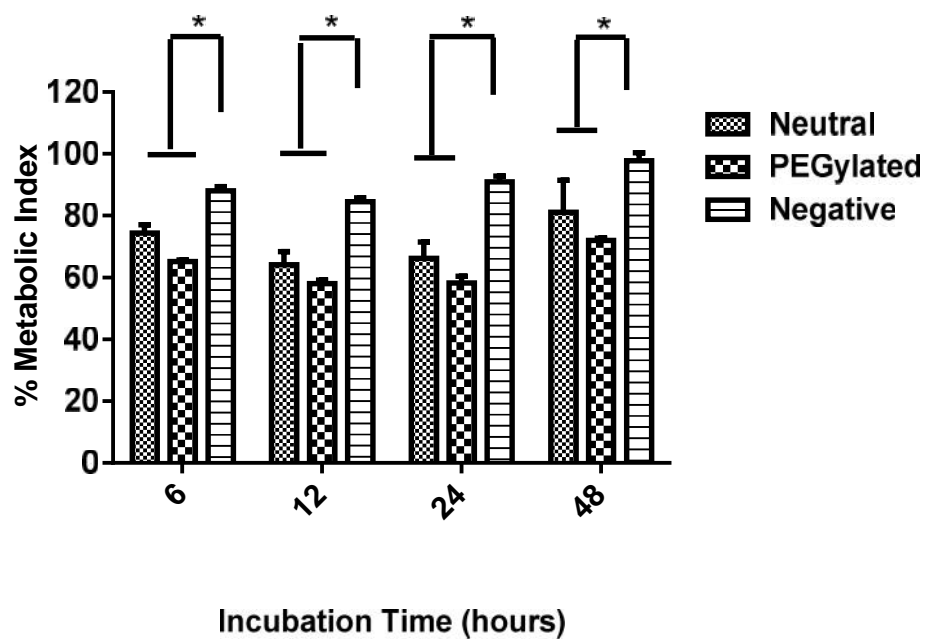


Figure 2.4: MTT assay showing percentage metabolic index of HUVECs at time points 6, 12, 24 and 48 hr. HUVECs were incubated with 100 nm hollow spheres. Data is represented as the mean  $\pm$  standard deviation ( $n = 3$ ). \* indicates statistical significance ( $p < 0.05$ ).

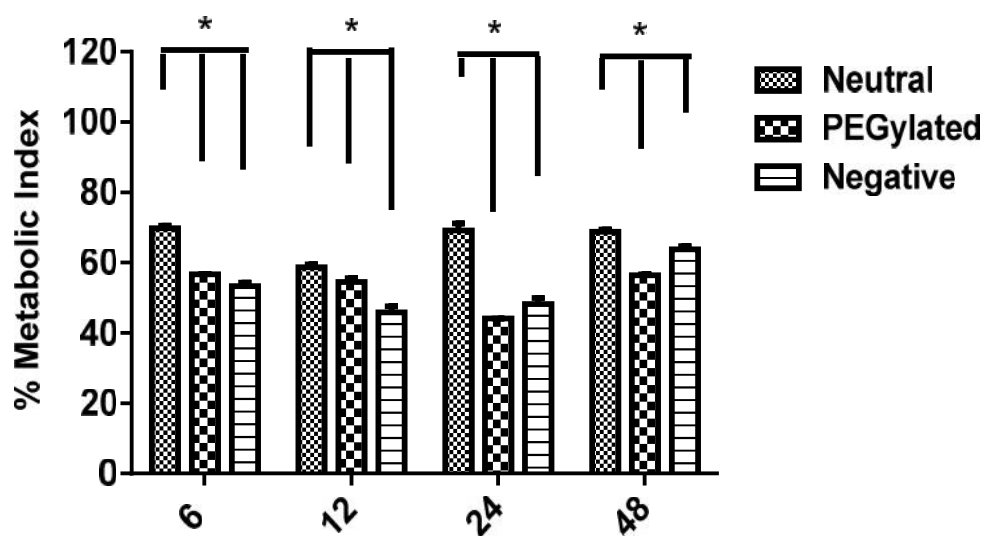


Figure 2.5: MTT assay showing percentage metabolic index of HUVECs at time points 6, 12, 24 and 48 hr. HUVECs were incubated with 300 nm hollow spheres. Data is represented as the mean  $\pm$  standard deviation ( $n = 3$ ). \* indicates statistical significance ( $p < 0.05$ ).

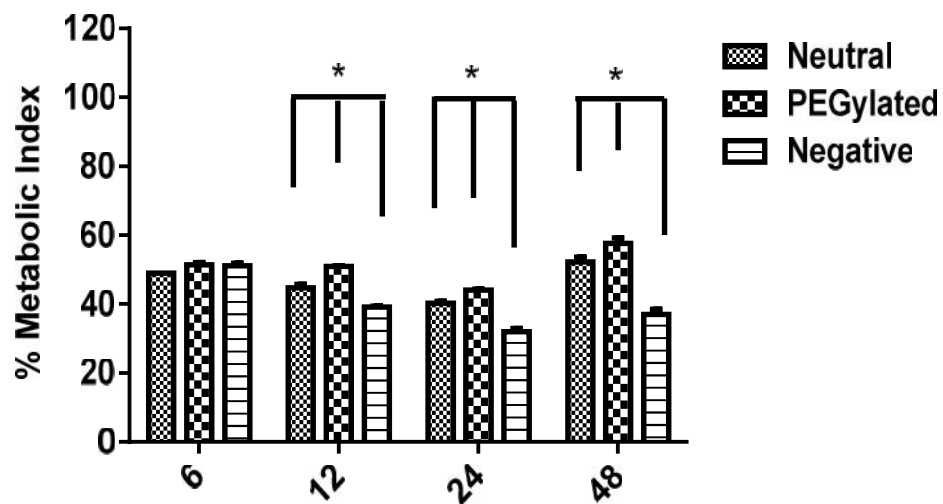


Figure 2.6: MTT assay showing percentage metabolic index of HUVECs at time points 6, 12, 24 and 48 hr. HUVECs were incubated with 500 nm hollow spheres. Data is represented as the mean  $\pm$  standard deviation ( $n = 3$ ). \* indicates statistical significance ( $p < 0.05$ ).

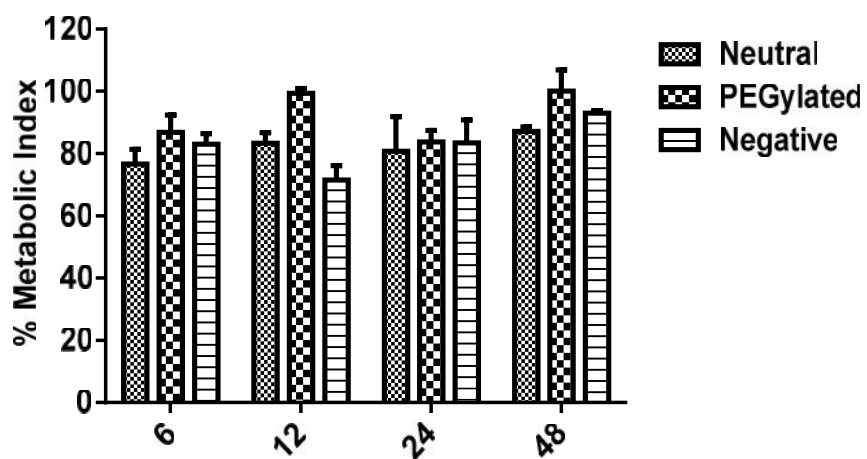
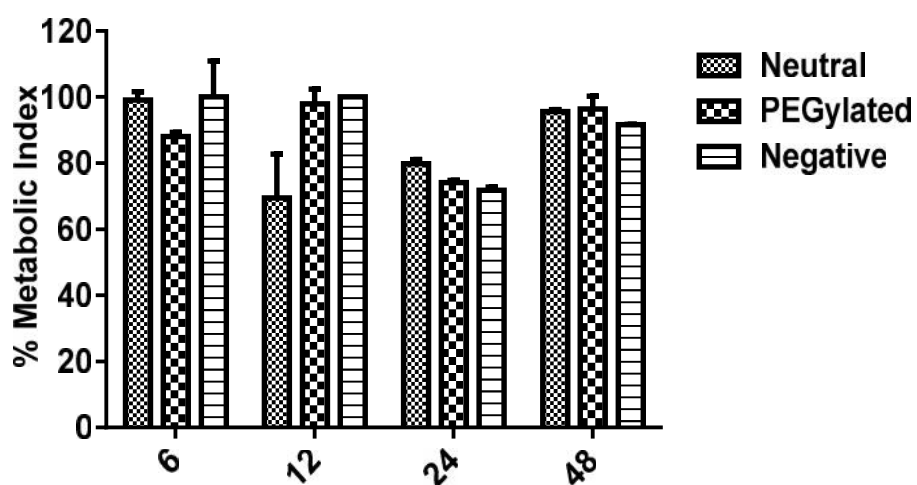
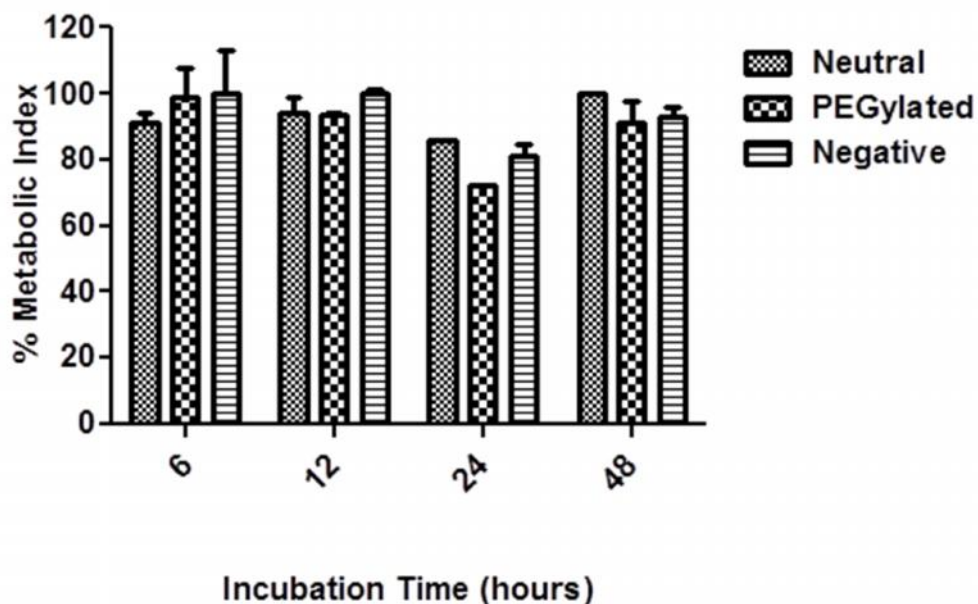


Figure 2.7: MTT assay showing percentage metabolic index of HUVECs at time points 6, 12, 24 and 48 hr. HUVECs were incubated with 1000 nm hollow spheres. Data is represented as the mean  $\pm$  standard deviation ( $n = 3$ ). No statistically significant effect of surface functionalization on cell metabolic activity was observed between hollow spheres.



**Figure 2.8: MTT assay showing percentage metabolic index of HUASMCs at time points 6, 12, 24 and 48 hr. HUASMCs were incubated with 100 nm hollow spheres. Data is represented as the mean  $\pm$  standard deviation ( $n = 3$ ). No statistically significant effect of surface functionalization on cell metabolic activity was observed between hollow spheres.**



**Figure 2.9: MTT assay showing percentage metabolic index of HUASMCs at time points 6, 12, 24 and 48 hr. HUASMCs were incubated with 300 nm hollow spheres. Data is represented as the mean  $\pm$  standard deviation ( $n = 3$ ). No statistically significant effect of surface functionalization on cell metabolic activity was observed between hollow spheres.**

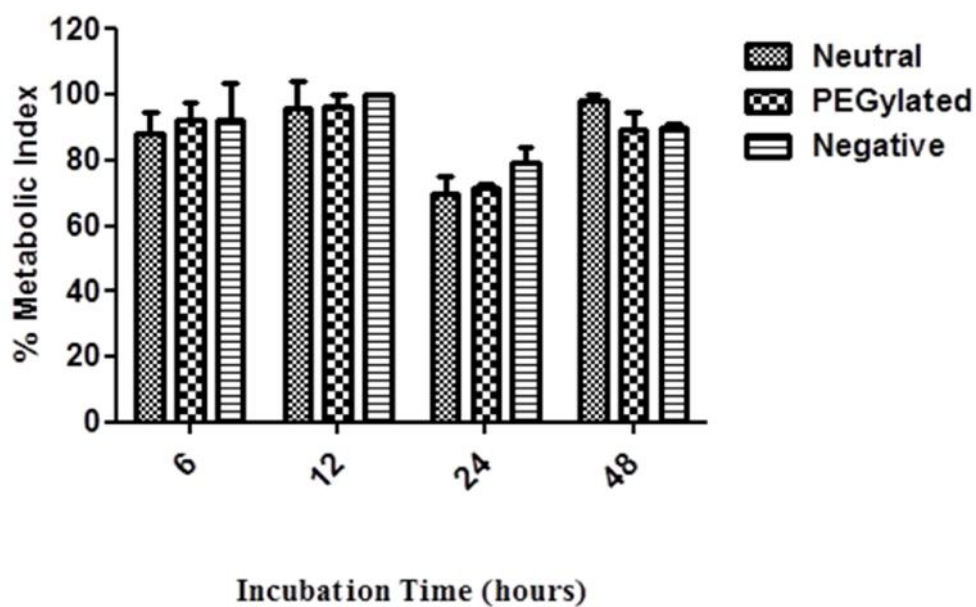


**Figure 2.10: MTT assay showing percentage metabolic index of HUASMCs at time points 6, 12, 24 and 48 hr. HUASMCs were incubated with 500 nm hollow spheres. Data is represented as the mean  $\pm$  standard deviation ( $n = 3$ ). No statistically significant effect of surface functionalization on cell metabolic activity was observed between hollow spheres.**

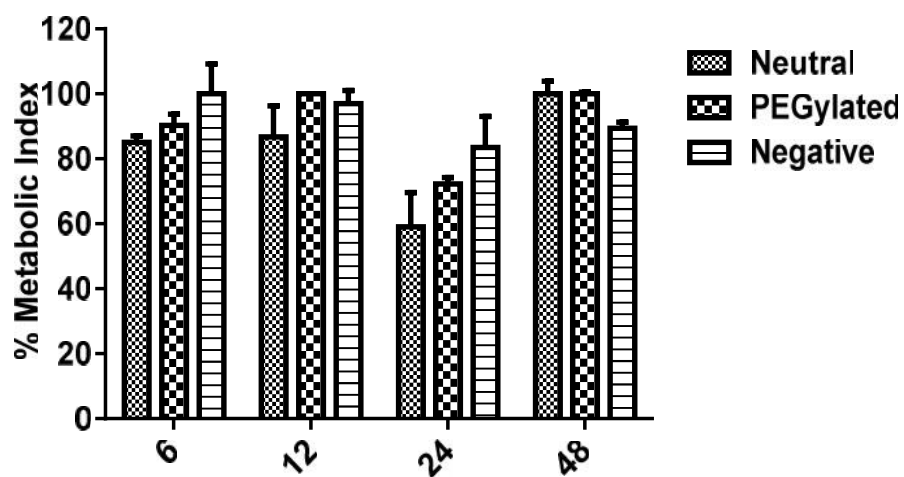


**Figure 2.11: MTT assay showing percentage metabolic index of HUASMCs at time points 6, 12, 24 and 48 hr. HUASMCs were incubated with 1000 nm hollow spheres. Data is represented as the mean  $\pm$  standard deviation ( $n = 3$ ). No statistically significant effect of surface functionalization on cell metabolic activity was observed between hollow spheres.**

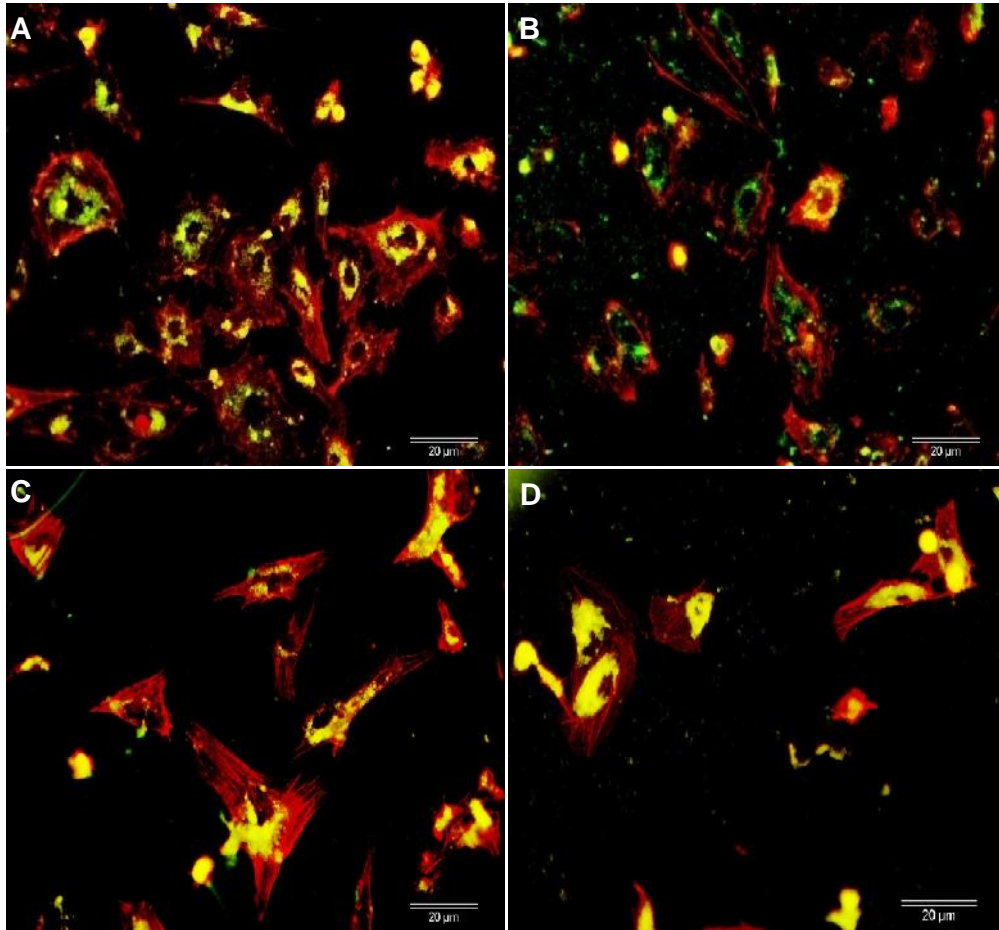


**Figure 2.12: Confocal micrographs of FITC labelled hollow spheres: (A) 100 nm and (B) 300 nm internalized into HUVECs and (C) 100 nm and (D) 300 nm internalized into HUASMCs. All images were taken after 24 hr incubation with cells. Red represents cytoskeleton and green for hollow spheres.**

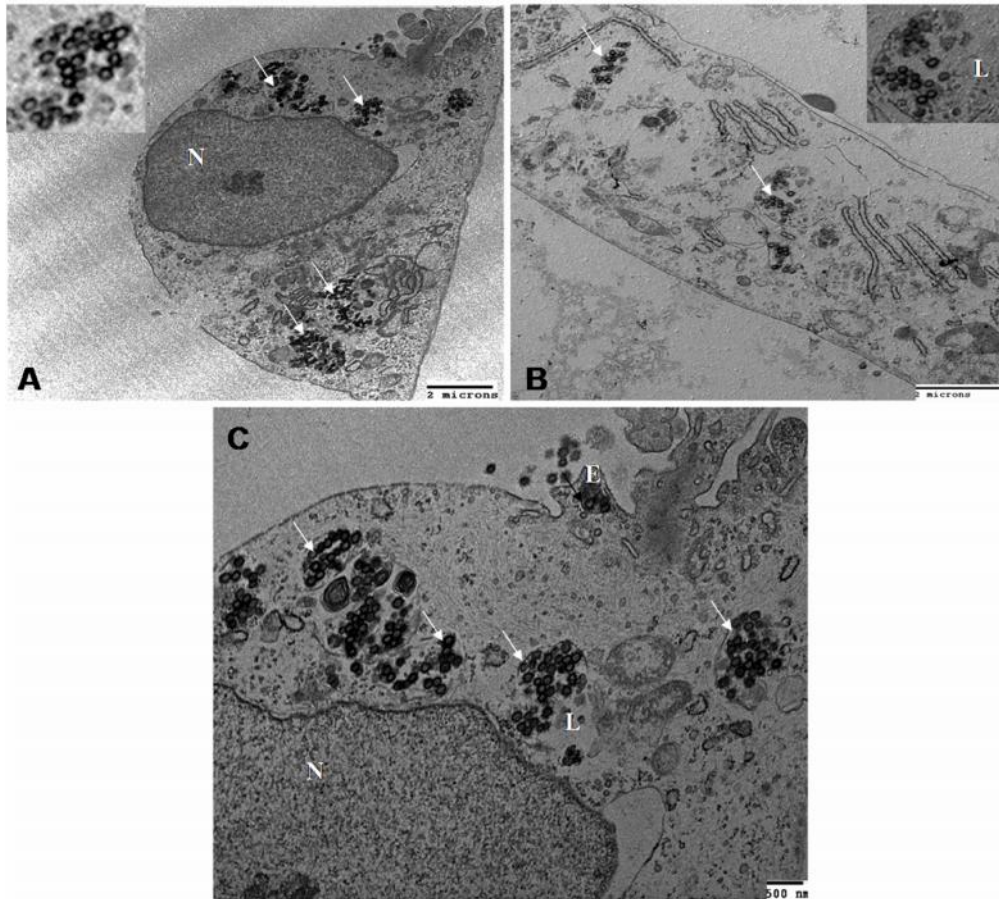


**Figure 2.13: TEM images illustrating 100 nm neutrally charged hollow spheres internalized into (A) HUVECs (inset shows the hollow spheres inside lysosome) and (B) HUASMCs (inset shows hollow spheres inside lysosome). (C) Higher magnification image of (A) showing endocytic internalization of hollow spheres from endosome (E) to lysosomes (L) near nucleus (N).**

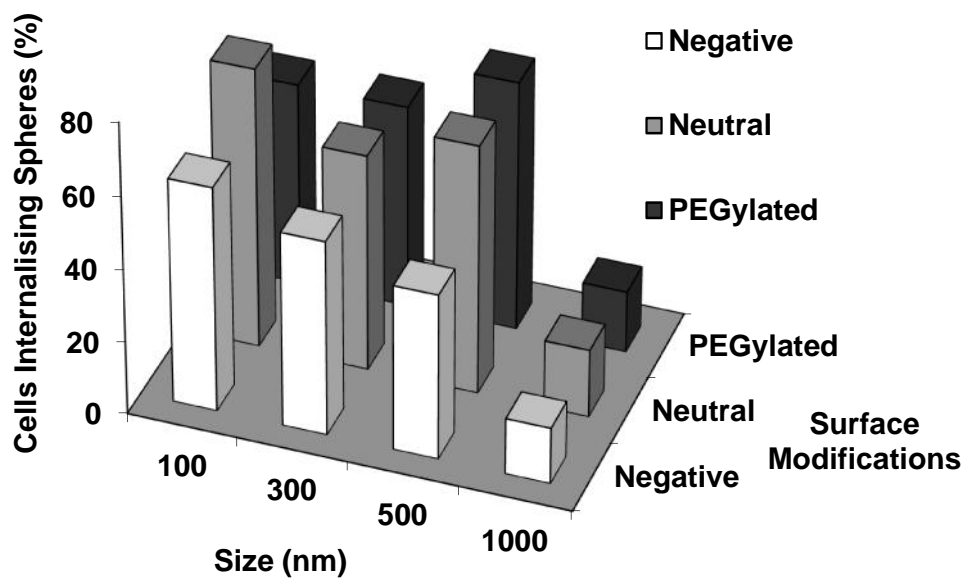


**Figure 2.14:** Flow cytometry data, elucidating the effect of size and surface modifications on the internalization efficiency of hollow spheres into HUVECs at 12 hr incubation.

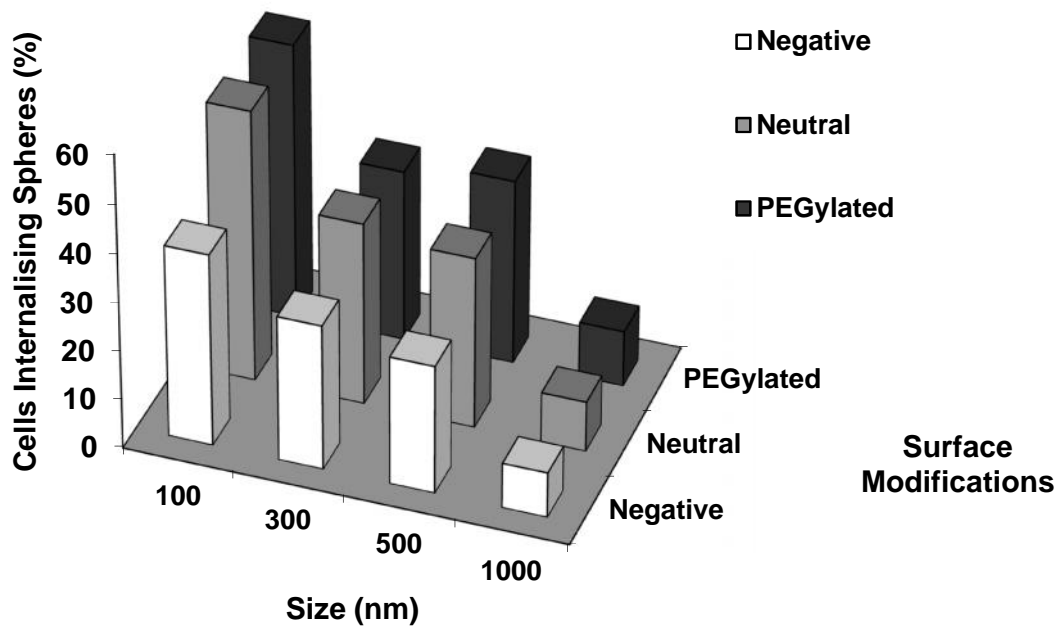
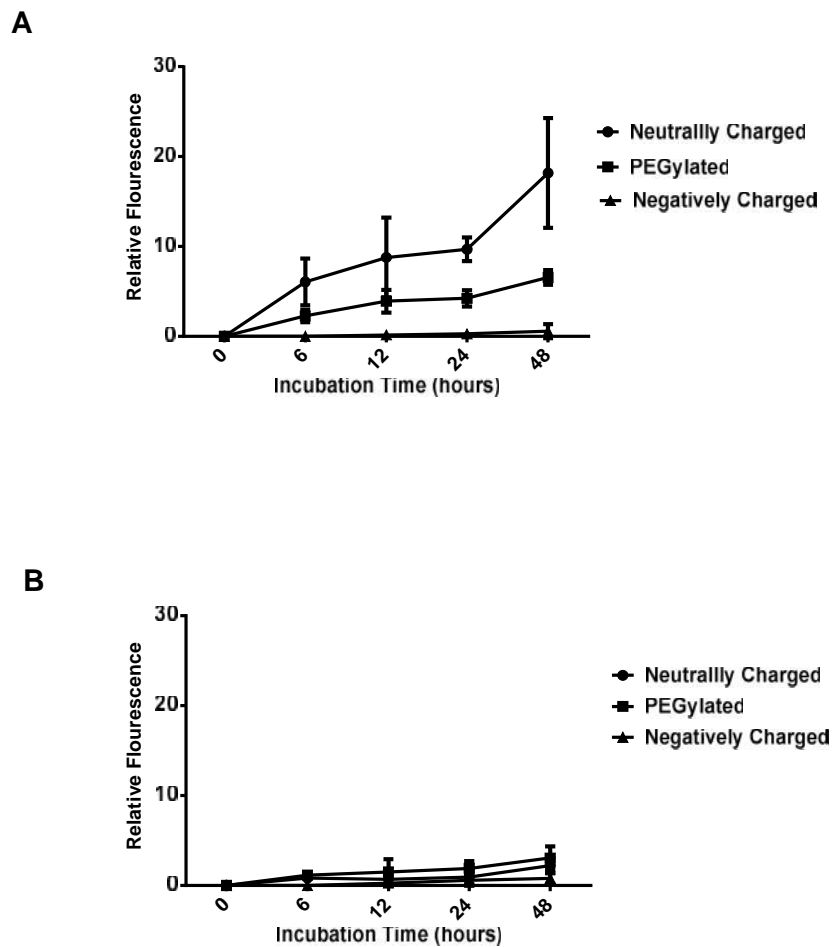
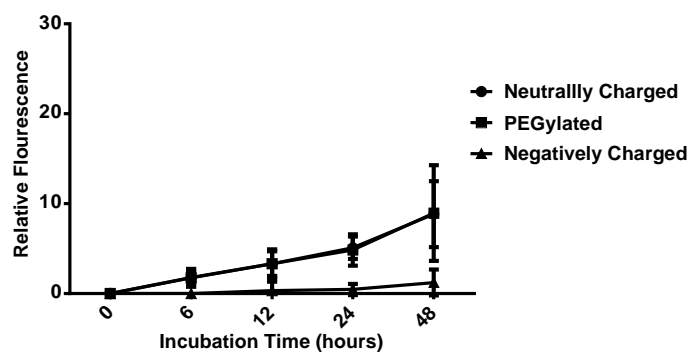


Figure 2.15: Flow cytometry data, elucidating the effect of size and surface modifications on the internalization efficiency of hollow spheres into HUASMCs at 12 hr incubation.



**Figure 2.16: High content analysis showing internalization of PEGylated, neutral and negatively charged hollow spheres of (A) 100 nm and (B) 300 nm with HUVECs over a time course of 6, 12, 24 and 48 hr. Data is represented as the mean  $\pm$  standard deviation ( $n = 3, p < 0.05$ ).**

A



B

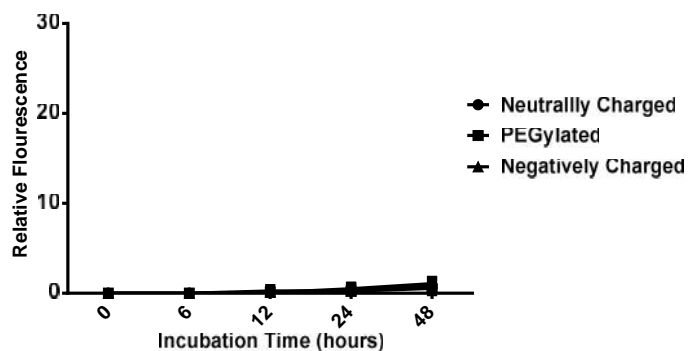
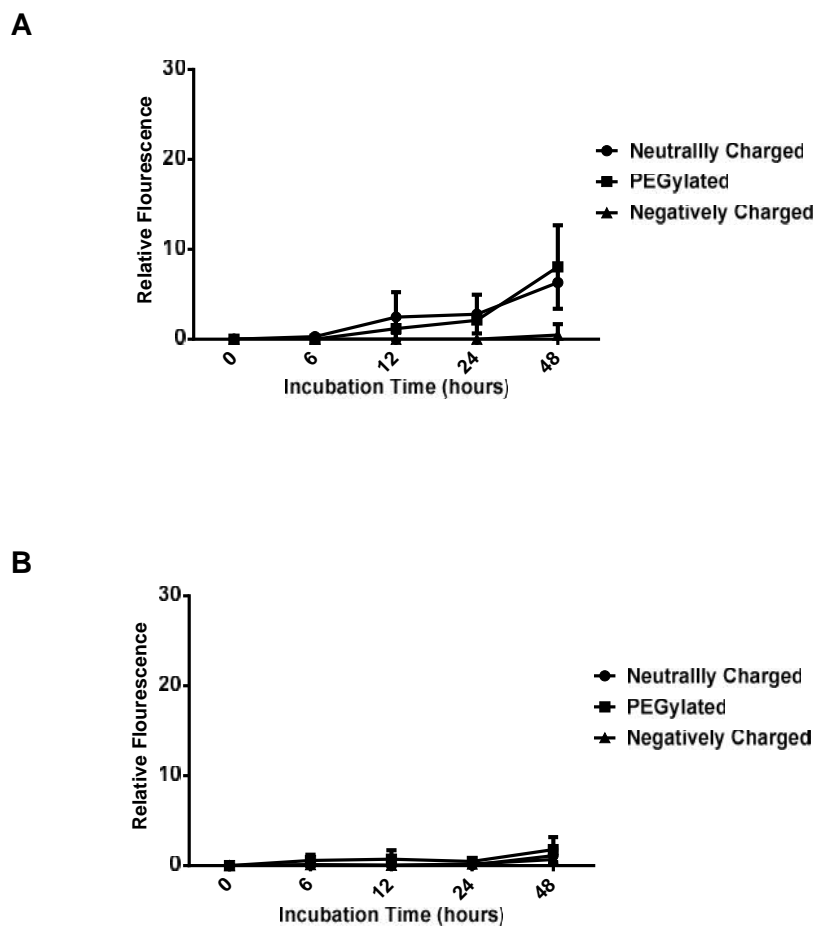
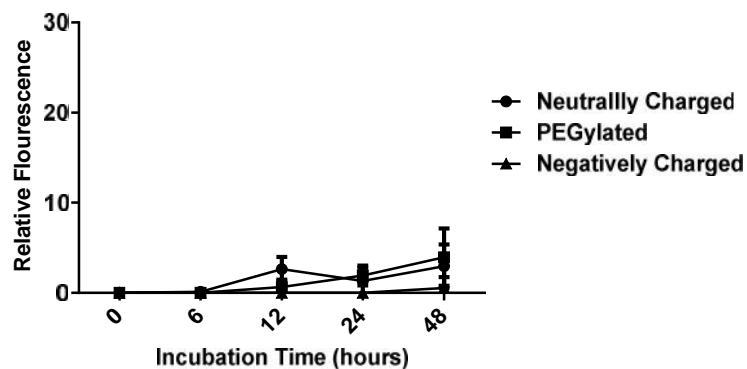


Figure 2.17: High content analysis showing internalization of PEGylated, neutral and negatively charged hollow spheres of (A) 500 nm and (B) 1000 nm with HUVECs over a time course of 6, 12, 24 and 48 hr. Data is represented as the mean  $\pm$  standard deviation ( $n = 3, p < 0.05$ ).



**Figure 2.18: High content analysis showing internalization of PEGylated, neutral and negatively charged hollow spheres of (A) 100 nm and (B) 300 nm with HUASMCs over a time course of 6, 12, 24 and 48 hr. Data is represented as the mean  $\pm$  standard deviation ( $n = 3, p < 0.05$ ).**

A



B

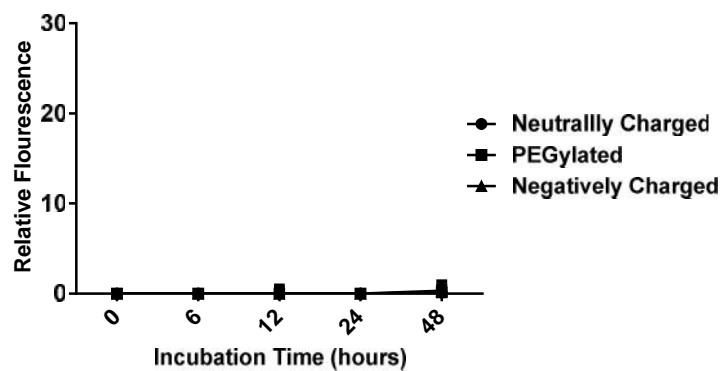


Figure 2.19: High content analysis showing internalization of PEGylated, neutral and negatively charged hollow spheres of (A) 500 nm and (B) 1000 nm with HUASMCs over a time course of 6, 12, 24 and 48 hr. Data is represented as the mean  $\pm$  standard deviation ( $n = 3, p < 0.05$ ).

**Table 2.1: Summary of effect of size (nm) and surface charge on all parameters investigated.**

|                        | Negative |     |     |      | Neutral |     |     |      | PEGylated |     |     |      |
|------------------------|----------|-----|-----|------|---------|-----|-----|------|-----------|-----|-----|------|
|                        | 100      | 300 | 500 | 1000 | 100     | 300 | 500 | 1000 | 100       | 300 | 500 | 1000 |
| <b>Cytotoxicity</b>    |          |     |     |      |         |     |     |      |           |     |     |      |
| <i>HUVEC</i>           | -        | ++  | +   | -    | -       | +   | ++  | -    | +         | +   | +   | -    |
| <i>HUASMC</i>          | -        | -   | -   | -    | -       | -   | -   | -    | -         | -   | -   | -    |
| <b>Internalization</b> |          |     |     |      |         |     |     |      |           |     |     |      |
| <i>HUVEC</i>           | -        | -   | -   | -    | +++     | ++  | +   | -    | +++       | ++  | +   | -    |
| <i>HUASMC</i>          | -        | -   | -   | -    | ++      | +   | -   | -    | ++        | +   | -   | -    |

1000 nm hollow spheres, regardless of surface charge, had low internalization with 9–13% of uptake in both cell types investigated. For all the sizes, negatively charged hollow spheres presented the lowest uptake profile compared to their respective PEGylated and neutral hollow spheres.

### *2.3.3.4 High Content Analysis of Cellular Internalization*

HCA enabled quantitative estimation of the internalization of FITC labelled hollow spheres of different parameters, including size, surface charges and time points when tested with HUVECs and HUASMCs. Cellular internalization was estimated in terms of relative fluorescence. The results showed that 100nm neutral hollow spheres were significantly more internalized ( $p < 0.05$ ) when compared with other sizes, for PEGylated and neutrally charged hollow spheres in both cell types, which is consistent with flow cytometric data, and showed a constant increase of internalization over time from a relative fluorescence value of 6 to 18 in HUVECs (Figures 2.16 and 2.17). Internalization is reduced in HUASMCs for all sizes and surface charges (Figures 2.18 and 2.19). PEGylated 100 nm hollow spheres show the same level of internalization with HUVECs and HUASMCs with an approximate relative fluorescence value of 8. Negatively charged spheres for all sizes resulted in less internalization in both type of cells. Also, neutral, PEGylated and negatively charged hollow spheres of 1000 nm size had much less uptake for all the time points. Overall, the interactions of 100 nm hollow spheres with both cell types result in a higher degree of internalization compared to the 300, 500 and 1000 nm size hollow spheres. The effect of size on internalization is inversely related [29, 30], while the neutrally charged hollow spheres appear to be more relevant than PEGylated and negatively charged hollow spheres for internalization. HUASMCs appear more resistant to internalization of hollow spheres than HUVECs.

## **2.4 Discussion**

A wide-ranging family of hollow spheres, with the potential to deliver drugs, compounds and/or genetic material, was developed with various sizes and surface charges. Sizes ranging between 100 and 1000 nm were prepared and samples were modified to obtain neutral surface charge and less negative surface charge (PEGylated). In order to evaluate the potential of these hollow spheres to be used as a delivery vehicle, cytotoxicity and cellular internalization were investigated (Table 2.1).

Surface charge and size exerted a significant influence on the hollow spheres' behaviour, most notably on toxicity and cellular uptake over time. HUVECs and HUASMCs showed different cytotoxicity responses when incubated with the hollow spheres which were quantified using MTT assay (Figures 2.4–2.11). Size and surface charge did not have any significant effect on

HUASMCs when compared with controls (Figure 2.8–2.11). However, surface charge showed a significant effect on the viability of HUVECs (Figure 2.4–2.7). The effect of surface charge was not significant with 1000 nm hollow spheres; however, for 100, 300 and 500 nm hollow spheres, surface charge did have a significant effect ( $p < 0.05$ ). Negatively charged 100 nm hollow spheres demonstrated reduced cytotoxic effects on cells compared to neutral and PEGylated hollow spheres. However, there was a transition to neutral and then PEGylated hollow spheres having greater viability with HUVECs at sizes 300 and 500 nm respectively. This suggests that there is a synergistic relationship between the size and surface charge that dictates their cytotoxicity. 1000 nm hollow spheres displayed the highest viability with PEGylated and neutral charge hollow spheres ( $p < 0.05$ ). However, there was no significant difference between 100 and 1000 nm hollow spheres when the surface charge was negative. This was attributed to the low internalization of 100 nm negatively charged spheres within the cells.

Cellular uptake of spheres is significantly dependent on size and surface charge, and 100 nm appeared to be an optimum size for internalization for neutral and PEGylated hollow spheres. Cellular internalization is also dependent on parameters, e.g. size, surface charge, incubation time and also the cell type. HUVECs and HUASMCs showed different internalization behaviour with these hollow spheres over different time points, varying size and charge. This was supported by flow cytometry and HCA data. 100 nm and other hollow spheres displayed relatively increased uptake within HUVECs compared to that of HUASMCs, with the exception of 1000 nm hollow spheres, where internalization was seen to be insignificant for both cell types. 100 nm neutral hollow spheres showed more uptake than 100 nm PEGylated hollow spheres, whereas there was no significant difference of internalization between 300 nm and 500 nm neutral and PEGylated hollow spheres. This indicates that there is a size limit beyond which surface modification has no influence on cellular internalization. Negative charge of the cell membrane is an obvious reason for the low internalization of negatively charged hollow spheres, and hence internalization of spheres into cells requires a holistic approach that takes account of size and surface charge.

### **2.5 Conclusions**

FITC labelled chitosan/PGA hollow spheres with definite hollow spheres size and surface charge were created for elucidating the combinatorial effects of physicochemical properties on cellular internalization and cell viability. It was clear that physicochemical differences such as alternation of size and zeta potential played a vital role in internalization behaviour of hollow spheres as well as on cell viability and blood compatibility. FITC labelled negative, neutral and

PEGylated hollow spheres showed cell-line-dependent internalization behaviour. The results were in accord with those of inorganic spheres and liposomes, indicating that size and surface charge of spheres are more important parameters than the sphere's composition [28]. Therefore, results obtained using tunable chitosan/PGA hollow spheres as a model system in the present investigation could be applied to other types of solid spheres as well as to hollow spheres. These results are of potential value as guidelines for predicting the behaviour of spheres for specific desired applications in biological and pharmaceutical fields, including design of nanometre to submicron-sized delivery vehicles.

## 2.6 References

- [1] Meier W. Polymer nanocapsule. *Chem Soc Rev* 2000; 29: 295–303.
- [2] Lensen D, Vriezema DM, van Hest JC. Polymeric microcapsules for synthetic applications. *Macromol Biosci* 2008; 8(11): 991–1005.
- [3] Zelikin AN, Becker AL, Johnston AP, Wark KL, Turatti F, Caruso F. A general approach for DNA encapsulation in degradable polymer microcapsules. *ACS Nano* 2007; 1(1): 63–9.
- [4] Rethore G, Mathew A, Naik H, Pandit A. Preparation of chitosan/polyglutamic acid spheres based on the use of polystyrene template as a nonviral gene carrier. *Tissue Eng Part C Methods* 2009; 15(4): 605–13.
- [5] Kuykendall DW, Zimmerman SC. Nanoparticles: a very versatile nanocapsule. *Nat Nanotechnol* 2007; 2(4): 201–2.
- [6] Kim E, Kim D, Jung H, Lee J, Paul S, Selvapalam N, Yang Y, Lim N, Park CG, Kim K. Facile, template-free synthesis of stimuli-responsive polymer nanocapsules for targeted drug delivery. *Angew Chem Int Ed Engl* 2010; 49(26): 4405–8.
- [7] Rethore G, Pandit A. Use of templates to fabricate nanoscale spherical structures for defined architectural control. *Small* 2010; 6(4): 488–98.
- [8] Caruso F, Caruso RA, Mohwald H. Nanoengineering of inorganic and hybrid hollow spheres by colloidal templating. *Science* 1998; 282(5391): 1111–4.
- [9] Alexis F, Pridgen E, Molnar LK, Farokhzad OC. Factors affecting the clearance and biodistribution of polymeric nanoparticles. *Mol Pharm* 2008; 5 (4): 505–15.
- [10] Chono S, Tanino T, Seki T, Morimoto K. Uptake characteristics of liposomes by rat alveolar macrophages: influence of particle size and surface mannose modification. *J Pharm Pharmacol* 2007; 59(1): 75–80.
- [11] Osaki F, Kanamori T, Sando S, Sera T, Aoyama Y. A quantum dot conjugated sugar ball and its cellular uptake: on the size effects of endocytosis in the subviral region. *J Am Chem Soc* 2004; 126(21): 6520–1.
- [12] Win KY, Feng SS. Effects of particle size and surface coating on cellular uptake of polymeric nanoparticles for oral delivery of anticancer drugs. *Biomaterials* 2005; 26(15): 2713–22.
- [13] Foged C, Brodin B, Frokjaer S, Sundblad A. Particle size and surface charge affect particle uptake by human dendritic cells in an in vitro model. *Int J Pharm* 2005; 298(2): 315–22.
- [14] Chithrani BD, Ghazani AA, Chan WC. Determining the size and shape dependence of gold nanoparticle uptake into mammalian cells. *Nano Lett* 2006; 6(4): 662–8.

- [15] Jiang W, Kim BY, Rutka JT, Chan, WC. Nanoparticle-mediated cellular response is size-dependent. *Nat Nanotechnol* 2008; 3(3): 145–50.
- [16] Lu F, Wu SH, Hung Y, Mou CY. Size effect on cell uptake in well-suspended, uniform mesoporous silica nanoparticles. *Small* 2009; 5(12): 1408–13.
- [17] Lee KD, Nir S, Papahadjopoulos D. Quantitative analysis of liposome–cell interactions in vitro: rate constants of binding and endocytosis with suspension and adherent J774 cells and human monocytes. *Biochemistry* 1993; 32(3): 889–99.
- [18] Warheit DB. How meaningful are the results of nanotoxicity studies in the absence of adequate material characterization? *Toxicol Sci* 2008; 101(2): 183–5.
- [19] Murdock RC, Braydich-Stolle L, Schrand AM, Schlager JJ, Hussain SM. Characterization of nanomaterial dispersion in solution prior to in vitro exposure using dynamic light scattering technique. *Toxicol Sci* 2008; 101(2): 239–53.
- [20] Prabhu BM, Ali SF, Murdock, RC, Hussain SM, Srivatsan M. Copper nanoparticles exert size and concentration dependent toxicity on somatosensory neurons of rat. *Nanotoxicology* 2010; 4(2): 150–60.
- [21] Napierska D, Thomassen LC, Rabolli V, Lison D, Gonzalez L, Kirsch-Volders M, Martens JA, Hoet PH. Size-dependent cytotoxicity of monodisperse silica nanoparticles in human endothelial cells. *Small* 2009; 5(7): 846–53.
- [22] Wittmaack K. In search of the most relevant parameter for quantifying lung inflammatory response to nanoparticle exposure: particle number, surface area, or what? *Environ Health Perspect* 2007; 115(2): 187–94.
- [23] Gojova A, Guo B, Kota RS, Rutledge JC, Kennedy IM, Barakat AI. Induction of inflammation in vascular endothelial cells by metal oxide nanoparticles: effect of particle composition. *Environ Health Perspect* 2007; 115(3): 403–9.
- [24] Mayer A, Vadon M, Rinner B, Novak A, Wintersteiger R, Frohlich E. The role of nanoparticle size in hemocompatibility. *Toxicology* 2009; 258(2–3): 139–47.
- [25] Gratton SE, Ropp PA, Pohlhaus PD, Luft JC, Madden VJ, Napier ME, DeSimone JM. The effect of particle design on cellular internalization pathways. *Proc Natl Acad Sci USA* 2008; 105(33): 11613–8.
- [26] Cortez C, Tomaskovic-Crook E, Johnston AP, Scott AM, Nice EC, Heath JK, Caruso, F. Influence of size, surface, cell line, and kinetic properties on the specific binding of A33 antigen-targeted multilayered particles and capsules to colorectal cancer cells. *ACS Nano* 2007; 1(2): 93–102.

- [27] Zauner W, Farrow NA, Haines AM. In vitro uptake of polystyrene microspheres: effect of particle size, cell line and cell density. *J Control Release* 2001; 71(1): 39–51.
- [28] Clift MJ, Rothen-Rutishauser B, Brown DM, Duffin R, Donaldson K, Proudfoot L, Guy K, Stone V. The impact of different nanoparticle surface chemistry and size on uptake and toxicity in a murine macrophage cell line. *Toxicol Appl Pharmacol* 2008; 232(3): 418–27.
- [29] Chung T-H, Wu S-H, Yao M, Lu C-W, Lin Y-S, Hung Y, Mou CY, Chen YC, Huang D. M. The effect of surface charge on the uptake and biological function of mesoporous silica nanoparticles in 3T3-L1 cells and human mesenchymal stem cells. *Biomaterials* 2007; 28(19): 2959–66.
- [30] Rejman J, Oberle V, Zuhorn IS, Hoekstra D. Size-dependent internalization of particles via the pathways of clathrin- and caveolae-mediated endocytosis. *Biochem J* 2004; 377: 159–69.

## Chapter 3

### **Tunable Elastin-like Polypeptide Hollow Spheres as a High Payload and Controlled Delivery Gene Depot**

Sections of this chapter have been previously published in:

Dash BC, Mahor S, Carroll O, Mathew A, Wang W, Woodhouse KA, Pandit A. Tunable Elastin-like Polypeptide Hollow Sphere as a High Payload and Controlled Delivery Gene Depot. *J Control Release* 2011; 15: 382–92.

### 3.1 Introduction

Self-assembly, a free-energy driven process, allows production of a variety of nanostructures that can be readily and finely tuned by molecular chemistry, assembly environment (pH, solvents, co-assembling molecules and temperature), and assembly kinetics [1, 2]. Polymeric and peptide amphiphiles tailored with self-assembly properties have been utilized to produce nanoparticles, nanotubes and nanofibers for applications ranging from drug delivery and biosensing to tissue engineering [1–5]. However, to be used as a promising gene delivery depot for therapeutic efficacy while at the same time minimizing undesired side-effects, these structures should 1) be non-detrimental to cell viability, non-inflammatory and biodegrade into non-toxic products; 2) be easy to synthesize with high yield and purity; 3) have readily accessible surface functional groups that can be used to tether different targeting moieties if necessary; 4) have high loading efficiency with controlled release; and 5) offer protection of the gene from endosomal degradation [6].

Elastin-like polypeptide (ELP) is one of the suitable candidates for various biomedical applications because of its biodegradable, non-toxic, non-inflammatory properties and efficient pharmacokinetics for the delivery of therapeutics [7–15]. ELPs are basically a class of polypeptide polymers composed of tetra, penta and hexapeptide tandem repeats of valine, proline, alanine and glycine. These polypeptides undergo phase transition above a certain critical temperature to form insoluble nano to microparticles that are reversible in nature [16–22]. Upon further incubation, these nano to microparticles coalesce to form larger aggregates or highly organized filamentous and fiber-like morphologies [21, 23–25]. This can increase their antigenicity or reduce their potential uptake by affecting access, and particle jamming [26–28]. Methods such as agitation or sonication can limit aggregation, but the mechanical stress may affect the loaded therapeutics. Additionally, an intrinsic adhesive property may cause the particles to coalesce again after a few treatments [27]. In two completely different studies, the Woodhouse group [16] and the Rodriguez-Cabello group [29] have demonstrated stable nano to microparticles of ELP, which is important for therapeutic delivery. Some of the recent studies are more focused on controlling the size and homogeneity of the ELP particles, which are two key factors in improving therapeutic efficacy. The strategies that describe stable, nearly monodisperse ELP particles include those by Chilkoti and colleagues [30] in which they demonstrated the fabrication of sub-100 nm sized particles from self-assembly of artificial recombinant chimeric protein conjugated to diverse hydrophobic molecules and chemotherapeutics; and by Kobatake and colleagues [27] in which the chimeric fusion protein

of ELP and polyaspartic acid chain self-assembled into sub-100 nm sized particles at 37°C. Also, in a recent study, Chaikof et al. have demonstrated thermally responsive micelle formation from recombinant amphiphilic diblock polypeptides based on elastin-mimetic sequences [23].

In this study, the specific objectives were to 1) fabricate monodispersed hollow spheres of various sizes using a chimeric ELP<sub>20–24</sub><sup>4</sup> of approximately 35 kDa synthesized by Woodhouse and colleagues (Figure 3.1) [21] and 2) characterize loading capacity of these hollow spheres to use them as a reservoir of plasmid DNA (*pDNA*) as well as a gene delivery vehicle. This chimeric ELP contains alternating hydrophobic blocks and cross-linking domains derived from human elastin protein; the chimeric ELP resembles amphiphilic block copolymers. The hydrophobic domains, as mentioned before, facilitate self-aggregation as well as elastomeric functions, while the cross-linking domains contain lysine residues, flanked by either alanine or proline, imparting the ability to undergo covalent cross-linking. Self-assembly and a slightly positive charge of ELP in aqueous solution assisted in a rapid fabrication of monodisperse ELP hollow spheres of tuneable sizes from nanometre to sub-micron range by using a template-based method (Figure 3.2). These hollow spheres are biodegradable, have less effect on cell viability with high *pDNA* loading efficiency, and exhibit a controlled release characteristic.

### 3.2 Materials and Methods

#### 3.2.1 Materials

Polystyrene (PS) beads of 100 and 300 nm, sulfuric acid, tetrahydrofuran (THF), DNase free water, agarose, sodium chloride, sodium acetate, sodium bicarbonate, poly-D-glutamic acid (PGA), bicinchoninic acid (BCA) kit, glutaraldehyde, sodium dodecyl sulfate (SDS), 30% acrylamide-bis and ammonium persulfate, Dulbecco's modified Eagle's medium (DMEM) with L-glutamine, Hank's balanced salt solution (HBSS), phosphate buffer saline (PBS), bovine serum albumin (BSA), sodium cacodylate, uranyl acetate hydrate and fetal bovine serum (FBS) were purchased from Sigma-Aldrich. Tetramethylethylenediamine was from BIO-RAD and PS beads of 500 and 1000 nm from GENTAUR. Quant-iT™ PicoGreen® dsDNA kit, alamarBlue®, fluorescein isothiocyanate (FITC), LysoTracker® Blue DND-22, cy3 and SimplyBlue™ SafeStain were from Invitrogen and trinitrobenzene sulfonic acid (TNBSA) were purchased from Pierce. Gaussia luciferase (*pCMV–GLuC*), green fluorescence protein (*pCMV–GFP*) plasmids and gaussia luciferase assay kit were purchased from New England BioLabs, and agar low viscosity resin kit, SEM carbon tabs and carbon coated copper grids from Agar Scientific. Ca<sup>2+</sup>-independent microbial transglutaminase (mTGase) was from Activa®WM. CM52 cation exchange resin was purchased from Whatman, and

transglutaminase (TGase) colorimetric microassay kit from Covalab. EP20–24<sup>4</sup> was provided by Elastin Specialties and poly (2-dimethyl-aminoethylmethacrylate) (PDMAEMA)-block-poly ethylene glycol methyl ether methacrylate (PEGMEMA)/ethylene dimethacrylate (EDGMA) was synthesized in the laboratory. Human umbilical vein endothelial cells (HUVECs) and EBM media were obtained from Lonza and rabbit adipose derived stem cells (ADSCs) were isolated using the standard protocol.

### **3.2.2 EP20–24 Polypeptide Expression and Purification**

EP20–24<sup>4</sup> relates to the recombinant ELP with exons 20–21–23–24–21–23–24–21–23–24–21–23–24 found in the human aortic elastin and was expressed and purified as reported previously [31]. ELP of 94% purity was obtained.

### **3.2.3 Purification of mTGase**

Ca<sup>2+</sup>-independent mTGase was purified as previously described [32, 33]. Briefly, the enzyme sample was dissolved in 20 mM sodium acetate buffer pH 5.8 at a concentration of 500 mg/ml and added to a glass column (1.5 × 30 cm) containing CM52 cation exchange resin pre-equilibrated with the above buffer at a flow rate of 2 ml/min. The sample was washed with two column volumes of the same buffer and eluted by a gradient of 10 column volumes from 0 to 0.5 M sodium chloride. The samples were analysed at 280 nm for protein and the pooled fractions were concentrated, dialyzed into PBS and analysed for enzyme activity using the transglutaminase colorimetric micro assay kit and purified guinea pig TGase (control) with known units of activity as standard (where 1 unit will catalyze the formation of 1 μmole of hydroxamate at pH 6.0 at 37°C using L-glutamic acid-monohydroxamate as the standard). Typical activity recovered was in the range of 0.5 U/mg mTGase.

### **3.2.4 Fabrication of Hollow Spheres**

ELP hollow spheres were fabricated using a template-based method [34–37]. Briefly, the fabrication method includes three processes: coating, cross-linking, and dissolution of the core to obtain the hollow sphere. PS beads of monodisperse sizes were sulfonated to create a negative surface charge on the sphere [35, 36]. These sulfonated PS beads were then used as a template. ELP of ~35 kDa was used to coat the sulfonated PS beads in PBS. The coating of ELP was further characterized at different time points (10, 30 and 60 min) and temperatures (4, 20 and 37°C) to illustrate the role of self-assembly. Also, the ELP requirement for each size of PS beads was quantified using different ratios of PS beads to ELP (20:1, 15:1 and 10:1 w/w). The coated beads were then washed three times with deionized water and incubated at different concentrations (20, 50 and 100 U/g of ELP) of mTGase for cross-linking. Finally, PS beads

were dissolved using THF to obtain the hollow spheres. Coating, cross-linking and hollow spheres were characterized using zeta sizer, scanning electron microscope (SEM), transmission electron microscope (TEM), BCA and TNBSA assays.

### **3.2.5 Size and Zeta Potential Analysis**

Zeta sizer (Malvern, Nano-ZS90) was used to characterize the ELP coating over sulfonated PS beads. 500 nm PS beads were sulfonated and used for the coating experiment. ELP coated beads of different parameters (incubation time point, temperature and concentration of ELP to that of a fixed quantity of PS beads) were resuspended in PBS for size and zeta potential analysis. In addition, the surface charge of hollow spheres was analysed. Stability of the pre-cross-linked and cross-linked spheres on days 1 and 15 was checked by performing size analysis.

### **3.2.6 ELP Adsorption Studies**

BCA assay was performed to optimize ELP requirement for the coating of 100, 300, 500 and 1000 nm size of PS beads and also to analyse the effect of incubation time and temperature on coating. BCA is a biochemical assay used to determine the total level of protein in a solution [38]. The total protein concentration is indicated by a change of the sample solution from green to purple in proportion to protein concentration, which can then be measured using colorimetric techniques at 562 nm. Briefly, after coating of ELP on PS beads, the coated beads were washed with water three times and then the amount of protein in the supernatant was quantified using BCA assay. Finally, the amount of ELP in the supernatant was deducted from the initial amount of ELP used to quantify the amount of ELP coated on the beads. BSA was used as a standard in the procedure.

### **3.2.7 TNBSA Assay for Cross-linking**

The cross-linking of ELP hollow spheres with mTGase was analysed using TNBSA. TNBSA is a hydrophilic modifying reagent for the detection of primary amines in samples containing amino acids, peptides or proteins [39]. It reacts readily with the primary amino groups of amino acids in aqueous solution at pH 8 to produce a yellow color. The colored derivatives are monitored at 335–345 nm. ELP, both with and without treatment of mTGase, was used for the assay. The mTGase of 20, 50 and 100 U/g were used to cross-link the ELP. In addition, ELP cross-linked with glutaraldehyde was used as a positive control.

### **3.2.8 SDS-PAGE Analysis for Cross-linking**

SDS polyacrylamide gel of 12% was used to characterize the cross-linking. The samples, ELP and mTGase alone and ELP treated with 0.001, 0.5, 1, 20 and 100 U/g of mTGase, were

electrophoresed under reducing conditions. The gel was stained with SimplyBlue™ SafeStain after electrophoresis as per manufacturer's instructions. Molecular weights were determined using a molecular weight marker.

### **3.2.9 Morphological Characterization**

#### *3.2.9.1 Surface Morphology Analysis using SEM*

SEM images were obtained using the Hitachi S-4700 field emission microscope operating with a beam voltage of 15 kV. A drop of sample containing hollow spheres was placed on adhesive carbon tabs mounted on SEM specimen stubs and then dried. The specimens were subsequently coated with gold using the Emitech K550 coating system.

#### *3.2.9.2 Internal Structure Analysis using TEM*

TEM measurements were performed using the Hitachi H-7500 microscope. The hollow spheres of all the four sizes were processed and embedded in resin. The resin embedded samples were then cut into sections of 90 nm thickness and observed under TEM. The detail regarding the processing of samples can be found in section 3.2.14.

### **3.2.10 Plasmid Propagation and Isolation**

pCMV-GLuc plasmid was transformed into XL1-Blue (Stratagene) competent cells and selected twice in antibiotic containing LB broth and on LB agar plates. Plasmid expansion was performed as recommended in the Giga-Prep (Qiagen) protocol and isolated using that kit. Plasmid purity was confirmed by UV spectroscopy (NanoDrop™ ND1000 Spectrophotometer, Thermo Scientific) and gel electrophoresis.

### **3.2.11 Polyplex Formulation**

Polyplexes were prepared using PDMAEMA polymer of 16 kDa [40] and pCMV-GLuc plasmid in PBS pH 7.4. The weight ratio of the polymer and pCMV-GLuc was optimized to 10:1. Polyplex of pCMV-GFP was prepared using a similar method.

### **3.2.12 Polyplex and Naked pDNA Loading Studies**

Briefly, 1 mg samples of 500 nm hollow spheres were resuspended in 300  $\mu$ l of PBS and polyplexes containing a predetermined amount of pDNA (20, 40, 80 and 160  $\mu$ g) were added (Figure 3.3). This mixture was then agitated for 12 hr at room temperature. The suspension was centrifuged at 13,000g and the sphere/polyplex complex was washed four times with ultra-pure water. The supernatant was collected to estimate the amount of pDNA, which was then deducted from the initial amount used to determine the loading efficiency of the hollow spheres. A similar approach was used for loading of naked pDNA in the hollow spheres. A comparison between solid spheres and hollow spheres for loading efficiency was performed.

300 nm sizes of hollow spheres were used against the same size of ELP solid spheres. For this particular experiment, 20  $\mu\text{g}$  of *pDNA* was used for loading in both hollow spheres and solid spheres, where ELP solid spheres of approximately 300 nm were fabricated by incubating 2 mg/ml of ELP solution with 20  $\mu\text{g}$  of *pDNA* at 37°C. The solid spheres were stable after cross-linking with mTGase and adding 20% of THF. A PicoGreen<sup>®</sup> assay was performed to quantify free *pDNA* for loading efficiency and release. To obtain free *pDNA*, polyplex samples collected during loading and release studies were treated with PGA of 10 mg/ml concentration at 37°C for 30 min with a modification of the protocol described [41]. Then, 100  $\mu\text{l}$  of PicoGreen<sup>®</sup> was added to a sample of similar volume and the fluorescence was analysed at 480 nm. A standard curve was prepared using naked *pDNA*. PGA was again used to quantify the amount of *pDNA* attached to the surface of the spheres as polyplexes. Briefly, the loaded hollow spheres were treated with 10 mg/ml of PGA for 30 min at 37°C. The samples were then centrifuged and the supernatant was collected for quantification of *pDNA* using PicoGreen<sup>®</sup> assay.

### **3.2.13 *In vitro* Release Studies**

To characterize the release pattern of the polyplex loaded hollow spheres, 1 mg of polyplex loaded hollow spheres of 100, 300, 500 and 1000 nm sizes was resuspended in PBS and incubated at 37°C. At every time point, the suspension was centrifuged and a sample of the supernatant taken. The 1000 nm hollow spheres were treated with enzymes elastase and protease 10 U/g of ELP sphere at pH 7.4 in PBS to investigate the enzyme triggered release from these hollow spheres. Released polyplexes were treated with PGA as mentioned in section 2.12 and quantified using PicoGreen<sup>®</sup> assay.

### **3.2.14 Imaging of Loaded Hollow Spheres by TEM**

The hollow spheres alone and polyplex loaded spheres were fixed with paraformaldehyde. The samples were washed in 0.2 M of sodium cacodylate buffer and spun to obtain a pellet. The samples were stained using 2% osmium tetroxide (diluted in 0.2 M sodium cacodylate buffer). The staining process was followed by washing in 0.2 M cacodylate buffer and then by dehydration process using a gradient of ethanol (30, 50, 70, 90 and 100% v/v). The samples were then left overnight in a solution of ethanol and resin (50:50). Finally, the solution was replaced with freshly prepared 100% resin and left for polymerization for three days at 60°C. The polymerized samples were cut into sections of 90 nm thickness using an ultramicrotome and then stained with uranyl acetate before observation under TEM.

### 3.2.15 Cell Culture Studies

HUVECs and rabbit ADSCs were grown in T75 flasks using EGM-2 and DMEM with 2 mM L-glutamine, 10% FBS and 1% ampicillin media respectively. The cells were incubated at 37°C in an atmosphere of 5% CO<sub>2</sub>. The culture medium was changed every 36 hr. The cells were then harvested and sub-cultured when >80% confluence was observed.

### 3.2.16 Cell Viability Studies

AlamarBlue<sup>®</sup> and PicoGreen<sup>®</sup> assays were performed to quantify the cell viability of polyplex loaded spheres in HUVECs and ADSCs. HUVECs and ADSCs were seeded at cell density of  $2 \times 10^4$  cell/well in a 48 well tissue culture plate, grown overnight and incubated with polyplex loaded hollow spheres of all the four sizes and with polyplex alone for 48 hr. Cells without treatment were kept as control. alamarBlue<sup>®</sup> assay was used to assess the cellular metabolic activity. The cells were washed with HBSS and replaced with 200  $\mu$ l of fresh HBSS with alamarBlue<sup>®</sup> (10% v/v). After 3 h incubation at 37°C in 5% CO<sub>2</sub>, 200  $\mu$ l of assay media was transferred to a 96 well plate, absorbance was read at 550 and 595 nm on a microplate reader (VarioskanFlash-4.00.53) and the percentage reduction of the dye was calculated. A PicoGreen<sup>®</sup> assay was then performed on the same plates used for alamarBlue<sup>®</sup> to quantify the DNA amount. Cells were repeatedly frozen at -80°C and thawed to lyse the cell and release the entire DNA content. Finally, fluorescence was measured at 480 nm. Cell viability was expressed in terms of amount of DNA.

### 3.2.17 Transfection Studies

Polyplex loaded hollow spheres of four different sizes were used for transfection efficiency using ADSCs and HUVECs. Briefly, 10,000 cells were seeded in 48 well plates and incubated for 48 h with hollow spheres containing polyplexes consisting of 2.5  $\mu$ g *p*DNA. Cells treated with polyplex, *p*DNA and hollow spheres containing *p*DNA were used as control with each containing 2.5  $\mu$ g of *p*DNA. All experiments were performed with serum in medium. After the 48 hr incubation period, 50  $\mu$ l media from all the samples were collected for quantification of luciferase expression using a gaussia luciferase assay kit. The luciferase assay was performed in accordance with manufacturer's instructions. In addition, transfection of released polyplexes was observed after 48 h of incubation with ADSCs under a fluorescence microscope. The luciferase expression level was expressed as relative light units (RLU).

### 3.2.18 Cellular Localization of Hollow Spheres

The cellular internalization pathway of 500 nm hollow spheres was characterized by TEM. ADSCs in T75 flasks were incubated with 500  $\mu$ g of spheres for 24 hr. Cells were washed three

times in 0.2 M sodium cacodylate buffer and fixed using paraformaldehyde. The cells were stained using 2% osmium tetroxide for 2 hr and washed three times in 0.2 M sodium cacodylate buffer. Then the cell layer was removed, treating the flask with propylene oxide for 5 min. The cell layer was collected from the flask and spun to obtain a pellet. The pellet was then processed in accordance with the method described in section 3.2.14 above, and observed under TEM.

### 3.2.19 Colocalization Studies

*pDNA* was labelled with cy3 dye. The naked *pDNA*-cy3 and polyplex (cy3-*pDNA* and polymer) were then loaded inside 500 nm sized hollow spheres. The hollow spheres were incubated with ADSCs for 24 hr followed by repeated washes with HBSS. LysoTracker Blue was used as per manufacturer's instructions to stain the lysosomes in live cells. Cells were kept in the incubator for 2 hr. The cells were fixed with 2% paraformaldehyde for 30 min and this was followed by several washes with PBS. The cells were then observed under the fluorescence microscope (Olympus IX81). LysoTracker Blue staining was tinted as blue and cy3 as red. The images were merged to characterize the colocalization.

## 3.3 Results

### 3.3.1 Fabrication of Hollow Spheres

Characterizations for coating were performed using 500 nm sulfonated PS beads as a model system. Within 10 min of incubation of PS beads and ELP in PBS at 37°C, an increase in size was observed from  $515 \pm 12$  nm to a value of  $592 \pm 35$  nm (Figure 3.4). Additionally, zeta potential increased from  $-38.06 \pm 2.4$  mV that of sulfonated PS beads to a value of  $-8.27 \pm 0.78$  mV (Figure 3.6); similar increases in zeta potential and size, however, were seen only after 6 and 24 hr of incubation at 20°C and 4°C respectively. No significant difference in size and zeta potential was found between 10, 30 and 60 min of incubation (Figures 3.5 and 3.7). Also, increases in size and zeta potential were observed with the increase in ELP amount from 50 to 75  $\mu\text{g}/\text{mg}$  of 500 nm PS beads, but no significant change was found between 75 and 100  $\mu\text{g}/\text{mg}$  of PS beads (Figures 3.4 and 3.6). BCA assays characterizing protein adsorption on PS beads were in accordance with the zeta sizer results (Figures 3.8 and 3.9). The adsorption of ELP on 100, 300, 500 and 1000 nm sulfonated PS beads was characterized using BCA assay (Figure 3.10). This result showed an inverse relationship between the size of PS beads and ELP adsorption. Coating was further characterized using SEM. The images showed the surface of the spheres as rough after coating with ELP (Figure 3.11).

TNBSA assay was performed to characterize the mTGase cross-linking of ELP and also to quantify the amount of free primary amino groups available on the surface. A decrease in the

amount of free amino groups was observed after incubation with mTGase of different concentrations: 20, 50 and 100 U/g of ELP; whereas there was no significant difference between the mTGase concentrations 50 and 100 U/g of ELP in terms of free amino groups (Figure 3.12). Glutaraldehyde cross-linking resulted in the least amount of surface free amino groups. MTGase cross-linking was further characterized using SDS-PAGE. The ELP had a distinct band around 35 kDa, which diminished to a lighter smear with a gradual increase in enzyme concentration from 0.5 U/g of ELP (Figure 3.13). However, few weaker bands were seen in the gel, which may be due to the remaining 6% impurity of ELP.

After dissolving the PS beads with THF, hollow spheres were observed under TEM. The TEM images of spheres revealed the transparency of ELP hollow spheres (Figure 3.14), while the SEM images revealed their rough surfaces (Figure 3.15). The sizes of the hollow spheres as estimated from their TEM images were  $100 \pm 9$ ,  $300 \pm 40$ ,  $500 \pm 30$ , and  $1000 \pm 90$  nm. The surface charge of all sizes of hollow spheres, as measured using a zeta sizer, was in the range of  $-20$  to  $-27$  mV (Figure 3.16). The stability of the pre-cross-linked and cross-linked hollow spheres was checked on days 1 and 15 by diffraction light scattering analysis. The size distribution was measured as size versus volume percentage. Pre-cross-linked spheres showed wider size distribution with high polydispersity index (PdI) above 0.6. The Z- average was above 6  $\mu\text{m}$  on both days (Figure 3.17A and B). Cross-linked spheres had a narrow size distribution of 145–170 nm with a PdI of 0.05 to 0.128 (Figure 3.17C and D).

### 3.3.2 Polyplex and *p*DNA Loading Studies

The loading efficiency was analysed by quantification of *p*DNA in the supernatant using PicoGreen<sup>®</sup> assay (Figures 3.19–3.24). The hollow spheres of 300 nm had 25% higher *p*DNA loading efficiency than that seen in self-assembled ELP solid spheres (Figure 3.18) of similar size (Figure 3.19). Also, the result showed that almost 98% of *p*DNA was loaded within the hollow spheres in the form of polyplex as compared to 54% of *p*DNA alone (Figure 3.20). The maximum *p*DNA loading capacity was investigated by taking different ratios of hollow sphere to polyplex while keeping the weight of spheres constant. This result showed an increasing amount of *p*DNA loading with increasing ratio. The maximum loading was approximately 70  $\mu\text{g}$  of *p*DNA/mg for 500 nm hollow spheres in the case of 1:80 (Figure 3.21). All the four different sizes of hollow spheres showed similar loading efficiency (Figure 3.22). For a precise understanding of the mechanism of loading, the hollow spheres were further characterized. Zeta potential analysis of 500 nm hollow spheres after loading showed an increase in surface charge from a negative value to a value near to +7 mV (Figure 3.23). The amount of *p*DNA on

the outer surface was determined to be 8–10% of the total amount loaded as assayed by PicoGreen<sup>®</sup> (Figure 3.24). The TEM analysis showed that hollow spheres with polyplexes appeared to be denser than did unloaded hollow spheres (Figure 3.25A1). The inner hollow space was filled with polyplexes and an approximately 50 nm thick layer of polyplex was observed on the surface of the hollow sphere (Figure 3.25A2), which disappeared after treatment with PGA (Figure 3.25A3). In addition, TEM was performed on different samples of the ratios of sphere to polyplex loaded samples (Figure 3.26). This result was consistent with the PicoGreen<sup>®</sup> assay showing a higher amount of polyplex loaded spheres in the case of the 1:80 ratios (Figure 3.26A3). Figures 3.27 and 3.28 showed the efficiency of the PGA method used to quantify pDNA from polyplex. The results showed similar emission values for naked pDNA and polyplex treated with PGA in a PicoGreen<sup>®</sup> assay (Figure 3.27), and when a similar pattern of bands run through an agarose gel were seen for both naked pDNA and PGA treated polyplex (Figure 3.28).

### 3.3.3 *In Vitro* Release Studies

The ELP hollow spheres showed a minimal release of polyplexes when incubated at 37°C. The release pattern was studied for up to 192 hr for all sizes. Spheres of 1 mg dry weight containing 70 µg of pDNA (complexed with polymer) were used for this study. The cumulative release profile of polyplexes was quantified in terms of the amount of pDNA released. No significant difference in release pattern was observed in any of the sizes up to 96 hr. A total of 6–7 µg of pDNA was released from the spheres. The release profile was found to be different at 192 h, whereas the 100 and 300 nm hollow spheres showed less release than 500 and 1000 nm hollow spheres (Figure 3.29). Spheres on exposure to enzymatic treatment released polyplexes much faster than did untreated spheres (Figure 3.30). Untreated hollow spheres released 20% of pDNA at 72 hr, whereas the release for the elastase and protease treated spheres was found to be approximately 85 and 71% respectively. Hollow spheres were found to be degraded as observed under SEM (Figure 3.31). To probe the expression ability of the released polyplexes, pDNA encoding green fluorescent protein (pCMV-GFP) was used. The polyplexes were collected after 360 hr and incubated with ADSCs. The cells showed GFP expression when observed under a fluorescence microscope after 48 hr of incubation (Figure 3.32).

### 3.3.4 Transfection and Cellular Viability Studies

The transfection efficiency of the spheres and their effect on cell viability were analysed to validate their use as a gene delivery vehicle. Polyplex loaded spheres of all the sizes showed similar cell viability to that of the control in the case of both ADSCs and HUVECs, whereas

the cells treated with polyplex alone showed less cell viability, as is evident from the alamarBlue<sup>®</sup> assay (Figures 3.33 and 3.34). Polyplex loaded hollow spheres of all the sizes showed greater luciferase expression than did *pDNA* and polyplex alone in both ADSCs and HUVECs (Figures 3.35 and 3.36). In addition, similar luciferase expression was found for all sizes of spheres without any significant difference in either ADSCs or HUVECs. In addition, an almost 10 times higher luciferase expression level was observed in the case of polyplex loaded spheres than in the naked *pDNA* loaded spheres (Figure 3.37).

### 3.3.5 Cellular Localization Studies

The cellular localization of the spheres was investigated under TEM using 500 nm hollow spheres and ADSCs. Their intracellular compartmentalization was identified by morphological criteria. The spheres were seen to adhere to the intact cell membrane (CM) in Figure 3.38A. One of the spheres was subsequently engulfed by a membrane protrusion, probably via macropinocytosis (Figure 3.38B). Figure 3.35C shows some of the spheres localized in early endosomes (clear vesicular structure close to the CM). Eventually, in Figure 3.38D and 3.38E, spheres were seen inside the lysosome (granulated vesicle near the nucleus). In addition, the hollow spheres were observed to escape from the lysosome into the cytoplasm (Figure 3.38F), preventing themselves from undergoing endosomal degradation.

### 3.3.6 Fluorescence Colocalization Studies

500 nm hollow spheres containing cy3-*pDNA* can be observed inside cells (Figure 3.39). *pDNA*- hollow spheres (Figure 3.39A1–A3) and polyplex- hollow spheres (Figure 3.39B1–B3) were uptaken by ADSCs. The merged images of cy3-*pDNA* and lysosomes stained with LysoTracker Blue showed colocalization of the spheres inside lysosomes in both cases. The intensity of cy3-*pDNA* was found to be less in the case of *pDNA*- hollow spheres than that of polyplex- hollow spheres.

## 3.4 Discussion

Gene therapy has a potential use in treating many genetic disorders [42]. Liposomes [43], synthetic polymers [44, 45], and particles [46, 47] have been used as non-viral gene delivery vehicles as alternatives to viral vectors. It is generally known that use of these cationic polymers or lipoplexes as transfecting agents can have a detrimental effect on cell viability [48]. Recent approaches to gene delivery systems aim at reducing cytotoxicity by using peptide-based delivery systems [49–51]. Chimeric ELP polymers have recently emerged as a promising class of biomaterial in a number of biomedical applications from tissue engineering to drug delivery [7].

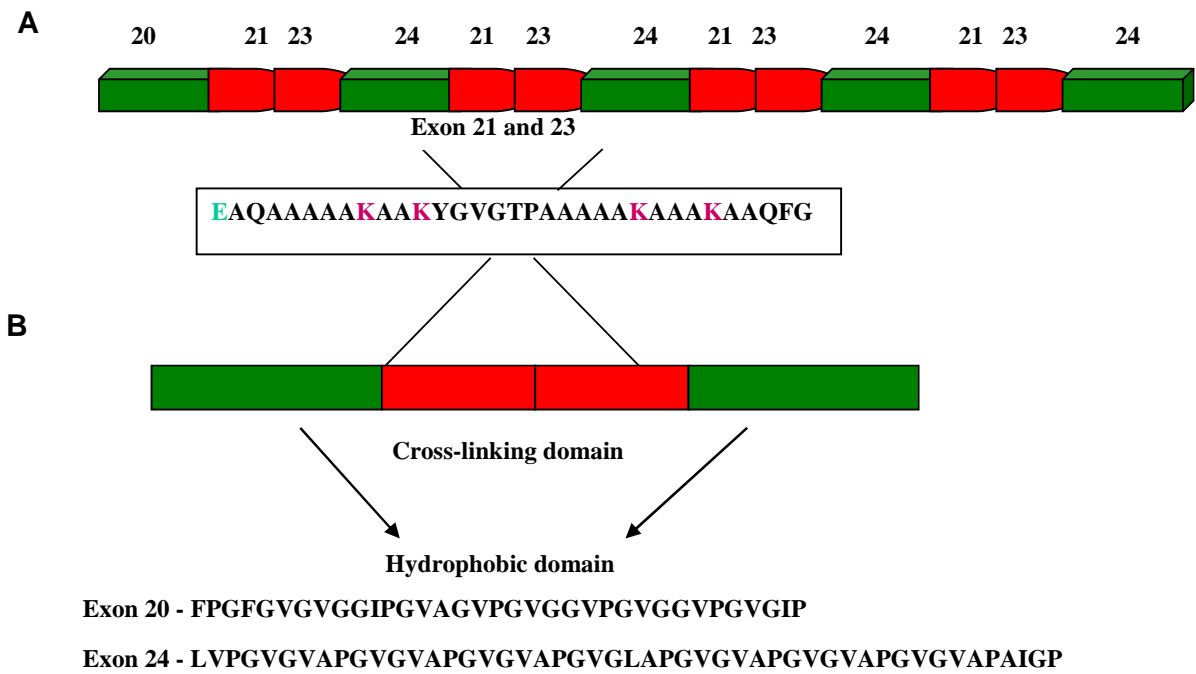


**Figure 3.1: Illustrating ELP<sub>20-24</sub><sup>4</sup> structure: (A) ELP<sub>20-24</sub><sup>4</sup> polypeptide sequence consisting of domains derived from human exons 20–21–23–24–21–23–24–21–23–24–21–23–24 and (B) showing amino acid sequence present in 20–21–23–24.**

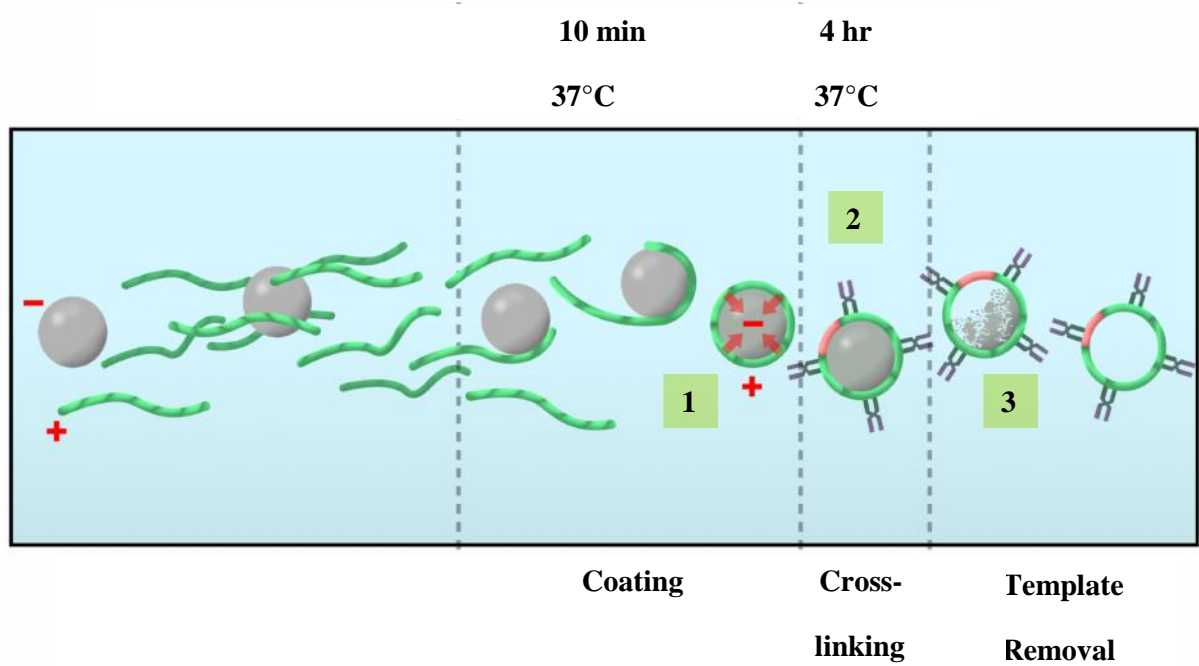


**Figure 3.2: Schematic representation of ELP hollow spheres fabrication using PS beads as a template. The process involves coating of ELP over sulfonated PS beads (Step 1), cross-linking with microbial transglutaminase (Step 2) and removal of PS bead to obtain the hollow spheres (Step 3).**

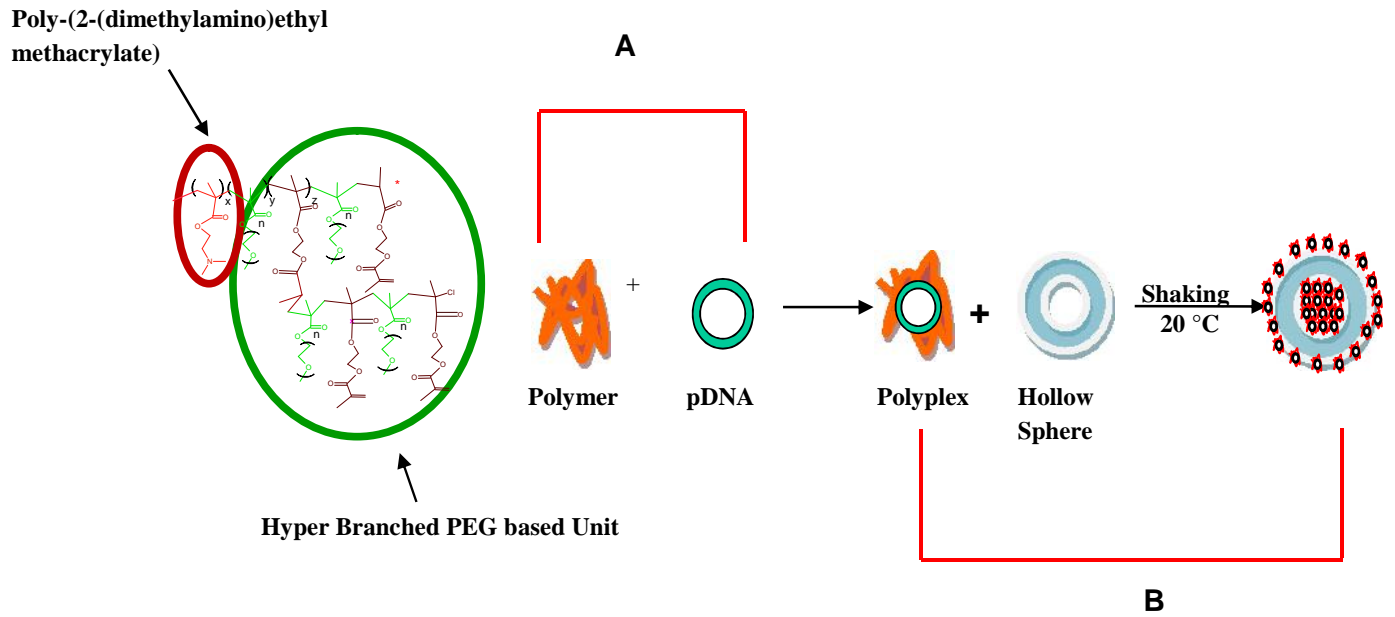
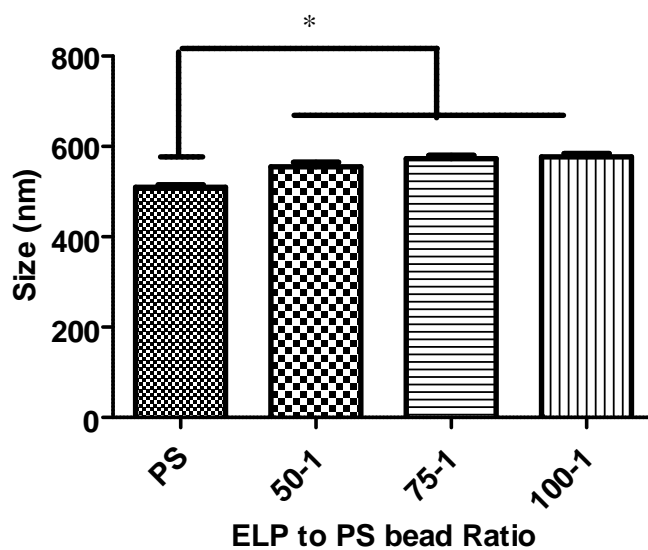
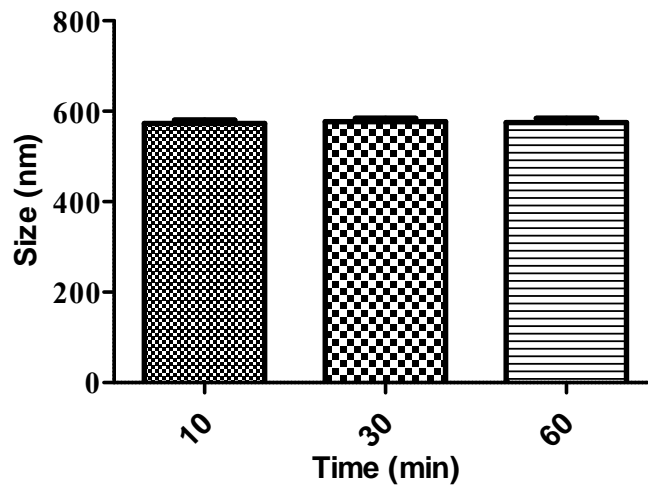


Figure 3.3: Schematic representation of (A) polyplex formation using the polymer and naked pDNA, (B) loading of polyplexes inside hollow spheres.



**Figure 3.4: Size analysis of coating of ELP over 500 nm PS beads at 37°C with different ratios of ELP to PS beads: statistical significance was determined by one-way ANOVA ( $n = 9, p < 0.05$ ). \* Represents statistical significance between PS beads alone and different ratios of ELP coated PS beads.**



**Figure 3.5: Size analysis of coating of ELP over 500 nm PS beads at 37°C over different time periods ( $n = 9$ ). No statistical significance was found between different groups.**

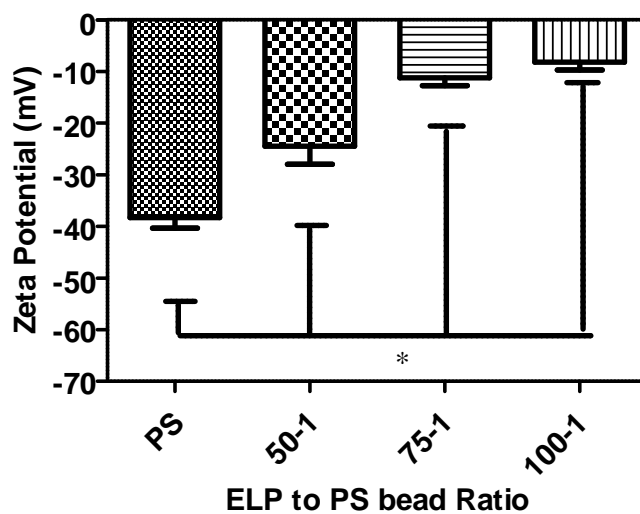


**Figure 3.6: Zeta potential analysis of ELP coating over 500 nm PS beads with different ratios of ELP to PS beads. Statistical significance was determined by one-way ANOVA ( $n = 9, p < 0.05$ ). \* Represents statistical significance between PS beads alone and different ratios of ELP coated PS beads.**

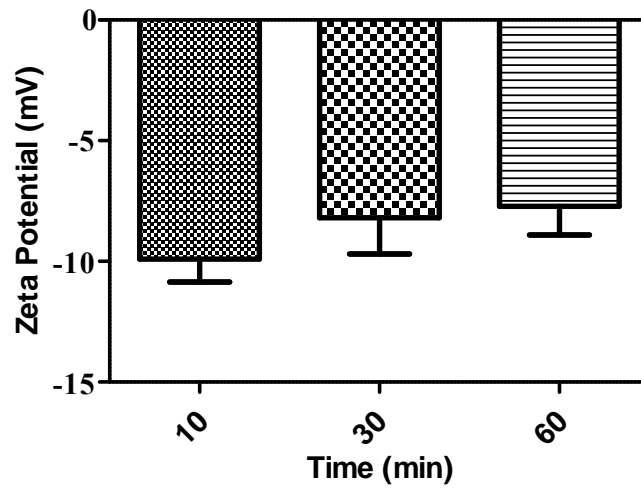


**Figure 3.7: Zeta potential analysis of ELP coating over 500 nm PS beads over different time periods ( $n = 9$ ). No statistical difference was found between different time points.**

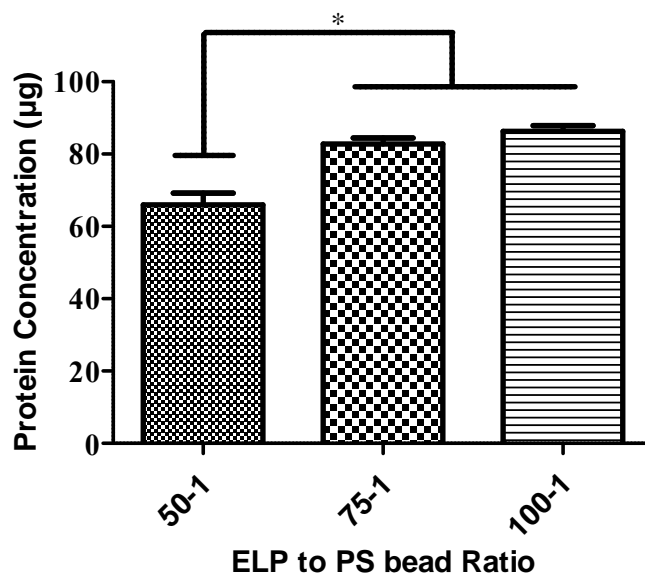


**Figure 3.8: BCA assay for quantification of coating over PS beads with different ratios of ELP to PS beads for 500 nm PS beads. Statistical significance was determined by one-way ANOVA ( $n = 6, p < 0.05$ ). \* Represents statistical significance between 50-1 to that of 75-1 and 100-1 groups.**

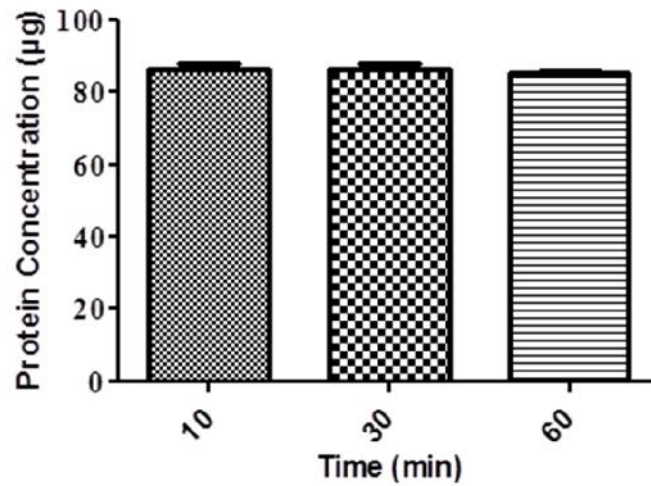


**Figure 3.9: BCA assay for quantification of coating of ELP on PS beads over different time points at 37°C ( $n = 6$ ). No statistical significance was found between different time points.**

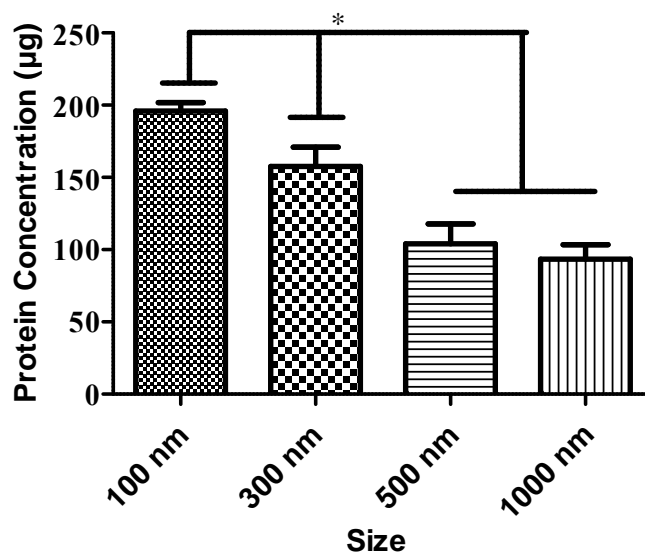


**Figure 3.10: Quantification of ELP required for coating of different sizes of PS beads using BCA assay. Statistical significance was determined by one-way ANOVA ( $n = 6, p < 0.05$ ). \* Represents statistical significance between various sizes in terms of their ELP requirement.**

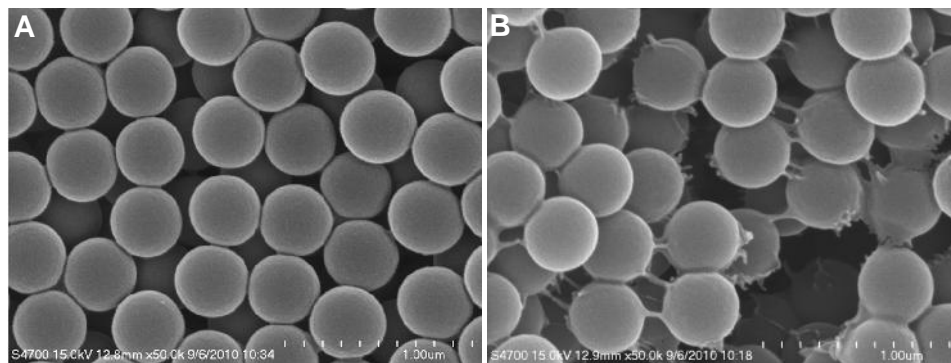


**Figure 3.11: SEM micrographs of 500 nm (A) uncoated and (B) ELP coated PS beads. The scale bars represent 1  $\mu\text{m}$ .**

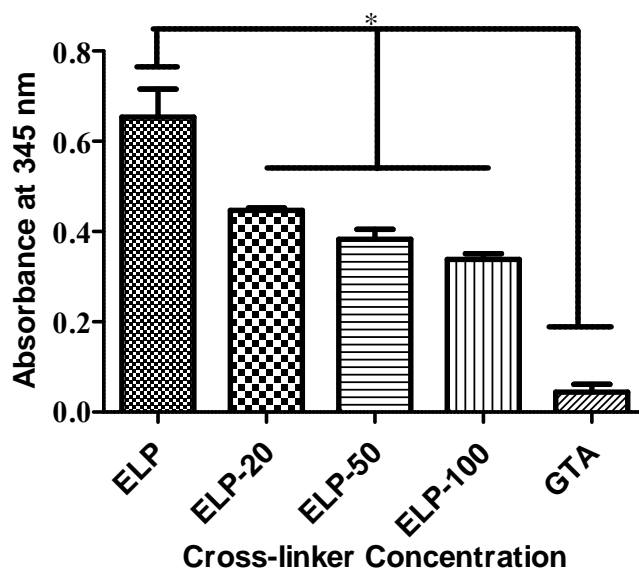


**Figure 3.12: TNBSA analysis to characterize the cross-linking of ELP with various amounts of mTGase enzyme. Glutaraldehyde and ELP alone were used as positive and negative controls respectively. Statistical significance was determined by one-way ANOVA ( $n = 9, p < 0.05$ ). \* Represents statistical difference between ELP and different ratios of ELP-mTGase along with GTA cross-linked ELP.**

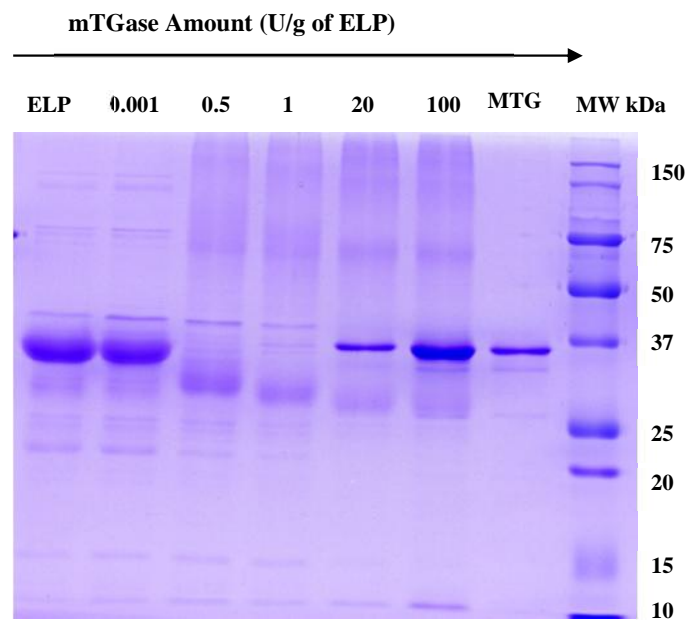


**Figure 3.13: SDS-PAGE showing the gradual cross-linking of ELP with increase in mTGase amounts. The gel was stained using SimplyBlue™ SafeStain.**

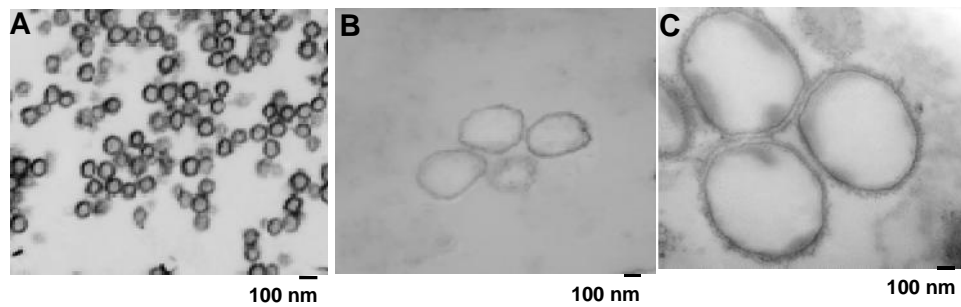


**Figure 3.14: TEM images of hollow spheres fabricated using (A) 100 nm, (B) 300 nm and (C) 1000 nm sizes of PS beads.**

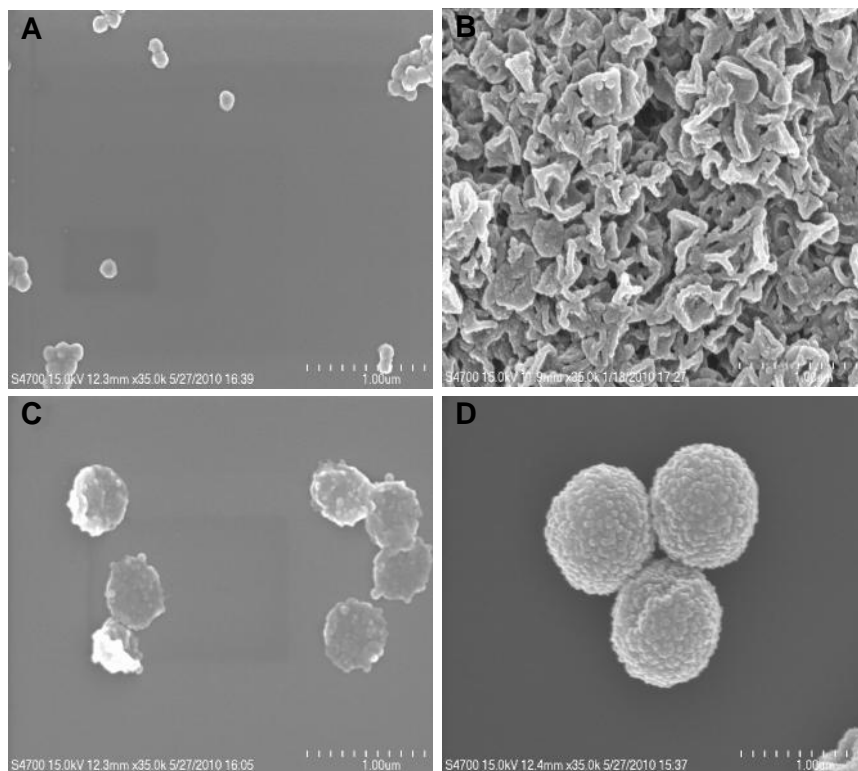


**Figure 3.15: SEM images of hollow spheres fabricated using (A) 100 nm, (B) 300 nm, (C) 500 nm and (D) 1000 nm sizes of PS beads.**

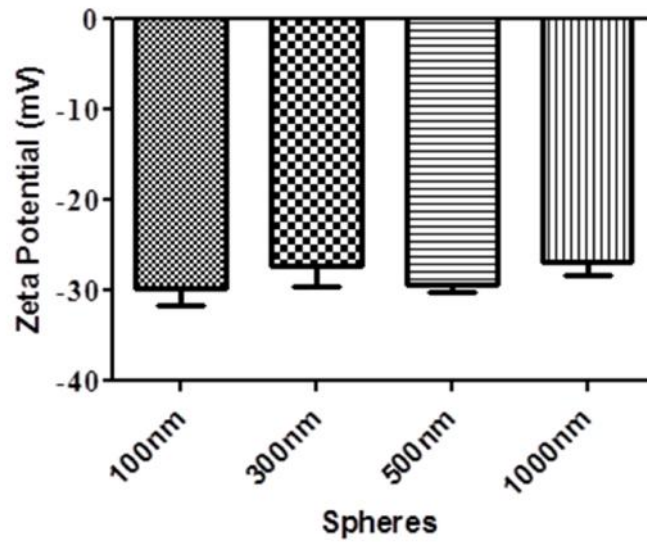


**Figure 3.16: Zeta potential analysis of hollow spheres fabricated using 100, 300, 500 and 1000 nm PS beads ( $n = 9$ ). No statistical significance was found between different groups.**

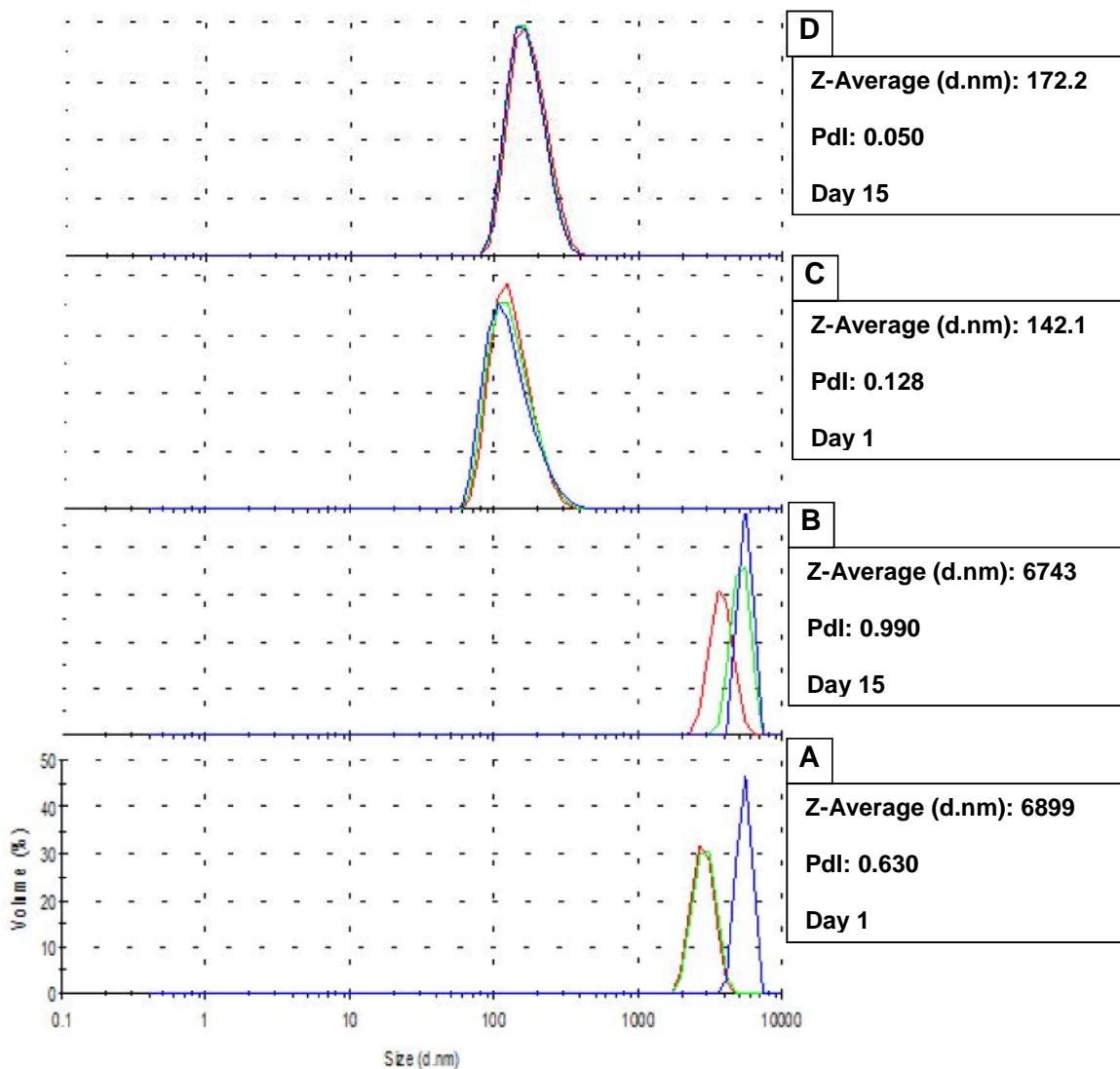


**Figure 3.17: Diffraction light scattering particle size analysis data of cross-linked and pre-cross-linked spheres made from 100 nm sulfonated PS beads. (A and B) Size distributions data of pre-cross-linked spheres on days 1 and 15 respectively. (C and D) Size distributions data of cross-linked spheres on days 1 and 15 respectively. Pdl, polydispersity index ( $n = 3$ ).**

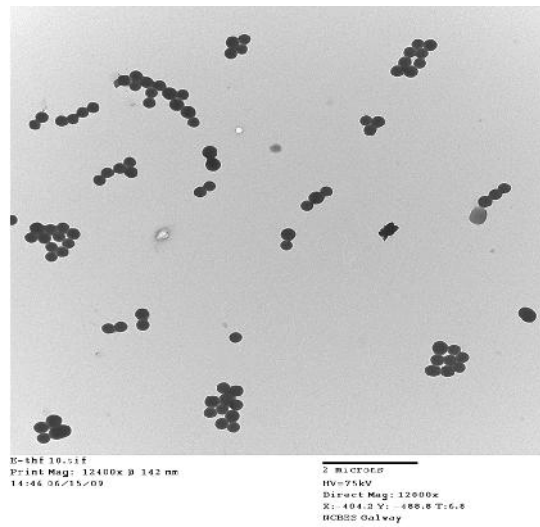


**Figure 3.18: TEM image of self-assembled ELP solid spheres cross-linked with mTGase and 20% THF. The scale bar represents 2  $\mu\text{m}$ .**

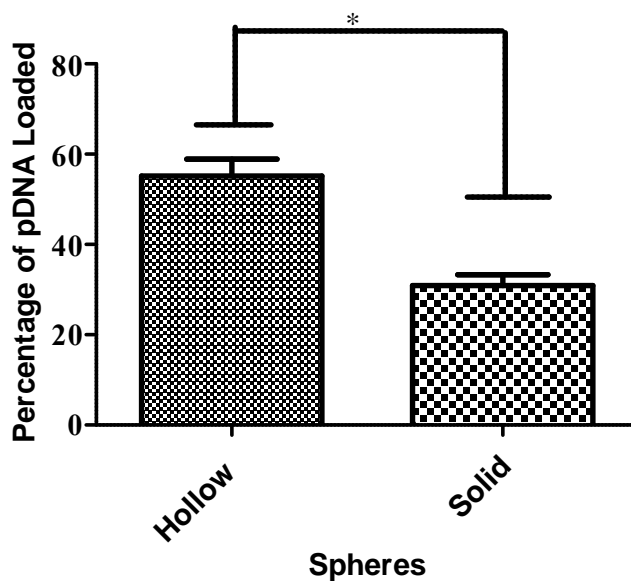


**Figure 3.19:** Comparison of *p*DNA loading efficiency of 300 nm hollow spheres and self-assembled ELP solid spheres of approx. 300 nm size. All the data are represented as mean  $\pm$  standard deviation ( $n = 3, p < 0.05$ ). Statistical analysis was performed using Student's *t*-test. \* Represents statistical significance between hollow spheres vs solid spheres.

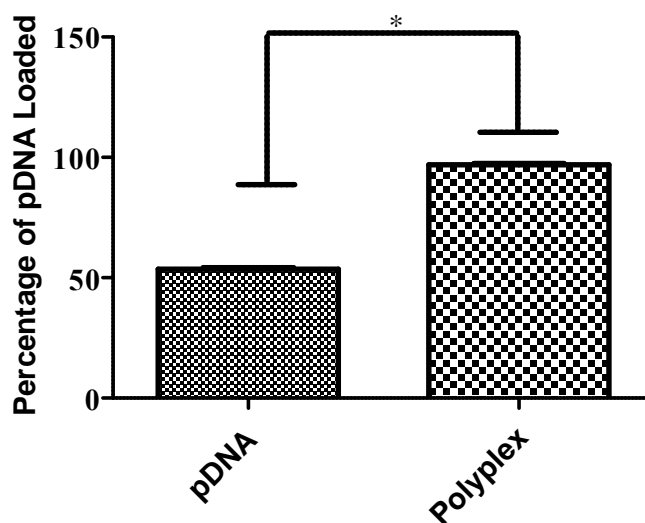


Figure 3.20: *pDNA* and polyplex loading behaviour of ELP hollow spheres. *pDNA* loading efficiency of 500 nm hollow spheres using naked *pDNA* and polyplex. All the data are represented as mean  $\pm$  standard deviation ( $n = 3$ ,  $p < 0.05$ ). Statistical analysis was performed using Student's *t*-test. \* Represents statistical significance between *pDNA* vs polyplex.

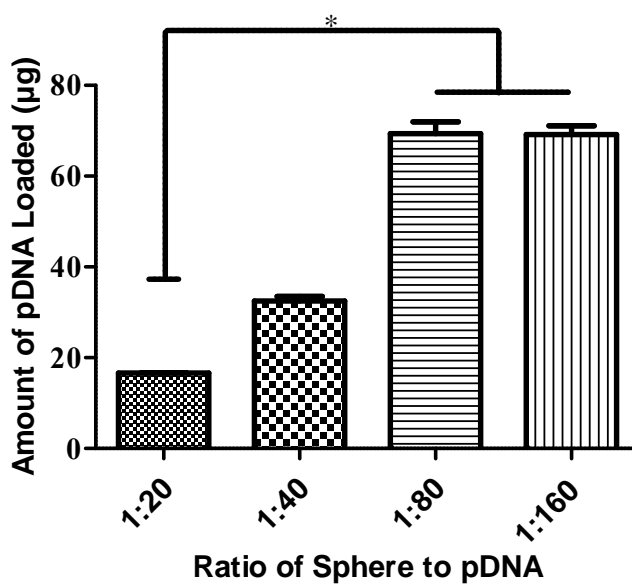
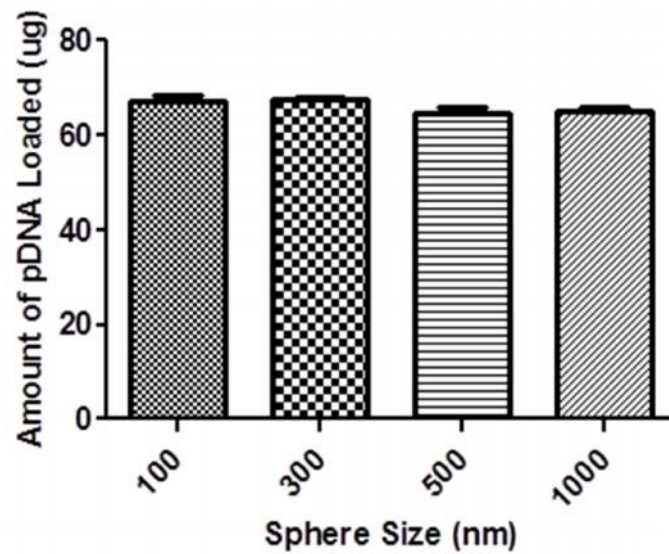
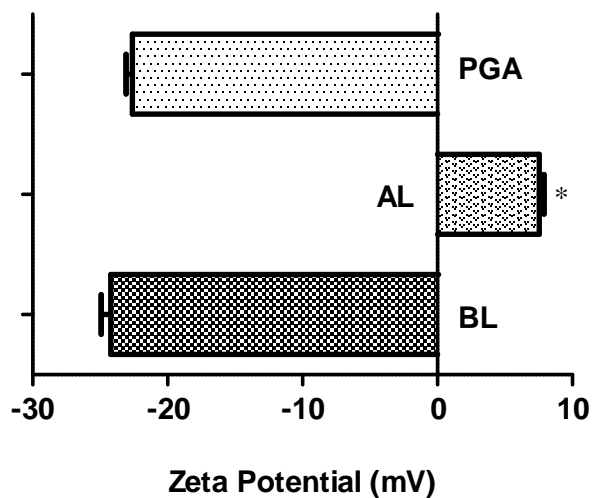


Figure 3.21: Polyplex loading efficiency of 500 nm hollow spheres with varying ratios of polyplex to sphere. All the data are represented as mean  $\pm$  standard deviation ( $n = 3$ ,  $p < 0.05$ ). Statistical analysis was performed using one-way ANOVA. \* Represents statistical significance between different ratio of sphere to pDNA.



**Figure 3.22: Polyplex loading efficiency of ELP hollow spheres of various sizes: 100 nm, 300 nm, 500 nm and 1000 nm. All the data are represented as mean  $\pm$  standard deviation ( $n = 3$ ). No statistical difference was found between different groups.**



**Figure 3.23: Zeta potential analysis of hollow spheres of 500 nm before loading (BL), after loading (AL) and after treatment with PGA to validate PGA method for quantification. All the data are represented as mean  $\pm$  standard deviation ( $n = 3$ ,  $p < 0.05$ ). Statistical analysis was performed using one-way ANOVA. \* Represents statistical difference between AN vs BL and PGA.**

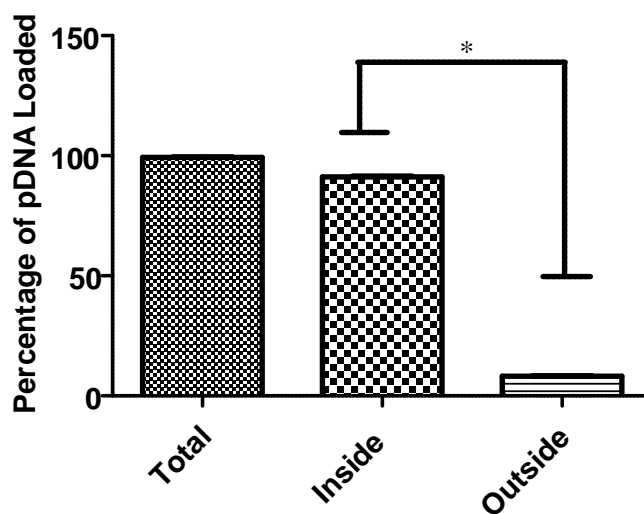


**Figure 3.24:** PicoGreen<sup>®</sup> assay showing quantification of polyplex loading outside spheres and inside the hollow spheres after treating the spheres with PGA. All the data are represented as mean  $\pm$  standard deviation ( $n = 3$ ,  $p < 0.05$ ). Statistical analysis was performed using one-way ANOVA. \* Represents statistical significance between inside vs outside.

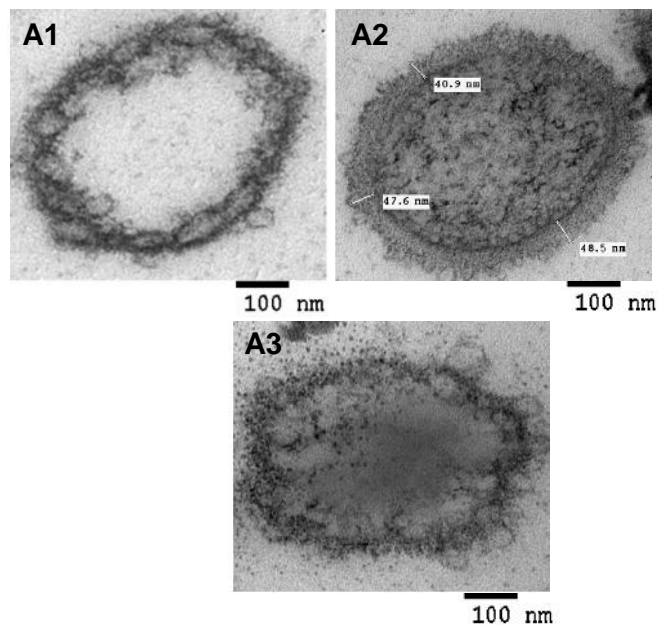


**Figure 3.25: TEM images of 500 nm hollow spheres. (A1) Hollow sphere without polyplex, (A2) hollow spheres loaded with polyplex and (A3) hollow spheres after PGA treatment.**

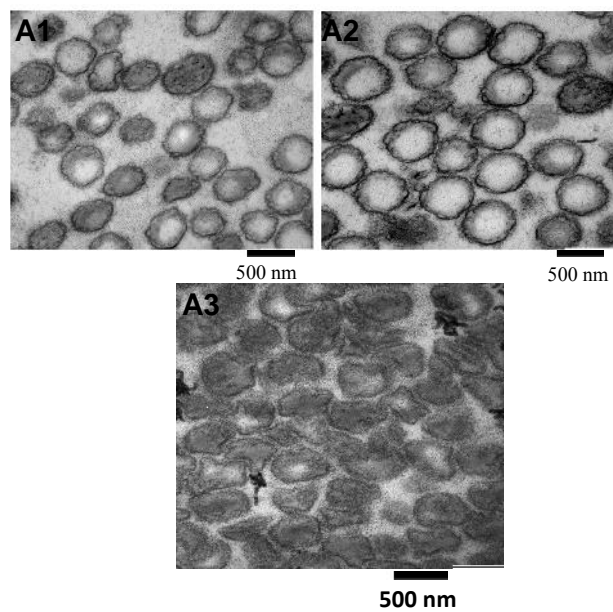


**Figure 3.26: TEM images of 500 nm hollow spheres. Hollow spheres loaded with different amounts of polyplex were investigated. (A1) 1:20 ratio shows minimal spheres loaded with polyplex, (A2) 1:40 with comparatively higher number of polyplex loaded spheres and (A3) 1:80 ratio showing almost all the spheres loaded with polyplex.**

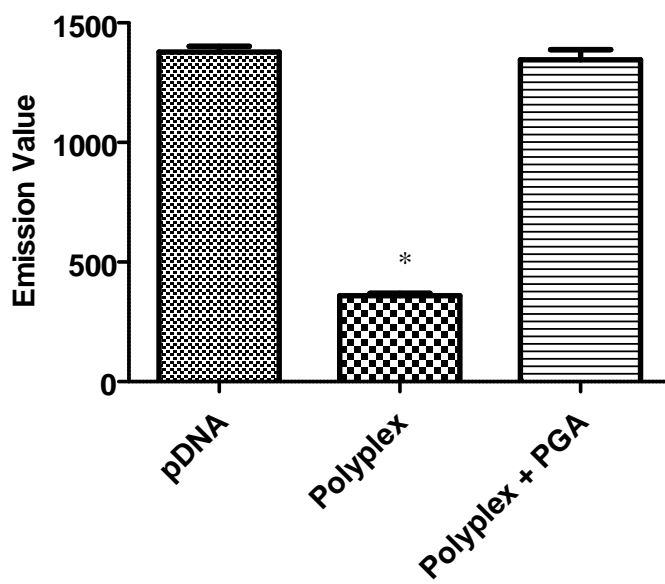


**Figure 3.27: PicoGreen<sup>®</sup> assay showing release of *pDNA* from the polyplex using polyglutamic acid. The emission values of naked *pDNA*, polyplex and polyplex treated with PGA. Statistical significance in Figure A was determined by one-way ANOVA ( $n = 3, p < 0.05$ ). \* Represents statistical significance between polyplex vs polyplex + PGA.**

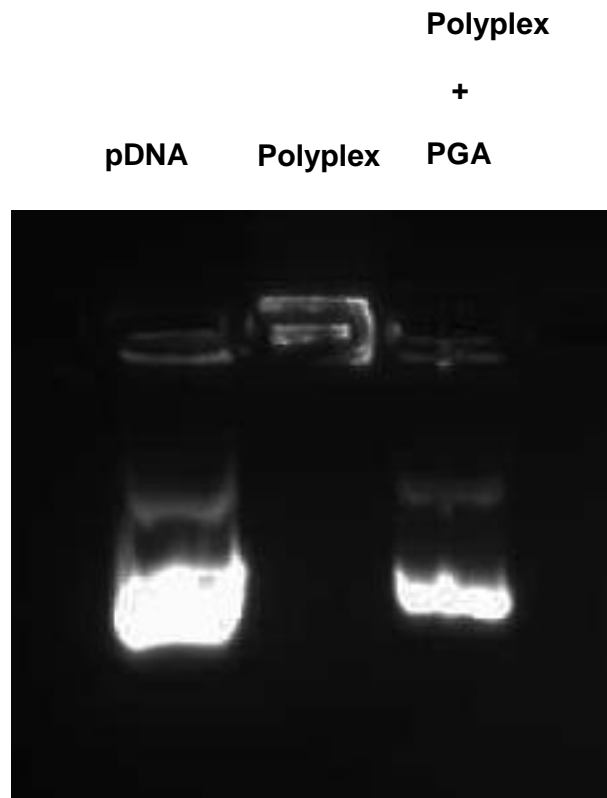


**Figure 3.28: Agarose gel showing naked *pDNA*, polyplex and polyplex treated with PGA.**

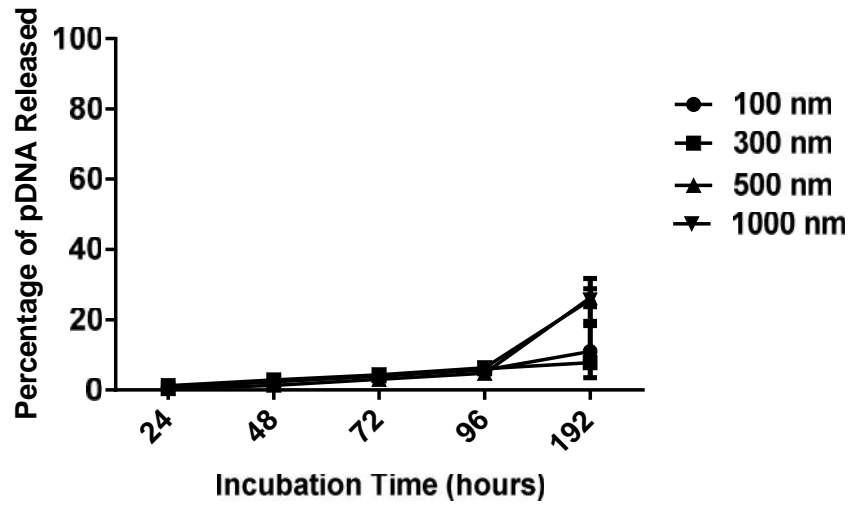


**Figure 3.29:** Cumulative release profile of *pDNA/polyplex* from all the four different sizes of hollow spheres tested at 37°C. All the data are represented as the mean  $\pm$  standard deviation ( $n = 3, p < 0.05$ ). Statistical analysis was performed using one-way ANOVA.

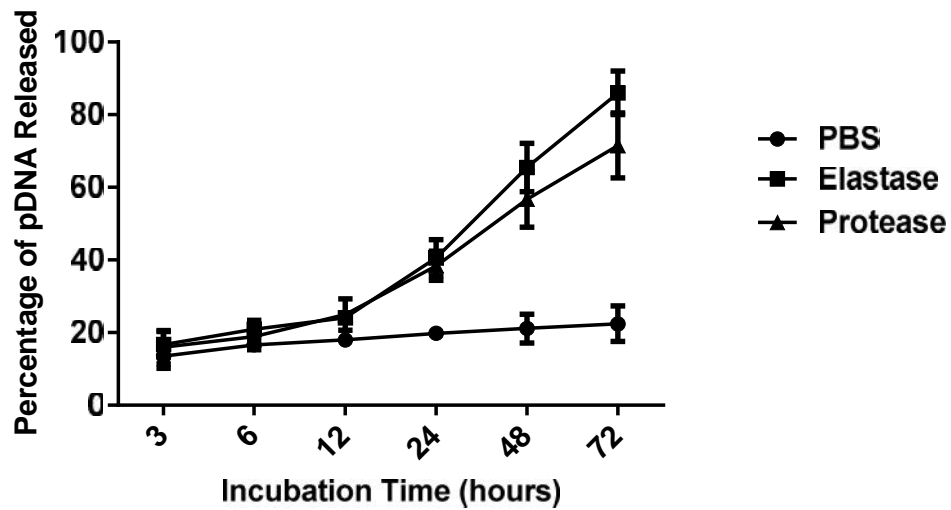


**Figure 3.30:** *In vitro* release study of 1000 nm hollow spheres in the presence of 10 U/g of human leukocyte elastase and protease (pH 7.4) in PBS. All the data are represented as the mean  $\pm$  standard deviation ( $n = 3, p < 0.05$ ). Statistical analysis was performed using one-way ANOVA.

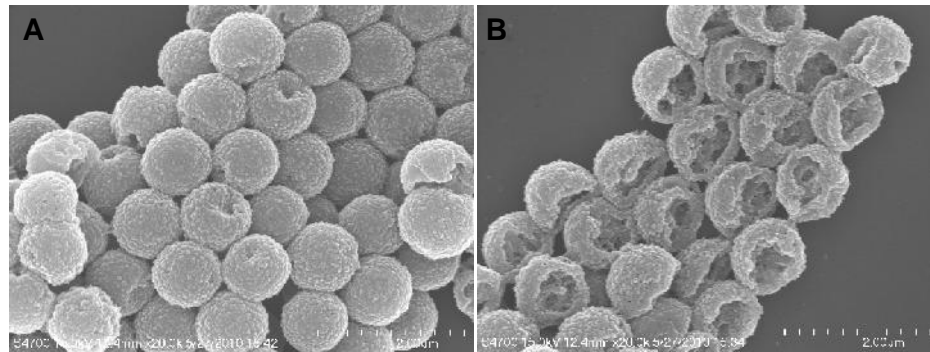


**Figure 3.31: SEM images of hollow spheres (A) untreated 1000 nm and (B) degrading 1000 nm hollow spheres in the presence of elastase after 72 hr. The scale bar represents 2  $\mu\text{m}$ .**

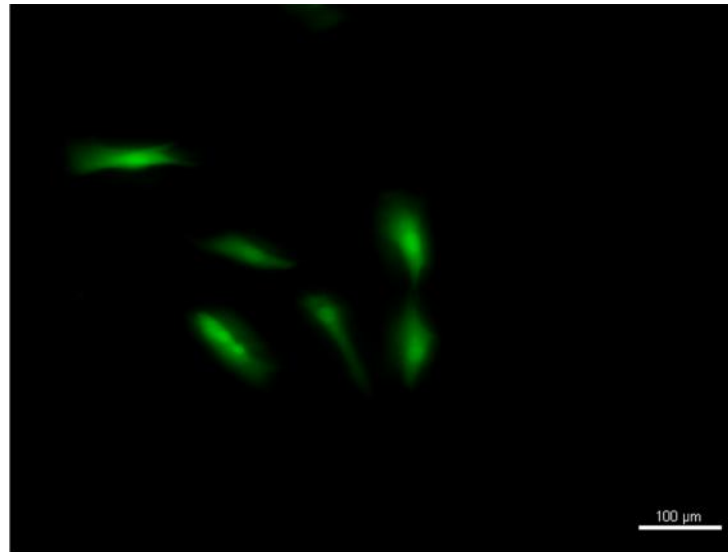


**Figure 3.32: Confocal image of ADSCs expressing GFP 48 hr after treatment with polyplexes. The scale bar represents 100  $\mu\text{m}$ .**

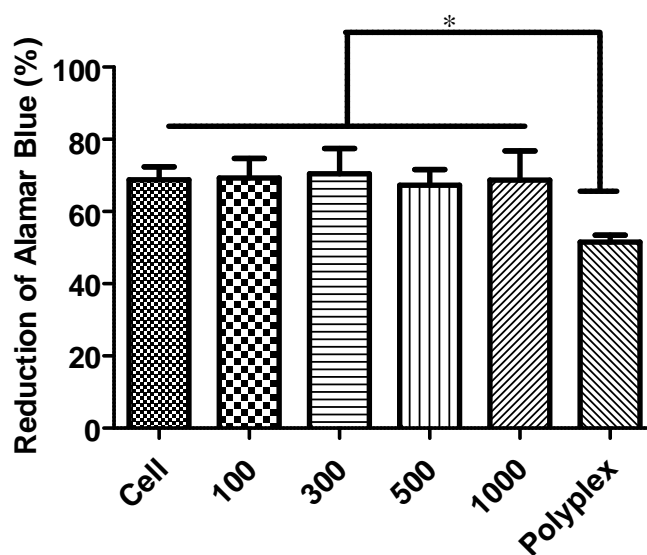


**Figure 3.33: AlamarBlue<sup>®</sup> assays showing the cell viability of loaded hollow spheres of all the four different sizes in ADSCs after 48 hr. All the data are represented as the mean  $\pm$  standard deviation ( $n = 3$ ,  $p < 0.05$ ). Statistical analysis was performed using one-way ANOVA. \* Represents polyplex vs other groups.**

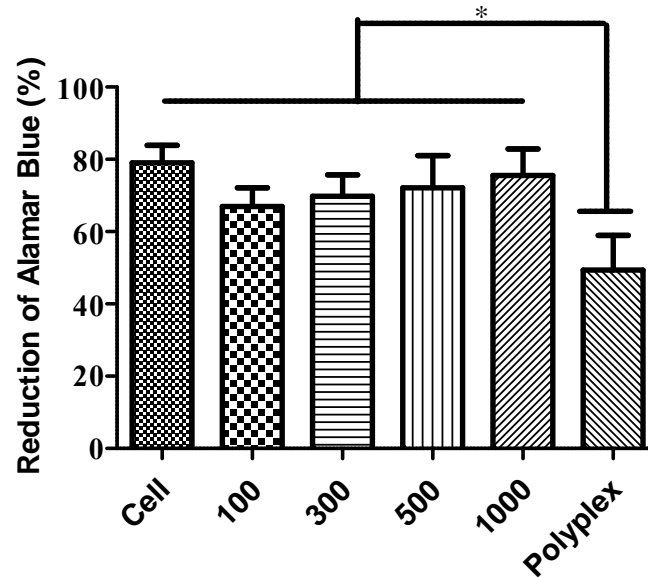


**Figure 3.34:** AlamarBlue<sup>®</sup> assays showing the cell viability of loaded hollow spheres of all the four different sizes in HUVECs after 48 hr. All the data are represented as the mean  $\pm$  standard deviation ( $n = 3, p < 0.05$ ). Statistical analysis was performed using one-way ANOVA. \* Represents polyplex vs other groups.

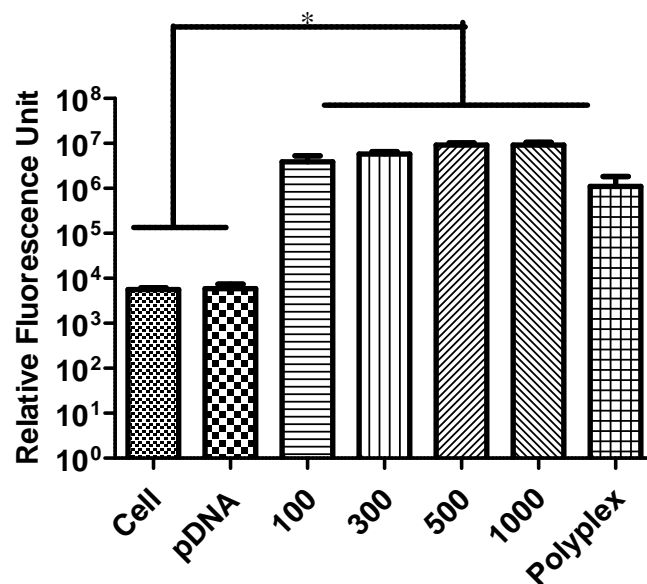


**Figure 3.35:** Gaussia luciferase assay for investigation of transfection efficiency of all the four different sizes of polyplex loaded hollow spheres in ADSCs. All the data are represented as the mean  $\pm$  standard deviation ( $n = 3$ ,  $p < 0.05$ ). Statistical analysis was performed using one-way ANOVA. \* Represents cell and pDNA groups vs other groups.

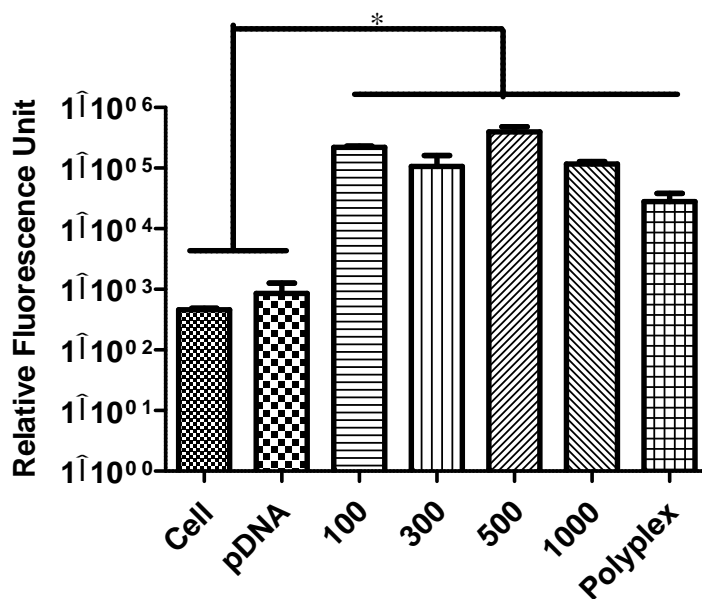
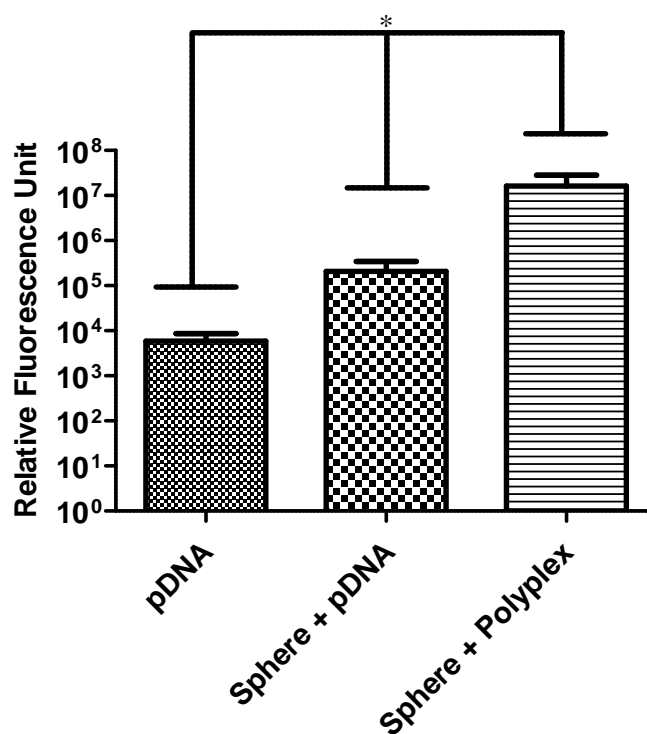
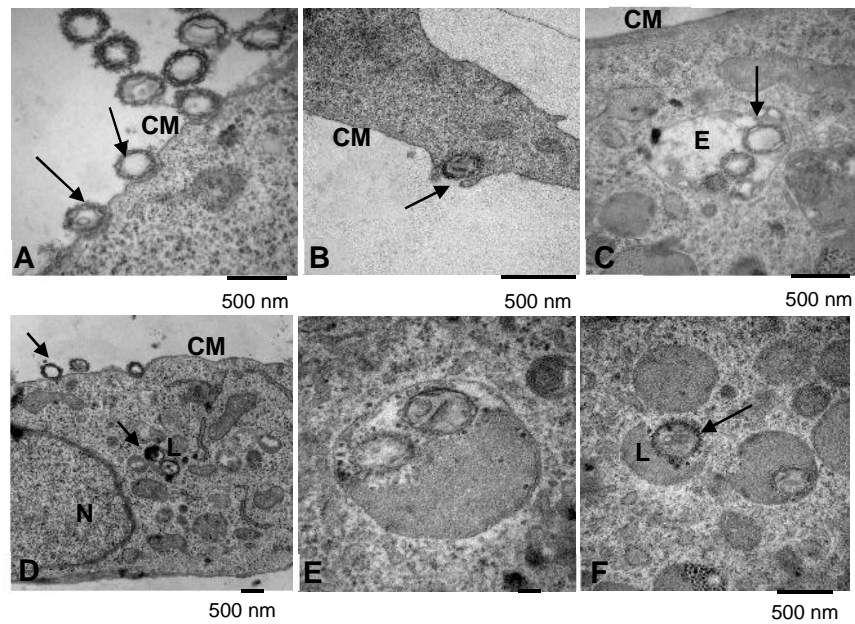


Figure 3.36: Gaussia luciferase assay for investigation of transfection efficiency of all the four different sizes polyplex loaded hollow spheres in HUVECs. All the data are represented as the mean  $\pm$  standard deviation ( $n = 3$ ,  $p < 0.05$ ). Statistical analysis was performed using one-way ANOVA. \* Represents cell and pDNA groups vs other groups.



**Figure 3.37: Polyplex loaded hollow spheres versus pDNA loaded hollow spheres using 500 nm hollow spheres. All the data are represented as the mean  $\pm$  standard deviation ( $n = 3$ ,  $p < 0.05$ ). Statistical analysis was performed using one-way ANOVA. \* Represents pDNA group vs sphere + pDNA and sphere + polyplex.**



**Figure 3.38:** TEM images showing the internalization pathway of 500 nm hollow spheres loaded with polyplexes within ADSCs. Hollow spheres were observed at different locations in the cell: (A) Attachment to cell membrane, (B) cell membrane engulfing a sphere, (C) in early endosomes, (D) lysosome near to nucleus, (E) rupturing the lysosomal membrane and (F) hollow spheres coming out of the lysosome by completely disrupting the lysosomal membrane. Cell membrane, endosomes, lysosome and nucleus are represented as CM, E, L and N respectively in the figures. The arrows point towards the localization of the hollow spheres inside the cell.

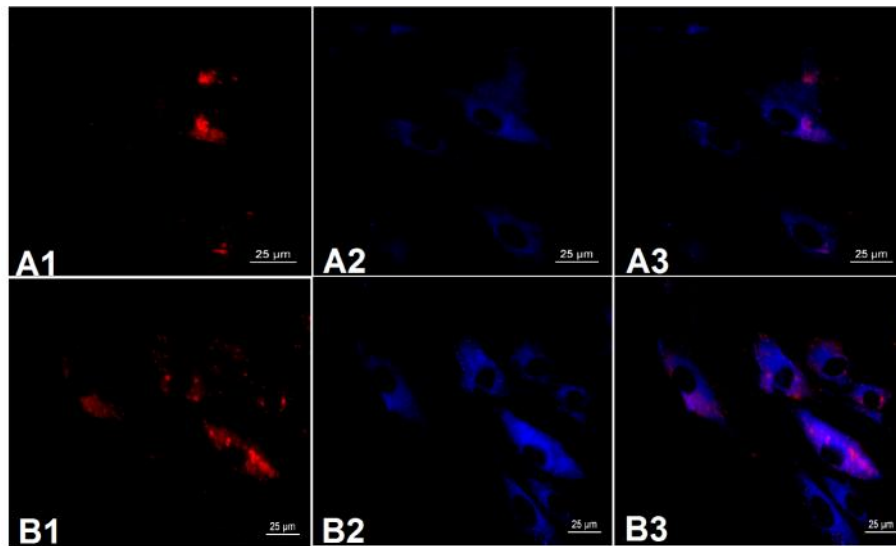


**Figure 3.39: Fluorescence images showing internalization of *pDNA*- hollow spheres (A1–A3) and polyplex- hollow spheres (B1–B3) by ADSCs. (A1 and B1). The images show fluorescence signal arising from *cy3-pDNA*. (A2 and B2) Lysosomal staining by LysoTracker Blue. (A3 and B3) Merged images of fluorescence signals: *cy3-pDNA* and LysoTracker Blue.**

A variety of drug delivery platforms, such as nano to microparticles, 2D films and 3D hydrogels, have been developed from ELPs for the purpose of local and controlled delivery of therapeutic molecules [7, 9, 10]. ELPs are non-toxic and possess a tunable range of biomechanical properties as a result of the precise control of pentapeptide sequence, block sequence, and processing conditions [7].

The primary goal of this study was to develop a gene delivery carrier based on ELP. The fabrication process of ELP hollow spheres comprised three distinct steps: coating of ELP on sulfonated PS beads, cross-linking, and dissolution of PS beads. In this study, we exploited both self-assembly and a slight positive charge of ELP for coating over a sacrificial PS bead. The increase in size and zeta potential as well as protein adsorption on the PS beads indicates coating of ELP over these beads. Also, the coating was rapid and efficient at 37°C, thus proving the role of the temperature-dependent self-assembly property of ELP. The amount of ELP required for coating beads is inversely related to the size of the PS beads. 100 nm with a higher surface area showed more ELP adsorption than did 1000 nm PS beads. Coating was followed by cross-linking, a crucial step as this provides the required stability and robustness to the sphere prior to the removal of the sacrificial core. Initially, an amine cross-linker, glutaraldehyde, was used which strongly cross-linked all the primary amine groups present on the surface of ELP to give a stable hollow sphere; however, the cross-linking resulted in a minimal number of surface functional groups becoming available for further surface modifications. This was evident from the results of the TNBSA assay for free amino group analysis. Therefore, the ability of mTGase to cross-link ELP coated beads was analysed. MTGase is an enzyme of bacterial origin and catalyses the acyl transfer reaction between an  $\epsilon$ -amino group of lysine residue and a  $\gamma$ -carboxamide group of glutamine residue by introducing covalent cross-links between proteins, peptides and various primary amines [32]. Additionally, its ease of production and  $\text{Ca}^{2+}$  independent activity make it more suitable than tissue TGase would be [32, 33]. MTGase catalyses the acyl transfer reaction between glutamine and lysine residues present in the cross-linking domains of ELP. The TNBSA assay was performed to characterize the mTGase cross-linking of ELP and also to quantify the number of free amino groups available on the surface. A decrease in this number was observed after cross-linking, which suggests that mTGase cross-linking results in a higher proportion of free amino groups on the surface of spheres than does cross-linking with glutaraldehyde. The ELP band on SDS-PAGE gel diminished after treatment with mTGase, probably as a result of covalent cross-linking of ELP.

Transparent hollow spheres were observed under TEM, after dissolving the core PS beads with THF. The hollow spheres showed a negative surface charge as mTGase cross-linked the amino groups leaving aside the maximum number of glutamic acids, contributing to the surface charge. The strong negative surface charge of these hollow spheres, imparted by glutamic acids, prevents their subsequent aggregation, while covalent cross-linking with mTGase provides the robustness. All the four different sizes of hollow spheres were nearly monodispersed as observed under TEM. This is a similar speculation to that made by Chaikof and colleagues, who hypothesized that a sufficiently high density of glutamic acid units prevents the association of the hydrophilic blocks and subsequently the aggregation by charge repulsion [23].

To demonstrate that hollow spheres are suitable as a gene depot due to high efficiency of *pDNA* loading, loading efficiency in the hollow spheres of 300 nm was compared to that of self-assembled ELP solid spheres of similar size. ELP in PBS at 37°C self assembles into a thermodynamically stable structure and forms solid spheres. During this process, the hydrophobic domains of ELP form the inner core and thus can facilitate encapsulation of only hydrophobic molecules. Also, the polar amino groups (lysine) present in the cross-linking domain remain on the outer surface and initiate charge interaction between amino groups and *pDNA*. Thus solid spheres are limited to surface charge availability on the outer surface of the sphere; while in the case of hollow spheres, a diffusion process leads to the loading of *pDNA* inside the hollow cores. Hence, between hollow and solid spheres of a similar size (300 nm), a higher loading was seen in the hollow spheres.

To further increase *pDNA* loading efficiency of hollow spheres and to provide protection against endosomal degradation, a hyper branched block copolymer was used and is a modification of the polymer as described in our previous study [40]. This linear PDMAEMA part of the copolymer binds *pDNA* with its tertiary amine groups, while the hyper branched PEGMEMA/EGDMA block shows better cell viability because of the PEG content. This polymer showed similar transfection efficiency to that of commercial transfection agents such as polyethyleneimine and degraded poly-(amidoamine) without any effect on cellular metabolic activity [40]. In the case of polyplexes, free *pDNA* was quantified for the loading efficiency. The method is more precise than the use of polyplex because polymer complexation with *pDNA* interferes with the reading [41]. PGA, being negatively charged when incubated with polyplex, forms an electrostatic interaction with the polymer by breaking its weak bond with *pDNA*. The result showed similar emission values of *pDNA* and polyplex after treatment with PGA (Figure 3.27). The result from agarose gel electrophoresis was consistent with that

of PicoGreen<sup>®</sup>, where a similar band pattern was observed between *p*DNA and PGA treated polyplex (Figure 3.28).

The loading of *p*DNA was greater when polyplex was used than it was with naked *p*DNA. The loading mechanism of *p*DNA alone is likely to be a diffusion-associated process and not that of a charge interaction. This is because both hollow spheres and *p*DNA are negatively charged. It is hypothesized that a higher efficiency of *p*DNA loading in the case of polyplex is likely due to 1) reduction of *p*DNA size when complexed with a polymer, 2) electrostatic interaction between slightly positively charged polyplex and negatively charged spheres, and 3) the diffusion process. Also, as evident from the PicoGreen<sup>®</sup> and TEM studies, the hollow spheres have a layer of polyplexes around their surface. The hollow spheres before and after treatment with PGA were analysed under TEM. The polyplex layer disappeared after the PGA treatment. A PicoGreen<sup>®</sup> assay of *p*DNA sample, collected from the supernatant, supported these data. The release of polyplexes from these hollow spheres was minimal. This might be due to an electrostatic interaction between polyplexes and spheres which prevents the polyplexes from flowing out of the hollow spheres. The release was found to be greater after being treated with protease and elastase. The SEM images showed degraded hollow spheres after treatment with elastase. The cellular expression of GFP by the treatment of polyplexes, collected from the release media, proved their bioactivity. Spheres of all four sizes of loaded *p*DNA showed similar cell viability in both the HUVECs and ADSCs as per alamarBlue<sup>®</sup> reduction assays and DNA quantification by PicoGreen<sup>®</sup> assays; polyplexes however showed less cell viability. Also, polyplex loaded spheres showed better luciferase expression level than polyplex and *p*DNA alone. The luciferase expression level of polyplex loaded hollow spheres was nearly 10 times higher than that of naked *p*DNA loaded spheres.

The TEM studies showed sub-cellular localization of the spheres inside the ADSCs. The spheres probably entered the cell via a macropinocytosis pathway and were transported to endosomes and finally to lysosomes. This suggests that the spheres might be following an endocytic pathway inside the cell. Although the study performed was not very detailed, the image showing a sphere breaking out of the lysosome shows the endosomal protection ability of polyplex loaded hollow spheres. The understanding is that the hydrophobic sequence present in ELP and the slightly positive charge of polyplex loaded hollow spheres are responsible for this lysosomal rupture and escape by means of a proton sponge effect phenomenon. In this phenomenon, a relatively hydrophobic weak base or cationic polymer becomes protonated inside the lysosome due to the low pH. The charged form of this molecule cannot cross the membrane of lysosome. This accumulation of charge causes an osmotic imbalance between

different sides of the membrane, thereby inducing swelling of the lysosome and, consequently, destabilization of the membrane [52]. Furthermore, in Figures 3.35A and D, the presence of an intact cell and nuclear membrane suggests that the spheres are not detrimental to cells. TEM studies showed hollow spheres in different cellular compartments within ADSCs. To further characterize and also to get a wider view of internalization, fluorescence studies were performed with spheres loaded with cy3-*pDNA*. *pDNA*- hollow spheres and polyplex- hollow spheres were internalized inside ADSCs and can be seen to be co-localized within lysosomes. The lesser intensity of *pDNA*- hollow spheres than that of polyplex- hollow spheres may be due to the lower efficiency of naked *pDNA* loading inside the hollow spheres.

### 3.5 Conclusions

In summary, fabrication of tunable and monodispersed ELP hollow spheres of various sizes (~100–1000 nm) using a template-based method was reported. The process was rapid, exploiting the self-assembly property and slight positive charge of ELP. Cross-linking with mTGase is a logical way to provide stability and robustness to the sphere while maintaining surface functional groups for further modifications. *pDNA* and polyplexes were efficiently loaded inside hollow spheres, a process governed by a diffusion process and charge interactions. The loading was more than that of self-assembled solid spheres. The high *pDNA* loading capability triggered by the enzymes elastase and protease, and the transfection ability of the released polyplexes, validates their use as a nucleic acid delivery depot. Moreover, higher luciferase expression of polyplex loaded spheres through endosomal protection further supports the use of hollow spheres as a gene transfection agent. The tethering of targeting ligands to the hollow spheres through established coupling protocols will further provide functionality to the hollow spheres for targeted gene delivery applications. Overall, the simple and efficient nature of the approach, coupled with the capability to fabricate tunable ELP hollow spheres in large quantities and the additional ability to post-functionalize the hollow spheres, provides exciting new opportunities for designing advanced ELP hollow spheres for use in a range of therapeutic and diagnostic applications.

### 3.6 References

- [1] Cui H, Webber MJ, Stupp SI. Self-assembly of peptide amphiphiles: from molecules to nanostructures to biomaterials. *Biopolymers* 2010; 94: 1–18.
- [2] Mann S. Self-assembly and transformation of hybrid nano-objects and nanostructures under equilibrium and non-equilibrium conditions. *Nat Mater* 2009; 8: 781–92.
- [3] Gazit E. Self-assembled peptide nanostructures: the design of molecular building blocks and their technological utilization. *Chem Soc Rev* 2007; 36: 1263–9.
- [4] Zhang S, Greenfield MA, Mata A, Palmer LC, Bitton R, Mantei JR, Aparicio C, de la Cruz MO, Stupp SI. A self-assembly pathway to aligned monodomain gels. *Nat Mater* 2010; 9: 594–601.
- [5] Ballister ER, Lai AH, Zuckermann RN, Cheng Y, Mougous JD. In vitro self-assembly of tailorable nanotubes from a simple protein building block. *Proc Natl Acad Sci USA* 2008; 105: 3733–8.
- [6] Storrie H, Mooney DJ. Sustained delivery of plasmid DNA from polymeric scaffolds for tissue engineering. *Adv Drug Deliv Rev* 2006; 58: 500–14.
- [7] Kim W, Chaikof EL. Recombinant elastin-mimetic biomaterials: emerging applications in medicine. *Adv Drug Deliv Rev* 2010; 62: 1468–78.
- [8] Woodhouse KA, Klement P, Chen V, Gorbet MB, Keeley FW, Stahl R, Fromstein JD, Bellingham CM. Investigation of recombinant human elastin polypeptides as non-thrombogenic coatings. *Biomaterials* 2004; 25: 4543–53.
- [9] Nettles DL, Chilkoti A, Setton LA. Applications of elastin-like polypeptides in tissue engineering. *Adv Drug Deliv Rev* 2010; 62: 1479–85.
- [10] Chilkoti A, Dreher MR, Meyer DE. Design of thermally responsive, recombinant polypeptide carriers for targeted drug delivery. *Adv Drug Deliv Rev* 2002; 54: 1093–111.
- [11] Chilkoti A, Christensen T, MacKay JA. Stimulus responsive elastin biopolymers: applications in medicine and biotechnology. *Curr Opin Chem Biol* 2006; 10: 652–7.
- [12] Rodriguez-Cabello JC. Smart elastin-like polymers. *Adv Exp Med Biol* 2004; 553: 45–57.
- [13] Rincon AC, Molina-Martinez IT, de Las Heras B, Alonso M, Bailez C, Rodriguez-Cabello JC, Herrero-Vanrell R. Biocompatibility of elastin-like polymer poly(VPAVG) microparticles: in vitro and in vivo studies. *J Biomed Mater Res A* 2006; 78: 343–51.

- [14] Rodriguez-Cabello JC, Prieto S, Arias FJ, Reguera J, Ribeiro A. Nanobiotechnological approach to engineered biomaterial design: the example of elastin-like polymers. *Nanomedicine (Lond)* 2006; 1: 267–80.
- [15] Mithieux SM, Weiss AS. Elastin. *Adv Protein Chem* 2005; 70: 437–61.
- [16] Osborne JL, Farmer R, Woodhouse KA. Self-assembled elastin-like polypeptide particles. *Acta Biomater.* 2008; 4: 49–57.
- [17] Wright ER, Conticello VP. Self-assembly of block copolymers derived from elastin-mimetic polypeptide sequences. *Adv Drug Deliv Rev* 2002; 54: 1057–73.
- [18] Yao XL, Conticello VP, Hong M. Investigation of the dynamics of an elastin-mimetic polypeptide using solid-state NMR. *Magn Reson Chem* 2004; 42: 267–75.
- [19] Mackay JA, Callahan DJ, Fitzgerald KN, Chilkoti A. Quantitative model of the phase behavior of recombinant pH-responsive elastin-like polypeptides. *Biomacromolecules.* 2010; 11: 2873–9.
- [20] Bessa PC, Machado R, Nummerger S, Dopler D, Banerjee A, Cunha AM, Rodriguez-Cabello JC, Redl H, van Griensven M, Reis RL, Casal M. Thermoresponsive self-assembled elastin-based nanoparticles for delivery of BMPs. *J Control Release.* 2010; 142: 312–8.
- [21] Bellingham CM, Lillie MA, Gosline JM, Wright GM, Starcher BC, Bailey AJ, Woodhouse KA, Keeley FW. Recombinant human elastin polypeptides self-assemble into biomaterials with elastin-like properties. *Biopolymers* 2003; 70: 445–55.
- [22] Keeley FW, Bellingham CM, Woodhouse KA. Elastin as a self-organizing biomaterial: use of recombinantly expressed human elastin polypeptides as a model for investigations of structure and self-assembly of elastin. *Philos Trans R Soc Lond B Biol Sci* 2002; 357: 185–9.
- [23] Kim W, Thevenot J, Ibarboure E, Lecommandoux S, Chaikof EL. Self-assembly of thermally responsive amphiphilic diblock copolypeptides into spherical micellar nanoparticles. *Angew Chem Int Ed Engl* 2010; 49: 4257–60.
- [24] Pepe A, Bochicchio B, Tamburro AM. Supramolecular organization of elastin and elastin-related nanostructured biopolymers. *Nanomedicine (Lond)* 2007; 2: 203–18.
- [25] Martino M, Perri T, Tamburro AM. Elastin-based biopolymers: chemical synthesis and structural characterization of linear and cross-linked poly(OrnGlyGlyOrnGly). *Biomacromolecules* 2002; 3: 297–304.
- [26] Ruenraroengsak P, Cook JM, Florence AT. Nanosystem drug targeting: facing up to complex realities. *J Control Release* 2010; 141: 265–76.

- [27] Fujita Y, Mie M, Kobatake E. Construction of nanoscale protein particle using temperature-sensitive elastin-like peptide and polyaspartic acid chain. *Biomaterials*. 2009; 30: 3450–7.
- [28] Aggarwal P, Hall JB, McLeland CB, Dobrovolskaia MA, McNeil SE. Nanoparticle interaction with plasma proteins as it relates to particle biodistribution, biocompatibility and therapeutic efficacy. *Adv Drug Deliv Rev* 2009; 61: 428–37.
- [29] Herrero-Vanrell R, Rincon AC, Alonso M, Reboto V, Molina-Martinez IT, Rodriguez-Cabello JC. Self-assembled particles of an elastin-like polymer as vehicles for controlled drug release. *J Control Release* 2005; 102: 113–22.
- [30] MacKay JA, Chen M, McDaniel JR, Liu W, Simnick AJ, Chilkoti A. Self-assembling chimeric polypeptide–doxorubicin conjugate nanoparticles that abolish tumours after a single injection. *Nat Mater* 2009; 8: 993–9.
- [31] Bellingham CM, Woodhouse KA, Robson P, Rothstein SJ, Keeley FW. Self-aggregation characteristics of recombinantly expressed human elastin polypeptides. *Biochim Biophys Acta* 2001; 1550: 6–19.
- [32] Zhu Y, Tramper J. Novel applications for microbial transglutaminase beyond food processing. *Trends Biotechnol* 2008; 26: 559–65.
- [33] O Halloran DM, Collighan RJ, Griffin M, Pandit AS. Characterization of a microbial transglutaminase cross-linked type II collagen scaffold. *Tissue Eng* 2006; 12: 1467–74.
- [34] Rethore G, Pandit A. Use of templates to fabricate nanoscale spherical structures for defined architectural control. *Small* 2010; 6: 488–98.
- [35] Rethore G, Mathew A, Naik H, Pandit A. Preparation of chitosan/polyglutamic acid spheres based on the use of polystyrene template as a nonviral gene carrier. *Tissue Eng Part C Methods* 2009; 15: 605–13.
- [36] Dash BC, Rethore G, Monaghan M, Fitzgerald K, Gallagher W, Pandit A. The influence of size and charge of chitosan/polyglutamic acid hollow spheres on cellular internalization, viability and blood compatibility. *Biomaterials* 2010; 31: 8188–97.
- [37] Caruso F, Caruso RA, Mohwald H. Nanoengineering of inorganic and hybrid hollow spheres by colloidal templating. *Science* 1998; 282: 1111–4.
- [38] Smith PK, Krohn RI, Hermanson GT, Mallia AK, Gartner FH, Provenzano MD, Fujimoto EK, Goeke NM, Olson BJ, Klenk DC. Measurement of protein using bicinchoninic acid. *Anal Biochem* 1985; 150: 76–85.

- [39] Bubnis WA, Ofner CM. The determination of epsilon-amino groups in soluble and poorly soluble proteinaceous materials by a spectrophotometric method using trinitrobenzenesulfonic acid. *Anal Biochem* 1992; 207: 129–33.
- [40] Newland B, Tai H, Zheng Y, Velasco D, Di Luca A, Howdle SM, Alexander C, Wang W, Pandit A. A highly effective gene delivery vector – hyperbranched poly(2-(dimethylamino)ethyl methacrylate) from in situ deactivation enhanced ATRP. *Chem Commun (Camb)* 2010; 46: 4698–700.
- [41] Kusonwiriawong C, Atuah K, Alpar OH, Merkle HP, Walter E. Cationic stearylamine-containing biodegradable microparticles for DNA delivery. *J Microencapsul* 2004; 21: 25–36.
- [42] Crystal RG. Transfer of genes to humans: early lessons and obstacles to success. *Science*. 1995; 270: 404–10.
- [43] Felgner PL, Gadek TR, Holm M, Roman R, Chan HW, Wenz M, Northrop JP, Ringold GM, Danielsen M. Lipofection: a highly efficient, lipid-mediated DNA-transfection procedure. *Proc Natl Acad Sci USA* 1987; 84: 7413–7.
- [44] Boussif O, Lezoualc'h F, Zanta MA, Mergny MD, Scherman D, Demeneix B, Behr JP. A versatile vector for gene and oligonucleotide transfer into cells in culture and in vivo: polyethylenimine. *Proc Natl Acad Sci USA* 1995; 92: 7297–301.
- [45] Lee H, Jeong JH, Park TG. PEG grafted polylysine with fusogenic peptide for gene delivery: high transfection efficiency with low cytotoxicity. *J Control Release* 2002; 79: 283–91.
- [46] Chavany C, Le Doan T, Couvreur P, Puisieux F, Helene C. Polyalkylecyanoacrylate nanoparticles as polymeric carriers for antisense oligonucleotides. *Pharm Res* 1992; 9: 441–9.
- [47] Alexakis T, Boadi DK, Quong D, Groboillot A, O'Neill I, Poncelet D, Neufeld RJ. Microencapsulation of DNA within alginate microspheres and crosslinked chitosan membranes for in vivo application. *Appl Biochem Biotechnol* 1995; 50: 93–106.
- [48] Fischer D, Bieber T, Li Y, Elsasser HP, Kissel T. A novel non-viral vector for DNA delivery based on low molecular weight, branched polyethylenimine: effect of molecular weight on transfection efficiency and cytotoxicity. *Pharm Res* 1999; 16: 1273–9.
- [49] Won YW, Yoon SM, Lee KM, Kim YH. Poly(oligo-D-arginine) with internal disulfide linkages as a cytoplasm-sensitive carrier for siRNA delivery. *Mol Ther* 2011; 19: 372–80.
- [50] Coles DJ, Toth I. Dendritic peptide-based carriers for gene delivery. *Curr Drug Deliv* 2009; 6: 338–42.

[51] Yang S, Coles DJ, Esposito A, Mitchell DJ, Toth I, Minchin RF. Cellular uptake of self-assembled cationic peptide–DNA complexes: multifunctional role of the enhancer chloroquine. *J Control Release* 2009; 135: 159–65.

[52] Varkouhi AK, Scholte M, Storm G, Haisma HJ. Endosomal escape pathways for delivery of biologicals. *J Control Release* 2011; 151: 220–8.

**Delivery of Therapeutic eNOS and IL-10 genes using an ELP-based  
Injectable System to Induce Angiogenesis and Modulate Inflammation  
Level in the Mouse Hind Limb Ischemic Limb**

Contents of this chapter are currently under preparation for manuscript submission:

Dash BC, Monaghan M, Thomas D, Carroll, O, Woodhouse K, O'Brien T, Pandit A. "Delivery of Therapeutic eNOS and IL-10 Genes using an ELP-based Injectable System to Induce Angiogenesis and Modulate Inflammation Level in the Mouse Hind Limb Ischemic Limb".

#### 4.1 Introduction

Critical limb ischemia (CLI) is a manifestation of peripheral artery disease (PAD), caused by the obstruction of blood flow to the limb [1, 2]. CLI affects around 500–1000 per million of the population in Europe and North America alone every year. Without endovascular treatment, CLI patients are at a very high risk of amputation, leading to severe morbidity and mortality. Thus, it is considered as a critical public health issue worldwide. The fundamental goal of CLI treatment is to relieve ischemic rest pain, heal ulcers, prevent limb loss and improve the quality of life, thereby extending the survival of the patient [1].

Considering the seriousness of the disease in terms of the high rate of gangrene progression in untreated patients, the majority of patients undergo surgical or endovascular revascularization therapy for limb salvage in CLI, which accounts for approximately 120–500 amputations performed per million people every year in Europe and North America. However, up to 30% of CLI patients are not suitable for such interventions because of high operative risk or unfavorable vascular anatomy [1, 3-5]. Therefore exploring new and more effective strategies for revascularization of ischemic limbs is imperative. A viable therapeutic alternative is necessary to promote angiogenesis through the delivery of proangiogenic drug (genes and growth factors) delivery and therapeutic cells for angiogenesis [6].

Understanding the pathophysiology of limb ischemia is a necessity for finding an effective treatment of this disease [4]. The two major pathways contributing pathophysiology of this disease are: inflammation and angiogenesis [7]. During an ischemic insult, most tissues in the body try to compensate for low levels of blood supply by mechanisms of angiogenesis, arteriogenesis, vascular remodeling, and hematopoiesis [7]. Among many proangiogenic growth factors, vascular endothelial growth factor (VEGF), angiopoietin 1, fibroblast growth factors (FGF) play an important role in regulating angiogenesis in ischemic tissue [8-12]. The ischemic tissue elicits an inflammatory response, triggered by the breakdown products of the muscle. The major proinflammatory cytokines released during this time are IL-1, TNF and IL-6 [13, 14]. Also, IL-10, an anti-inflammatory cytokine has shown to be up-regulated in the ischemic tissue [15]. Despite the endogenous up-regulation of the proangiogenic factors, this is insufficient to compensate for the progressive deterioration of the tissue, due to the lack of blood supply. Hence, delivering soluble growth factors/cytokines or therapeutic genes could help in slowing down the tissue damage and promote tissue repair [16-18].

The major proangiogenic growth factors which have progressed to the clinical trials for the treatment of CLI are VEGF and FGF [19, 20]. eNOS is a major proangiogenic factor which is known to play an important role in angiogenesis by synthesis of NO. NO is a gaseous molecule with a wide range of targets, including the regulation of vessel tone and angiogenesis in wound healing, inflammation, ischemic cardiovascular diseases and other cardiovascular malignant diseases [21]. IL-10 is a major anti-inflammatory cytokine which inhibits proinflammatory activity of monocytes and macrophages by inhibiting expression of MHC class II and co-stimulatory molecule such as B7-1/B7-2c and limits the production of proinflammatory cytokines [22]. It is established to be produced by macrophages, dendritic cells (DC), B cells, and various subsets of CD4- and CD8-T cells. The role of IL-10 during infection is to inhibit the activities of T helper cell (Th)-1 cells, natural killer (NK) cells, and macrophages [15, 23].

Gene therapy is an evolving field and has grown from using naked *pDNA* alone to using viral and non-viral vectors for better transfection efficiency [24]. In comparison, delivery of therapeutic genes using viral vectors is considered more efficient than that of non-viral vectors. However, due to safety concerns, the use of non-viral vectors are preferred. In addition, viral vectors are known to cause immunogenic and inflammatory response [25]. Various cationic polymers have been developed so far to form a complex of *pDNA*/polymer (polyplex) to transfect the gene of interest to cells [24, 26, 27]. The polyplex helps in reduction in the size of the *pDNA* and helps it in crossing the cell membrane barrier efficiently. Also, *pDNA* micro-carriers have been developed to load and release genes of interest in a spatio-temporal manner. Recently, elastin-like polypeptide (ELP) has been used to fabricate hollow micro-spheres of a gene delivery depot [28]. ELP is used for various biomedical applications due to its biodegradable, non-toxic, non-inflammatory properties and efficient pharmacokinetics for the delivery of therapeutics [7-15]. ELPs are namely a class of polypeptide polymers composed of tetra, penta and hexapeptide tandem repeats of amino acids valine, proline, alanine and glycine. A variety of drug delivery platforms, such as micelles, nano-/micro-particles, hydrogels and films have been developed from ELP for the purpose of local and controlled delivery of bioactive molecules [29-34]. ELP self-assembles into a range of supramolecular structures from the nano- to the micron scale that facilitate the loading of hydrophobic drugs into local microenvironments. This self-assembly property of ELP can be readily modulated by variation of size, composition and sequence of the polypeptides that comprise the blocks which enables precise control of

molecular self-assembly through subtle changes in temperature, pH, and ionic strength of the aqueous solution. Therefore, ELP copolymers hold significant promise as drug delivery vehicles [34, 35].

In this study, for the first time a combined gene therapy for angiogenesis and inflammation has been considered for the treatment of CLI. It was hypothesized that the dual release of eNOS and IL-10 using an ELP based delivery platform will modulate inflammation and increase the blood perfusion in the ischemic tissue. The overall goal of this study was to deliver therapeutic genes eNOS and IL-10 to treat the ischemic environment and to characterize at a molecular level, the role of eNOS and IL-10 and assess the effect on angiogenic and inflammatory pathways (Figure 4.1). The specific objectives are: 1) fabrication of an ELP based dual delivery system, 2) determination of a therapeutic dose for eNOS and IL-10 and 3) delivery of eNOS and IL-10 in a hind limb ischemia mouse model to characterize at a molecular level the role of eNOS and IL-10 in angiogenic and inflammatory pathways.

## **4.2 Materials and Methods**

### **4.2.1 Materials**

Polystyrene (PS) beads of 0.1, 0.3, 10  $\mu\text{m}$  sulphuric acid, tetrahydrofuran (THF), DNase free water, agarose, sodium chloride, sodium acetate, sodium bicarbonate, poly-D-glutamic acid (PGA), glutaraldehyde, Dulbecco's modified eagle's medium (DMEM) with L-glutamine, Hank's balanced salt solution (HBSS), phosphate buffer saline (PBS), bovine serum albumin (BSA), fetal bovine serum (FBS) were purchased from Sigma-Aldrich. PS beads of diameter 0.5 and 1  $\mu\text{m}$  were obtained from GENTAUR. Quant-iT<sup>TM</sup> PicoGreen<sup>®</sup> dsDNA kit, alamarBlue<sup>®</sup>, fluorescein isothiocyanate (FITC) and trinitrobenzene sulfonic acid (TNBSA) were obtained from Thermo Scientific. Gaussia luciferase (pCMV-GLuC). Ca<sup>2+</sup>-independent microbial transglutaminase (mTGase) was purchased from Activa<sup>®</sup>WM. CM52 cation exchange resin was purchased from Whatman<sup>®</sup>, and transglutaminase (TGase) colorimetric microassay kit was purchased from Covalab. EP20-24<sup>4</sup> was provided by Elastin Specialties and SuperFect<sup>®</sup> was purchased from QIAGEN. Human umbilical vein endothelial cells (HUVECS) and endothelial growth basal medium (EBM-2) along with the kits were obtained from Lonza and human acute monocytic leukemia cell line (THP1) were obtained from ATCC. Human eNOS and IL-10 ELISA kit from R&D Systems. Multiplex cytokine measurement kit from Meso Scale Discovery and RT-PCR array and kits from QIAGEN.

#### 4.2.2 EP20-244 Polypeptide Expression and Purification

EP20-24<sup>4</sup> relates to the recombinant ELP with exons 20-21-23-24-21-23-24-21-23-24-21-23-24 found in the human aortic elastin and was expressed and purified as reported previously [36]. ELP of 94% purity was obtained from Elastin Specialties, Canada.

#### 4.2.3 Purification of mTGase

Ca<sup>2+</sup>-independent mTGase was purified as previously described [37]. Briefly, the mTGase enzyme sample was dissolved in 20 mM sodium acetate buffer (pH 5.8) at a concentration of 500 mg/ml and added to a glass column (1.5 x 30 cm) containing CM52 cation exchange resin pre-equilibrated with the above buffer at a flow rate of 2 ml/min. The sample was washed with two column volumes of the same buffer and eluted by a gradient of 10 column volumes from 0 to 0.5 M sodium chloride. The samples were analyzed at 280 nm for eluted protein. Pooled fractions were concentrated, dialyzed into PBS and analyzed for enzyme activity using the transglutaminase colorimetric micro assay kit and purified guinea pig TGase (control) with known units of enzyme activity as standard (where 1 unit will catalyze the formation of 1  $\mu$ mole of hydroxamate at pH 6.0 at 37 °C using L-glutamic acid-monohydroxamate as the standard). Typical activity recovered was in the range of 0.5 U/mg mTGase.

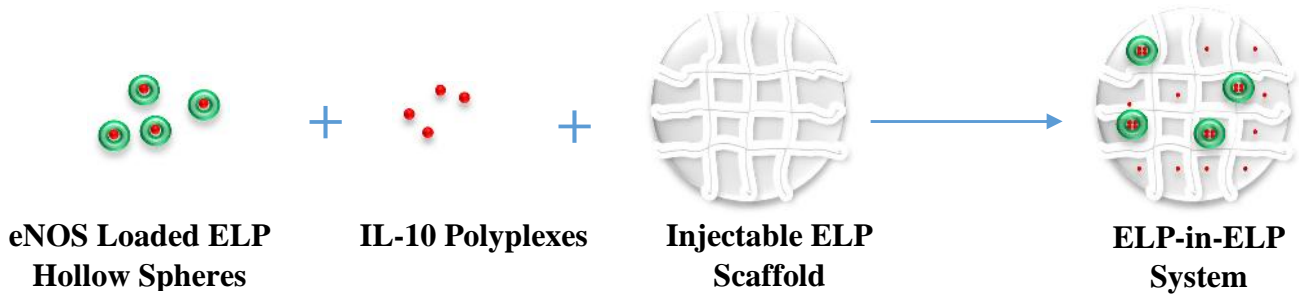
#### 4.2.4 Fabrication of Hollow Spheres

ELP hollow spheres were fabricated using a template-based method [38-40] as described previously [28]. Briefly, the fabrication method includes three steps: coating, cross-linking, and dissolution of the PS core to obtain hollow ELP spheres. Monodispersed PS beads were sulfonated to create a negative surface charge on the sphere [38-40]. These sulfonated PS beads were then used as a template. ELP of ~ 35 kDa was used to coat the sulfonated PS beads in PBS. The coated beads were then cross-linked using mTGase. Finally, PS beads were dissolved using THF to obtain hollow spheres.

#### 4.2.5 Fabrication of In Situ Injectable Scaffold

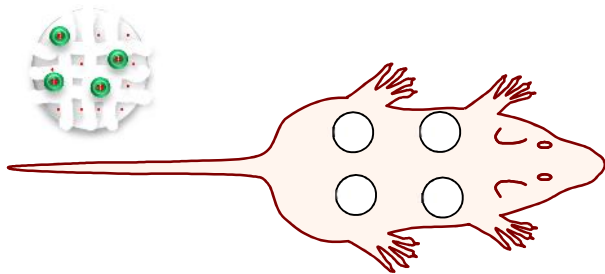
A scaffold capable of gelling in situ was fabricated using ELP and mTGase (Figure 4.2). Briefly, various concentrations of ELP and mTGase were used for fabrication of the scaffold. ELP with 2, 5 and 10 % (weight/volume) were dissolved in water and with 25, 50 and 100 U of mTGase (U/g of ELP concentration) with several combinations. The ELP/mTGase solutions were incubated in a water bath at 37 °C.

*In vitro* ELP-in-ELP System Fabrication



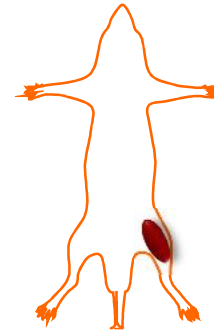
Nine Different Treatments Groups of IL-10 and eNOS (See Table 1)

*In vivo* Animal Study



**Subcutaneous Dose Response Study**

1. Saline
2. ELP Scaffold/Hollow Sphere
3. IL-10 (10 µg)
4. eNOS (20 µg)
5. IL-10(10 µg)/ eNOS (20 µg)



**Ischemic Study**

- Volume Fraction of Inflammatory Cells
- Surface and Length Density of Blood Vessel
- Inflammatory Cytokines Analysis

- Lase Doppler Perfusion Imaging
- Volume Fraction of Inflammatory Cells
- Surface and Length Density of Blood Vessel
- RT-PCR Analysis for Angiogenic and Inflammatory Factors

**Figure 4.1:** A schematic showing the overall goal of this study. The study includes (A) an *in vitro* fabrication of the ELP-in-ELP injectable system and (B) delivery of the therapeutic genes heNOS and hIL-10 in a subcutaneous study to determine a therapeutic dose for heNOS and hIL-10 and a final *in vivo* study in a mouse model of HLI.

Gelation was characterized at different time points ranging from 5 to 30 min. The combination of ELP and mTGase concentrations (10 % of ELP and 100 U of mTGase) gelling at 10 min was further characterized for its cross-linking and cell viability.

#### **4.2.6 TNBSA Assay for Cross-linking**

The cross-linking of ELP hollow spheres with mTGase has been characterized previously [28] and cross-linking of an ELP scaffold with mTGase was performed similarly. TNBSA is a hydrophilic modifying reagent for the detection of primary amines in samples containing amino acids, peptides or proteins [41]. It reacts readily with the N-terminal amino groups of amino acids in aqueous solution at pH 8 to produce a yellow color. The colored derivatives are detected at 335-345 nm. ELP, both with and without treatment of mTGase was used for the assay. mTGase concentrations of 20, 50 and 100 U/g of ELP were used to cross-link ELP. In addition, ELP cross-linked with glutaraldehyde was used as a positive control. For this particular experiment, the cross-linked ELP scaffolds were hydrolyzed in 1N HCL to hydrolyze into a solution. The hydrolyzed ELP solution was then used for the assay.

#### **4.2.7 Cell Viability**

MTT assay was performed to quantify the cell viability of HUVECS in contact with the scaffold. Injectable ELP scaffolds were fabricated in a 96 well tissue culture plate. Briefly, 100  $\mu$ l mixture of ELP and mTGase were plated in several wells of a 96 well plate and were incubated at 37 °C for 10 min. The ELP scaffolds were then equilibrated for 24 hr using EGM-2 medium. The medium was discarded after 24 hr of equilibration. HUVECs were harvested using 0.25% of trypsin-EDTA. Finally, HUVECs were seeded at cell density of  $1 \times 10^4$  cell/well for 24 hr. The culture medium was replaced with fresh medium after 24 hr of seeding. HUVECs on tissue culture plates were kept as a positive control and glutaraldehyde cross-linked scaffolds as negative control. MTT assay was used to assess the cell viability. The scaffolds seeded with HUVECS, along with controls were washed with HBSS and replaced with 200  $\mu$ l of fresh MTT (0.5 mg/ml) solution. This was followed by 4 hr incubation at 37 °C in 5% CO<sub>2</sub>. After the required incubation this MTT solution was decanted carefully and 200  $\mu$ l dimethyl sulfoxide (DMSO) was added to dissolve the formed formazan crystals. The absorbance of the solution was measured at 595 nm on a microplate reader (VarioskanFlash-4.00.53).

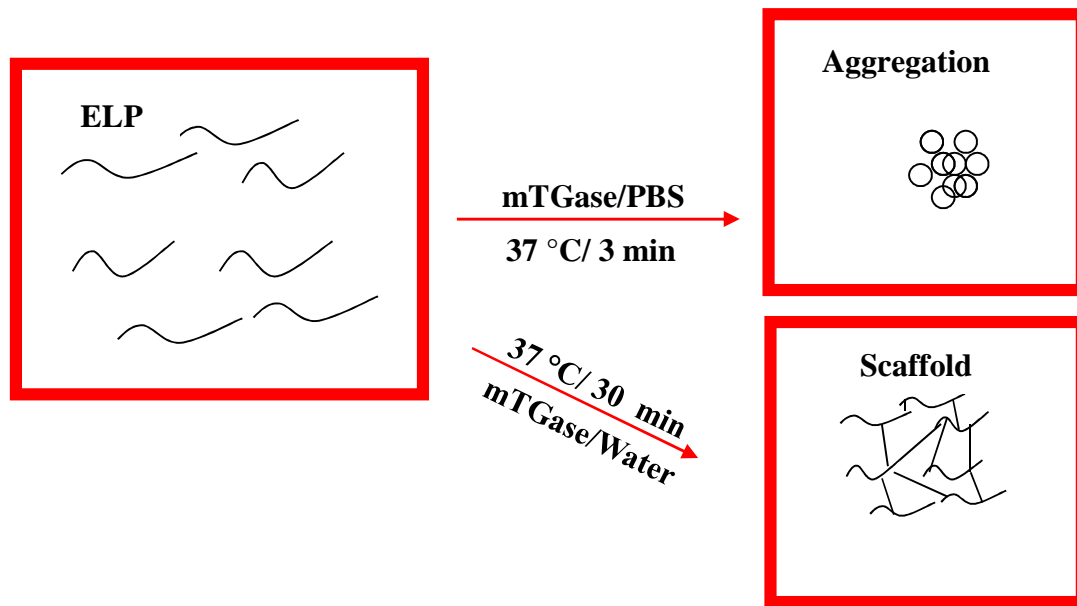


**Figure 4.2:** A schematic representation of injectable elastin-like polypeptide scaffold fabrication method. Elastin-like polypeptide and microbial transglutaminase (mTGase) mixture solution in water forms the scaffold when incubated at 37 °C. The mixture solution of elastin-like polypeptide and mTGase forms aggregated structure rather than a scaffold.

#### **4.2.8 Propagation of Plasmid and Isolation**

Plasmid pCMV-GLuc, human eNOS (heNOS) and human IL-10 (hIL-10) plasmids were transformed into XL1-Blue (Stratagene) competent cells and selected twice in ampicillin antibiotic containing LB broth and on LB agar plates. Plasmid expansion was performed as recommended in the Giga-Prep (Qiagen) protocol and isolated using that kit. Plasmid purity was confirmed by UV spectroscopy (NanoDrop™ ND1000 Spectrophotometer, Thermo Scientific) and gel electrophoresis.

#### **4.2.9 Formulation of Polyplex**

Polyplexes were prepared using commercially available SuperFect® and pCMV-GLuc, heNOS and hIL-10 plasmids in PBS pH 7.4. The weight: weight ratios of SuperFect® and plasmids were optimized to 20:1.

#### **4.2.10 *In Vitro* Internalization Study of ELP Hollow Spheres using Flow Cytometry**

HUVECs and THP1 cells were grown in T25 tissue culture flasks for flow cytometry studies. HUVECs were cultured using EBM-2 medium and THP1 non adherent cells were cultured in RPMI-1640 supplemented with 10% FBS and 1% P/S and L-glutamine at 37 °C in humidified 5% CO<sub>2</sub>. Culture of adherent macrophages from THP1 monocytes were achieved by using phorbolmyristate acetate (PMA) in a differentiation media and were activated using TNF . Briefly, the THP1 cells at a density of 800,000-1,000,000 cells/ml, were cultured on tissue culture plates in a RPMI-1640 differentiation media containing 5 g/L glucose, 1 % P/S and L-glutamine and PMA at a final concentration of 100 ng/ml for 24 h.

For the flow cytometry analysis HUVECs, activated and non-activated THP1 were incubated with FITC labeled ELP hollow spheres of 0.1, 0.5, 1 and 10 μm sizes at a concentration of 50μg/ml concentration. After the desired incubation time, cells were trypsinized and resuspended in a buffer (1% BSA in PBS). Cells were then analyzed using flow cytometry for internalization efficiency.

#### **4.2.11 *In Vitro* Release Study**

*In vitro* dual release studies of pDNA were performed on the injectable ELP-in-ELP (ELP hollow spheres embedded within ELP scaffold) system. The injectable system comprised of scaffold and 1μm ELP hollow spheres which were loaded separately with pCMV-GLuc. Two different samples of ELP-in-ELP were prepared, where one of the group was carrying pDNA in the scaffold and another group in the ELP hollow spheres. The systems were tested for the release

of *pDNA* with and without treatment of enzyme elastase. Briefly, 250 mg samples of 1  $\mu\text{m}$  ELP hollow spheres were re-suspended in 300  $\mu\text{l}$  of PBS and polyplexes containing 20  $\mu\text{g}$  of *pDNA* (20) were added. This mixture was then agitated for 12 h at room temperature. The suspension was centrifuged at 13,000g and the ELP hollow sphere/polyplex complexes were washed four times with MilliQ purified water. The ELP hollow sphere/polyplexes were then mixed with ELP solution containing mTGase and incubated at 37  $^{\circ}\text{C}$  to form a gel encapsulating the ELP hollow spheres. In another sample, ELP solution 10 % (w/v) was mixed with mTGase and 20  $\mu\text{g}$  pCMV-GLuc polyplexes along with the ELP hollow spheres without *pDNA* in it. Both the samples were incubated in PBS with elastase at 37  $^{\circ}\text{C}$  for 10 days to characterize their release profile. The supernatants were collected and quantified using PicoGreen<sup>®</sup> assay, the same way as mentioned in chapter 3. Briefly, the supernatants with polyplexes were treated with high concentration (10mg/ml) of poly-D-glutamic acid (PGA) for 30 min to break the SupeFect/*pDNA* bond in order to get free *pDNA*. Finally, this free *pDNA* was used to quantify the release pattern from scaffold.

#### **4.2.12 *In Vivo* Studies**

The ability of an injectable ELP system to deliver two therapeutic genes of interest (eNOS and IL-10) and their therapeutic doses was investigated in an *in vivo* subcutaneous mouse model. Subsequently, a unilateral hind limb ischemic model was created to test the effect of hIL-10 and heNOS expression in an ischemic condition. Male C57BL/6 mice of 10 weeks old were used for this study. All experimental procedures and protocols were approved by the Ethics Committee of the National University of Ireland, Galway under the license (B100/4131) granted by the Department of Health and Children, Dublin, Ireland. Mice were housed in group of three per cage under controlled temperature and humidity conditions. Mice were fed a regular chow diet and had access to water.

#### **4.2.13 Subcutaneous Dose Response Study**

Animals were anaesthetized using intra-peritoneal injection of ketamine (80-100 mg/kg) with xylazine (10 mg/kg). The skin overlying the scruff and back of each of the animal was shaved. Four random samples were injected in 4 different places in each mouse. The total sample volume was kept at 100  $\mu\text{l}$  with different formulations of eNOS (10 and 20  $\mu\text{g}$ ) and IL-10 (10 and 20  $\mu\text{g}$ ) encapsulated with in ELP hollow spheres and scaffolds respectively. The total number of treatment groups were nine including the control group of ELP scaffold/hollow spheres alone. Two different time points, day 7 and 14 were taken to study both inflammation and angiogenesis

with six animals for each treatment group. The animals were sacrificed at days 7 and 14 and the tissue samples were harvested. Each tissue sample was equally dissected into two halves. One half of the sample was fixed with 4% formaldehyde for histological and immunohistochemical analysis and the other half was divided again into two halves and stored at – 80 °C for protein and mRNA analysis.

#### **4.2.14 Hind Limb Ischemic Study**

Mice were anaesthetized using a combination of ketamine (80-100 mg/kg) and xylazine (10 mg/Kg) administered intraperitoneally. The limbs of the mice were shaved and a sterilized using iodine before the surgery. The femoral artery was exposed by performing an incision in the skin overlying the middle portion of the hind limb of each mouse (unilateral). Left femoral artery and vein were ligated proximal to profunda femoris and excised. The overlying skin was then closed using a surgical suture. Animals were closely monitored until full recovery from anesthesia. Laser Doppler perfusion imaging (LDPI) was performed before and after surgery to assess the perfusion level in the ischemic limbs. ELP injectable system containing IL-10 and eNOS were injected intramuscularly. There were five treatment groups in total including control saline and empty scaffold/empty hollow sphere alone. Blood perfusion level was monitored over different time points (1, 2 and 3 weeks) using LDPI. Animals were housed separately post-surgery under controlled temperature and humidity conditions. Postoperative buprenorphine was administered for analgesia. Their functional recovery was checked at the end of three weeks by assessing walking and necrosis using a score from 1 to 4 for severity. Animals were sacrificed at different time periods (week 1 and 3) with CO<sub>2</sub> asphyxiation. The tissue sections were processed for histological evaluation and protein and mRNA expression analysis as described previously.

#### **4.2.15 Histology and Immunohistochemistry**

Samples from subcutaneous implants were paraffin embedded whereas for ischemic study tissue samples were frozen embedded using cryo-OCT compound. Blocks were cut into sections of 5 µm thickness. Nine sections were cut from each block from three different depths with 100 µm intervals. Slides were stained with H & E using standard protocol. The images for identification of inflammatory cells and blood vessels were taken at 400X magnification in the beginning for consistency.

Identification of blood vessels was confirmed by immunofluorescence staining of the endothelial cell membrane marker CD31 using standard protocols. Briefly, tissue sections from the paraffin

embedded samples were deparaffinized and processed through a gradient of alcohol from 100% ethanol to 50% and finally in water. Furthermore, enzymatic antigen retrieval was carried out at 37 °C using 1X proteinase K solution in TE buffer (50 mM Tris Base, 1 mM EDTA, pH 8.0). The primary antibody used was polyclonal rabbit anti-CD31 (Abcam, Dublin, Ireland) (1:100 in 0.01 M PBS containing 1% BSA, 0.1% cold fish skin gelatin), with an incubation time of overnight at 4 °C. Blocking buffer was added to three slides as negative control. Secondary goat anti-rabbit IgG Alexa Fluor® 488 (1:400 in 0.01 M PBS, Invitrogen, Ireland) was applied for 45 min at room temperature, followed by DAPI as a counterstain.

Identification of macrophages was confirmed by immunohistochemistry using a standard protocol. Briefly, enzymatic antigen retrieval was carried out at 37 °C using 1X proteinase K (20 mg/ml) solution in TE buffer (50 mM Tris Base, 1 mM EDTA, pH 8.0). The primary antibody used was rabbit polyclonal macrophage CD 68 (Abcam, Dublin, Ireland) (1:100 in 0.01 M PBS containing 1% BSA, 0.1% cold fish skin gelatin), with an overnight incubation at 4 °C. Blocking buffer was added to three slides as negative control. Secondary goat anti-rabbit IgG Alexa Fluor® 488 (1:400 in 0.01 M PBS, Invitrogen, Ireland) was applied for 45 min at room temperature, followed by DAPI as a counterstain.

#### 4.2.15.1 Stereology

Six fields of view of the H & E stained slides were captured at 400 X magnification. The volume fraction of inflammatory cells was measured using a 192-point grid. The surface density and length density of blood vessels were measured using a cycloidal line grid.

##### 4.2.15.1.1 Inflammation

Volume fraction ( $V_V$ ) is a relative parameter best estimated by point counting [42]. The number of neutrophil- and macrophage- cell nuclei intersecting grid points was counted ( $P_P$ ). This number was divided by the total number of grid points for each field of view ( $P_T$ ), and a cumulative volume fraction of inflammatory cells calculated for the six fields of view on each section. The following formula was used to calculate volume fraction of inflammatory cells<sup>1</sup>.

$$V_V = \frac{P_P}{P_T} \quad (1)$$

#### 4.2.15.1.2 Angiogenesis

A cycloidal grid of 40 micron radius was overlaid on each field of view [42]. The grid consisted of six test lines, each comprising 10 cycloid arcs. Therefore, the total length ( $L_T$ ) of cycloid arcs was 2400 mm. The number of times a blood vessel intersected (I) an arc was counted, and the following standard equation was used to measure the surface density ( $S_V$ ). The following formula was used to calculate surface density of blood vessels<sup>2</sup>.

$$S_V = 2 \times \frac{I}{L} \quad (2)$$

Length density of blood vessels was measured by rotating each captured field of view by 90 degrees. The cycloidal grid was placed in the same orientation as described above. The grid now consisted of eight test lines, each comprising eight cycloid arcs of radius 40 microns. The total length of test line ( $L_T$ ) was therefore 2560 mm. The number of intersections between blood vessels ( $I_L$ ) and test line was counted, and the length density ( $L_V$ ) of blood vessels was calculated using the following equation, where  $T_S$  is the thickness of the section. The following formula was used to calculate length density of blood vessels<sup>3</sup>.

$$L_V = \frac{2 \times I_L}{T_S} \quad (3)$$

This distance is critical to determine the efficiency of new blood vessels as it measures the zone of diffusion around blood vessels.

#### 4.2.16 Quantification of heNOS and hIL-10 Level

Protein analysis was conducted on tissue homogenates using human IL-10 and eNOS ELISA kit from R&D Systems. Briefly, tissue samples were suspended in Tissue Extraction Reagent (Sigma, Dublin, IE) at 20 mg/mL. The samples were incubated for 5 minutes at 4 °C and then homogenized using a Tissue Ruptor (Qiagen, Crawley, UK). Homogenates were centrifuged at 10,000g for 10 minutes to remove particulates. The IL-10 and eNOS content in the supernatant was then analyzed and normalized to the total protein content, as analyzed using the bicinchoninic acid assay.

#### 4.2.17 Multiplex Cytokine Measurements

A mouse inflammatory cytokine multiplex array (Meso Scale Discovery, Gaithersburg, MD) was used to analyze the relative levels of a variety of different inflammatory cytokines. Briefly, tissue lysates extracted as mentioned above were added to plates carrying antibodies for interferon gamma (IFN- $\gamma$ ), interleukin 1 $\beta$ , -10, -4, -2, -5, -12 (IL-1 $\beta$ , IL-10, IL-4, IL-6, IL-2, IL-5, IL-12), tissue necrosis factor alpha (TNF- $\alpha$ ), IFN- $\gamma$ , IL-1 $\beta$ , IL-4, IL-5, IL-12, IL-2, KC/GRO/CINC (which is the mouse analog of human IL-8). The plate was then imaged with a SECTOR<sup>®</sup> Imager 2400 (Meso Scale Discovery, Gaithersburg, MD).

#### 4.2.18 RT-PCR Analysis

RNA was isolated using RNeasy<sup>®</sup> Micro Kit (QIAGEN), following the manufacturer's protocol. Briefly, cells were homogenized by Trizol and then phase separated using chloroform. The quantity of RNA isolated was checked spectrophotometrically using a NanoDrop. The quality was checked using Agilent RNA. The isolated RNA was first reverse transcribed using Reverse Transcription System (QIAGEN). The cDNA thus obtained was then used for real time PCR reaction (ABI StepOnePlus<sup>™</sup> Real-Time PCR System, software v2.1). The PCR array was designed (QIAGEN) for 16 genes: angiopoietin 1 (ANG-1), fibroblast growth factor 1 (FGF1), platelet derived growth factor B (PDGFB), serpinF1, vascular endothelial growth factor A and B (VEGFA and VEGFB), IFN- $\gamma$ , IL-1 $\beta$ , IL-10, IL-4, IL-6, IL-2, TNF- $\alpha$ , leptin, matrix metalloproteinase 9 (MMP9) with their specific primers and RT<sup>2</sup> SYBR Green Mastermix (QIAGEN) was used under standard conditions to perform the RT-PCR. *18s rRNA* was used as a reference gene to normalise the qRT-PCR data.

#### 4.2.19 Statistics

All bar charts represent mean  $\pm$  standard deviation. One-way ANOVA, with Tukey's multiple comparisons test was carried out. Pearson's correlation analysis was carried out for each group between the following parameters: surface density, volume fraction of inflammatory cells, eNOS and IL-10 expression.  $P < 0.05$  was considered statistically significant. Tests were carried out using statistical software (GraphPad Prism, USA).

### **4.3 Results**

#### **4.3.1 Internalization Study of Hollow Spheres**

Various sizes of ELP hollow spheres were screened to determine the cellular uptake efficiency. Flow cytometry was performed on cells treated with FITC-labelled ELP hollow spheres of 0.1, 0.5, 1 and 10  $\mu\text{m}$  sizes of ELP hollow spheres (Figure 4.3 and 4.4). The cells used were HUVECS and activated and non-activated macrophages (THP1). Human cell lines instead of mouse were used in this study to evaluate the clinical relevance of these hollow spheres. The activated and non-activated macrophages showed a higher uptake of 10  $\mu\text{m}$  ELP HS compared to 0.1, 0.5 and 1  $\mu\text{m}$  sized hollow spheres (Figure 4.3). Although the internalisation of ELP hollow spheres into HUVECS did not show any defined pattern, as shown in the case of macrophages,; ELP hollow spheres of 0.5, 1 and 10  $\mu\text{m}$  size showed more uptake in the HUVECs compared to 1  $\mu\text{m}$  size of hollow spheres (Figure 4.4).

#### **4.3.2 Fabrication of Injectable Scaffold and its Characterization**

An injectable ELP scaffold was fabricated using mTGase as a cross-linker (Figure 4.5). A 20% ELP scaffold and mTGase of 100 U/g of ELP concentration was found to be the optimal ratio of ELP and mTGase to fabricate the scaffold with a gelation time of 10 min at 37 °C. The successful cross-linking of the ELP scaffold was verified by TNBSA assay and it was shown that the cross-linked ELP scaffold has less free primary amino groups after cross-linking with mTGase than that of ELP without mTGase (Figure 4.6).

Cellular cytotoxicity of ELP scaffold was measured using HUVECs. Metabolic activity using MTT assay revealed that ELP scaffold cross-linked with mTGase is non-cytotoxic similar to the control, on tissue culture plastic. The ELP scaffold cross-linked with GTA as a negative control showed higher cellular cytotoxicity than that of ELP/mTGase and the control (Figure 4.7).

#### **4.3.3 *In Vitro* Release Study**

A release study was performed using the ELP-inELP injectable system comprising both ELP hollow spheres and the ELP injectable scaffold as gene delivery depot (Figure 4.8). Two different sample groups were used for this study: 1) ELP injectable scaffold containing pCMV-GLuc and 2) ELP hollow spheres containing pCMV-GLuc. The release profile of these systems was monitored for 10 days and a cumulative release profile was calculated.

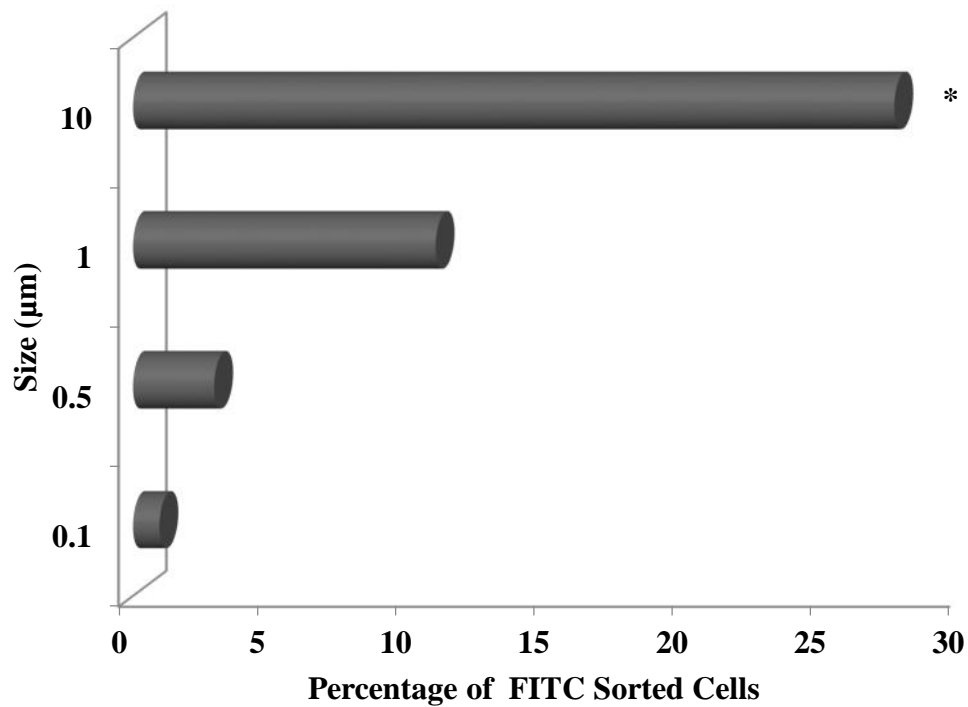


**Figure 4.3: Flow cytometry data, elucidating the effect of size on the internalization efficiency of elastin-like polypeptide hollow spheres into activated macrophages THP1 at 24 h incubation. Statistical significance was performed by one-way ANOVA (n=3, p<0.05). \* represents significant difference of 10 µm from rest of the hollow spheres.**

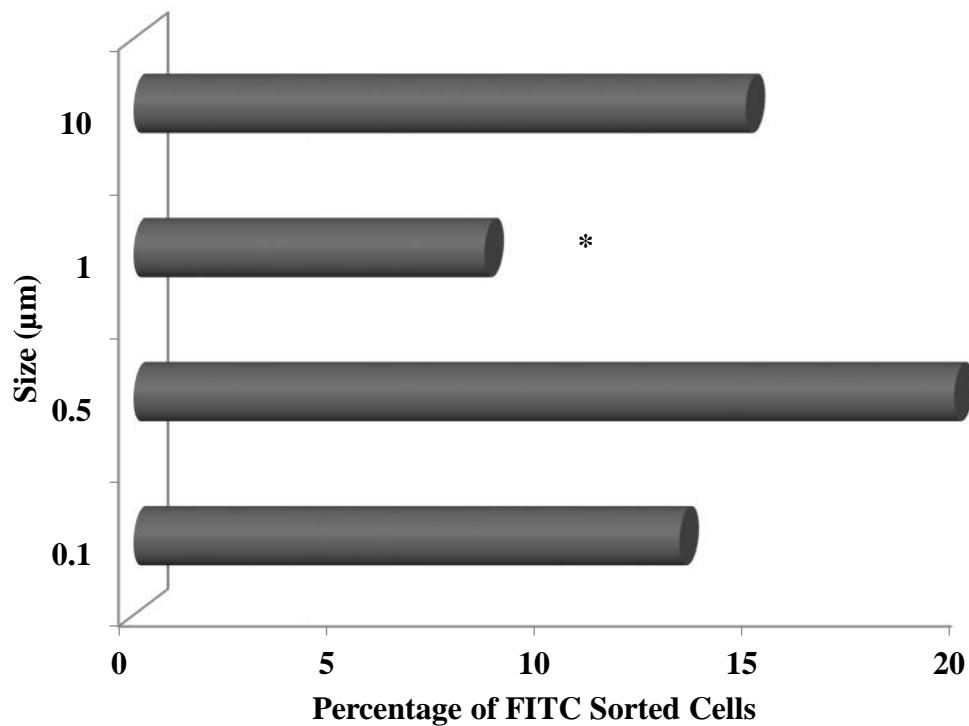


**Figure 4.4:** Flow cytometry data, elucidating the effect of size on the internalization efficiency of elastin-like polypeptide hollow spheres into human umbilical vein endothelial cells at 24 h incubation. Statistical significance was performed by one-way ANOVA (n=3, p<0.05). \* represents significant difference of 1 µm from rest of the hollow spheres.

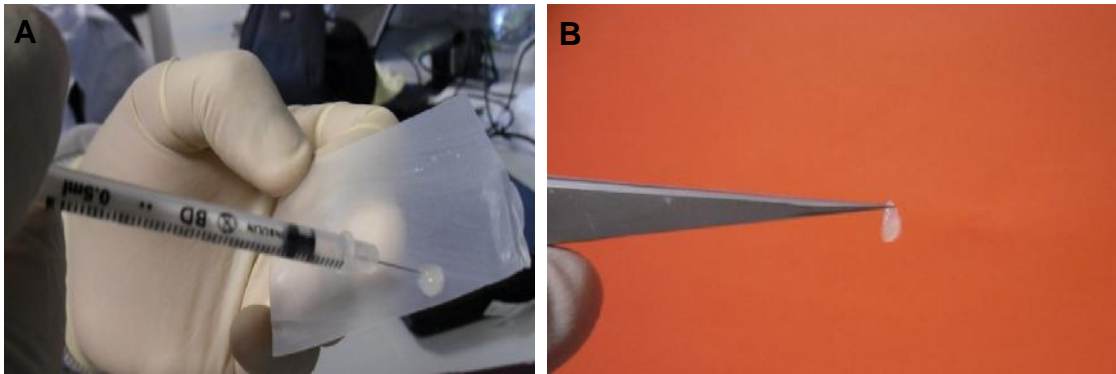


**Figure 4.5: Photographic image (A) injection of elastin-like polypeptide/mTGase mix solution on a parafilm sheet and (B) solidified elastin-like polypeptide based scaffold after gelation.**

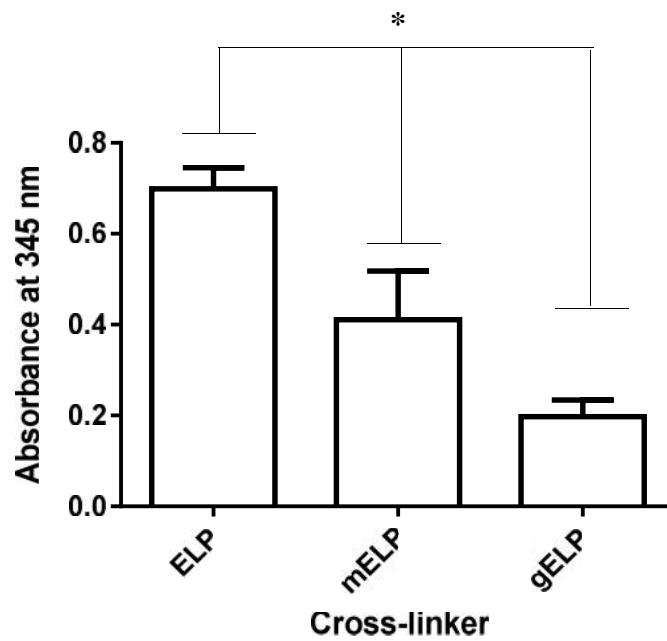


**Figure 4.6:** TNBSA analysis to characterize the cross-linking of elastin-like polypeptide scaffold with mTGase enzyme of 100U/g of ELP. Glutaraldehyde and elastin-like polypeptide alone were used as positive and negative controls respectively. Statistical significance was determined by one-way ANOVA (n=3, p<0.05).

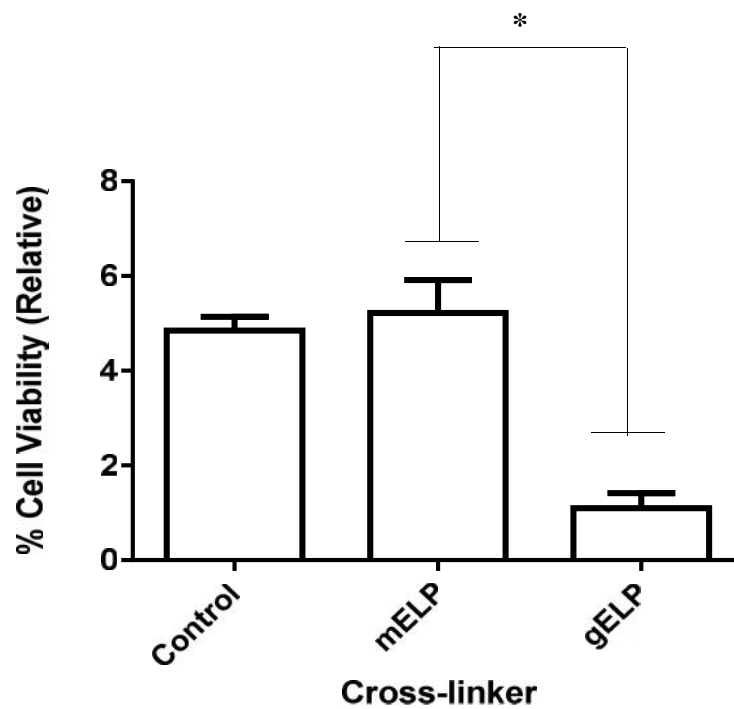


**Figure 4.7:** MTT assay was used to characterize the cellular metabolic activity of elastin-like polypeptide scaffold with mTGase enzyme. Glutaraldehyde and elastin-like polypeptide alone were used as negative and positive controls respectively. Statistical significance was determined by one-way ANOVA (n=3, p<0.05).

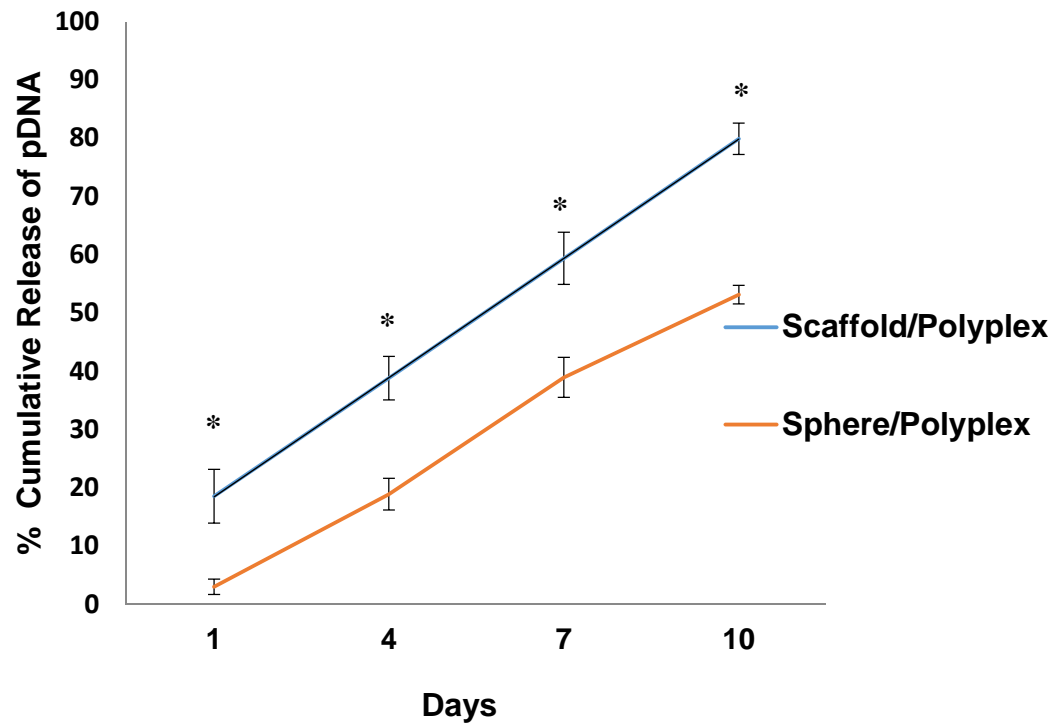


**Figure 4.8:** Cumulative release profile of *pDNA*/polyplex from the injectable system: elastin-like polypeptide scaffold/polyplex and elastin-like polypeptide hollow spheres/polyplex at 37 °C and treated with elastase. All the data are represented as the mean  $\pm$  standard deviation (n=3, p<0.05). Statistical significance was performed using t-test.

The scaffold/polyplex sample group released 20% of *pDNA* by day one as compared to ELP hollow sphere/polyplex which was near to 0%. By day four, the scaffold/polyplex group released around 40% of its *pDNA* and nearly 90% by the end of ten days. The ELP hollow sphere/polyplex released a significantly lower percentage of *pDNA* as compared to scaffold/polyplex. At day 4 the release for ELP hollow sphere/polyplex was only 20% and almost 50% by day ten.

#### **4.3.4 *In Vivo* Subcutaneous Study**

An *in vivo* subcutaneous study was performed in C57BL/6 mice to determine a combination of dose for eNOS and IL-10. Nine different samples were used (Table 4.1). This *in vivo* subcutaneous study was performed to characterize the degradation profile of the injectable ELP system and also to elucidate an appropriate therapeutic dose to induce angiogenesis and reduce inflammation *in vivo*. The degradation of the ELP scaffold is shown in the figure 4.9. H & E sections of the tissue sections revealed a 40-50% higher degradation of the scaffold from day 7 to day 14 (Figure 4.9).

##### *4.3.4.1 Angiogenesis and Inflammation Analysis of Subcutaneous Mouse Model*

Inflammation was measured as volume fraction of the infiltrated inflammatory cells from the H & E sections (Figure 4.10). At day 7, the volume fraction of inflammatory cells decreased 30% in the case of IL-10 treatment groups compared to ELP alone and eNOS alone treatments. There was no significant difference observed between any treatment groups in the amount of inflammatory cells on day 14. CD68 immunostaining, a macrophage marker, showed similar results and showed IL-10 to be effective in reducing macrophage level (Figure 4.13 and 4.14). Surface and length density of blood vessels were measured from the H & E sections of the subcutaneous implants of different treatment groups and control (Figure 4.11 and 4.12). Two different time points, day 7 and 14, were analysed for this study. On day 7 the control and IL-10 treatment alone groups showed similar levels of blood vessel density level of around 30 mm<sup>2</sup> whereas the eNOS treatment groups showed blood vessel density around 50 mm<sup>2</sup>. A trend towards an increase in the blood vessel surface density was found in the eNOS treatment groups. On day 14 the blood vessel density increased up to 139 mm<sup>2</sup> and was significantly higher from that seen in control groups and IL-10 treatment alone groups (40 up to 55 mm<sup>2</sup>). The eNOS doses of both 10 and 20 µg showed significantly enhanced surface density of blood vessels at day 14. The sample treatment group IL-10 (20 µg)/eNOS (20 µg) showed 62% less blood vessel density, while, IL-10 (10 µg) /eNOS (20 µg) showed a 30% less blood vessel surface density than eNOS

20 µg alone on day 14. Based on the blood vessel surface density data, treatment groups such as: ELP alone, IL-10 (10 µg) alone, eNOS (20 µg) alone and IL10 (10 µg)/eNOS (20 µg) were used to characterize the length density. The length density of all the four treatment groups were found to be similar on day 7. On day 14 both the eNOS treatment groups showed 30-50% higher length density of blood vessels compared to ELP and IL-10 (10 µg) alone. Furthermore, immunostaining of the blood vessels using CD31 supported histological data for vessel density (Figure 4.15). The results showed higher blood vessel in the treatment groups eNOS (20 µg) and IL10 (10 µg)/eNOS (20 µg).

#### 4.3.4.2 *heNOS and hIL-10 Expression in the Subcutaneous Mouse Model*

The spatio-temporal expression of heNOS and hIL-10 was studied *in vivo*. Human eNOS and IL-10 protein levels were measured using ELISA. The expression was measured in terms of pg/mg of protein. On day 7 eNOS treated samples showed eNOS expression at the level of 40-60 pg/mg of eNOS. On day 14 the heNOS treated groups showed an increase in heNOS expression level which falls within a range 80-100 pg/mg of protein (Figure 4.16).

Similar to heNOS, hIL-10 protein expression level was measured for day 7 and day 14. The IL-10 treated group showed expression of hIL-10 from range of 800-1100 pg/mg of protein on day 7. And on day 14 the expression level of hIL-10 treated groups showed less expression, the expression level ranging from 400-700 pg/mg of protein (Figure 4.17). The control and eNOS alone groups showed an insignificant expression value for both day 7 and 14.

#### 4.3.4.3 *Inflammatory Markers*

Nine inflammatory markers comprising of both pro- and anti-inflammatory cytokines were analysed to determine the pro and anti-inflammatory cytokines expressed on day 7 and 14 (Figure 4.18 and 4.19). Samples from day 7 and 14 were used to extract protein and multiplex ELISA was performed to analyse the expression of different mouse inflammatory markers. TNF showed no significant difference in their expression level for all the treatment groups. The result is similar for both day 7 and 14. IFN was found to be expressed more in ELP alone compared to IL-10, eNOS and IL-10/eNOS treatment groups on day 7 while heNOS treated group showed significantly lower level of IFN than other groups on day 14.

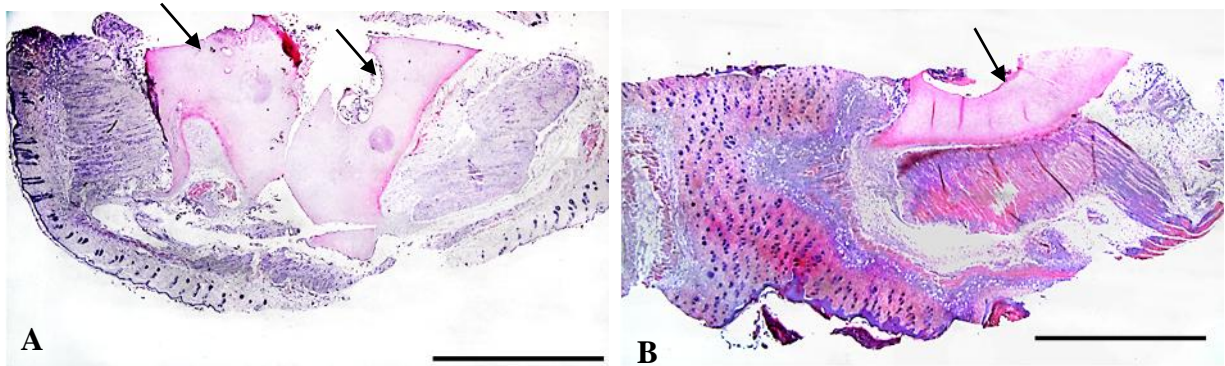


**Figure 4.9: H & E staining of subcutaneous implant showing degradation of elastin-like polypeptide scaffold by A) day 7 and B) day 14. Arrows indicate elastin-like polypeptide scaffold at the site of implantation. The scale bar represents 100  $\mu\text{m}$ .**

**Table 4.1:** The table contains nine different treatment groups used for the subcutaneous dose study.

| <b>Treatment Groups</b>                 | <b>Abbreviation</b>   | <b>hIL-10<br/><i>p</i>DNA<br/>(<math>\mu</math>g)</b> | <b>heNOS<br/><i>p</i>DNA<br/>(<math>\mu</math>g)</b> |
|-----------------------------------------|-----------------------|-------------------------------------------------------|------------------------------------------------------|
| <b>Scaffold/Hollow Sphere</b>           | <b>ELP</b>            |                                                       |                                                      |
| <b>Scaffold-IL 10/Hollow Sphere</b>     | <b>IL10-10</b>        | <b>10</b>                                             |                                                      |
| <b>Scaffold-IL 10/Hollow Sphere</b>     | <b>IL10-20</b>        | <b>20</b>                                             |                                                      |
| <b>Scaffold/Hollow Sphere-eNOS</b>      | <b>eNOS10</b>         |                                                       | <b>10</b>                                            |
| <b>Scaffold/Hollow Sphere-eNOS</b>      | <b>eNOS20</b>         |                                                       | <b>20</b>                                            |
| <b>Scaffold-IL10/Hollow Sphere-eNOS</b> | <b>IL10-10/eNOS10</b> | <b>10</b>                                             | <b>10</b>                                            |
| <b>Scaffold-IL10/Hollow Sphere-eNOS</b> | <b>IL10-10/eNOS20</b> | <b>10</b>                                             | <b>20</b>                                            |
| <b>Scaffold-IL10/Hollow Sphere-eNOS</b> | <b>IL10-20/eNOS10</b> | <b>20</b>                                             | <b>10</b>                                            |
| <b>Scaffold-IL10/Hollow Sphere-eNOS</b> | <b>IL10-20/eNOS20</b> | <b>20</b>                                             | <b>20</b>                                            |

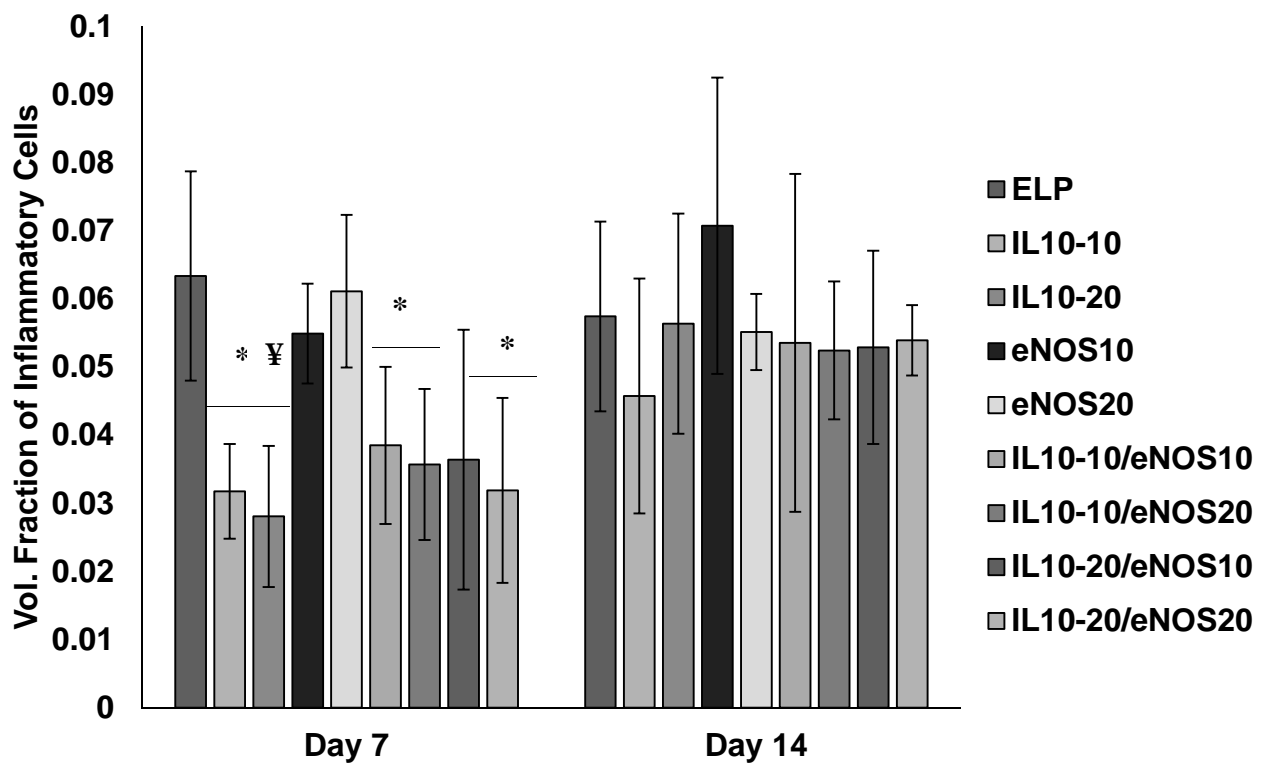


**Figure 4.10: Volume fraction of inflammatory cells in the subcutaneous implant area A) day 7 and B) day 14. Nine different doses of eNOS and IL-10 were implanted. Elastin-like polypeptide scaffold was used as a control. Statistical significance by one way ANOVA ( $n = 6$ ,  $p < 0.05$ ). \* represents the groups IL-10 treatments groups with statistical difference from ELP and eNOS alone treatment groups on day 7. ¥ represents significant difference between IL-10-10 and 20 treatment groups of day 7 and all the treatment groups of day 14.**

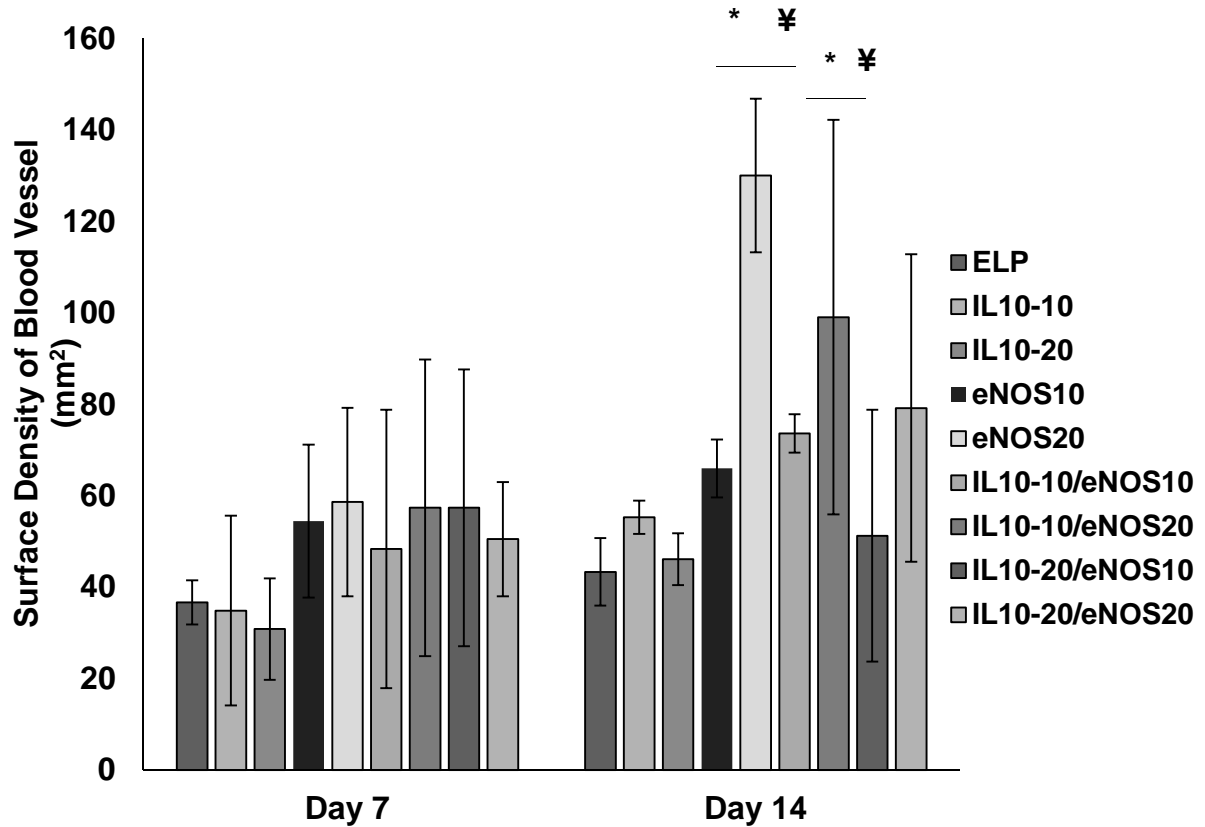


**Figure 4.11 : Surface density of blood vessels in the subcutaneous implant area day 7 and day 14. Nine different doses of eNOS and IL-10 were implanted. Elastin-like polypeptide scaffold was used as a control. Statistical significance by one way ANOVA (n = 6, p < 0.05). \* represents the groups eNOS20 and IL10-10/eNOS20 with statistical difference from ELP alone and IL-10 treatment groups on day 14. ¥ represents significant difference between eNOS20 and IL10-10/eNOS20 groups of day 14 from that of day 7.**

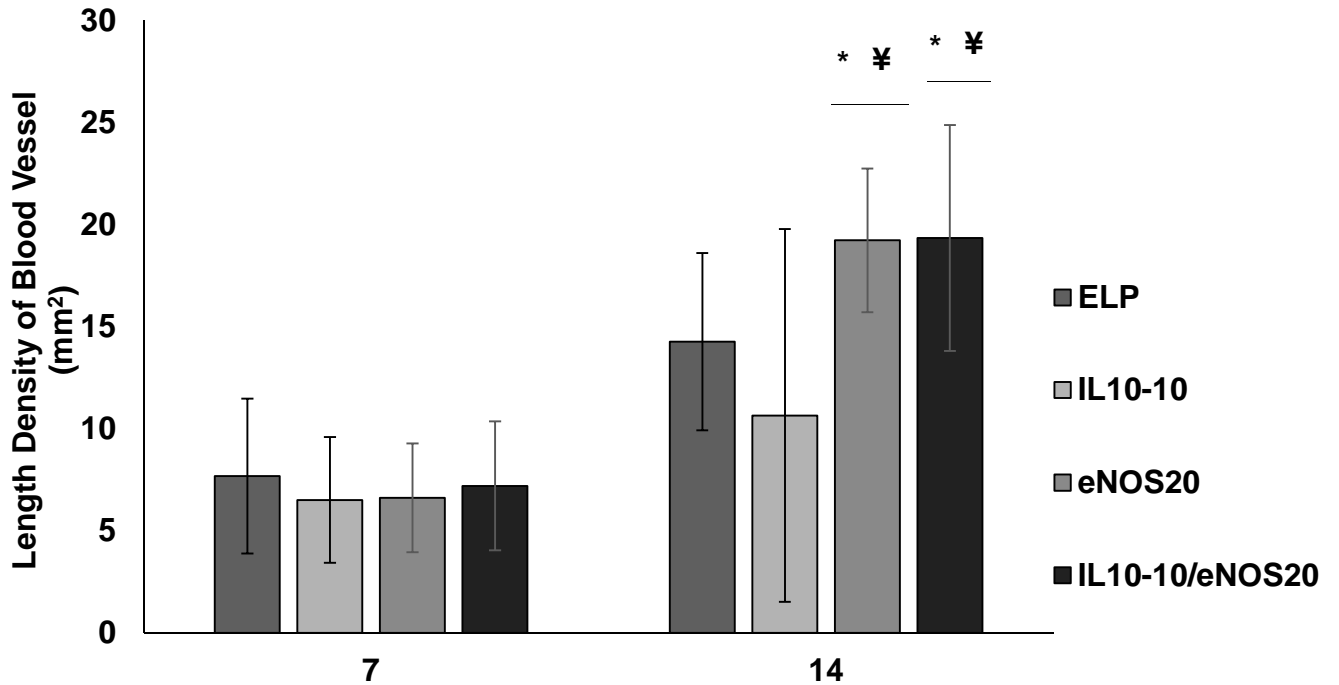


**Figure 4.12:** Length density of blood vessels in the subcutaneous implant area at day 7 and 14. Elastin-like polypeptide scaffold was used as a control. Statistical significance by one way ANOVA ( $n = 6$ ,  $p < 0.05$ ). \* represents the groups eNOS20 and IL10-10/eNOS20 with statistical difference from ELP alone and IL10-10 treatment groups on day 14. ¥ represents significant difference between eNOS20 and IL10-10/eNOS20 groups of day 14 from that of day 7.

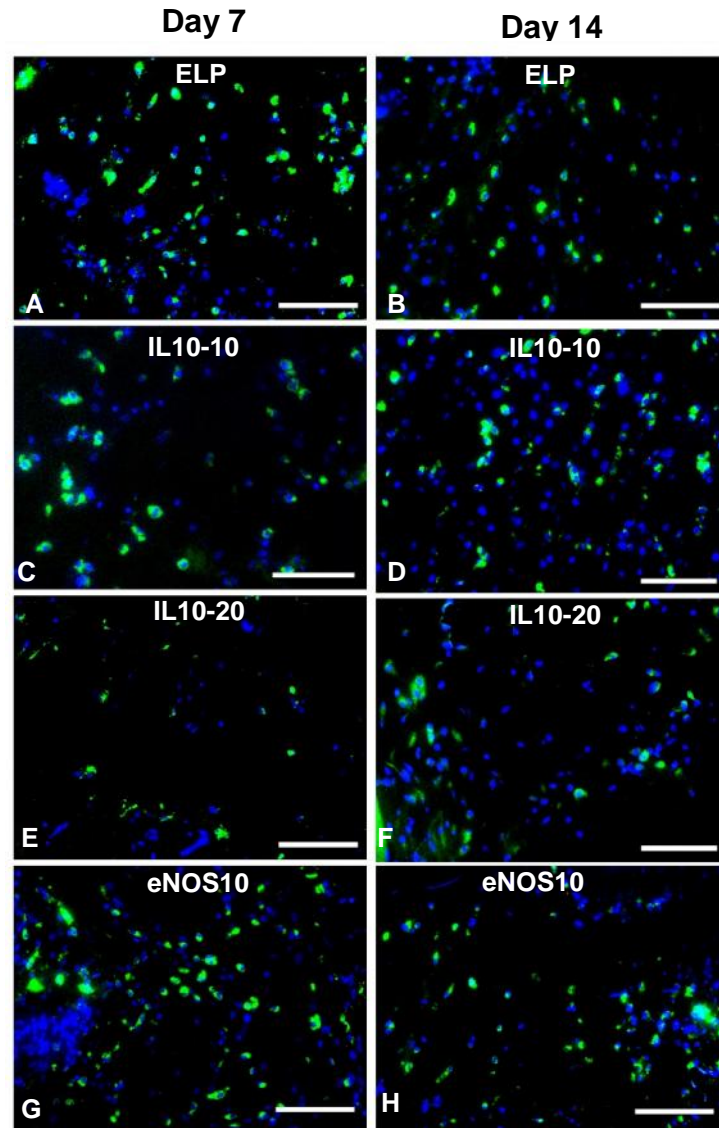


**Figure 4.13: CD68 immunostaining for macrophages (stained as green cells) at day 7 and 14 in various treatments in the subcutaneous implant study. (A, B) ELP, (C,D) IL10-10, (E,F) IL10-20 (G,H) eNOS10. The scale bar represents 100  $\mu$ m.**

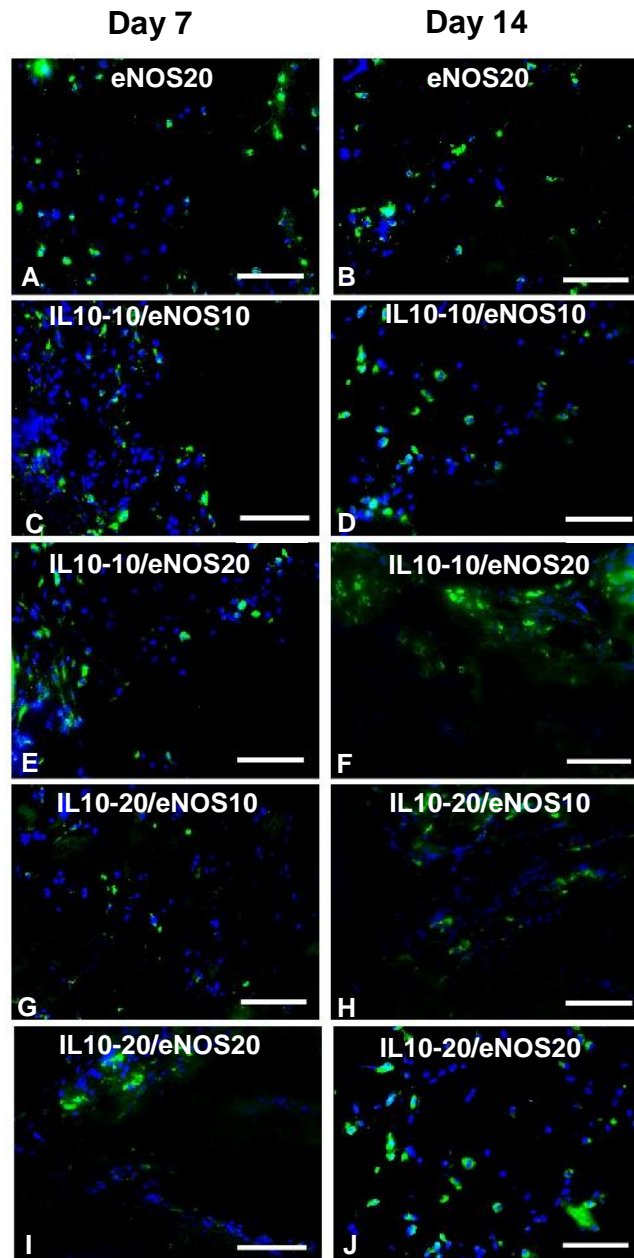


**Figure 4.14** CD68 immunostaining for macrophages (stained as green cells) at day 7 and 14 in various treatments in the subcutaneous implant study. (A,B) eNOS20, (C,D) IL10-10/eNOS10, (E,F) IL10-10/eNOS20 and (G,H) IL10-20/eNOS10 and (I,J) IL10-20/eNOS20. The scale bar represents 100  $\mu$ m.

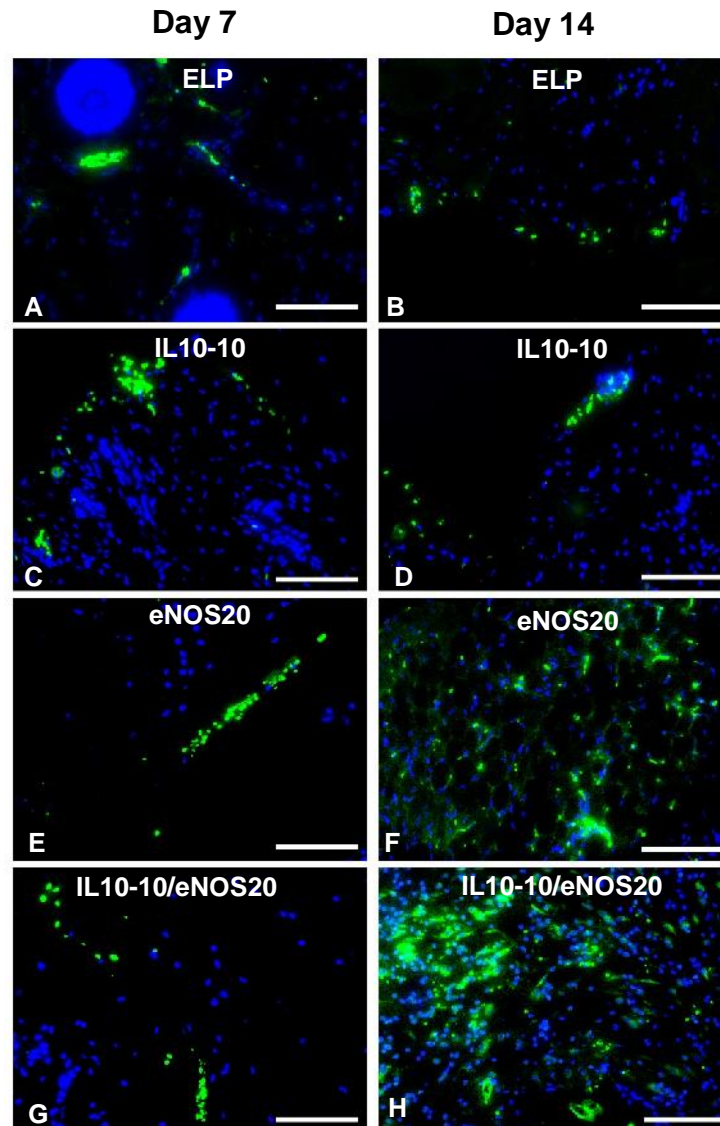


**Figure 4.15:** CD31 immunostaining for blood vessels (stained as green cells) at day 7 and 14 in various treatments in the subcutaneous implant study. (A, B) ELP, (C, D) IL10-10, (E, F) eNOS20 and (G, H) IL10-10/eNOS20. The scale bar represents 100  $\mu\text{m}$ .

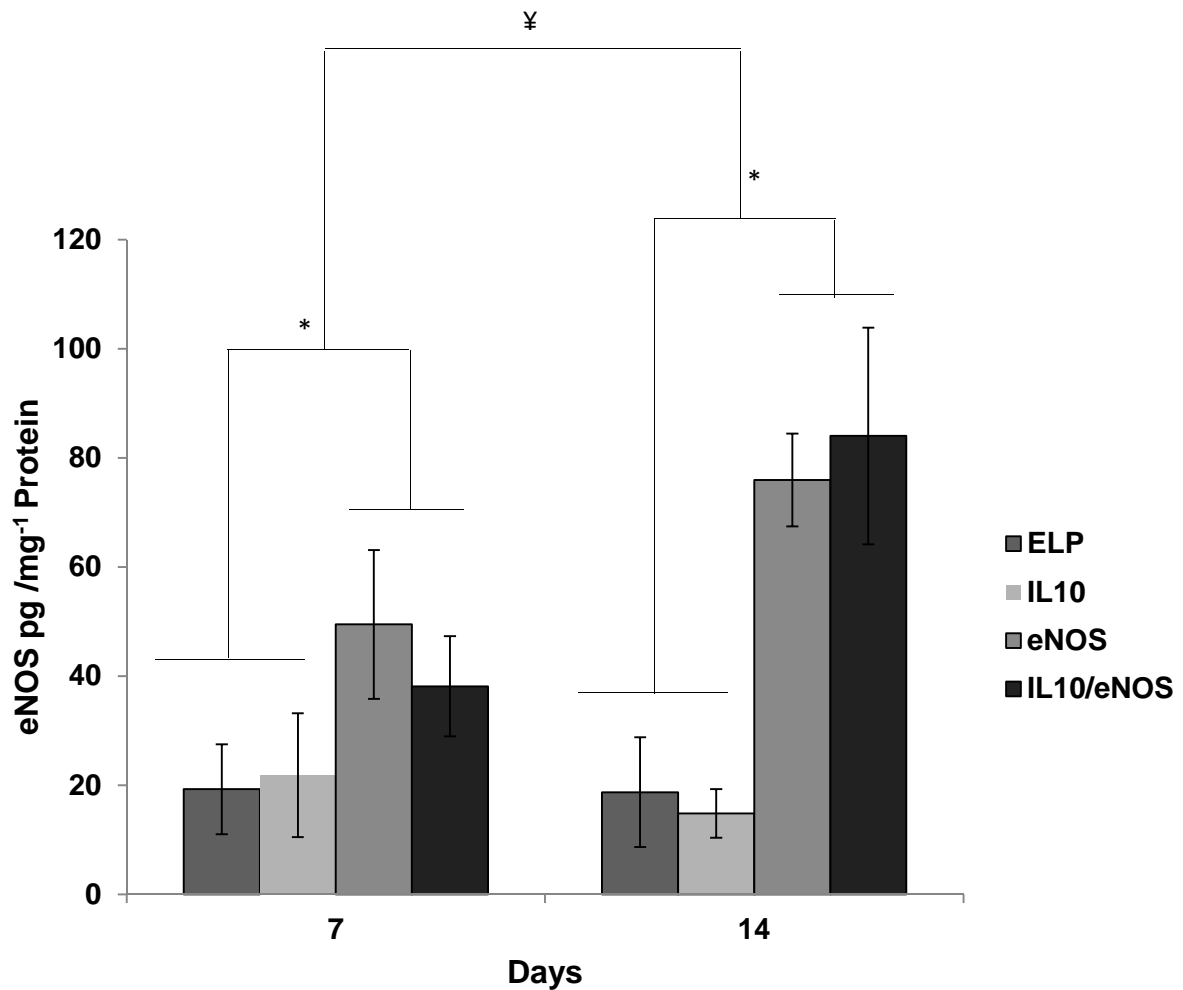


**Figure 4.16: Human eNOS expression in the subcutaneous implant for day 7 and 14.** Elastin-like polypeptide scaffold only was kept as a control. Statistical significance by one way ANOVA ( $n = 6$ ,  $p < 0.05$ ). \* represents significance difference between eNOS containing treatment groups with rest of the groups and ¥ represents significant difference between the day 7 and 14 expression of eNOS.

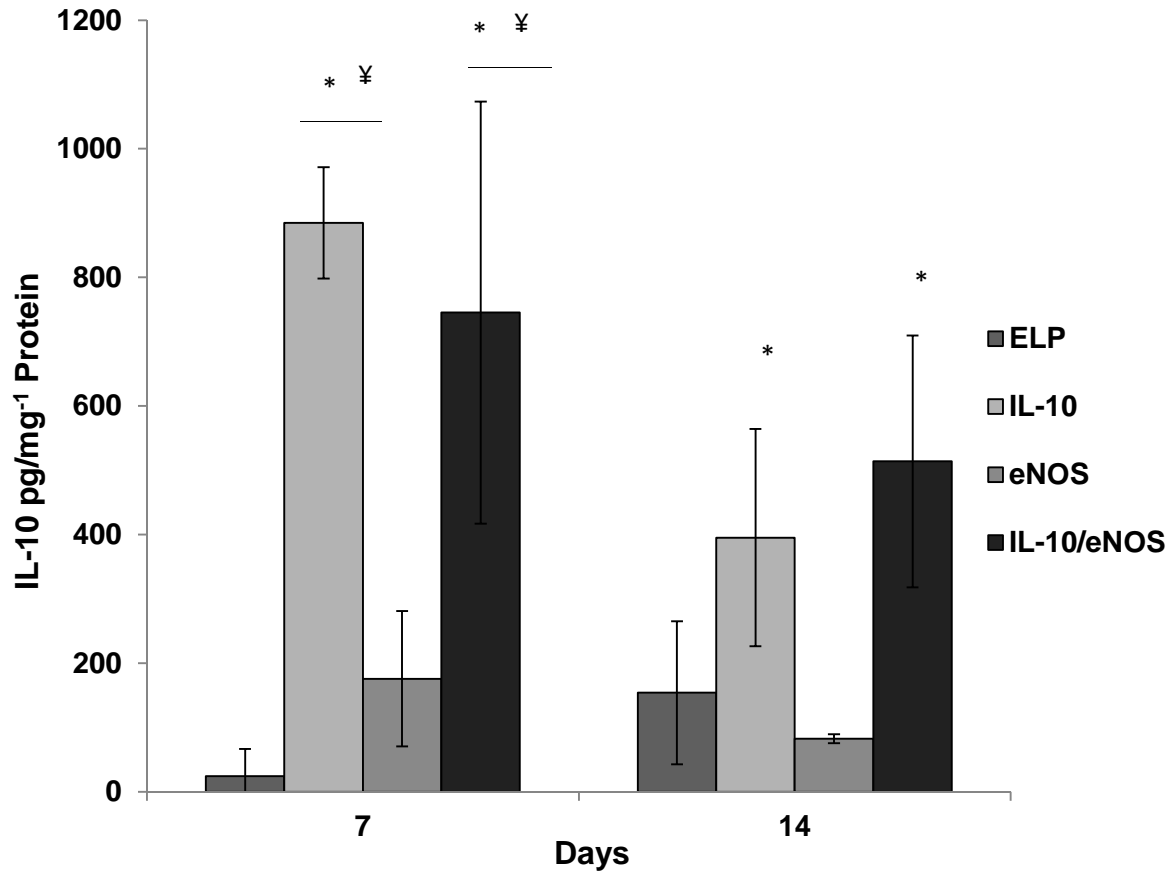


**Figure 4.17: Human IL-10 expression in the subcutaneous implant for day 7 and 14. Elastin-like polypeptide scaffold only was kept as a control. Statistical significance by one way ANOVA ( $n = 6, p < 0.05$ ). \* represents significance difference between IL-10 containing treatment groups with rest of the groups and ¥ represents significant difference between the day 7 and 14 expression of IL-10.**

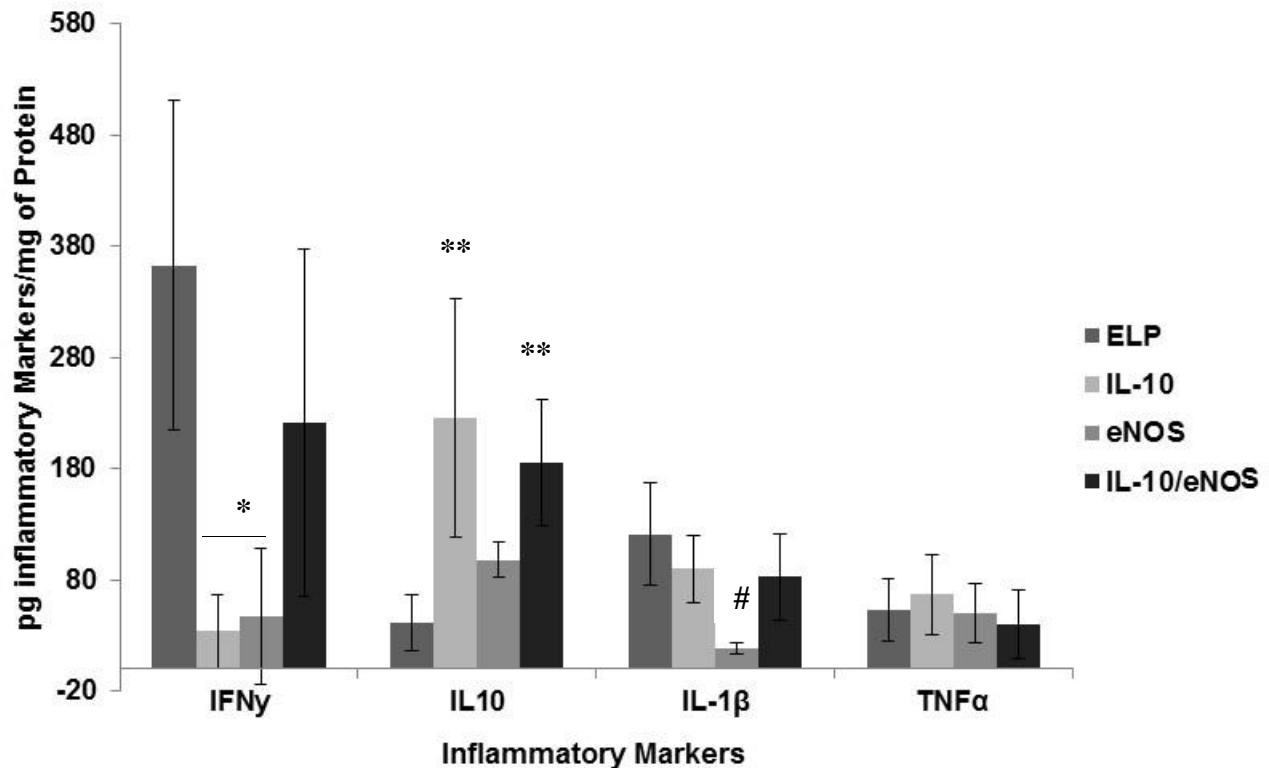


**Figure 4.18: Screening of inflammatory cytokines expressed in the subcutaneous implant by day 7.** Elastin-like polypeptide scaffold only was kept as a control. Statistical significance by one way ANOVA ( $n = 6$ ,  $p < 0.05$ ). \* represents statistical significance of Interleukin-10 and eNOS only treatment groups from ELP and IL-10/eNOS treatment groups. \*\* represents statistical significance of IL-10 and IL-10/eNOS from rest of the treatment groups. # represents statistical significance of eNOS treatment group from rest of the treatment groups.

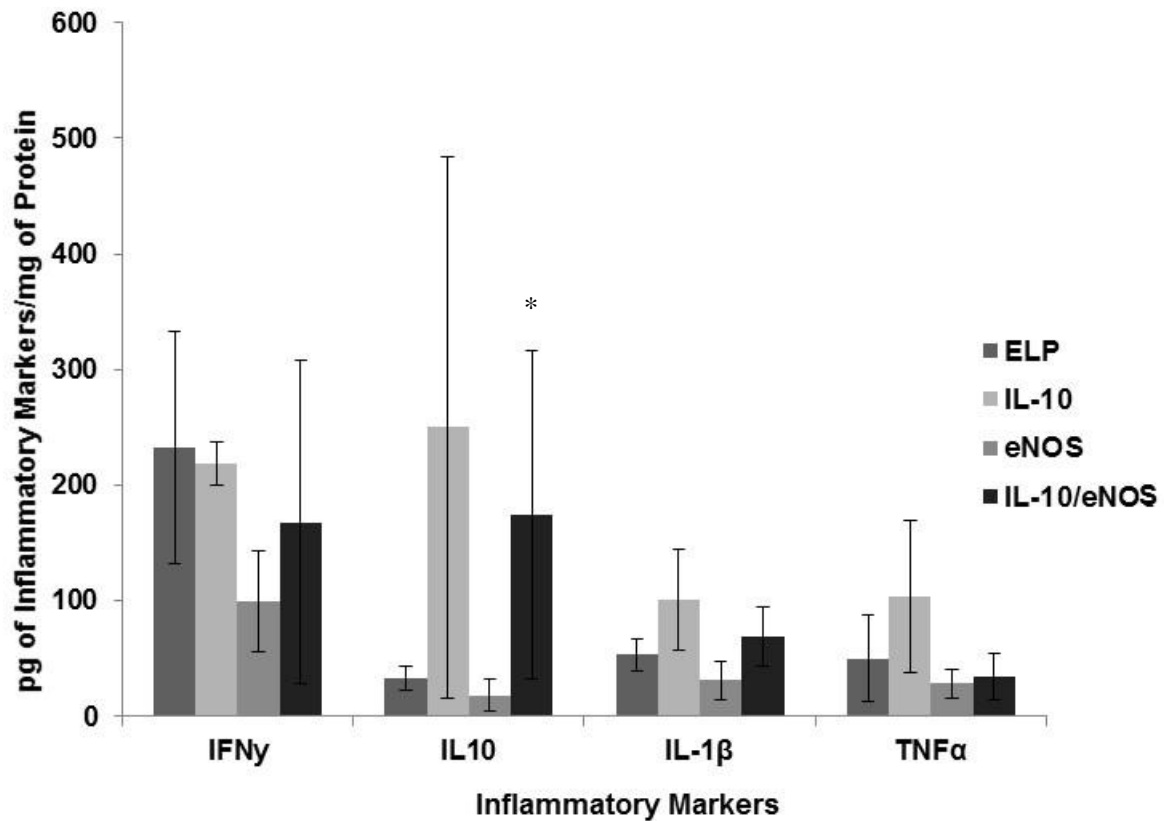


**Figure 4.19: Screening of inflammatory cytokines expressed in the subcutaneous implant by day 14. Elastin-like polypeptide scaffold only was kept as a control. Statistical significance by one way ANOVA (n = 6, p < 0.05). \* represents statistical significance of IL-10/eNOS treatment groups from the rest of the groups.**

IL-1 expression level showed significantly less in eNOS treated group as compared to others on day 7 whereas there was no significant difference between all the groups on IL-1 expression level by day 14. IL-10 treatment groups have more expression of mIL-10 on both day 7 and 14.

#### **4.3.5 Hind Limb Ischemia Study**

Unilateral hind limb ischemia in a mouse model was successfully generated by permanent ligation of the left femoral artery and vein. Blood perfusion was used as a measure to assess the effect of the treatments on angiogenesis. Blood perfusion was measured after the surgery every week until day 21 using LDPI. Blood perfusion is represented as a ratio of perfusion in ischemic limb to non-ischemic limb (Figure 4.20 and 4.21). The results showed that eNOS treatment groups had 40-50% more perfusion than IL-10, ELP and control saline groups. Most of the saline injected animals showed severely necrotic limbs after 21 days, and ELP and hIL-10 alone showed a 10-15% of perfusion. The functional recovery of the ischemic limb after treatment was measured using external parameters like necrosis of the foot, discoloration of the skin and plantar flexion (Figure 4.22). Saline groups showed minimal functional recovery where out of seven animals, three animals showed severely necrotic limbs. The ELP, hIL-10 and heNOS alone treated groups showed minimal functional recovery compared to saline. Five out of seven ischemic mice showed functional recovery in the case of heNOS/hIL-10 treatment.

##### *4.3.5.1 Angiogenesis and Inflammation Levels in the Ischemic Tissue*

Skeletal muscle samples were cryofixed and sections 5 $\mu$ m were stained with H & E to measure blood vessel density. The blood vessel density was measured in terms of surface and length density (Figure 4.23 and 4.24). Day 7 results showed no significant difference between control saline and different treatment groups such as ELP alone, IL-10 (10  $\mu$ g), eNOS (20  $\mu$ g), and IL-10 (10  $\mu$ g)/eNOS (20  $\mu$ g). By day 21, eNOS and IL-10/eNOS treatment groups showed a 60% increase in the surface blood vessel density. A similar trend was seen in the case of length density measurement, where at day 21 eNOS and eNOS/IL-10 treatment groups showed a 50% increase in the blood length density compared to saline, ELP and IL-10 alone treatment groups.

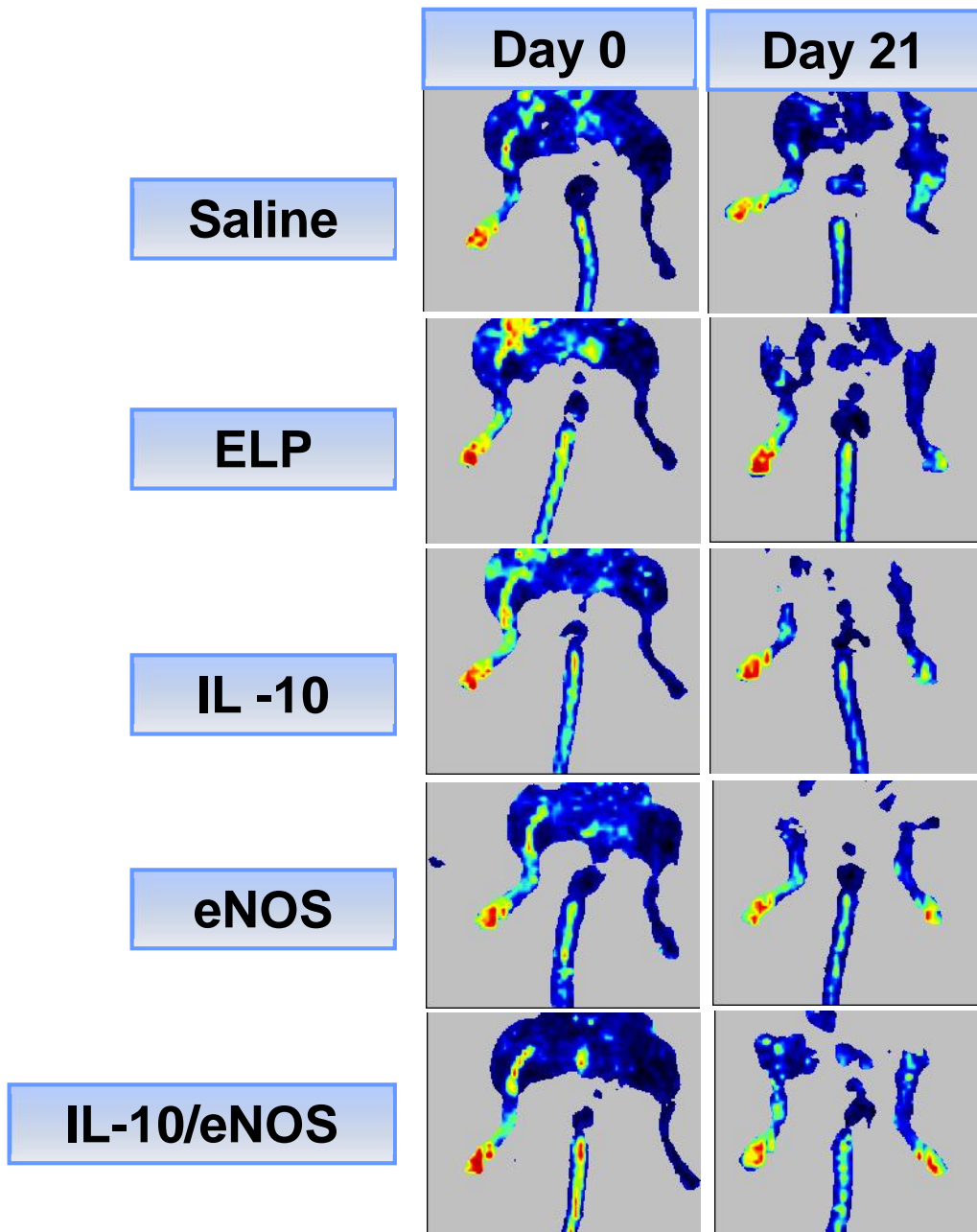


**Figure 4.20: Improvement of blood flow recovery at the ischemic site following eNOS treatment. Representative laser doppler perfusion imaging (LDPI) at week 0 (10 min after the ischemic surgery) and week 3 are shown. In these digital color-coded images, maximum perfusion values are in red, medium values in yellow to green and the lowest values in dark blue.**

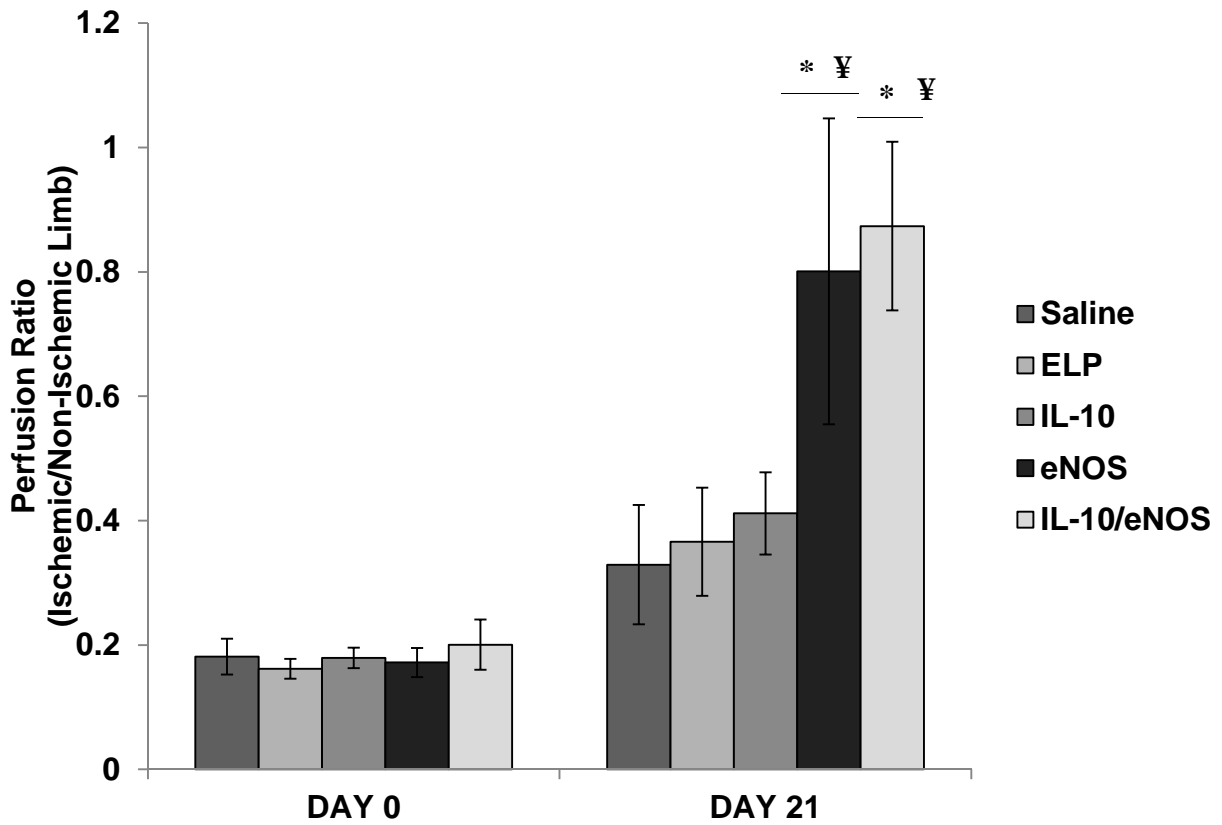


**Figure 4.19: Blood perfusion measurement of ischemic limb in mouse model. Elastin-like polypeptide scaffold only was kept as a control. Statistical significance by one way ANOVA ( $n = 7$ ,  $p < 0.05$ ). \* represents statistical significance of eNOS and IL-10/eNOS20 treatment groups from rest of the treatment groups.**

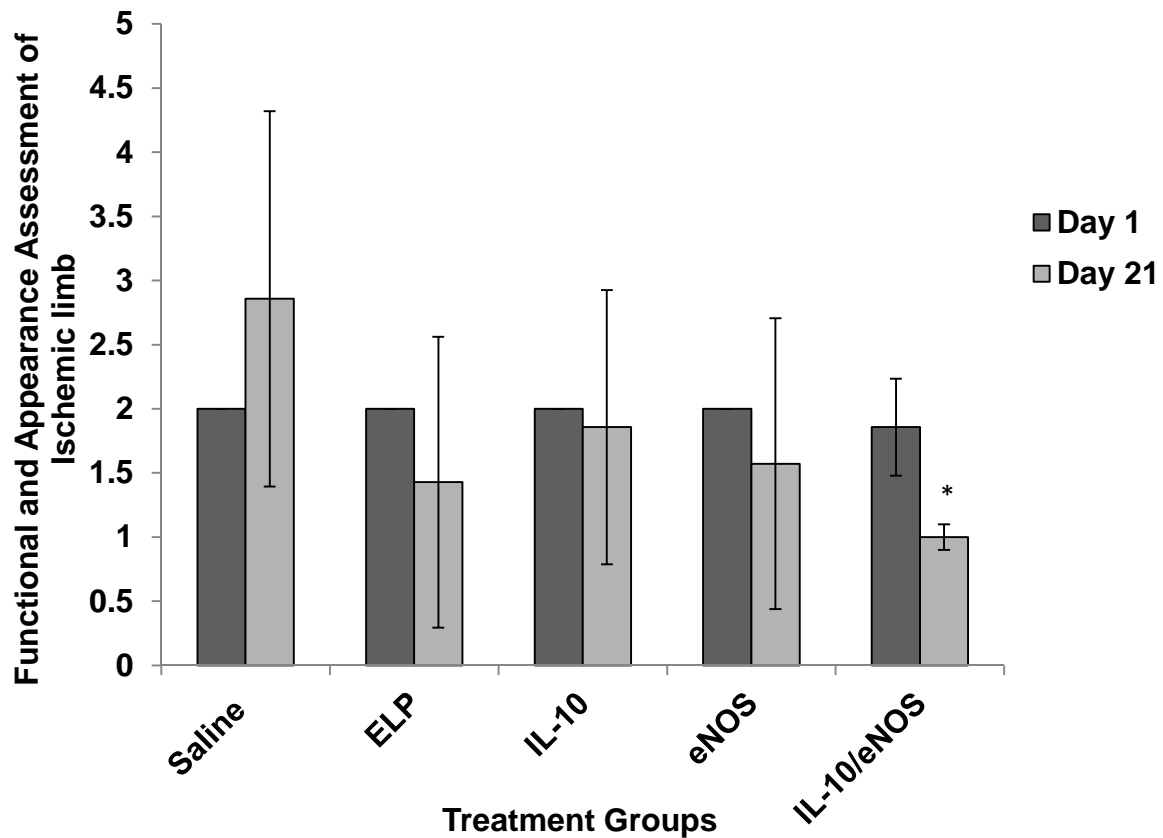


**Figure 4.22: Functional recovery assessment of ischemic mice. Elastin-like polypeptide scaffold only was kept as a control. Measurements were performed by observing parameters such as 1) plantar flexion but mild discoloration, 2) No plantar flexion and mild discoloration, 3) No plantar flexion and moderate to severe discoloration and 4) necrosis. Statistical significance by one way ANOVA ( $n = 7$ ,  $p < 0.05$ ). \* represents statistical significance IL-10/eNOS20 treatment groups from rest of the treatment groups.**

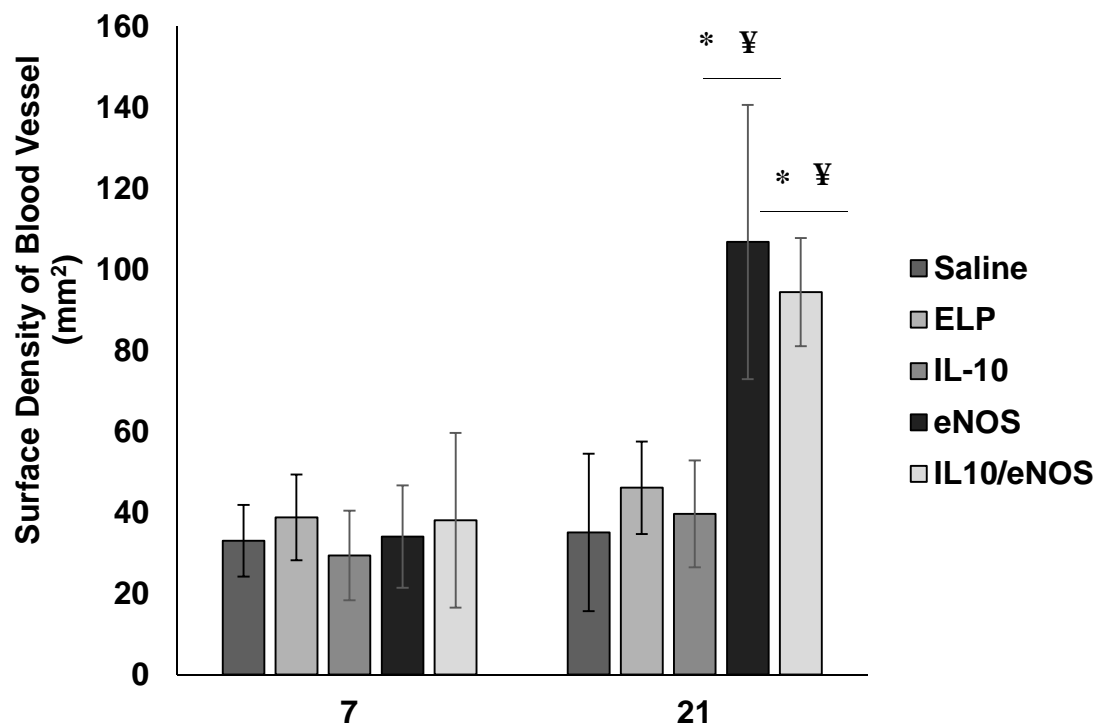


**Figure 4.20 :** Surface density of blood vessels in the ischemic tissue day 7 and 21. Five different doses of eNOS and IL-10 were implanted. Elastin-like polypeptide scaffold was used as a control. Statistical significance by one way ANOVA ( $n = 7$ ,  $p < 0.05$ ). \* represents statistical significant difference from the rest of the treatment groups at day 21. ¥ represents statistical significant difference between day 7 and 21.

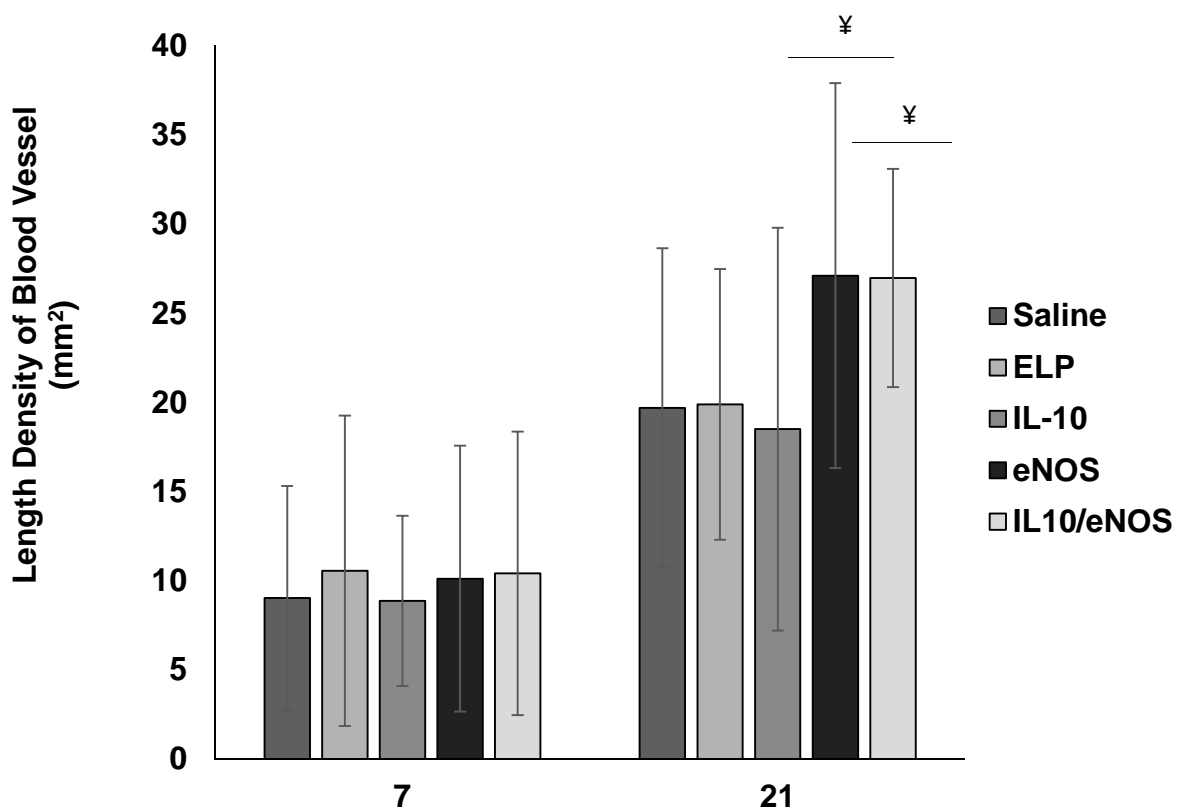


**Figure 4.21: Length density of blood vessels in the ischemic tissue at day 7 and 21. Five different doses of eNOS and IL-10 were implanted. Elastin-like polypeptide scaffold was used as a control. Statistical significance by one way ANOVA ( $n = 7$ ,  $p < 0.05$ ). ¥ represents statistical significant difference between day 7 and 21.**

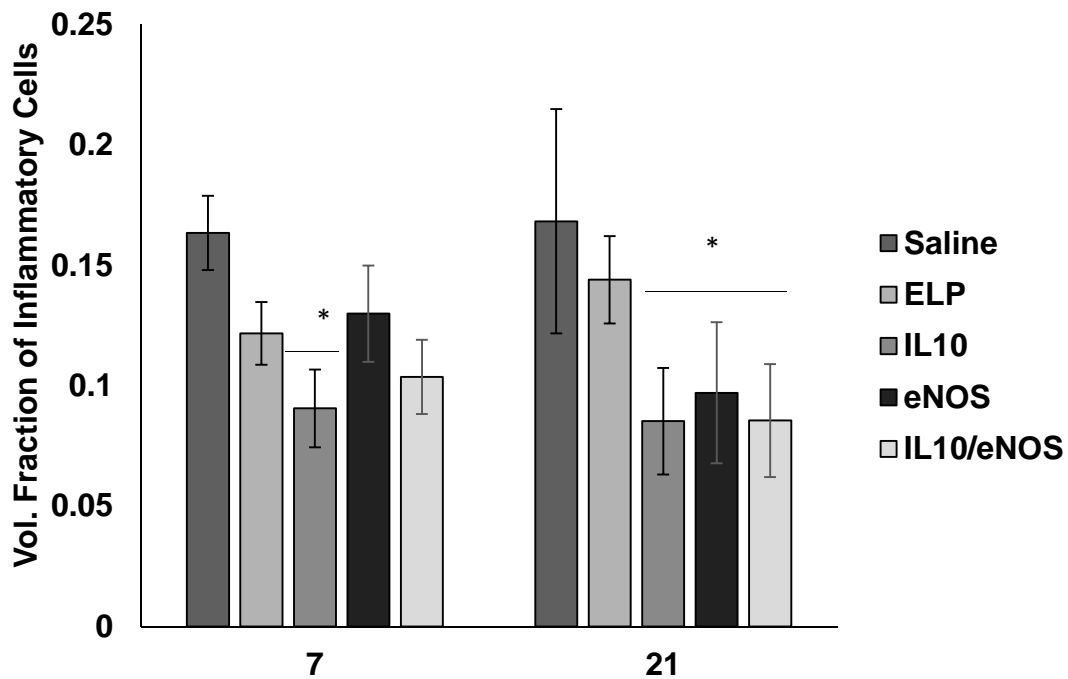


**Figure 4.22: Volume fraction of inflammatory cells in the ischemic tissue at day 7 and day 21. Five different doses of eNOS and IL-10 were implanted. Elastin-like polypeptide scaffold was used as a control. Statistical significance by one way ANOVA ( $n = 7$ ,  $p < 0.05$ ). \* represents statistical significance of IL-10 and IL-10/eNOS20 treatment groups from rest of the treatment groups.**

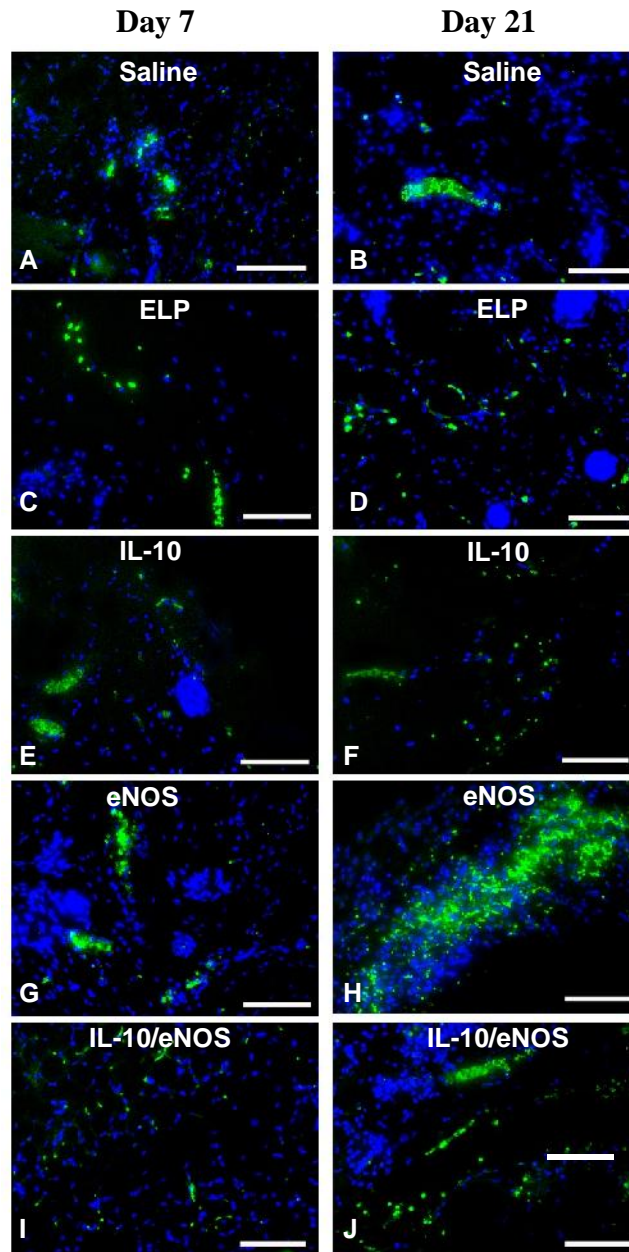


**Figure 4.23:** CD31 staining of blood vessels (stained as green cells) at day 7 and 21 in various treatments in the ischemic study. (A, B) Saline (C, D) ELP, (E, F) IL-10, (G, H) eNOS and (I, J) IL-10/eNOS. The scale bar represents 100  $\mu\text{m}$ .

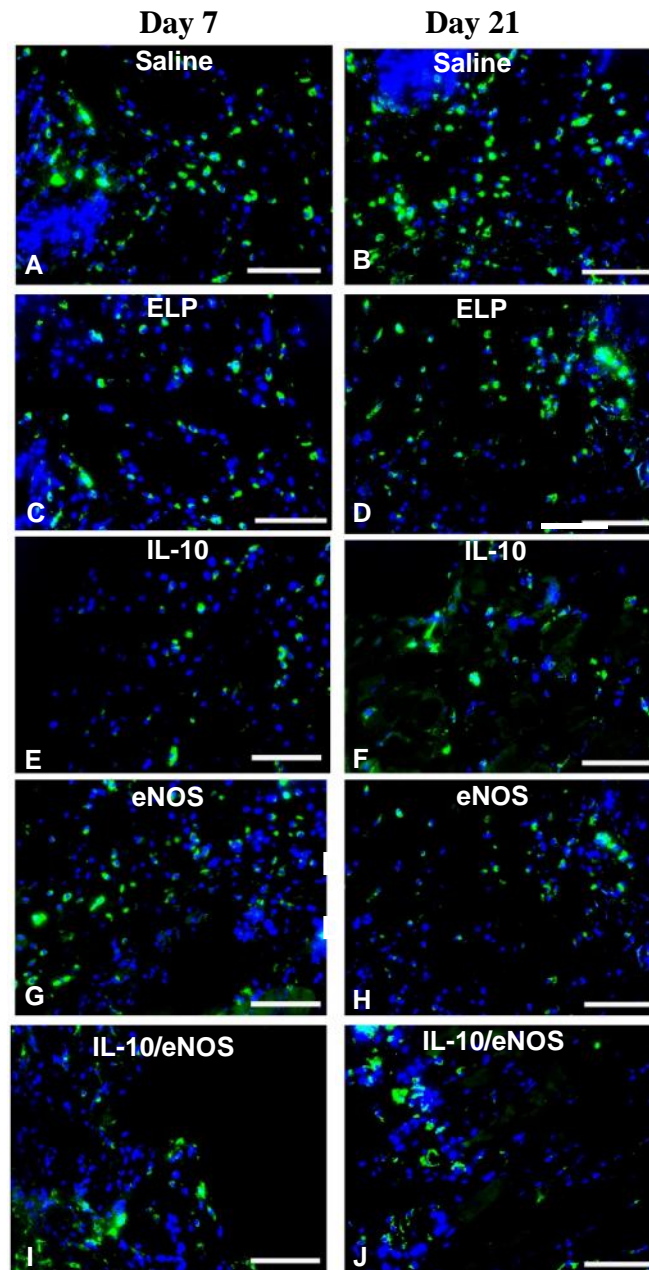


**Figure 4.24:** CD68 staining of macrophages (stained as green cells) at day 7 and 14 in various treatments in the ischemic study. (A, B) Saline (C, D) ELP, (E, F) IL-10, (G, H) eNOS and (I, J) IL-10/eNOS. The scale bar represents 100  $\mu\text{m}$ .

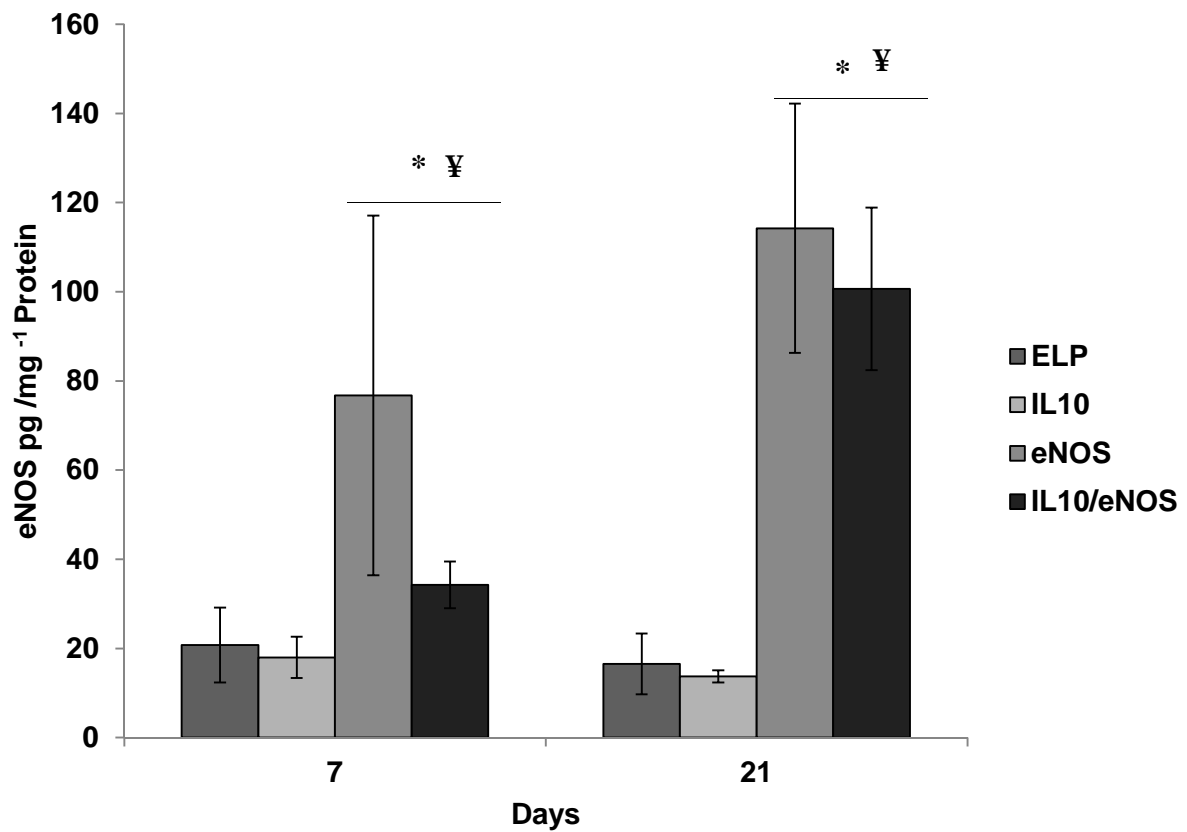


**Figure 4.25: Human eNOS expression in the ischemic tissue for day 7 and 21. Elastin-like polypeptide scaffold only was kept as a control. Statistical significance by one way ANOVA ( $n = 7$ ,  $p < 0.05$ ). \* represents statistical significance of eNOS and IL-10/eNOS treatment groups from Scaffold and IL-10 groups and ¥ represents significant difference between the day 7 and 21 expression of eNOS.**

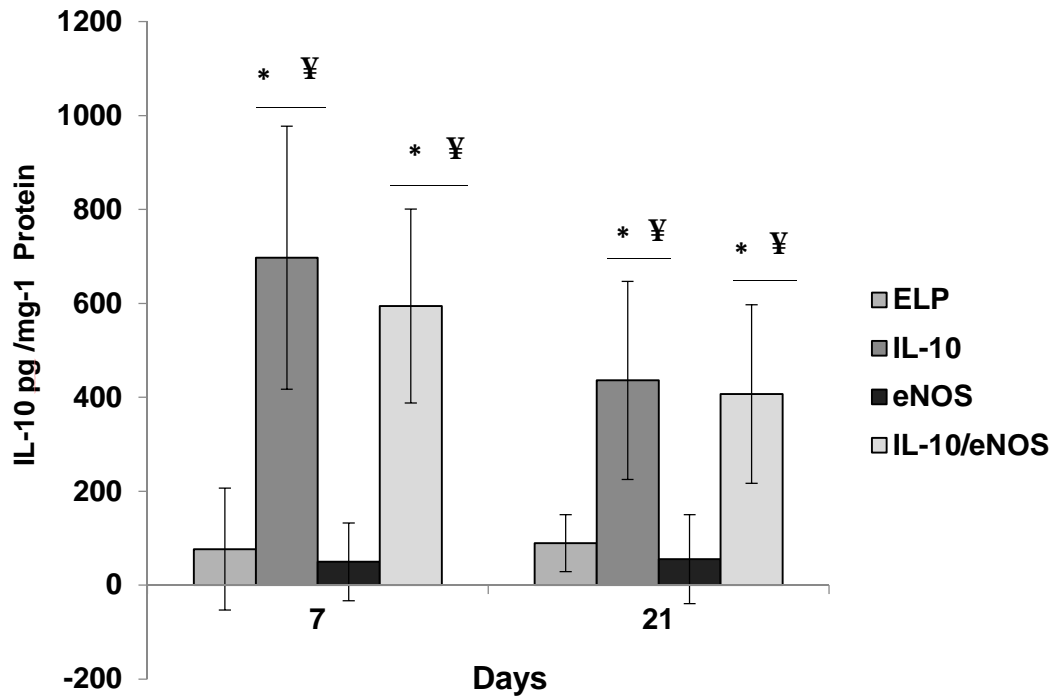


**Figure 4.26: Human IL-10 expression in the ischemic tissue for day 7 and 21. Elastin-like polypeptide scaffold only was kept as a control. Statistical significance by one way ANOVA ( $n = 7$ ,  $p < 0.05$ ). \* represents significant difference of IL-10 treatment groups than rest of the groups and ¥ represents significant difference between the day 7 and 21 expression of IL-10.**

The volume fraction of inflammatory cells reduced by 35% and 50% in the case of IL-10 treatment groups such as IL-10 (10  $\mu$ g) and IL-10 (10  $\mu$ g)/eNOS (20  $\mu$ g) than saline for both days 7 and day 21 respectively (Figure 4.25). Furthermore, on day 21 eNOS alone treatment showed 50% less inflammatory cells than saline and ELP alone. These results were further validated using immunofluorescence staining of endothelial cells by CD31 (Figure 4.26) and CD68 (Figure 4.27) for inflammatory cells. CD68 immunostaining data showed that overall macrophages are less for IL-10 treated groups for day 7 and 21. The endothelial cells staining by CD31 showed more blood vessel in the eNOS treated groups on day 21.

Human eNOS expression in the ischemic tissue was analysed for different treatment groups by ELISA (Figure 4.28). It was observed that eNOS treated groups such as IL-10 (10  $\mu$ g)/eNOS (20  $\mu$ g) and eNOS (20  $\mu$ g) significantly up-regulated expression of eNOS at day 7 and 21 compared to other groups. Also, at day 21 the expression level of eNOS for eNOS treated groups was seen to be significantly more than day 7 expression. A similar trend was found in the case of IL-10 expression where, IL-10 treatment groups such as IL-10 (10  $\mu$ g) and IL-10 (10  $\mu$ g)/eNOS (20  $\mu$ g) showed a significant up-regulation of IL-10 compared to other groups by day 7 and 21. And, expression level decreased significantly from day 7 to day 21 (Figure 4.29).

#### **4.3.6 RT-PCR Analysis**

RT-PCR was performed to analyze gene expression of major angiogenic and inflammatory factors. The expression of inflammatory markers IFN  $\gamma$ , IL-10, IL-4, IL-6, TNF  $\alpha$ , IL-2 and IL-1  $\beta$  was analyzed (Figure 4.31). IL-10/eNOS treatment group showed 2-6 folds higher up-regulation of IL-4 on day 21 from its earliest time point of day 7 (Figure 4.31). Also, IL-4 expression level was significantly higher in the case of IL-10/eNOS group when compared to ELP and IL-10 alone. Furthermore, IL-1  $\beta$  was found to be up regulated at day 7 and was significantly, 5-20 folds, more expressed than day 21 scaffolds, IL-10 and eNOS treatment groups.

On day 21, eNOS treatment groups showed upregulation of FGF1, PDGFB, VEGFA and VEGFB. eNOS alone treated group was found to have significantly, 10-18 folds, increased expression of FGF1 from that of IL-10/eNOS and 3-4 folds from IL-10 and ELP groups on day 21. Similarly, eNOS alone treated group was seen to have a significant increased expression of PDGFB from that of ELP and IL-10/eNOS groups at day 21 (Figure 4.30). And, in the case of VEGFA the upregulation at day 21 was significantly higher compared to ELP, IL-10 and eNOS/IL-10 treatment groups. Furthermore, VEGFB expression in the eNOS alone treatment significantly

increased, around 4-5 folds, more than ELP, 2 fold more than IL-10, and 5 fold more than that of eNOS/IL-10 groups.

Moreover, the factors that showed higher expression compared to day 7 expression level were Angpt1, FGF1, SerpinF1, VEGFA, VEGFB and PDGFB. Angpt1, an important proangiogenic factor was up-regulated significantly, by 2-3 folds, from day 7 to day 21 in eNOS and IL-10/eNOS treatment groups (Figure 4.30). Similarly, a significant 2 to 10 folds increase in expression level of SerpinF1 was seen from day 7 to day 21 for the eNOS treated groups such as eNOS and IL-10/eNOS (Figure 4.30). FGF1 was found to have a significantly increased expression level from day 7 to day 21 for eNOS and IL-10 treatments except for scaffold and eNOS/IL-10 treatment groups (Figure 4.30). Also, a significant increase in expression of PDGFB from day 7 to day 21 was seen in the eNOS alone group. Furthermore, VEGFA showed 2 to 12 folds significant up regulation by 21 days in all the groups except IL-10/eNOS group (Figure 4.30). Also, a significantly increased expression of VEGFB was seen from day 7 to day 21 for both IL-10 and eNOS alone treatment groups (Figure 4.30).

#### **4.3.7 Relation between Angiogenesis and Inflammation in a Subcutaneous Model**

The ratio of each parameter from day 14: day 7 for subcutaneous study and day 21: day 7 for hind limb ischemia study were calculated to represent the change in cellularity and vascularity over time. Pearson's correlations were obtained in order to assess whether the angiogenic and inflammatory parameters correlated with each other over time (Table 4.2 and 4.3). The significant correlation found was in the IL-10/eNOS group, where surface area increase is correlated with the increase in length of vessels in the subcutaneous tissue (Table 4.2). Furthermore, in the ischemic study a negative correlation was observed between expression of IL-10 and volume fraction of inflammatory cells in the ELP treatment group. And, a positive correlation was seen in between expression of IL-10 and length density in the IL-10 treatment group (Table 4.3).

#### **4.4 Discussion**

In this study, an injectable ELP delivery system was designed to deliver therapeutic genes IL-10 and eNOS. The aims of this study were to reduce the early onset of inflammation followed by stimulation of angiogenesis in the ischemic tissue. This approach necessitated a delivery vehicle which will spatio-temporally release two different genes. Previous studies have already reported the fabrication of ELP hollow spheres of various sizes and their use as a gene depot [28]. However, a screening of various sizes of ELP hollow spheres was performed by characterizing their

internalization pattern into endothelial cells and macrophages. These cells were chosen for the study as they are abundantly found in ischemic tissue [43, 44]. This screening was performed to find a suitable size ELP hollow sphere which can be used to load *pDNA* inside with minimal internalization into both endothelial cells and macrophages. The FACS study showed that ELP hollow spheres of 10  $\mu\text{m}$  were engulfed by both activated and non-activated macrophages compared to 1  $\mu\text{m}$ , 0.5 and 0.1  $\mu\text{m}$  ELP hollow spheres, while HUVECs internalized 0.1 and 0.5  $\mu\text{m}$  size spheres more than 1  $\mu\text{m}$  spheres. Thus considering the amount of *pDNA* that can be loaded within ELP hollow spheres without internalization by macrophages and endothelial cells, 1  $\mu\text{m}$  ELP hollow sphere was chosen to be the gene depot. The previous study performed on size and loading efficiency showed that there was no significant difference between various sizes of spheres for their *pDNA* loading efficiency. However, the larger the ELP hollow sphere, the more *pDNA* can be loaded for a spontaneous release of the *pDNA*.

An injectable scaffold was fabricated so that combining both ELP hollow spheres and injectable scaffold they can be used to deliver dual therapeutic genes IL-10 and eNOS. The biomaterial system used was an ELP scaffold which would be injectable and gel *in situ* without causing any cytotoxicity. In this study, the ELP injectable scaffold was fabricated by using mTGase, as the cross linker. MTGase is an enzyme of bacterial origin and catalyses the acyl transfer reaction between an  $\alpha$ -amino group of lysine residue and a  $\gamma$ -carboxamide group of glutamine residue by introducing covalent cross-links between proteins, peptides and various primary amines [37]. Additionally, its ease of production and  $\text{Ca}^{2+}$  independent activity make it more suitable than tissue TGase [37]. MTGase catalyzes the acyl transfer reaction between glutamine and lysine residues present in the cross-linking domains of ELP. The TNBSA assay showed a decrease in the amount of free amino groups in the mTGase and GTA cross-linked groups. The amount of free amino groups available after cross-linking was reduced greatly after cross-linking with GTA compared to that of mTGase. This further explains the role mTGase as a mild cross-linker leaving free amino groups in the scaffold. These free amino groups help the scaffold to hold negatively charged *pDNA* or neutrally charged polyplexes with the help of an electrostatic interaction and thus were released only by treating with enzyme like elastase. Free amino groups played an important role in binding *pDNA* complexes which are released only under the action of protease and elastase enzymes [28]. The release data showed that the dual delivery system released *pDNA* with the treatment of elastase which is abundant in the ischemia area [45].

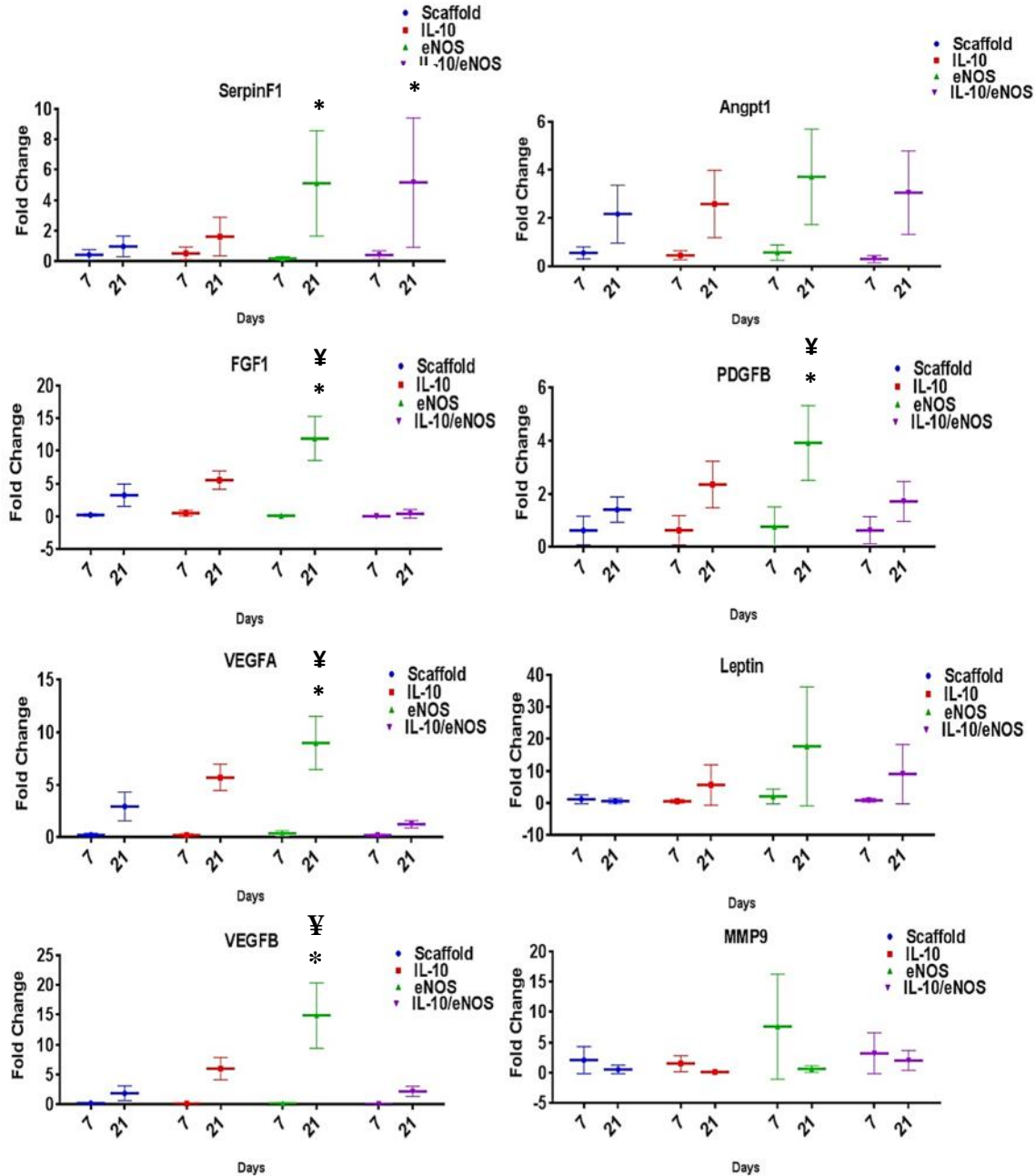


**Figure 4.30: RT-PCR data showing differential regulation of angiogenic factors with respect to treatment groups ELN, IL-10, eNOS and IL-10/eNOS in the ischemic tissue on day 7 and 21. The differential regulation angiogenic factors studied are: angiopoietin 1, serpinF1, fibroblast growth factor 1, platelet derived growth factor B, vascular endothelial cell growth factors A and B, leptin and matrix metalloproteinase protein 9. Statistical significance was determined by one way ANOVA (n = 3, p < 0.05).\* represents a significant difference in the upregulation of a factor on day 21 compared to its early time point day 7. ¥ represents a significant difference in the upregulation of a factor on day 21 compared rest of the treatment groups.**

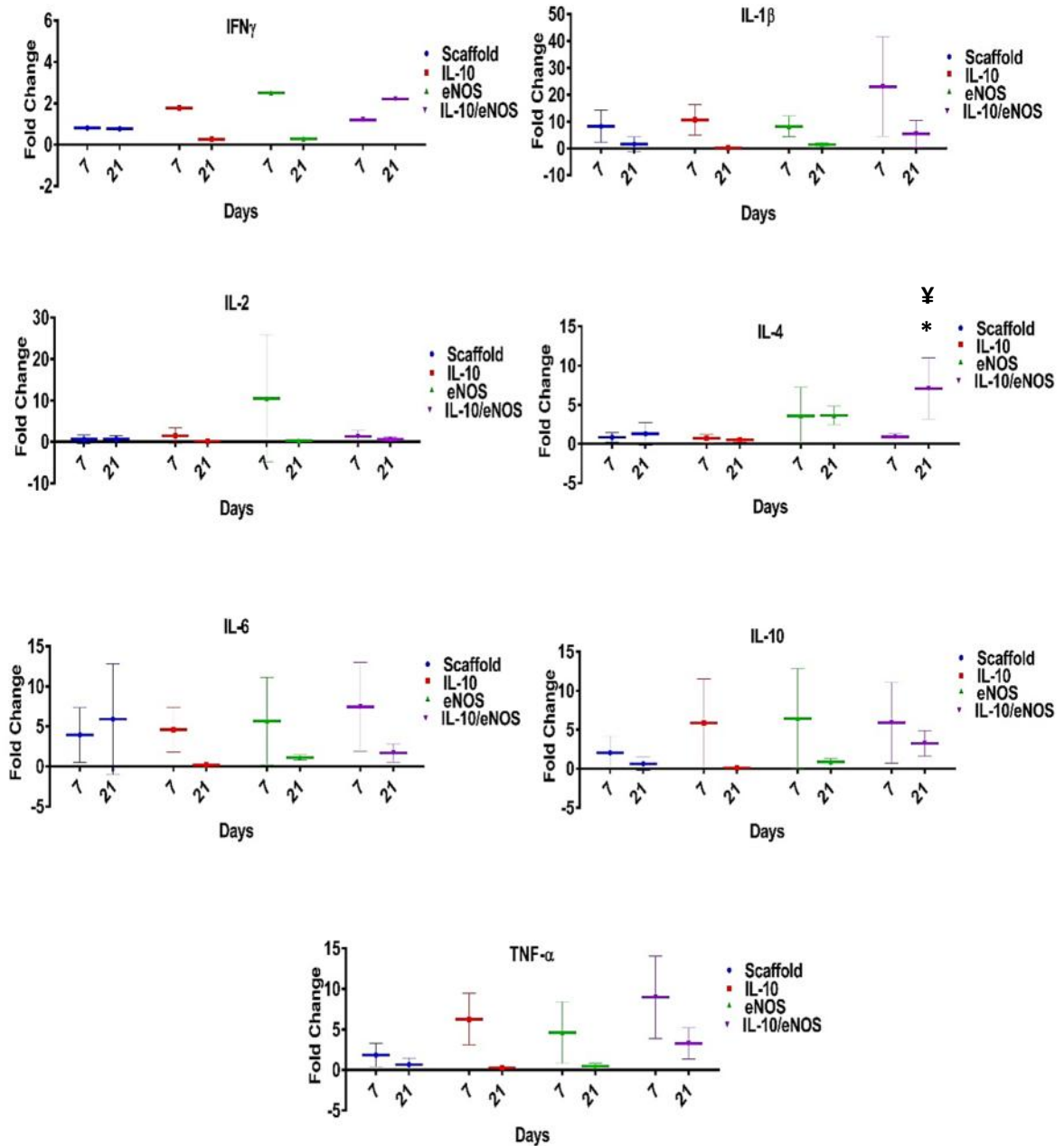


**Figure 4.31: RT-PCR data showing differential regulation of inflammatory factors with respect to treatment groups ELP, IL-10, eNOS and IL-10/eNOS in the ischemic tissue on day 7 and 21. The differential regulation inflammatory factors studied are: Interleukin-1 $\beta$ , -2, -4, -6 and -10, tissue necrosis factor- $\alpha$  and interferon  $\gamma$ . Statistical significance was determined by one way ANOVA (n = 3, p < 0.05). \* represents a significant difference in the upregulation of a factor on day 21 compared to its early time point day 7. ¥ represents a significant difference in the upregulation of a factor on day 21 compared rest of the treatment groups.**

| IL-10/eNOS |       |       |       |       | eNOS |       |       |       |       |
|------------|-------|-------|-------|-------|------|-------|-------|-------|-------|
|            | I     | L     | eNOS  | IL-10 |      | I     | L     | eNOS  | IL-10 |
| SD         | -0.88 | 0.97* | -0.98 | 0.79  | SD   | -0.23 | -0.44 | -0.68 | -0.52 |
| I          |       | -0.88 | 0.94  | -0.41 | I    |       | -0.49 | -0.29 | 0.57  |
| L          |       |       | -0.98 | 0.79  | L    |       |       | 0.22  | -0.52 |
| eNOS       |       |       |       | -0.68 | eNOS |       |       |       | 0.54  |
| IL-10      |       |       |       |       | ELP  |       |       |       |       |
| SD         | 0.31  | 0.89  | 0.95* | -0.47 | SD   | 0.45  | 0.75  | -0.44 | 0.40  |
| I          |       | 0.05  | 0.15  | -0.84 | I    |       | 0.89  | 0.33  | -0.54 |
| L          |       |       | 0.98* | -0.06 | L    |       |       | 0.17  | -0.28 |
| eNOS       |       |       |       | -0.22 | eNOS |       |       |       | -0.94 |

**Table 4.2: Pearson's correlations' values between angiogenic and inflammatory parameters as a function of time in the subcutaneous implant study. I=change in inflammatory cells, L= change in length density of vessels, eNOS= change in eNOS expression, SD= change in surface of vessels density, IL-10= change in IL-10 expression, all between 7 and 14 days. \* indicates significance ( $P < 0.05$ ).**

| IL-10/eNOS |       |       |       |       | eNOS |       |       |       |        |
|------------|-------|-------|-------|-------|------|-------|-------|-------|--------|
|            | I     | L     | eNOS  | IL-10 |      | I     | L     | eNOS  | IL-10  |
| SD         | -0.55 | 0.36  | -0.86 | 0.008 | SD   | -0.10 | -0.92 | -0.54 | 0.77   |
| I          |       | -0.52 | 0.13  | 0.82  | I    |       | -0.60 | -0.72 | -0.15  |
| L          |       |       | 0.10  | -0.37 | L    |       |       | 0.75  | -0.23  |
| eNOS       |       |       |       | -0.41 | eNOS |       |       |       | 0.44   |
| IL-10      |       |       |       |       | ELP  |       |       |       |        |
| SD         | -0.74 | -0.70 | 0.23  | -0.69 | SD   | -0.90 | -0.90 | -0.59 | 0.90   |
| I          |       | 0.50  | -0.81 | -0.34 | I    |       | 0.71  | 0.47  | -0.95* |
| L          |       |       | 0.31  | 0.97* | L    |       |       | 0.31  | -0.83  |
| eNOS       |       |       |       | -0.09 | eNOS |       |       |       | -0.26  |

**Table 4.3: Pearson's correlations' values between angiogenic and inflammatory parameters as a function of time in the hind limb ischemic tissue study. I=change in inflammatory cells, L= change in length density of vessels, eNOS= change in eNOS expression, SD= change in surface density of vessels, IL-10= change in IL-10 expression, all between 7 and 21 days. \* indicates significance (P < 0.05).**

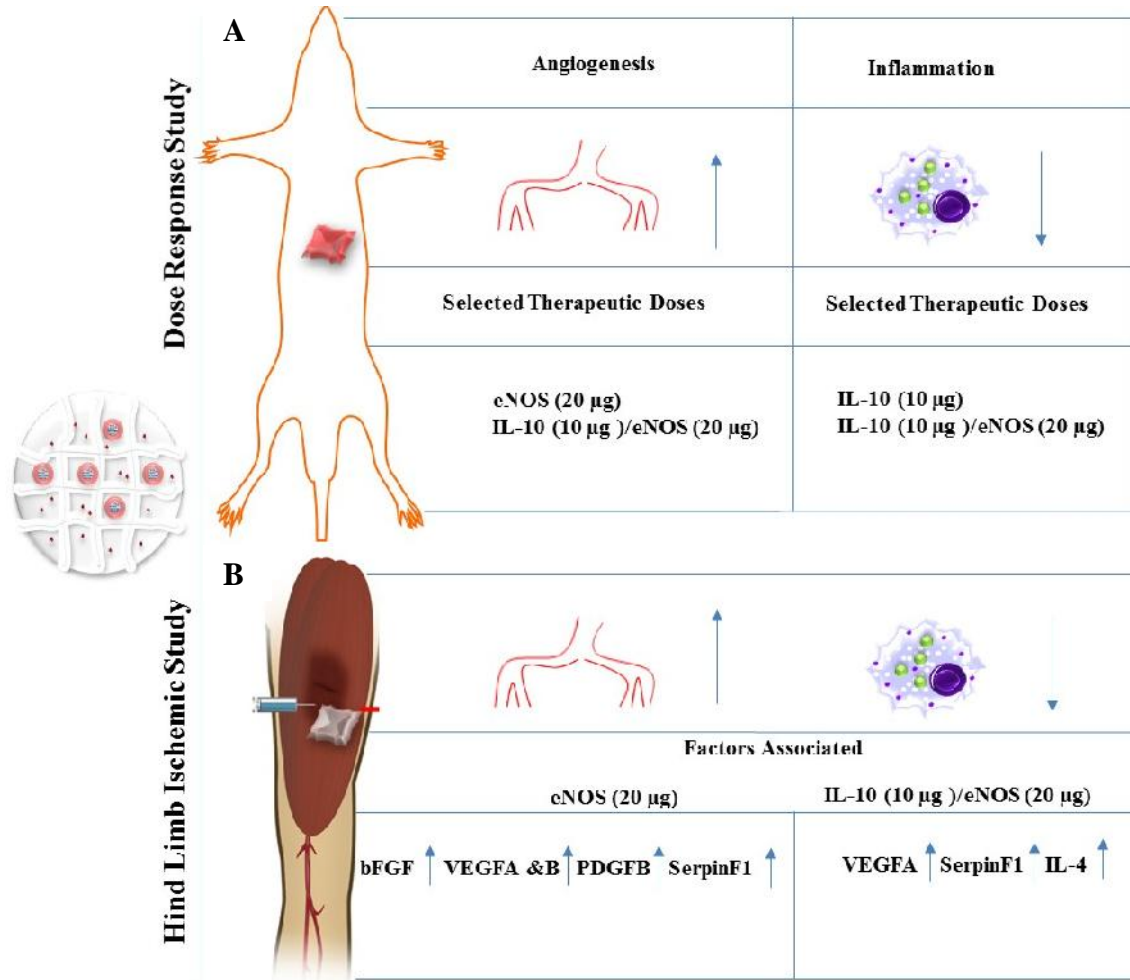


**Figure 4.27:** The schematic summarizes (A) dose response study to determine therapeutic doses of eNOS and IL-10 to enhance angiogenesis and modulate inflammation and (B) the therapeutic goal (in terms of changes in the angiogenesis and inflammation level in the ischemic tissue) achieved by the treatment group eNOS and IL-10/eNOS and the key factors associated with these changes at a molecular level.

Also, *pDNA* was released faster from the scaffold than from ELP hollow spheres. Thus, this system as designed was able to load two different genes at the same time and deliver them spatio-temporally.

To further validate the use of the ELP injectable system *in vivo* and to determine a therapeutic dose of eNOS and IL-10, a subcutaneous study was performed in the mouse model. ELISA data showed higher expression of heNOS and hIL-10. Day 7 showed more hIL-10 expression and it decreased at day 14. In contrast, heNOS expression increased by day 14, while at day 7 there was reduced expression compared to day 14. The pattern of expression of heNOS and hIL-10 can be correlated to the *in vitro* release and the *in vivo* degradation profile of the ELP injectable system. In the ELP injectable system hIL-10 *pDNA* was loaded inside the scaffold and heNOS *pDNA* inside the ELP hollow spheres and thus with the initial degradation of the scaffold, IL-10 was released earlier than eNOS. This leads to the higher expression of IL-10 by day 7 while for eNOS the highest expression was by day 21. A highest dose of 20  $\mu\text{g}$  and lowest of 10  $\mu\text{g}$  was chosen for both the *pDNA* to perform the dose study. Combinations of both the genes including all the doses were used to do the dosage study.

In total, nine samples were implanted subcutaneously on the back of the mice. The histology data for angiogenesis and inflammation was in accordance with the hIL-10 and heNOS expression data. By day 14 there was a difference between different groups with and without heNOS in the amount of vessel and length density. On the other hand, by day 7 a reduction in the volume of inflammatory cells can be noticed with IL-10 treatment groups as the IL-10 released from the scaffold reduces the minor inflammation caused by implantation. However, by day 14 there was no big difference in the level of inflammatory cells between all the groups. The reason might be that the subcutaneous mouse model used here in this study is not a perfect model to study inflammation for longer period. The angiogenesis data obtained from the stereology showed that eNOS treatment groups such as eNOS (20  $\mu\text{g}$ ) and IL-10 (10  $\mu\text{g}$ )/eNOS (20  $\mu\text{g}$ ) indicated comparatively more blood vessel density than eNOS in combination with a bigger dose of IL-10 such as IL-10 (20  $\mu\text{g}$ )/eNOS (20  $\mu\text{g}$ ) and IL-10 (20  $\mu\text{g}$ )/eNOS (10  $\mu\text{g}$ ). This might be due to inhibitory effect of IL-10 on angiogenesis [46], when used at a higher dose as seen here. The eNOS at a dose of 20  $\mu\text{g}$  showed higher surface and length density of blood vessels and in a combination with IL-10  $\mu\text{g}$  reduced the inflammation level without inhibiting angiogenesis. Thus, the treatment group IL-10 (10  $\mu\text{g}$ )/eNOS (20  $\mu\text{g}$ ) was chosen for the ischemic study. Moreover, blood vessel surface density

was found to have a correlation with the length density in the IL-10/eNOS treatment group. The correlation study showed an increase in surface density and length density with an increase in eNOS expression.

The immunostaining for CD68 and CD31 were in accordance with the histology data for macrophages and vessel density data respectively. The CD68, a universal marker for a wide array of macrophages, was found to be reduced with the treatment of IL-10 and so eNOS treated showed more blood vessel density stained with CD31. The dose study further assessed the combined effect of IL-10 and eNOS. The IL-10/eNOS treatment groups showed an apparent decrease in the level of inflammatory cells by day 7 and an increase in blood vessel density by day 14. But with an increase in dose of the IL-10 the level of blood vessel density decreased. This inhibitory effect on angiogenesis might be because of the anti-angiogenic activity of IL-10.

Ischemic study was performed using mouse model of unilateral ischemia. There were five groups: saline, eNOS (20  $\mu$ g), IL-10 (10  $\mu$ g), eNOS (20  $\mu$ g)/IL-10 (10  $\mu$ g) and ELP alone. The treatment groups that showed higher blood perfusion measured using LDPI were groups with eNOS. Saline showed a higher amputation rate. And ELP and IL-10 (10  $\mu$ g) showed minimal blood perfusion. The histological data was in accordance with the LDPI as surface and length density of blood vessels were significantly higher in the case of eNOS treated samples. The correlation study showed a decrease in inflammation with an increase in IL-10 expression in one of the treatment group. This was further proven by immunostaining with CD31. ELISA test for heNOS showed similar pattern as seen in the case of subcutaneous dose study. Human eNOS was expressed significantly by day 21 and thus a higher blood perfusion was seen by three weeks' time. eNOS treatment groups enhanced protein expression of eNOS much more than its endogenous level (< 50 ng/mg of protein) in skeletal muscle [47, 48]. Also, the expression level of eNOS was very similar to that observed in lipoplex mediated eNOS delivery. Similarly, IL-10 treatment groups enhanced the level IL-10 protein expression in the skeletal muscle and was significantly higher compared to that of Superfect<sup>TM</sup> only (< 100 pg/mg of protein) [49]. eNOS is a major proangiogenic factor and induces angiogenesis by mobilization of vascular endothelial cell and endothelial progenitor cells. eNOS produces NO, which acts as a signaling molecule in the angiogenic pathway. On the other hand, IL-10 acts on proinflammatory cytokines and macrophages to reduce the inflammation level in the ischemic tissue. IL-10 containing treatment groups significantly reduced the amount of inflammatory cells as per the stereological analysis of

the H&E sections. This was further proven by CD68 immunostaining of macrophages. The ELISA data showed earlier release of IL-10 and thus a significant reduction in the amount of inflammatory cells was seen in the IL-10 treatment groups. IL-10 in combination with eNOS showed increased vascularization of the ischemic tissue with reduced inflammation by three week.

Furthermore, a mechanistic study was performed to understand the cross-talk of IL-10 and eNOS in the ischemic muscle with respect to inflammation and angiogenesis. Ischemic angiogenesis, as mentioned, is regulated by several angiogenic factors, the major factors being: VEGF, PDGFB and bFGF and angiopoietin 1 [16-18, 50]. eNOS treatment group induced up-regulation of VEGFA and B, potent angiogenic cytokines which also increases vascular permeability with the help of nitric oxide. But eNOS treatment groups also showed an increase in Ang-1 expression, which helps in the formation of stable vessel as Ang-1 protects blood vessels from increased plasma leakage, which contributes to their stabilization. Furthermore, eNOS treatment groups also showed an increasing level of serpinF1, an anti-angiogenic factor. SerpinF1 is known to inhibit the migration and proliferation of endothelial cells induced by VEGF [51], and then further inhibits angiogenesis by interacting with specific cell surface receptors. This anti-angiogenic activity of serpinF1 is critical for the regulation of angiogenesis. Another major proangiogenic factors upregulated with the treatment of eNOS is PDGFB. PDGFB helps in stabilization of newly formed blood vessels [52, 53]. eNOS thus upregulates major proangiogenic factors such as bFGF, VEGF(A and B) and PDGFB to induce angiogenesis. It is known that a short exposure of PDGFB and FGF-2 in the ischemic tissue would be sufficient to establish stable and functional vessels [54]. This shows the role of eNOS in establishing a stable and functional vascular network through upregulation of bFGF and PDGFB. Also, what can be noticed is a decrease in the expression of these specific growth factors in the presence of IL-10 thus suggesting an inhibitory effect of IL-10 on angiogenesis. ELP scaffold itself helps in upregulation of these major growth factors but the effect is less than that with eNOS alone. Ischemia leads to damage of the local tissue and thus is a site for inflammation. The major proinflammatory cytokines are: IFN , TNF and IL-6 [14]. These were seen to be downregulated by 21 days in the IL-10 treatment groups but with no significant difference compared to other groups. Factors such as IL-6 and TNF are considered to be proangiogenic factors as they enhance the angiogenesis level in ischemic condition [55-57]. No significant effect of IL-10 alone was found on IL-4 factor, whereas IL-10/eNOS treatment group showed an enhanced level of IL-4, anti-inflammatory cytokine. So far several studies have

proposed that maintaining a balance between the pro and anti-angiogenic factors is critical for the regulation of angiogenesis [58-60]. Thus use of a combination of eNOS and IL-10 can provide a balance in angiogenesis by inducing a differential expression of proangiogenic and antiangiogenic factors in the ischemic tissue. The results have been briefly summarized in the figure 4.32.

### **4.5 Conclusions**

In summary, this study reported the fabrication of an injectable ELP based system to deliver IL-10 and eNOS in a spatio-temporal manner. The injectable system was assembled by using ELP hollow spheres and injectable ELP scaffold as two separate gene delivery depot. The results showed that 1  $\mu\text{m}$  ELP hollow spheres when used as a depot are less internalized in to the cells predominantly found in an ischemic tissue such as: endothelial cells and macrophages. The delivery system showed a spatio-temporal release of two different genes. A dose of eNOS (20  $\mu\text{g}$ ) and IL-10 (10  $\mu\text{g}$ ) reduced inflammation level and increased angiogenesis in both subcutaneous and ischemic mouse model. The dosage study also showed an inhibitory effect of IL-10 on angiogenesis especially when a high dose of 20  $\mu\text{g}$  was used. RT-PCR study showed that eNOS induced major proangiogenic factors by week one and three and helped in vascularisation of the ischemic tissue. And along with IL-10, it reduces the early onset of inflammation level by inhibiting major proinflammatory cytokines. Although use of IL-10 reduced the angiogenic potential of ischemic tissue, later on this was compensated by eNOS induced upregulation of proangiogenic factors.

Overall, the study was designed to show a holistic approach towards the treatment of ischemic condition rather than focussing only on angiogenesis and to understand an underlying mechanism between inflammation and angiogenesis by using eNOS and IL-10. The study showed the importance of a dose study before any gene therapy. This study opens up more opportunities to do further preclinical studies in larger animals before moving to clinical trials. Additionally, the ELP-based injectable system shows its potential to be used in any disease model for gene delivery.

#### 4.6 References

- [1] Ouriel K. Peripheral arterial disease. *Lancet*. 2001;358:1257-64.
- [2] Tulsyan N, Ouriel K, Kashyap VS. Emerging drugs in peripheral arterial disease. *Exper Opin. Emerging Drugs*. 2006;11:75-90.
- [3] Lumsden AB, Davies MG, Peden EK. Medical and endovascular management of critical limb ischemia. *J Endovasc Ther*. 2009;16:II31-62.
- [4] Mangiafico RA, Mangiafico M. Medical treatment of critical limb ischemia: current state and future directions. *Curr Vasc Pharmacol*. 2011;9:658-76.
- [5] Slovut DP, Sullivan TM. Critical limb ischemia: medical and surgical management. *Vasc Med*. 2008;13:281-91.
- [6] Lavu M, Gundewar S, Lefer DJ. Gene therapy for ischemic heart disease. *J Mol Cell Cardiol*. 2011;50:742-50.
- [7] Eliason JL, Wakefield TW. Metabolic consequences of acute limb ischemia and their clinical implications. *Sem Vasc Surg*. 2009;22:29-33.
- [8] Boutin AT, Weidemann A, Fu Z, Mesropian L, Gradin K, Jamora C. Epidermal sensing of oxygen is essential for systemic hypoxic response. *Cell*. 2008;133:223-34.
- [9] Cao Y. Monotherapy versus combination therapy of angiogenic and arteriogenic factors for the treatment of ischemic disorders. *Curr Mol Med*. 2009;9:967-72.
- [10] Cao Y, Hong A, Schulten H, Post MJ. Update on therapeutic neovascularization. *Cardiovasc Res*. 2005;65:639-48.
- [11] Makino Y, Cao R, Svensson K, Bertilsson G, Asman M, Tanaka H. Inhibitory PAS domain protein is a negative regulator of hypoxia-inducible gene expression. *Nature*. 2001;414:550-4.
- [12] Lendahl U, Lee KL, Yang H, Poellinger L. Generating specificity and diversity in the transcriptional response to hypoxia. *Nat Rev Genet*. 2009;10:821-32.
- [13] Swain MG, Appleyard CB, Wallace JL, Maric M. TNF-alpha facilitates inflammation-induced glucocorticoid secretion in rats with biliary obstruction. *J hepatol*. 1997;26:361-8.
- [14] Khawaja FJ, Kullo IJ. Novel markers of peripheral arterial disease. *Vasc Med*. 2009;14:381-92.
- [15] Moore KW, de Waal Malefyt R, Coffman RL, O'Garra A. Interleukin-10 and the interleukin-10 receptor. *Annu Rev Immunol*. 2001;19:683-765.

- [16] Cao Y. Molecular mechanisms and therapeutic development of angiogenesis inhibitors. *Adv Cancer Res.* 2008;100:113-31.
- [17] Cao Y. Positive and negative modulation of angiogenesis by VEGFR1 ligands. *Science signaling.* 2009;2:re1.
- [18] Cao Y. Angiogenesis: What can it offer for future medicine? *Exp Cell Res.* 2010;316:1304-8.
- [19] Shimamura M, Nakagami H, Taniyama Y, Morishita R. Gene therapy for peripheral arterial disease. *Expert Opin Biol Ther.* 2014;14:1175-84.
- [20] Shimamura M, Nakagami H, Koriyama H, Morishita R. Gene therapy and cell-based therapies for therapeutic angiogenesis in peripheral artery disease. *BioMed Res Int.* 2013;2013:186215.
- [21] O'Connor DM, O'Brien T. Nitric oxide synthase gene therapy: progress and prospects. *Expert Opin Biol Ther.* 2009;9:867-78.
- [22] Fiorentino DF, Bond MW, Mosmann TR. Two types of mouse T helper cell. IV. Th2 clones secrete a factor that inhibits cytokine production by Th1 clones. *J Exp Med.* 1989;170:2081-95.
- [23] Couper KN, Blount DG, Riley EM. IL-10: the master regulator of immunity to infection. *J Immunol.* 2008;180:5771-7.
- [24] Crystal RG. Transfer of genes to humans: early lessons and obstacles to success. *Science.* 1995;270:404-10.
- [25] Thomas CE, Ehrhardt A, Kay MA. Progress and problems with the use of viral vectors for gene therapy. *Nat Rev Genet.* 2003;4:346-58.
- [26] Lee H, Jeong JH, Park TG. PEG grafted polylysine with fusogenic peptide for gene delivery: high transfection efficiency with low cytotoxicity. *J Control Release.* 2002;79:283-91.
- [27] Felgner PL, Gadek TR, Holm M, Roman R, Chan HW, Wenz M. Lipofection: a highly efficient, lipid-mediated DNA-transfection procedure. *Proc Natl Acad Sci U S A.* 1987;84:7413-7.
- [28] Dash BC, Mahor S, Carroll O, Mathew A, Wang W, Woodhouse KA, Pandit A. Tunable elastin-like polypeptide hollow sphere as a high payload and controlled delivery gene depot. *J Control Release.* 2011;152:382-92.
- [29] Chiellini F, Piras AM, Errico C, Chiellini E. Micro/nanostructured polymeric systems for biomedical and pharmaceutical applications. *Nanomed (Lond).* 2008;3:367-93.

- [30] Kwon GS, Okano T. Soluble self-assembled block copolymers for drug delivery. *Pharm Res.* 1999;16:597-600.
- [31] Kim W, Chaikof EL. Recombinant elastin-mimetic biomaterials: Emerging applications in medicine. *Adv Drug Deliv Rev.* 2010;62:1468-78.
- [32] Chilkoti A, Christensen T, MacKay JA. Stimulus responsive elastin biopolymers: Applications in medicine and biotechnology. *Curr Opin Chem Biol.* 2006;10:652-7.
- [33] Nettles DL, Chilkoti A, Setton LA. Applications of elastin-like polypeptides in tissue engineering. *Adv Drug Deliv Rev.* 2010;62:1479-85.
- [34] Almine JF, Bax DV, Mithieux SM, Nivison-Smith L, Rnjak J, Waterhouse A. Elastin-based materials. *Chem Soc Rev.* 2010;39:3371-9.
- [35] Kataoka K, Harada A, Nagasaki Y. Block copolymer micelles for drug delivery: design, characterization and biological significance. *Adv Drug Deliv Rev.* 2001;47:113-31.
- [36] Bellingham CM, Woodhouse KA, Robson P, Rothstein SJ, Keeley FW. Self-aggregation characteristics of recombinantly expressed human elastin polypeptides. *Biochim Biophys Acta.* 2001;1550:6-19.
- [37] Zhu Y, Tramper J. Novel applications for microbial transglutaminase beyond food processing. *Trends Biotechnol.* 2008;26:559-65.
- [38] Rethore G, Pandit A. Use of templates to fabricate nanoscale spherical structures for defined architectural control. *Small.* 2010;6:488-98.
- [39] Rethore G, Mathew A, Naik H, Pandit A. Preparation of chitosan/polyglutamic acid spheres based on the use of polystyrene template as a nonviral gene carrier. *Tissue Eng Part C.* 2009; 15: 605-13.
- [40] Dash BC, Rethore G, Monaghan M, Fitzgerald K, Gallagher W, Pandit A. The influence of size and charge of chitosan/polyglutamic acid hollow spheres on cellular internalization, viability and blood compatibility. *Biomaterials.* 2010;31:8188-97.
- [41] Bubnis WA, Ofner CM, 3rd. The determination of epsilon-amino groups in soluble and poorly soluble proteinaceous materials by a spectrophotometric method using trinitrobenzenesulfonic acid. *Anal Biochem.* 1992;207:129-33.
- [42] Garcia Y, Breen A, Burugapalli K, Dockery P, Pandit A. Stereological methods to assess tissue response for tissue-engineered scaffolds. *Biomaterials.* 2007;28:175-86.

- [43] Dai Q, Thompson MA, Phippen AM, Cherwek H, Taylor DA, Annex BH. Alterations in endothelial cell proliferation and apoptosis contribute to vascular remodeling following hind-limb ischemia in rabbits. *Vasc Med* 2002;7:87-91.
- [44] Brechot N, Gomez E, Bignon M, Khallou-Laschet J, Dussiot M, Cazes A. Modulation of macrophage activation state protects tissue from necrosis during critical limb ischemia in thrombospondin-1-deficient mice. *PloS One*. 2008;3:e3950.
- [45] Dinerman JL, Mehta JL, Saldeen TG, Emerson S, Wallin R, Davda R. Increased neutrophil elastase release in unstable angina pectoris and acute myocardial infarction. *J Am Coll Cardiol*. 1990;15:1559-63.
- [46] Silvestre JS, Mallat Z, Duriez M, Tamarat R, Bureau MF, Scherman D. Antiangiogenic effect of interleukin-10 in ischemia-induced angiogenesis in mice hindlimb. *Circ Res*. 2000;87:448-52.
- [47] Brito LA, Chandrasekhar S, Little SR, Amiji MM. Non-viral eNOS gene delivery and transfection with stents for the treatment of restenosis. *Biomed Eng*. 2010;9:56.
- [48] Montes de Oca M, Torres SH, De Sanctis J, Mata A, Hernandez N, Talamo C. Skeletal muscle inflammation and nitric oxide in patients with COPD. *Eur Resp J*. 2005;26:390-7.
- [49] Holladay C, Power K, Sefton M, O'Brien T, Gallagher WM, Pandit A. Functionalized scaffold-mediated interleukin 10 gene delivery significantly improves survival rates of stem cells in vivo. *Mol Ther*. 2011;19:969-78.
- [50] Cao Y. Tumor angiogenesis and molecular targets for therapy. *Front Biosci*. 2009;14:3962-73.
- [51] Ren JG, Jie C, Talbot C. How PEDF prevents angiogenesis: a hypothesized pathway. *Med Hypotheses*. 2005;64:74-8.
- [52] Hellberg C, Ostman A, Heldin CH. PDGF and vessel maturation. Recent results in cancer research *Fortschritte der Krebsforschung Progres dans les recherches sur le cancer*. 2010;180:103-14.
- [53] Bategay EJ, Rupp J, Iruela-Arispe L, Sage EH, Pech M. PDGF-BB modulates endothelial proliferation and angiogenesis in vitro via PDGF beta-receptors. *J Cell Biol*. 1994;125:917-28.
- [54] Cao R, Brakenhielm E, Pawliuk R, Wariaro D, Post MJ, Wahlberg E, et al. Angiogenic synergism, vascular stability and improvement of hind-limb ischemia by a combination of PDGF-BB and FGF-2. *Nat Med*. 2003;9:604-13.

- [55] Sainson RC, Johnston DA, Chu HC, Holderfield MT, Nakatsu MN, Crampton SP, et al. TNF primes endothelial cells for angiogenic sprouting by inducing a tip cell phenotype. *Blood*. 2008;111:4997-5007.
- [56] Jee SH, Chu CY, Chiu HC, Huang YL, Tsai WL, Liao YH, et al. Interleukin-6 induced basic fibroblast growth factor-dependent angiogenesis in basal cell carcinoma cell line via JAK/STAT3 and PI3-kinase/Akt pathways. *J Invest Dermatol*. 2004;123:1169-75.
- [57] Huang SP, Wu MS, Shun CT, Wang HP, Lin MT, Kuo ML, et al. Interleukin-6 increases vascular endothelial growth factor and angiogenesis in gastric carcinoma. *J Biomed Sci*. 2004;11:517-27.
- [58] Mentlein R, Held-Feindt J. Angiogenesis factors in gliomas: a new key to tumour therapy? *Die Naturwissenschaften*. 2003;90:385-94.
- [59] Ribatti D. Endogenous inhibitors of angiogenesis: a historical review. *Leuk Res*. 2009;33:638-44.
- [60] Nyberg P, Xie L, Kalluri R. Endogenous inhibitors of angiogenesis. *Cancer Res*. 2005;65:3967-79.

## **Chapter 5**

### **Summary and Future Directions**

## 5.1 Introduction

Critical limb ischemia (CLI) is considered as a serious public health issue with almost 27 million individuals in Europe and North America being affected by it. The fundamental goal of CLI treatment is to relieve ischemic pain, heal ulcers, prevent limb loss and improve the quality of life, thereby extending the survival of the patient. Surgical or endovascular revascularization therapies represent the gold standard for limb salvage in CLI. Nevertheless, such interventions are not suitable for up to 30% of CLI patients because of high operative risk or unfavourable vascular anatomy. Since the chronic nature of CLI is multifactorial, development of a gene delivery system capable of delivering multiple therapeutic genes based on the pathophysiology of CLI in a spatiotemporally controlled manner is required. The overall goal in this project was to treat the CLI by developing an injectable ELP based gene delivery system with controlled release.

## 5.2 Summary

### 5.2.1 Phase I – Chitosan Hollow Sphere as a Model System

The objective of Phase I (Chapter 2) was to use chitosan/polyglutamic acid (PGA) hollow spheres as a model system to elucidate the combinatorial effects of physicochemical properties such as size and surface charge on cell viability and, most importantly, on cellular internalization. This was achieved by fabricating multiple sizes of hollow spheres with different surface charges and assessing their *in vitro* internalisation profile using various methods such as flow cytometry and high content analysis. The hollow spheres of chitosan/PGA were fabricated using mono-dispersed polystyrene beads. The surface charge of the chitosan/PGA hollow spheres was negative and was modified with methoxyethanol amine (MEA) and polyethylene glycol (PEG) surface functionalization to obtain neutral surface charge and PEGylated surfaces or less negative surface charge. Surface charge and size exerted a significant influence on the sphere's property, most notably on toxicity and cellular uptake over time. Human umbilical endothelial cells (HUVECs) and human umbilical artery smooth muscle cells (HUASMCs) have different cytotoxicity responses when incubated with the spheres. Size and surface charge had no significant effect on HUASMCs when compared with controls. However, surface charge had a significant effect on the viability of HUVECs. The effect of surface charge was not significant with 1000 nm spheres; however, for 100, 300 and 500 nm there was a synergistic relationship between the size and surface charge that dictates their cytotoxicity. Cellular uptake is significantly dependant on size and surface charge and 100 nm appears to be an optimum size for internalization for neutral and PEGylated spheres. Cellular internalization is also dependent on a number of parameters, including size, surface

charge, incubation time and also the cell type. HUVECs and HUASMCs show different internalization behaviour with these spheres over different time points, varying size and charge. It is clear that the internalisation behaviour and cell viability of these hollow spheres depend not only on physicochemical differences such as size and zeta potential, but also dependent on cell type. The results are in accord with those of inorganic spheres and liposomes, indicating that size and surface charge of spheres are more important parameters than are the sphere's composition. Therefore, results obtained using tuneable chitosan/PGA hollow spheres as a model system in the present investigation can be applied to other types of solid spheres as well as to hollow spheres.

### **5.2.2 Phase II – Elastin-like Polypeptide Hollow Sphere as Gene Delivery Depot**

Based on the results obtained from chitosan/PGA spheres, hollow spheres from elastin-like polypeptide (ELP) were developed in Phase II (Chapter 3). ELP was chosen as the material for the application as it is known for its biodegradable, non-toxic, non-inflammatory and proangiogenic properties [1].

In this phase, the primary goal was to develop a gene delivery carrier based on ELP. Tuneable mono-dispersed ELP hollow spheres of 100, 300, 500 and 1000 nm were reported. The fabrication process of ELP hollow spheres comprised of three distinct steps: coating of ELP on sulfonated PS beads, cross-linking with mTGase, and dissolution of PS beads. The process was rapid, exploiting the self-assembly property and the slight positive charge of ELP. Cross-linking with a non-toxic microbial trans-glutaminase (mTGase) was a logical way to provide stability and robustness to the sphere while maintaining surface functional groups for further modifications. The hollow spheres showed a negative surface charge as mTGase cross-linked the amino groups leaving aside the maximum number of glutamic acids contributing to the surface charge. This negative surface charge of the hollow spheres prevents their subsequent aggregation, while covalent cross-linking with mTGase provides the robustness. Transmission electron microscope (TEM) and zetasizer data showed that all the four different sizes of hollow spheres are mono-dispersed. Plasmid DNA and polyplexes were efficiently ( $\sim 70 \mu\text{g } p\text{DNA}/\text{mg}$  of hollow sphere) loaded inside hollow spheres, a process governed by diffusion and charge interactions. Moreover, higher luciferase expression of polyplex loaded spheres through endosomal protection further validates hollow spheres as an effective gene vector reservoir system. Also, polyplex loaded spheres showed better luciferase expression level than do polyplex and *pDNA* alone in human umbilical vein endothelial cells and adipose derived stem cells (ADSCs). The luciferase expression level of polyplex loaded hollow spheres was nearly 10 times higher than that seen with *pDNA* loaded spheres. The TEM studies showed sub-

cellular localization of the hollow spheres inside the ADSCs. It is likely that the spheres entered the cell via a macropinocytosis pathway and were transported to endosomes and finally to lysosomes. Thus the spheres followed an endocytic pathway inside the cell. The high *pDNA* loading capability, triggered release by the enzymes elastase and protease, and the transfection ability of the released polyplexes, validates their use as a nucleic acid delivery depot.

### **5.2.3 Phase III – Dual Delivery Release System**

In this phase (chapter 4), the fabrication of a dual gene delivery system using ELP as the biomaterial was reported. The dual delivery system was designed with goal of delivering human endothelial nitric oxide synthase (heNOS) and human interleukin 10 (hIL-10) to the ischemic tissue in a spatio-temporal manner. The injectable ELP delivery system was fabricated by combining ELP hollow spheres (chapter 3) and an injectable ELP scaffold. The previous chapter described the fabrication of ELP hollow spheres and their use as a gene depot. The ELP injectable scaffold was fabricated by using ELP and mTGase as the cross linker. A 10% weight/volume ratio of ELP was used for this purpose. The mix of solution of ELP and mTGase was prepared in water and incubated at 37 °C. This solution solidified to make a scaffold within 10 min. Trinitrobenzene sulfonic acid assay (TNBSA) proved the cross-linking of ELP by mTGase. In addition, MTT assay demonstrated non-cytotoxicity of the ELP scaffold. Furthermore, screening of various sizes of ELP hollow spheres was performed in this study by characterizing their internalization pattern into cells such as HUVECS and activated and non-activated macrophages (THP1 cells). The flow cytometry study showed that ELP hollow spheres of 1000 nm were less internalized to either of these cells. Thus, hollow spheres of 1000 nm were chosen to be used as a depot. The release data using ELP scaffold and hollow spheres showed that *pDNA* from scaffold was released faster than it was with hollow spheres. Thus, ELP injectable system as designed was able to load two different genes at the same time and deliver them spatio-temporally at two different time points.

### **5.2.4 Phase IV – *In Vivo* Animal Study**

In this phase (chapter 4), a subcutaneous dose study was performed in the mouse model to determine a therapeutic dose of hIL-10 and heNOS. The selected therapeutic doses were then used to treat the ischemic mice. In the ELP-inELP system, hIL-10 was loaded inside the scaffold and heNOS inside the ELP hollow spheres. A highest dose of 20 µg and a lowest of 10 µg was chosen for both the *pDNA* to perform the dose study. Combinations of both the genes including all the doses were used to conduct dosage study. In total, nine various treatment groups were tested *in vivo*. ELISA data showed higher expression of heNOS and hIL-10 by day 14 and 7 respectively. The histology data for angiogenesis and inflammation was in

accordance with the hIL-10 and heNOS expression data. Blood vessel density was greater on day 14 in the heNOS treatment groups, whereas there was a reduced level of inflammatory cells by day 7 in the case of hIL-10 treated groups. The data showed that heNOS (20 µg) and hIL-10 (10 µg)/heNOS (20 µg) showed comparatively more blood vessel density than others. The immunostaining for CD68 and CD31 was in accordance with the histology data for inflammatory cells and vessel density data respectively. Ischemic study was performed using mouse model of unilateral ischemia. There were five groups: saline, heNOS (20 µg), hIL-10 (10 µg), heNOS (20 µg)/hIL-10 (10 µg) and ELP-inELP system only. The treatment groups that showed higher blood perfusion measured using LDPI were the groups with heNOS treatment groups. Saline group showed signs of severe necrosis. And ELP injectable system only and hIL-10 (10 µg) groups showed minimal blood perfusion but not enough to improve the ischemic condition. The histological data was in accordance with the LDPI as surface and length density of blood vessels were significantly higher in the case of heNOS treated samples. This was further proved by immunostaining with CD31. Human IL-10 treatment groups showed reduction in the level of inflammation cells. Furthermore, a mechanistic study showed proangiogenic activity of eNOS by up-regulating major proangiogenic growth factors such as vascular endothelial growth factors (VEGFA and B), platelet derived growth factor B (PDGFB) and fibroblast growth factor 1 (FGF1). These factors help in formation of a stable vascular network. Combination of eNOS/IL-10 showed up-regulation of some anti-angiogenic factors such as serpinF1, IL-4 and down regulation of IL-6 and tumor necrosis factor alpha (TNF- ), which are known to be proangiogenic. It has been proposed that maintaining a balance between the pro and anti-angiogenic factors is critical for the regulation of angiogenesis [2].

### **5.3 Limitations**

#### **5.3.1 Phase I**

The chitosan/PGA hollow sphere was used as a model to study internalisation and cell viability behaviour with respect to size and surface charge. The chitosan/PGA hollow spheres are tuneable with respect to their size and surface charge with a few limitations to their use as a therapeutic gene delivery vehicle. The first limitation is their processing time. The fabrication process is time consuming and takes more than two days to obtain the chitosan/PGA hollow spheres. The second limitation is lower gene loading ability. The hollow spheres load genes inside the hollow core via a diffusion process and the negative surface charge of these hollow spheres and compact surface create hindrance in this process.

Biomaterial surface properties and their degradation products play an important role in activating inflammatory responses when they are implanted as a medical device [3]. Chitosan by-products can induce inflammation which impact its use in the clinic [4, 5]. This limitation can be overcome by using extracellular matrix (ECM)-based materials to fabricate hollow spheres and have been mitigated in the chapter 3 by using ELP as a suitable biomaterial to fabricate the hollow spheres.

The *in vitro* internalisation study was optimal for testing a wide variety of cell types, various sizes and surface charge of hollow spheres. In this chapter, all the internalisation study was conducted on monocultures. And, the majority of the optimization steps used two-dimensional cultures of HUVECS and HUASMCs. This was an ideal setting for comparing an array of hollow spheres of various size and charge. However, *in vitro* systems, especially two-dimensional cell sheets, do not consistently represent *in vivo* conditions.

Furthermore, *pDNA* release from chitosan hollow spheres was performed using chitosanase. Chitosanase is only produced by microbes and plants and so the human body lacks this enzyme [6]. So *in vivo* release is likely to show a different pattern from that of *in vitro*.

### 5.3.2 Phase II

ELP hollow spheres were fabricated in order to increase the loading efficiency of *pDNA* and to greatly reduce the probability of an inflammation when used *in vivo*. The ELP hollow spheres showed high *pDNA* loading efficiency and a spatio-temporal release of *pDNA*. The high loading efficiency and spatio-temporal release are due to an electrostatic interaction between the polyplexes and ELP hollow spheres and hence ELP hollow spheres are limited to loading of only charged drug molecules. Another method of *pDNA* encapsulation that has been reported includes tethering of *pDNA* on to a template and then coating the surface with a polymer and finally dissolving the template in order to obtain the *pDNA* only inside the hollow capsules [7]. The next strategy for fabricating ELP hollow spheres can adopt this method so that it can be more efficient to encapsulate *pDNA* then loading them just by a diffusion process. Furthermore, all the *in vitro* transfection and internalization studies were performed in a two dimensional culture system of HUVECS and ADSCs. In this Phase, all testing was conducted on monocultures that received nutrients via cell culture media. This was an ideal environment for comparing an array of formulations with minimal ethical concerns. However, *in vitro* systems, especially two-dimensional cell sheets, do not consistently represent *in vivo* conditions. Therefore, while most optimization was conducted using *in vitro* systems, the *in vivo* experiments were conducted in Phase IV.

### 5.3.3 Phase III

The *in vitro* internalisation study was performed to screen a defined size of ELP hollow spheres that will be suitable as a depot. This screening was performed using cells such as activated and non-activated THP1 macrophage and HUVECS. The first limitation of this study is that the study was done in a two dimensional *in vitro* setting which is not similar to an ischemic tissue micro environment and furthermore cells picked for this study were only a few representative cells found abundantly in the ischemic tissue. Therefore, while most of these optimizations were conducted in two dimensional cell culture system, the *in vivo* experiments discussed in Phase IV included the ischemic study.

Additionally, a poly (2-dimethyl-aminoethylmethacrylate) (PDMAEMA) - block- poly ethylene glycol methyl ether methacrylate (PEGMEMA) / ethylene dimethacrylate (EDGMA) was synthesized in our laboratory to be used as a transfecting agent. The transfecting agent was found not to be efficient enough to transfect the cells in an *in vivo* set up. Therefore, in the Phase IV a commercially available partially degraded dendrimer known as Superfect™ was used. Superfect™ effectively transfects a variety of cell types [8-10], even in the presence of serum. In addition, it has been used *in vivo*.

The *in vitro* release was performed, where the scaffold released the *pDNA* faster than that the hollow spheres did. This release was seen to be spatio-temporal. Therefore, while the *pDNA* release was conducted using *in vitro* systems, the *in vivo* experiments discussed in Phase IV included release of dual therapeutic genes eNOS and IL-10. The expression profile was characterised to assess the spatio-temporal release of the genes as observed *in vitro*.

### 5.3.4 Phase IV

Angiogenesis and inflammation are the two most vital processes that are associated with ischemic pathophysiology [11]. In this phase, eNOS and IL-10 were delivered using an ELP based injectable system. An *in vivo* dose response study was performed to determine a therapeutic dose for eNOS and IL-10. And finally ischemic tissue were treated with eNOS and IL-10. The various parameters studied to investigate the change in angiogenesis were: histology to observe new blood vessel formations and CD31 staining for endothelial cells. The angiogenic factors such as angiopoietin 1 (ANGPT1), FGF1, platelet derived growth factor B (PDGFB), serpinF1, VEGFA and VEGFB, leptin and matrix metalloproteinase 9 (MMP9) were analysed to gain a further depth in the mechanism. This study is limited with the number of cells or factor analysed. The only cells investigated were endothelial cells whereas there are other cells which contribute in the angiogenesis process such as endothelial progenitor cells (EPCs), pericytes and macrophages and were not investigated in this study [12-14]. Similarly

there are several other angiogenic factors whose roles were not analysed in this phase and these include VE-cadherin, integrin, NOTCH signalling related molecules, hypoxia inducing factors and stromal cell derived growth factors [12].

As with angiogenesis, inflammation was monitored using several parameters such as stereological analysis of volume fraction of inflammatory cells in the tissue as well as inflammatory factors including IFN- $\gamma$ , IL-1, IL-10, IL-4, IL-6, IL-2, and TNF- $\alpha$ . This analysis was limited to only macrophages and monocytes, while the role of few other cells such as B-Cells and T-cells has not been investigated [15, 16]. Another area to be investigated is the involvement of M1 and M2 macrophages with respect to inflammation and healing. Likewise, there are other factors such as IFN- $\beta$  and IFN- $\gamma$ , IL-3, granulocyte-macrophage colony stimulating factor, and granulocyte colony stimulating factor which were not studied in this set up [15-17].

Furthermore, this study did not focus on skeletal muscle injury and its regeneration since these are major parts of ischemic pathophysiology but/and distinct from angiogenesis and inflammation [18]. The time course of molecular events associated with skeletal muscle damage and regeneration *in vivo* is still not clearly defined. An initial transcriptional analysis has shown that the ischemic skeletal muscle undergoes a transition through a functional adaptation stage with recovery of contractile force prior to full regeneration [17]. Factors such as myoD and Myf-5 have been known to help in muscle regeneration along with satellite cells [17]. Further investigation is needed to explore the interactions of skeletal muscle injury and regeneration physiological process with major physiological processes such as angiogenesis, and inflammation, when treated with eNOS and IL-10.

The present study focussed on localised delivery of eNOS from a biodegradable ELP scaffold which leads to significant recovery in animal models through sustained and localized release to the ischemic regions. However, this requires invasive local delivery into the ischemic tissue, and also requires multiple, appropriately spaced injections to target large or anatomically distinct regions of tissue ischemia in human patients. An alternative method is to deliver therapeutic angiogenic factor by introducing it into the blood stream, with subsequent targeting to ischemic regions.

#### **5.4 Conclusions**

The conclusions derived from the research performed in the current project can be summarized as follows:

#### 5.4.1 Phase I

The objective of this phase was to use chitosan/PGA hollow spheres as a model system to study the effect size and surface charge on internalisation and cell viability.

##### Conclusions:

- Chitosan/PGA hollow spheres of various sizes (100, 300, 500 and 1000 nm) and surface charge (negative, neutral and less negative) were fabricated.
- Variation of size and zeta potential played a vital role in internalization behaviour of chitosan hollow spheres as well as in cell viability.
- FITC labelled negative, neutral and PEGylated chitosan hollow spheres showed cell-line-dependent internalization behaviour.

#### 5.4.2 Phase II

The objective of this study was to fabricate ELP based hollow spheres to be used as gene delivery depot.

##### Conclusions:

- ELP based hollow spheres of various sizes (100, 300, 500 and 1000 nm) were fabricated using the template based method and using mTGase as the cross-linker.
- The ELP hollow spheres were of neutral surface charge with a few primary amino groups outside.
- Plasmid DNA and polyplexes were efficiently loaded inside the hollow spheres, a process governed by diffusion and charge interactions.
- *In vitro* release of pDNA was triggered by elastase and protease enzymes. Furthermore, the transfection ability of the released polyplexes from the hollow spheres validate their use as a gene delivery depot.
- The polyplex loaded and unloaded hollow spheres showed higher luciferase expression without any cytotoxicity in HUVECs and ADSCs.
- The polyplex loaded hollow spheres showed endosomal escape and can be used as a nucleic acid transfer vector.

#### 5.4.3 Phase III

The objective of this study was to fabricate an injectable dual gene delivery ELP based system.

##### Conclusions:

- ELP hollow spheres of size 1000 nm showed comparatively less internalization in HUVECs and activated and non-activated macrophages and were thus selected as the suitable size to be used as a gene depot.

- Injectable ELP scaffold was fabricated using ELP of 10 % (w/v) and mTGase as cross-linker.
- The ELP scaffold was found to be non-cytotoxic.
- *In vitro* release showed a spatio-temporal release, where *pDNA* from scaffold released faster than *pDNA* loaded inside ELP hollow spheres.

#### 5.4.4 Phase IV

The objectives of this study were to determine a therapeutic dose of heNOS and hIL-10 in a subcutaneous model of mouse and to treat the ischemic limb using the therapeutic dose of hIL-10 and heNOS.

#### Conclusions:

- Injectable ELP based gene delivery system was found to be degrading from day 7 to day 14 when implanted subcutaneously.
- The combination of doses hIL-10 (10 µg)/heNOS (20 µg) increased surface density of blood vessels by day 14 and reduced the volume fraction of inflammatory cells by day 7.
- The expression heNOS and hIL-10 was found to be spatio-temporal. A higher IL-10 expression was seen by day 7, while for eNOS the highest expression level was at day 14. The similar expression pattern was seen for heNOS and hIL-10 in the ischemic limb.
- The treatment groups' heNOS (20 µg) and hIL-10 (10 µg)/heNOS (20 µg) were seen to increase blood perfusion level by day 21 in the ischemic hind limb of the mice. The surface and length density increased by day 21 in these treatment groups. Also, a reduced level of inflammatory cells was seen by day 7 and 21.
- The treatment groups with heNOS up-regulated major proangiogenic growth factors such as VEGFA, VEGFB, FGF1 and PDGFB, whereas hIL-10 acted as anti-inflammatory and anti-angiogenic factors by down-regulating cytokines such as TNF- and IL-6.

#### 5.5 Future Directions

The assessment in various phases of the study has spanned efforts in developing a spatio-temporal gene delivery ELP injectable system capable of delivering multiple genes in a controlled manner and then investigating the system in a preclinical model with successful enhancement of angiogenesis and reduction of inflammation. Also, the study focussed on the role eNOS and IL-10 play at a molecular level in an ischemic set up. The possible directions the current project can take are i) gene and protein and cell screening in an ischemic pathophysiology, ii) genetically engineered cell-based therapy, iii) targeted delivery of therapeutics to ischemic limb and iv) tissue engineered blood vessels for use as vascular grafts. These directions have been summarized schematically in figure 5.1.

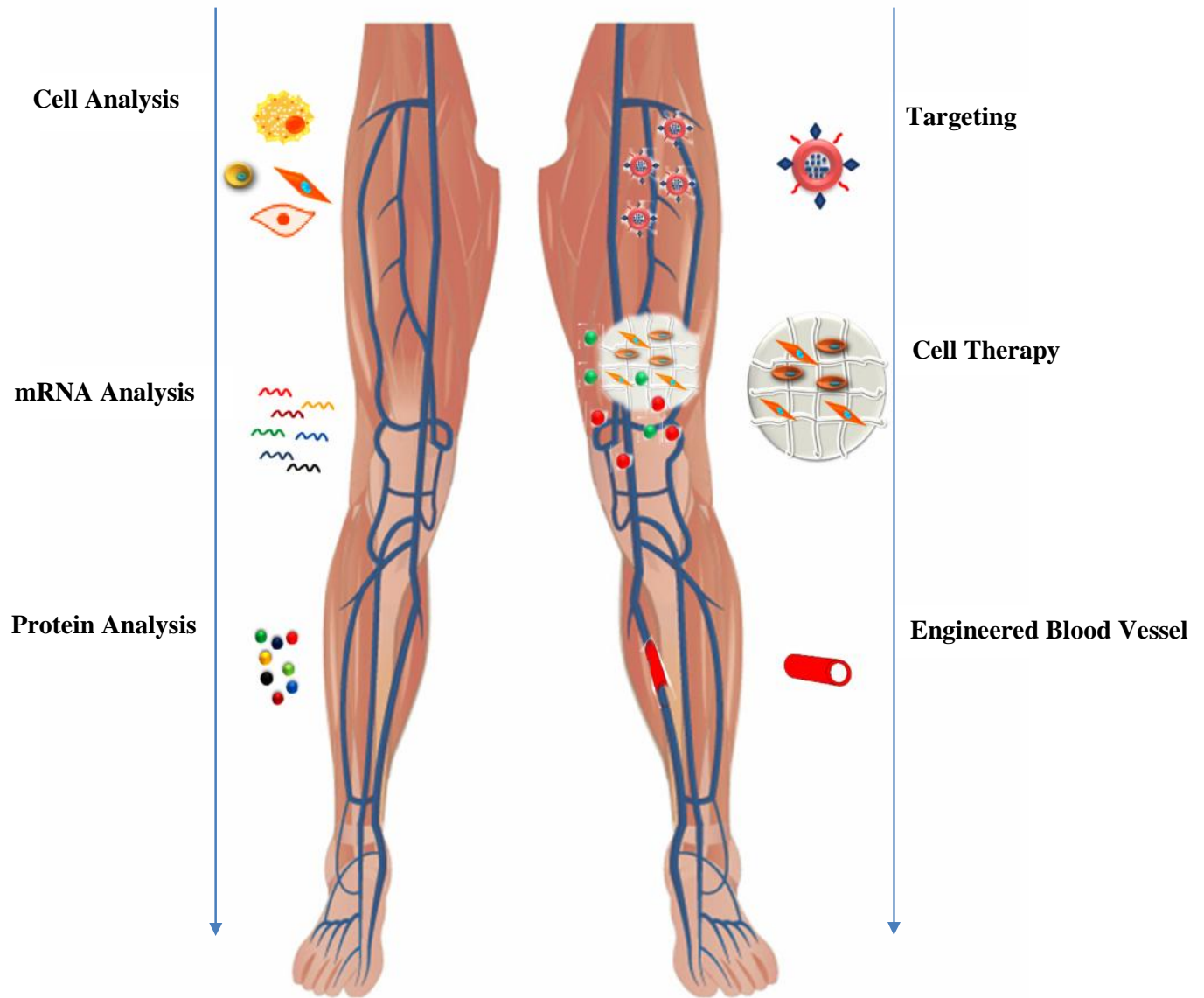


**Figure 5.1:** A schematic showing an overview of future applications stemming from the current study. The future studies both aim for understanding the pathophysiology of the CLI with respect to its cellular, molecular and biochemical aspects and also treating the condition via targeted delivery of drugs, cell therapy and engineered blood vessel.

### **5.5.1 Gene and Protein and Cell Screening in an Ischemic Pathophysiology**

Limb ischemia is a severe clinical problem that may result in a significant high rate of morbidity and mortality. Despite extensive experimental work that is directed toward the treatment and prevention of established ischemic injuries, the clinical outcome has not appreciably changed over the past decades [19, 20]. This may be related to the fact that the pathophysiology of this complex event at a molecular level is still not completely understood. To date a few molecular pathways related to inflammation and angiogenesis have been assessed. The next step of this research can include a) Assessment of mRNA, protein and understanding of cellular regulation with respect to inflammation, angiogenesis and muscle regeneration (Figure 5.2).

#### *5.5.1.1 Assessment of mRNA Regulation with Respect to Inflammation, Angiogenesis and Muscle Regeneration*

In this research, inflammation and angiogenesis were the major targets for the therapeutic treatment for ischemia. The tissues were analysed for mRNA for a few inflammatory molecules and angiogenic markers. The time course of molecular events of angiogenesis and inflammation that leads to skeletal muscle damage is largely undetermined [19, 20]. Also, molecular events that accompany muscle regeneration can be investigated to obtain new therapeutic targets. The hypothesis of this study is that with different time course there will be a differential regulation of angiogenic, inflammatory and skeletal muscle regenerative factors in the ischemic limb. The overall objective of this study is to investigate the expression of a subset of genes at mRNA level that encode mediators of inflammation, angiogenesis and muscle regeneration. To conduct this study, unilateral ischemia will be created in a mouse model by ligating the femoral artery. The hind limb ischemia model will be used to correlate the time course of muscle damage at the histological and functional levels with changes in mRNA expression level. Histopathology and muscle function measurements will be performed to accompany the mRNA data. The gene expression analysis will be done at different time points such as 0, 4h, day 3, day 7, day 14 and day 21.

#### *5.5.1.2 Assessment of Protein Regulation with Respect to Inflammation, Angiogenesis and Muscle Regeneration*

One of the first cellular functions to be affected by limb ischemia in the muscle tissue is protein synthesis. Although ischemia is one of the strongest stimuli of gene induction in the skeletal muscle, confirmation of protein expression and/or protein function is an absolute requirement. Protein analysis is critical to determine whether a specific protein plays a role in the ischemic pathophysiology. This approach will lead to identification of an acceptable candidate that will be a likely target for future therapeutic strategies. The hypothesis of this study is that with

different time course there will be a differential regulation of angiogenic, inflammatory and skeletal muscle regenerative factors in the ischemic limb at a protein level.

In order to investigate differential protein expression in the ischemic tissue, unilateral ischemia will be created in a mouse model by ligating femoral artery. Antibody arrays will be performed on the muscle tissue lysates as these arrays have the potential for mass analysis of protein level changes. A commercial antibody microarray will be performed to analyse protein expression level in the ischemic tissue as well as site specific phosphorylations of a variety of low abundant protein kinases, phosphatases and other regulatory proteins. Protein expression analysis will be done over different time points such as 0, 4h, day 3, day 7, day 14 and day 21.

#### *5.5.1.3 Assessment of Cell Regulation with Respect to Inflammation, Angiogenesis and Muscle Regeneration*

Cells form a major part in the ischemic pathophysiology. Endothelial progenitor cells and macrophages have already been reported to be found in ischemic tissue. [19-26]. Histological analysis performed in this research showed inflammatory cells such as macrophages, neutrophils, and basophils. Angiogenic cells include mostly endothelial cells. The hypothesis of this study is that with different time course in ischemia, various cells related to angiogenesis, and inflammation and muscle regeneration will be differentially recruited in the ischemic tissue. The study will involve investigation into different cell lines such as T Cells, B cells, endothelial progenitor cells (EPCs), pericytes and satellite cells and their recruitment during ischemic condition over different time points. The procedure for experiment will be similar where unilateral ischemia will be created in mice model by ligating femoral artery. Along with tissue samples, blood samples will be collected for flow cytometry analysis using specific cell surface markers. The analysis will be conducted at different time points such as 0, 4h, day 3, 7, 14 and 21.

#### **5.5.2 Cell Therapy for Critical Limb Ischemia**

Cell-based therapy promises to be a suitable option for mitigating the major problems associated with CLI. For example, a variety of cell populations, including MSCs, bone marrow mononuclear cells (BM-MNC) and EPCs have been investigated for use in the treatment of ischemic diseases in preclinical and clinical trials [27-30]. Therapeutic activity has been attributed to stimulation of reparative angiogenesis through direct incorporation of progenitor cells into neovessels and paracrine stimulation of endothelial cell growth [31, 32].

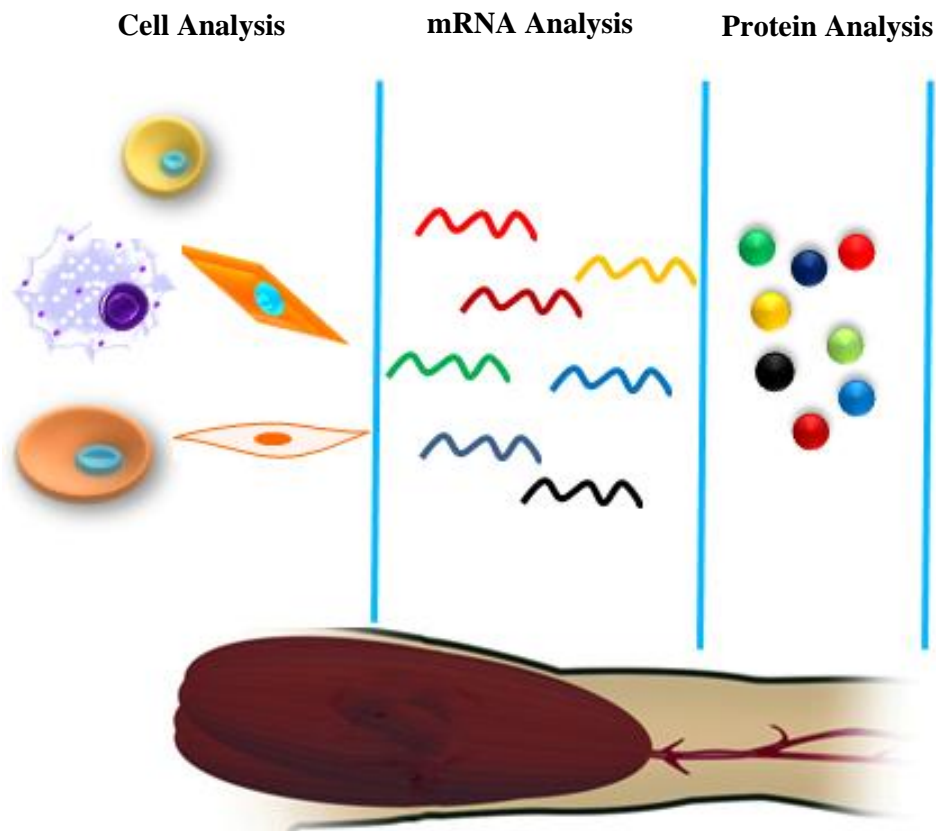


**Figure 5.2: A schematic elucidating the future studies which aim at understanding the pathophysiology of the CLI with respect to its cellular, molecular and biochemical aspects.**

Around 80 clinical cell therapy trials have been conducted during the past six years in which a patient's own cells were isolated, often multiplied *in vitro*, and re-infused either systemically or into the ischemic tissue. These trials, while reassuring as to the safety of cell therapy, indicate that present approaches have significant limitations [33]. Research into different cell lines indicates that the vast majority (typically 90%) of transplanted cells will rapidly die due to the presence of low oxygen, glucose and pH in ischemic microenvironment [34].

Furthermore, control over the fate of the cells is lost once they are intramuscularly injected in a dispersed fashion. Intravascular injection, by contrast, has the drawback that cells cannot reach the target tissue if the main artery is completely occluded. Various techniques, such as scaffold usage, priming of the cells, and physical and chemical stimuli have been shown to improve the performance of transplanted cells. Cell-based angiogenesis may therefore benefit from tissue engineered strategies to better administer cells and optimize their specific homing. The rapidly evolving field of biomaterial science allows specific design of biomaterials to support transplanted cells within the ischemic environment [35]. Herein, the structure, dimensions, and shape of constructs are pivotal to better mimic the native architecture of extracellular matrix. An optimal biomaterial to support cell therapy should provide a three-dimensional environment to enhance biomechanical properties of extracellular matrix [36]. In some scaffold, bioactive signals can be incorporated to specifically modulate stem cell behaviour [37]. Thus the goal of transplanting cells in a biomaterial is to optimize the cellular microenvironment to maintain cell viability and function. Hydrogels, which have physical and chemical properties similar to the natural ECM, are frequently used as scaffolds. Natural materials which form hydrogels, such as collagen, fibrin and elastin, have been investigated as scaffolds. Furthermore, bioactive signals can be incorporated in biomaterials to additionally enhance cell survival, retention, proliferation, and differentiation.

The priming of cells basically targets any functional step that influences cell fate from the application on: adhesion/transmigration homing, migration, engraftment, survival, cell-cell interaction, repair capacity, differentiation, and retention. Potential tools for modification include drugs, small molecules, naked and vector facilitated plasmids, and epigenetic reprogramming [38, 39]. Priming of dysfunctional autologous cells from cardiovascular patients via any of these tools may allow for a 'resetting of impaired biopotency'. Few of the major proangiogenic growth factors which have been exploited in order to prime cells are vascular endothelial growth factors (VEGF-A), platelet derived growth factors (PDGF-BB) and stromal cell- derived factor (SDF-1) [12]. VEGF regulates the process of angiogenesis predominantly. VEGF-A, the main component of the VEGF family, stimulates angiogenesis in

healthy and diseased microenvironment by signalling through VEGF receptor-2. For vessels to function properly, they must be mature and covered by mural cells. PDGF-BB contributes to this process. To stabilize endothelial cell channels, angiogenic endothelial cells release PDGF-BB to chemo-attract PDGF receptor-<sup>+</sup> pericytes. SDF-1, a chemokine, promotes revascularization of ischemic organs by recruiting pro-angiogenic immune cells and endothelial progenitor cells [12].

A second obstacle to achieving successful cell-based angiogenesis has been the difficulty in the identification of the optimal cell population for vascularisation [40]. Total bone marrow cells and cells sorted for CD133, CD34, and VEGFR-2 (VEGFR-2; CD133<sup>+</sup>CD34<sup>+</sup>VEGFR-2<sup>+</sup> cells) have been principally used in clinical trials [41, 42]. However, these cells may not represent the best option because they do not generate a stable and robust collateralization. Furthermore, they are extracted from a niche that is significantly damaged by the ongoing disease and associated risk factors as demonstrated by recent studies [43]. Cells endowed with the capacity to stabilize provisional neovascularisation such as pericytes are warranted. Recent work by the group of Madeddu has demonstrated the therapeutic potential of foetal and adult pericytes in models of diabetic ulcers, limb ischemia and myocardial infarction [44-47].

Keeping all limitations and shortcomings in mind, the idea to realize effective ischemic tissue repair by using only one cell type or growth factor is likely to remain challenging. Combined, precisely timed, multi-step approaches incorporating various progenitor and stromal cells, paracrine factors, and specifically bioengineered tools such as engineering cells to secrete a desired growth factor and designing biomaterial for cell delivery are needed in order to advance this exciting field to the next level for true ischemic tissue repair. The hypothesis of this project is that the primed endothelial cells and pericytes with SDF-1, VEGF-A and PDGF-B genes, encapsulated in ELP based biomaterial system, will enhance blood perfusion level in the ischemic tissue of a mouse model of hind limb ischemia.

The project proposes a multidisciplinary approach to achieve rational design of sophisticated combined ELP-based biomaterial carriers for delivery of combined vascular cells (endothelial cells and pericytes) modified to allow controlled release of major proangiogenic factors within the microenvironment (Figure 5.3). The objectives are i) to design and develop an injectable ELP scaffold for encapsulation of human pericytes and endothelial cells and *in vitro* characterization, ii) to engineer pericytes and endothelial cells to release proangiogenic growth factors SDF-1, VEGF-A and PDGF-B and characterization of their *in vitro* and *in vivo* angiogenic potential in a subcutaneous mouse model, iii) to conduct *in vivo* ischemic study in diabetic mouse for induction of reparative angiogenesis in the ischemic microenvironment.

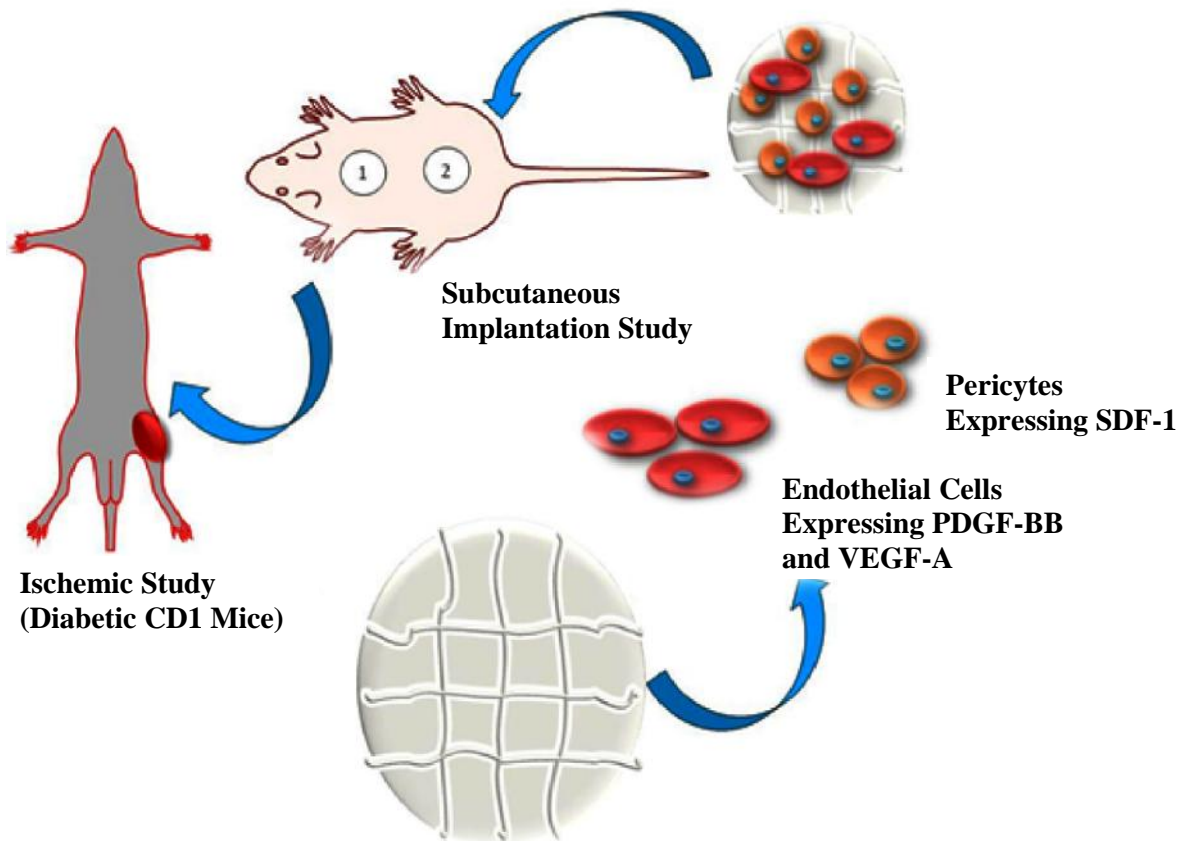


**Figure 5.3: A schematic showing the future study which aims at using cell therapy to treat the ischemic condition. The engineered endothelial cells and pericytes will be implanted in subcutaneously in mice and finally in an ischemic mouse model.**

In order to achieve these goals, pure human pericytes and endothelial cells will be engineered with the proangiogenic genes. The purified engineered cells will be isolated using FACS sorting. Injectable ELP scaffold of different viscosity will be tested for their cell encapsulation ability and cytotoxicity. The engineered pericytes and endothelial cells, encapsulated within an injectable ELP scaffold, will then be implanted in a mouse model of unilateral ischemia. Laser doppler perfusion imaging will be performed to assess the blood perfusion level in addition to histological analysis to investigate cell viability after implantation and blood vessel density.

### **5.5.3 Hollow Sphere Modifications for Targeting**

In this thesis, elastin hollow spheres have been used as a gene depot for a localised delivery in the ischemic muscle. These ELP hollow spheres can be modified further to be used as a targeted drug delivery vehicle (Figure 5.4). These modifications can be considered to create ELP hollow spheres with properties of (a) evading immune barriers to become an efficient drug delivery system, and (b) targeting ischemic muscle

#### *5.5.3.1 Evading Immune Barriers for an Efficient Drug Delivery System*

Nano and microparticles have been used as delivery systems for drugs and vaccines and have a considerable advantage over conventional delivery systems. These systems are often tailored to have controlled release of the drug/vaccine and also to provide protection from metabolism and degradation [48, 49]. However, these particles are eventually cleared by the body's immune cells such as macrophages and dendritic cells (DC) irrespective of the route of their administration [50]. These cells are phagocytic in nature and active in eliminating pathogens or antigens by non-specific or receptor-mediated phagocytosis and thus form a barrier against drug delivery [50]. DCs act as antigen presenting cells and present the processed antigens on their surface through major histocompatibility complex (MHC). The MHC–antigen complex can be recognized by T cell receptors and activates cytotoxic CD8+ T cells [51]. Recent studies in DC and macrophages revealed significantly improved antigen presentation when the antigen was bound to the surface of microparticles and internalised by phagocytosis compared to the uptake of soluble antigen. Cationic microparticles especially have been demonstrated in an earlier study to enhance phagocytosis by DC [52].

One of the strategies to avoid phagocytosis of the particles by macrophages is by making the surface of the particles hydrophilic. A significant number of studies have been conducted along with theoretical interpretations of the role of macrophages in phagocytosis. These results suggest that phagocytosis increases with particle size for hydrophobic particles and decrease for hydrophilic particles. Moreover, it is generally accepted that more hydrophilic surfaces (as a result of PEGylation) result in reduced phagocytosis by postponing opsonisation, or the

binding of proteins that increase recognition and receptor-specific attachment by macrophages adsorption of proteins which increases phagocytosis [53-56].

Another possible strategy can be to tether p53 or MDM2 on the particle's surface. This strategy follows the tumor's immune evasion mechanism. Tumors escape the immune system by various strategies, one of which is through their expression of self-antigens, such as p53 or MDM2, to which dendritic and T cells have been peripherally or centrally tolerated [57]. Thus, surface functionalization of nano or microparticles with these antigens can be an option to avoid phagocytosis of these particles.

The hypothesis of this study is that ELP hollow spheres tethered with PEG moieties and p53 or MDM2 antigens will evade immune barriers. The objective of this study is to fabricate ELP hollow spheres with PEG and p53 and/or MDM2 antigens. The project will focus on a multiple approach of modification of size and surface chemistry to achieve microparticles which will allow evasion of the immune barrier to become an efficient drug delivery vehicle.

ELP hollow spheres will be chemically conjugated with PEG moieties and p53 and/or MDM2 antigens. The ELP hollow spheres will be tested *in vitro* for their internalisation property with cells such as macrophages and DCs and can be finally characterised in an *in vivo* set up.

#### 5.5.3.2 ELP Hollow Spheres Targeting Ischemic Muscle

The present study focussed on localised delivery of eNOS for angiogenesis in the ischemic muscle. Another method of delivery of this therapeutic angiogenic factor can be its introduction into the blood stream, with subsequent targeting strategies to ischemic regions. The hypothesis of these projects is that ELP hollow spheres can be targeted to the ischemic tissue. The objectives are to I) tether VEGF-A moiety on the ELP hollow spheres to target the ischemic tissue and II) tether mannose on the ELP hollow spheres to deliver these spheres to the ischemic tissue.

**Approach I:** Ischemia in peripheral tissue leads to up-regulated expression of a variety of angiogenic factors and, most importantly, VEGF receptors 1 and 2 [58]. The up-regulation of VEGF receptor 1 and 2 can be exploited to target ischemia. The ELP hollow spheres fabricated in this project can be PEGylated with the free amino group present on the surface of the ELP hollow spheres. Briefly, surface functionalization of ELP spheres will be performed by using PA-functionalized amino terminated PEG and EDC-NHS as cross-linker. Moreover, VEGF-A targeting moiety will be tethered to the surface of the ELP hollow spheres with their free amino groups and using EDC-NHS as cross-linker. The modification of the hollow sphere with PEG will help it to prevent opsonisation and VEGF-A moiety will target the ischemic muscle. These experiments can be performed in a unilateral ischemic mice model. The targeting will be

monitored at different time points 0, 3, 6, 12, 24 and 48 hr after the ischemic surgery. The hollow spheres will be initially loaded with a fluorescent agent to quantify the amount of ELP hollow spheres deposited in the ischemic tissue at different time points. Also, biodistribution of ELP hollow spheres will be measured in liver, kidney, lung, heart and spleen along with skeletal muscle. This optimization will be followed by the delivery therapeutic gene of interest using targeted ELP hollow spheres.

**Approach II:** The pathophysiology of ischemia not only involves an up-regulation of angiogenic factors, but also has a highly inflammatory environment [11, 19]. The tissue macrophage can be found abundantly and changes with different time period [59]. This fact can be used to modify the hollow spheres with a macrophage targeting moiety such as mannose [60-62]. The hollow spheres can be tethered with mannose. Briefly, mannose will be complexed with polyethylenimine and then the PEI/mannose complex will be conjugated with the free amino groups of ELP hollow spheres using EDC/NHS cross-linker. A unilateral ischemic mouse model will be created. The hollow spheres will be tagged with a suitable fluorescent agent and will be delivered through the blood stream into the ischemic site. The targeting will be monitored over different time points such as 0, 3, 6, 12, 24 and 48 hr after the ischemic surgery. Biodistribution of ELP hollow spheres tethered with mannose will be measured in liver, kidney, lung, heart and spleen along with skeletal muscle at different time points. This optimization will be followed by the delivery therapeutic gene of interest using mannose receptor targeted ELP hollow spheres.

#### **5.5.4. Tissue Engineered Blood Vessel using an ELP Scaffold**

With millions of patients diagnosed with CLI and over a quarter million undergoing bypass surgery every year, there is a pressing need to develop functional small diameter vascular grafts for clinical applications. Over the last few decades there have been various tissue engineering approaches in the development of biological vascular grafts [63-67]. However, before clinical trials are undertaken, a number of challenges need to be resolved. One of these is the lack of elastin even after long culture periods [64]. It has already been reported that SMCs are capable of producing large amounts of collagen matrix when cultured in a bioreactor for more than eight weeks but not elastin [64].

The hypothesis of the study is that ELP along with smooth muscle cells (SMCs) can be used to fabricate stronger blood vessels. The objectives of this study are: 1) to fabricate an ELP-based blood vessel; 2) Implant the blood vessels in the abdominal aorta of nude rats.

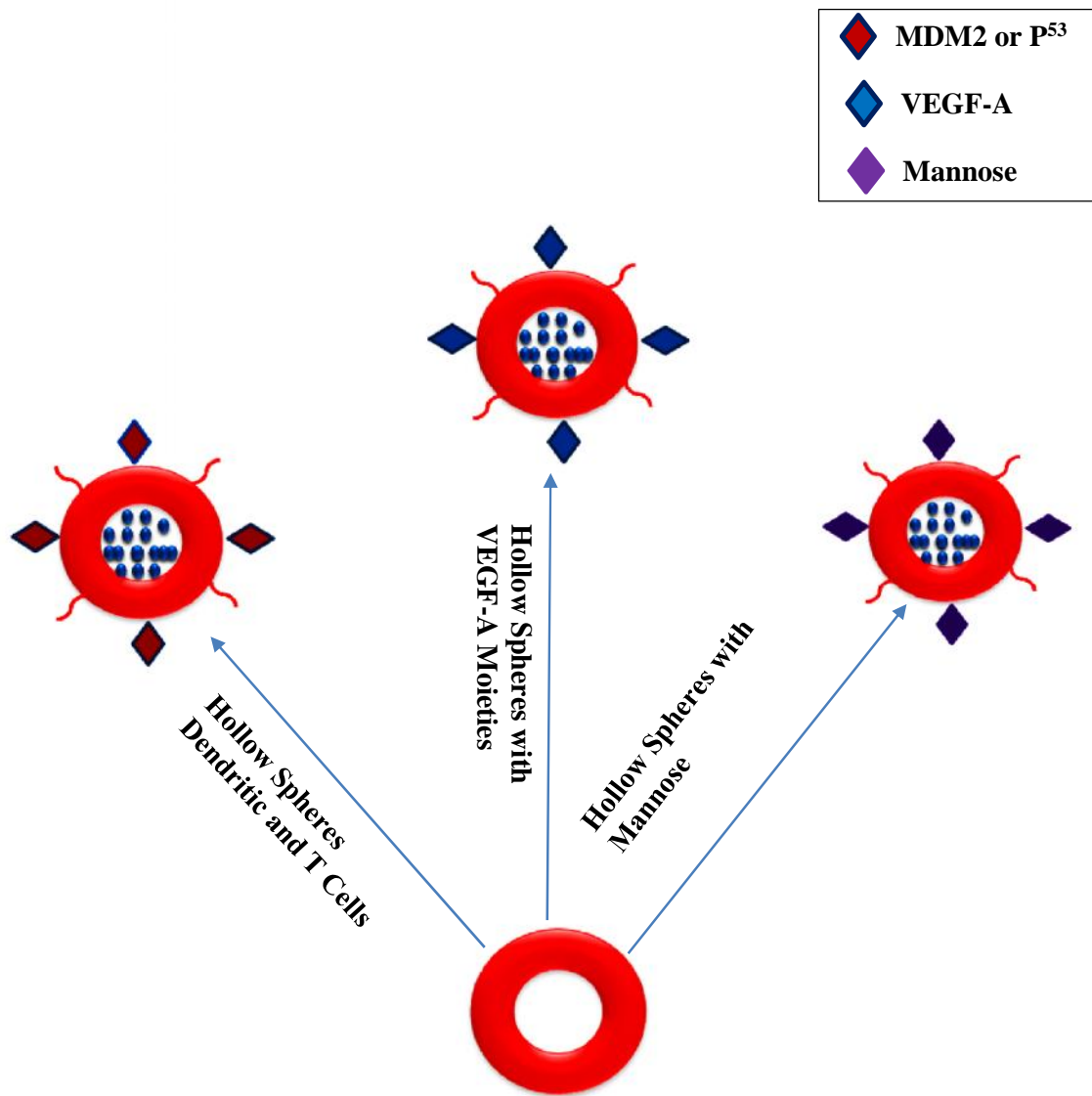


**Figure 5.4:** A schematic presenting ways in which ELP hollow spheres can be engineered further to evade the immune system and surface functionalized to target the ischemic area.

In this study, ELP along with SMCs will be used to generate a tissue engineered graft. Briefly, an ELP gel will be fabricated as a small vascular graft and SMCs will be encapsulated and cultured for 4 weeks in a bioreactor (Figure 5.5). This will be followed by mechanical testing of the vessel grafts by performing suture retention and burst pressure measurements. The vascular grafts will then be implanted in the abdominal aorta of nude rats to further characterize there *in vivo* application.

### **5.5.5 Tumor Xenograft Implantation using an Elastin-based Biomaterial System**

The use of transplantable human tumors (tumor xenograft) in mice is a very common set of practices to screen new anti-cancer drugs or therapies for their efficacy as anti-cancer treatment. These models frequently involve human tumor xenografts grown either subcutaneously or in the organ type in which the tumor originated in immune deficient hosts such as athymic (nude) or severe combined immune deficient (SCID) mice or other immunocompromised mice. They are grown for 1-8 weeks depending upon the number of cells used or the initial size of the tumor [68].

The key advantages of using human tumor xenografts to examine therapeutic responses to drugs are: 1) use of actual human tumor tissue, featuring the complexity of genetic and epigenetic abnormalities that exist in the human tumor population and 2) they can also be used in the development of individualized molecular therapeutic approaches within a few weeks [69].

Despite the enormous efforts applied in preclinical studies for anticancer drug screening on the basis of xenograft models, very few efficacious agents are clinically relevant at well-tolerated doses [70]. One of the reasons may be the use of immune-depressed mouse model which is physiologically not relevant in terms of i) drug bioavailability, depending on its administration, absorption, metabolism and delivery; and ii) interaction between human cancer cells in the graft and the mouse stroma, vasculature and infiltrating cells. Also, according to a recent report, transplantation of human solid tumor in immune-deficient mice is susceptible to lymphangiogenesis [69, 71].

The use of an immune-competent mouse model is a more clinically relevant set-up for tumor xenograft. But, this model can induce an immune response leading to rejection of the transplanted tumor [72]. This rejection might be a result of the activation of the immune system due to surgical trauma that initiates the inflammatory cascade and the presence of foreign antigens associated with the cells promoting a more chronic adaptive response [73]. Biomaterial chemistry and architecture can be manipulated to prevent up-regulation of inflammation, which may be a step towards reducing immune rejection.

**ELP Scaffold Embedded  
with Primary SMCs**

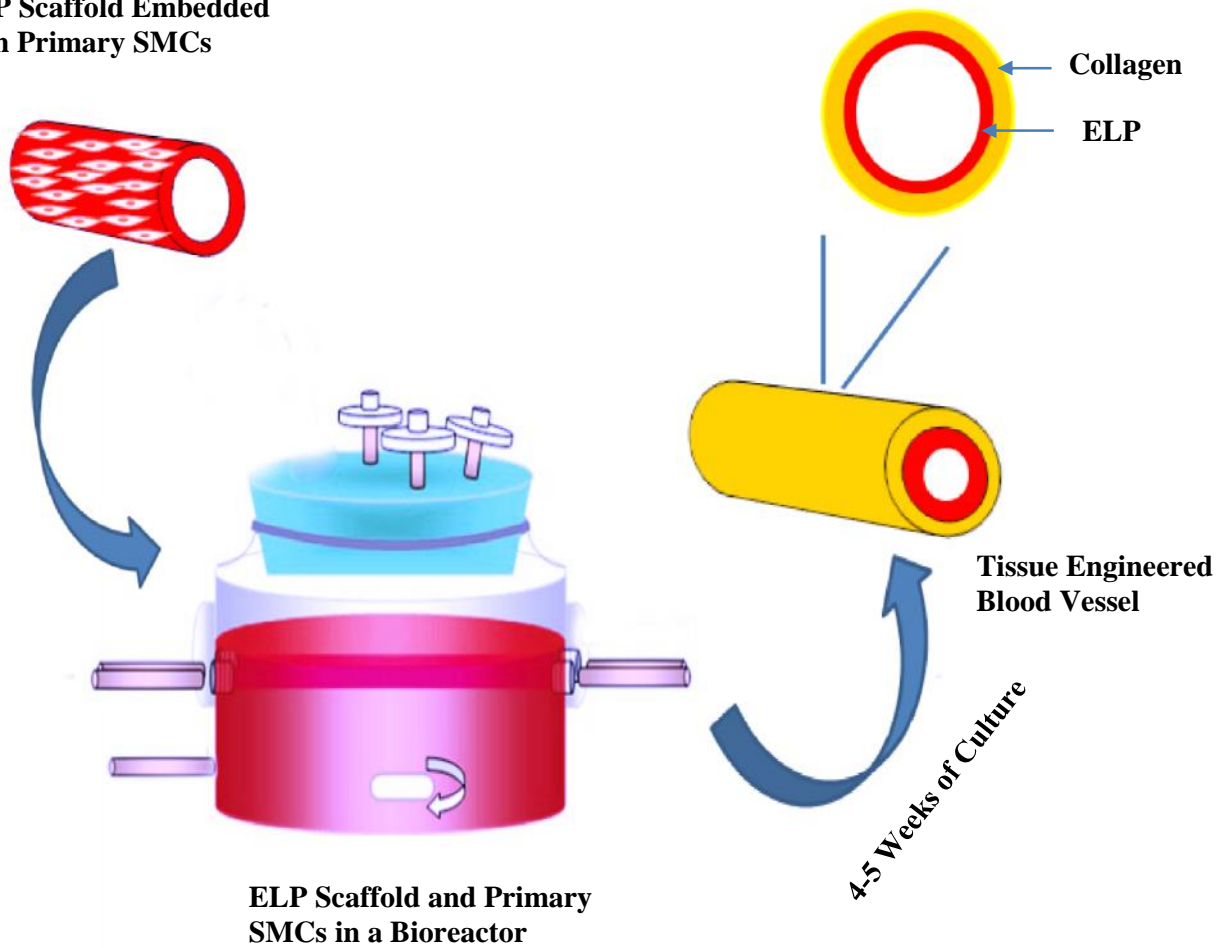


**Figure 5.5: A schematic showing the fabrication of an ELP-based tissue engineered blood vessel. SMCs will be embedded while fabricating the ELP scaffold and then cultured in a bioreactor for 4-5 weeks. The blood vessels will be harvested and characterised for their mechanical strength before the implantation.**

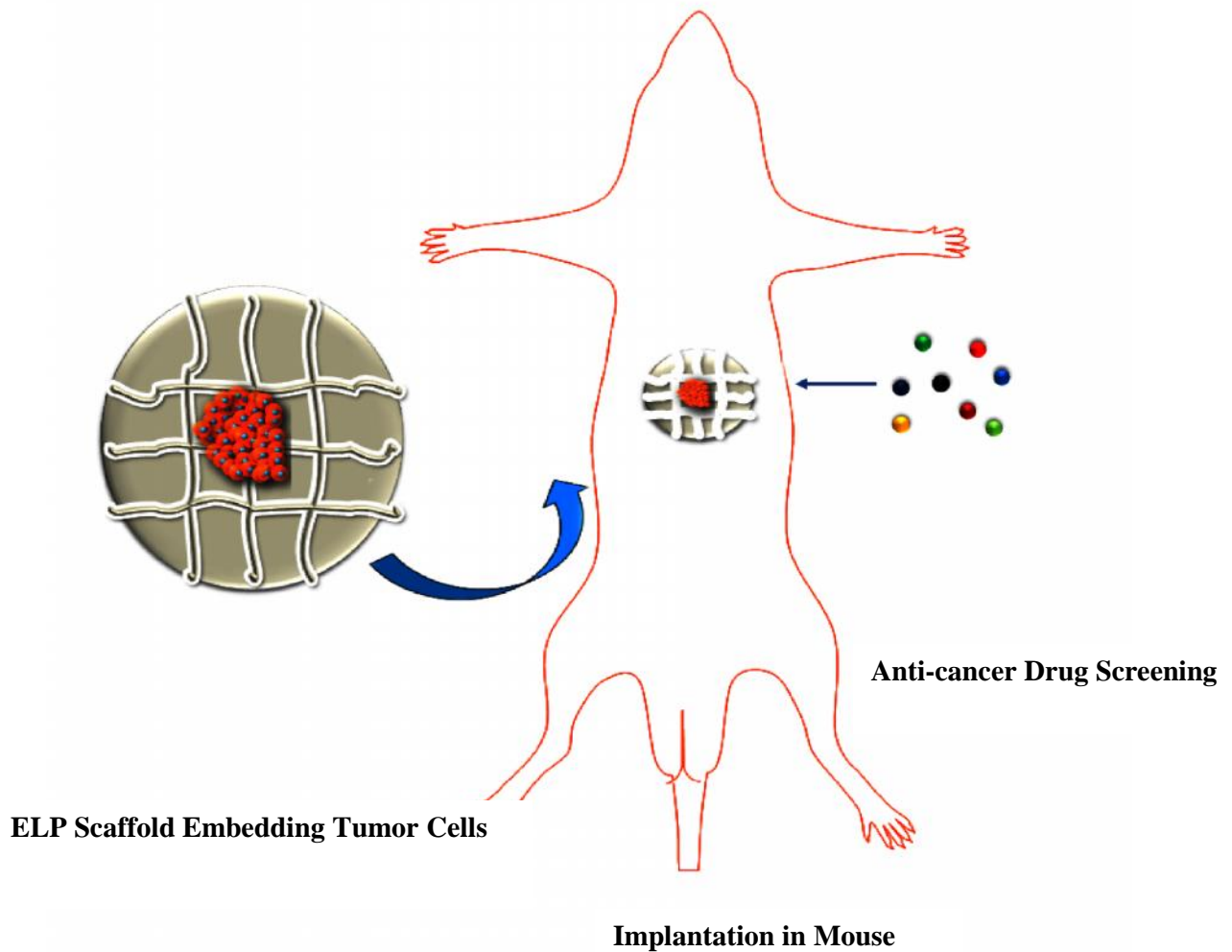


**Figure 5.6: A schematic showing encapsulation of tumor within the ELP scaffold for xenograft studies and anti-cancer drug screening.**

Generally, hydrophobic materials tend to enhance monocyte adhesion relative to hydrophilic materials leading to a local immune response at the implant site. Implantation of ECM based materials such as elastin that is hydrophilic or has a neutral charge has decreased monocyte/macrophage adhesion and reduced foreign-body giant cell formation *in vitro* [73].

The hypothesis of this study is that ELP biomaterial system can reduce tumor xenograft immune rejection. This project proposes the use of an ECM-based biomaterial system to help in the reduction of tumor xenograft immune rejection in an immune-competent mouse model with an overall goal of studying the tumor xenograft in a clinically relevant set-up (Figure 5.6). This study will focus on 1) development of an ELP based scaffold for transplantation of tumor xenografts, 2) *in vivo* tumor growth/viability study by subcutaneous and orthotopic implantation, and 3) anti-cancer drug efficacy testing. In order to achieve these goals, ELP of 94% purity will be used to develop an injectable scaffold of various viscosity and their tumor cells encapsulation ability and toxicity will be assessed. The injectable ELP scaffold along with tumor cells will be injected on subcutaneous and orthotopic sites in a mouse model. Furthermore, *in vivo* survival of these encapsulated tumor cells will be characterised by live fluorescent imaging technique. Drug screening will be performed using this model to assess the anti-cancer activity of various drugs.

## 5.6. Conclusions

In conclusion, an injectable ELP-based delivery system has been developed to deliver therapeutic genes heNOS and hIL-10 to ischemic limb. *In vitro*, it was demonstrated that ELP hollow spheres alone can act as a reservoir system and can efficiently load high amount of *p*DNA. It has been demonstrated that the injectable scaffold along with ELP hollow spheres can be used as dual delivery gene depot and can release the reporter genes in a spatio-temporal manner. *In vivo*, it was demonstrated that the injectable ELP system carrying heNOS and hIL-10 can effectively mediate transfection and have therapeutic benefits. In the subcutaneous dose response study, heNOS (20  $\mu$ g), hIL-10 (10  $\mu$ g) and hIL-10(10  $\mu$ g) /heNOS(20  $\mu$ g) have been shown to enhance angiogenesis and modulate inflammation. In the model of hind limb ischemia, ELP injectable system-mediated gene therapy of heNOS and hIL-10 effectively increased blood perfusion in the ischemic limb and reduced inflammation level. Also, heNOS was shown to improve angiogenesis through the upregulation of major proangiogenic growth factors such as VEGFA, VEGFB, PDGFB and FGF1. And, IL-10 significantly up-regulated IL-4 to reduce inflammation level. This improvement in the ischemic limb suggests that a therapeutic benefit exists in combining heNOS and hIL-10 gene therapy and thus is an effective combinatorial approach for ischemic limb healing.

### 5.7. References

- [1] Nettles DL, Chilkoti A, Setton LA. Applications of elastin-like polypeptides in tissue engineering. *Adv Drug Delivery Rev.* 2010;62:1479-85.
- [2] Ren JG, Jie C, Talbot C. How PEDF prevents angiogenesis: a hypothesized pathway. *Med Hypotheses.* 2005;64:74-8.
- [3] Anderson JM, Rodriguez A, Chang DT. Foreign body reaction to biomaterials. *Semin Immunol.* 2008;20:86-100.
- [4] Barbosa JN, Amaral IF, Aguas AP, Barbosa MA. Evaluation of the effect of the degree of acetylation on the inflammatory response to 3D porous chitosan scaffolds. *J Biomed Mater Res A.* 2010;93:20-8.
- [5] Farrugia BL, Whitelock JM, Jung M, McGrath B, O'Grady RL, McCarthy SJ, Lord, M. S. The localisation of inflammatory cells and expression of associated proteoglycans in response to implanted chitosan. *Biomaterials.* 2014;35:1462-77.
- [6] Thadathil N, Velappan SP. Recent developments in chitosanase research and its biotechnological applications: a review. *Food Chem.* 2014;150:392-9.
- [7] Zelikin AN, Becker AL, Johnston AP, Wark KL, Turatti F, Caruso F. A general approach for DNA encapsulation in degradable polymer microcapsules. *ACS Nano.* 2007;1:63-9.
- [8] Uchida E, Mizuguchi H, Ishii-Watabe A, Hayakawa T. Comparison of the efficiency and safety of non-viral vector-mediated gene transfer into a wide range of human cells. *Biol Pharm Bull.* 2002;25:891-7.
- [9] Dennig J, Duncan E. Gene transfer into eukaryotic cells using activated polyamidoamine dendrimers. *Rev Mol Biotechnol.* 2002;90:339-47.
- [10] Bielinska AU, Chen CL, Johnson J, Baker JR. DNA complexing with polyamidoamine dendrimers: Implications for transfection. *Bioconjug Chem.* 1999;10:843-50.
- [11] Khawaja FJ, Kullo IJ. Novel markers of peripheral arterial disease. *Vasc Med.* 2009;14:381-92.
- [12] Carmeliet P, Jain RK. Molecular mechanisms and clinical applications of angiogenesis. *Nature.* 2011;473:298-307.
- [13] Cao Y. Molecular mechanisms and therapeutic development of angiogenesis inhibitors. *Adv Cancer Res.* 2008;100:113-31.
- [14] Cao Y. Therapeutic angiogenesis for ischemic disorders: what is missing for clinical benefits? *Discov Med.* 2010;9:179-84.
- [15] Nylaende M, Kroese A, Strandén E, Morken B, Sandbaek G, Lindahl AK, Arnesen H.

Markers of vascular inflammation are associated with the extent of atherosclerosis assessed as angiographic score and treadmill walking distances in patients with peripheral arterial occlusive disease. *Vasc Med.* 2006;11:21-8.

[16] Ouriel K. Peripheral arterial disease. *Lancet.* 2001;358:1257-64.

[17] Paoni NF, Peale F, Wang F, Errett-Baroncini C, Steinmetz H, Toy K. Time course of skeletal muscle repair and gene expression following acute hind limb ischemia in mice. *Physiol Genomics.* 2002;11:263-72.

[18] Grounds MD. Towards understanding skeletal muscle regeneration. *Pathol Res and Pract.* 1991;187:1-22.

[19] Blaisdell FW. The pathophysiology of skeletal muscle ischemia and the reperfusion syndrome: a review. *Cardiovascular surgery.* 2002;10:620-30.

[20] Duran WN, Takenaka H, Hobson RW, 2nd. Microvascular pathophysiology of skeletal muscle ischemia-reperfusion. *Semin Vasc Surg.* 1998;11:203-14.

[21] Tongers J, Roncalli JG, Losordo DW. Role of endothelial progenitor cells during ischemia-induced vasculogenesis and collateral formation. *Microvasc Res.* 2010;79:200-6.

[22] Leff JA, Repine JE. Blood cells and ischemia-reperfusion injury. *Blood Cell.* 1990;16:183-91; discussion 91-2.

[23] Christov C, Chretien F, Abou-Khalil R, Bassez G, Vallet G, Authier FJ. Muscle satellite cells and endothelial cells: close neighbors and privileged partners. *Mol. Biol Cell.* 2007;18:1397-409.

[24] Kokovay E, Li L, Cunningham LA. Angiogenic recruitment of pericytes from bone marrow after stroke. *J Cereb Blood Flow Metabol.* 2006;26:545-55.

[25] Brechot N, Gomez E, Bignon M, Khallou-Laschet J, Dussiot M, Cazes A. Modulation of macrophage activation state protects tissue from necrosis during critical limb ischemia in thrombospondin-1-deficient mice. *PloS One.* 2008;3:e3950.

[26] Zhao M, Fernandez LG, Doctor A, Sharma AK, Zarbock A, Tribble CG. Alveolar macrophage activation is a key initiation signal for acute lung ischemia-reperfusion injury. *Am J Physiol Lung Cell Mol Physiol.* 2006;291:L1018-26.

[27] Jackson KA, Majka SM, Wang H, Pocius J, Hartley CJ, Majesky MW. Regeneration of ischemic cardiac muscle and vascular endothelium by adult stem cells. *J Clin Invest.* 2001;107:1395-402.

[28] Mamidi MK, Pal R, Dey S, Bin Abdullah BJ, Zakaria Z, Rao MS. Cell therapy in critical limb ischemia: current developments and future progress. *Cytotherapy.* 2012;14:902-16.

- [29] Welt FG, Losordo DW. Cell therapy for acute myocardial infarction: curb your enthusiasm? *Circulation*. 2006;113:1272-4.
- [30] Iba O, Matsubara H, Nozawa Y, Fujiyama S, Amano K, Mori Y. Angiogenesis by implantation of peripheral blood mononuclear cells and platelets into ischemic limbs. *Circulation*. 2002;106:2019-25.
- [31] Hur J, Yoon CH, Kim HS, Choi JH, Kang HJ, Hwang KK. Characterization of two types of endothelial progenitor cells and their different contributions to neovasculogenesis. *Arterioscler Thromb Vasc Biol*. 2004;24:288-93.
- [32] Yoon CH, Hur J, Oh IY, Park KW, Kim TY, Shin JH. Intercellular adhesion molecule-1 is upregulated in ischemic muscle, which mediates trafficking of endothelial progenitor cells. *Arterioscler Thromb Vasc Biol*. 2006;26:1066-72.
- [33] Rosenzweig A. Cardiac cell therapy--mixed results from mixed cells. *N Engl J Med*. 2006;355:1274-7.
- [34] Hofmann M, Wollert KC, Meyer GP, Menke A, Arseniev L, Hertenstein B. Monitoring of bone marrow cell homing into the infarcted human myocardium. *Circulation*. 2005;111:2198-202.
- [35] Laflamme MA, Murry CE. Regenerating the heart. *Nat Biotechnol*. 2005;23:845-56.
- [36] Mooney DJ, Vandenburgh H. Cell delivery mechanisms for tissue repair. *Cell Stem Cell*. 2008;2:205-13.
- [37] Tongers J, Webber MJ, Losordo DW. Bioengineering to enhance progenitor cell therapeutics. *Tex Heart Inst J*. 2009;36:140-4.
- [38] Penn MS, Mangi AA. Genetic enhancement of stem cell engraftment, survival, and efficacy. *Circ Res*. 2008;102:1471-82.
- [39] Chavakis E, Koyanagi M, Dimmeler S. Enhancing the outcome of cell therapy for cardiac repair: progress from bench to bedside and back. *Circulation*. 2010;121:325-35.
- [40] Dimmeler S, Zeiher AM. Wanted! The best cell for cardiac regeneration. *J Am Coll Cardiol*. 2004;44:464-6.
- [41] Peichev M, Naiyer AJ, Pereira D, Zhu Z, Lane WJ, Williams M. Expression of VEGFR-2 and AC133 by circulating human CD34(+) cells identifies a population of functional endothelial precursors. *Blood*. 2000;95:952-8.
- [42] Urbich C, Dimmeler S. Endothelial progenitor cells: characterization and role in vascular biology. *Circ Res*. 2004;95:343-53.

- [43] Oikawa A, Siragusa M, Quaini F, Mangialardi G, Katare RG, Caporali A. Diabetes mellitus induces bone marrow microangiopathy. *Arterioscler Thromb Vasc Biol.* 2010;30:498-508.
- [44] Invernici G, Emanuelli C, Madeddu P, Cristini S, Gadau S, Benetti A. Human fetal aorta contains vascular progenitor cells capable of inducing vasculogenesis, angiogenesis, and myogenesis in vitro and in a murine model of peripheral ischemia. *Am J Pathol.* 2007;170:1879-92.
- [45] Barcelos LS, Duplaa C, Krankel N, Graiani G, Invernici G, Katare R. Human CD133+ progenitor cells promote the healing of diabetic ischemic ulcers by paracrine stimulation of angiogenesis and activation of Wnt signaling. *Circ Res.* 2009;104:1095-102.
- [46] Campagnolo P, Cesselli D, Al Haj Zen A, Beltrami AP, Krankel N, Katare R. Human adult vena saphena contains perivascular progenitor cells endowed with clonogenic and proangiogenic potential. *Circulation.* 2010;121:1735-45.
- [47] Katare R, Riu F, Mitchell K, Gubernator M, Campagnolo P, Cui Y. Transplantation of human pericyte progenitor cells improves the repair of infarcted heart through activation of an angiogenic program involving micro-RNA-132. *Circ Res.* 2011;109:894-906.
- [48] LaVan DA, Lynn DM, Langer R. Moving smaller in drug discovery and delivery. *Nat Rev Drug Discov.* 2002;1:77-84.
- [49] Langer R. New methods of drug delivery. *Science.* 1990;249:1527-33.
- [50] Moghimi SM, Hunter AC, Murray JC. Nanomedicine: current status and future prospects. *FASEB J.* 2005;19:311-30.
- [51] Kim J, Mooney DJ. In vivo modulation of dendritic cells by engineered materials: towards new cancer vaccines. *Nano Today.* 2011;6:466-77.
- [52] Thiele L, Diederichs JE, Reszka R, Merkle HP, Walter E. Competitive adsorption of serum proteins at microparticles affects phagocytosis by dendritic cells. *Biomaterials.* 2003;24:1409-18.
- [53] Mitragotri S, Lahann J. Physical approaches to biomaterial design. *Nat Mater.* 2009;8:15-23.
- [54] Kawaguchi H, Koiwai N, Ohtsuka Y, Miyamoto M, Sasakawa S. Phagocytosis of latex particles by leucocytes. I. Dependence of phagocytosis on the size and surface potential of particles. *Biomaterials.* 1986;7:61-6.
- [55] Chen H, Langer R, Edwards DA. A film tension theory of phagocytosis. *J Colloid Interface Sci.* 1997;190:118-33.

- [56] Champion JA, Walker A, Mitragotri S. Role of particle size in phagocytosis of polymeric microspheres. *Pharm Res.* 2008;25:1815-21.
- [57] Seliger B. Strategies of tumor immune evasion. *BioDrugs.* 2005;19:347-54.
- [58] Cao Y. Angiogenesis: What can it offer for future medicine? *Exp Cell Res.* 2010;316:1304-8.
- [59] Lambert JM, Lopez EF, Lindsey ML. Macrophage roles following myocardial infarction. *Int J Cardiol.* 2008;130:147-58.
- [60] Zhu L, Chen L, Cao QR, Chen D, Cui J. Preparation and evaluation of mannose receptor mediated macrophage targeting delivery system. *J Control release.* 2011;152 Suppl 1:e190-1.
- [61] Ruan GX, Chen YZ, Yao XL, Du A, Tang GP, Shen YQ. Macrophage mannose receptor-specific gene delivery vehicle for macrophage engineering. *Acta Biomater.* 2014;10:1847-55.
- [62] Harris N, Super M, Rits M, Chang G, Ezekowitz RA. Characterization of the murine macrophage mannose receptor: demonstration that the downregulation of receptor expression mediated by interferon-gamma occurs at the level of transcription. *Blood.* 1992;80:2363-73.
- [63] Quint C, Kondo Y, Manson RJ, Lawson JH, Dardik A, Niklason LE. Decellularized tissue-engineered blood vessel as an arterial conduit. *Proc Natl Acad Sci U S A.* 2011;108:9214-9.
- [64] Niklason LE. Building stronger microvessels. *Nat Biotechnol.* 2011;29:405-6.
- [65] Sundaram S, Niklason LE. Smooth muscle and other cell sources for human blood vessel engineering. *Cells Tissues Organs.* 2012;195:15-25.
- [66] Niklason LE, Gao J, Abbott WM, Hirschi KK, Houser S, Marini R, Langer, R. Functional arteries grown in vitro. *Science.* 1999;284:489-93.
- [67] Gui L, Boyle MJ, Kamin YM, Huang AH, Starcher BC, Miller CA, Niklason, L. Construction of tissue-engineered small-diameter vascular grafts in fibrin scaffolds in 30 days. *Tissue Eng Part A.* 2014;20:1499-507.
- [68] Richmond A, Su Y. Mouse xenograft models vs GEM models for human cancer therapeutics. *Dis Model Mech.* 2008;1:78-82.
- [69] Luconi M, Mannelli M. Xenograft models for preclinical drug testing: implications for adrenocortical cancer. *Mol Cell Endocrinol.* 2012;351:71-7.
- [70] Suggitt M, Bibby MC. 50 years of preclinical anticancer drug screening: empirical to target-driven approaches. *Clin Cancer Res.* 2005;11:971-81.
- [71] Chen K, Ahmed S, Adeyi O, Dick JE, Ghanekar A. Human solid tumor xenografts in immunodeficient mice are vulnerable to lymphomagenesis associated with Epstein-Barr virus. *PLoS One.* 2012;7:e39294.

[72] Nilsson B, Korsgren O, Lambris JD, Ekdahl KN. Can cells and biomaterials in therapeutic medicine be shielded from innate immune recognition? *Trends Immunol.* 2010;31:32-8.

[73] Boehler RM, Graham JG, Shea LD. Tissue engineering tools for modulation of the immune response. *BioTechniques.* 2011;51:239-40.

## **Appendices**

**A List of reagents / Compounds used****Table A.1: List of compounds and reagents used in this study**

| <b>Material</b>                               | <b>Supplier</b>                             |
|-----------------------------------------------|---------------------------------------------|
| Agarose                                       | Sigma-Aldrich Ireland Ltd., Dublin, Ireland |
| Ampicillin                                    |                                             |
| Bovine serum albumin                          |                                             |
| Sulphuric acid                                |                                             |
| Tetrahydrofuran                               |                                             |
| 2, methoxy ethylamine                         |                                             |
| Poly-D-glutamic acid                          |                                             |
| Bicinchoninic acid                            |                                             |
| 2-(N-morpholino)ethanesulfonic acid           |                                             |
| N-hydroxysuccinimide                          |                                             |
| 1-Ethyl-3-(3-dimethylaminopropyl)carbodiimide |                                             |
| Sodium cacodylate                             |                                             |
| Elastase                                      |                                             |
| Protease                                      |                                             |
| LB agar                                       |                                             |
| DMEM                                          |                                             |
| Isopropanol                                   |                                             |
| Uranyl acetate hydrate                        |                                             |
| Tetramethylethylenediamine                    |                                             |
| DMSO                                          |                                             |
| Eosin                                         |                                             |
| Ethanol                                       |                                             |
| Fetal bovine serum                            |                                             |
| Fish gelatin                                  |                                             |
| Formaldehyde                                  |                                             |
| Glutaraldehyde                                |                                             |
| Glycerol                                      |                                             |
| Goat serum                                    |                                             |
| Hank's balanced salt solution                 |                                             |
| Hematoxylin                                   |                                             |
| Kanamycin                                     |                                             |
| LB agar                                       |                                             |
| LB broth                                      |                                             |
| L-Glutamine                                   |                                             |
| Polystyrene beads 100 and 300nm               |                                             |
| Penicillin-streptomycin                       |                                             |
| Phosphate buffered saline                     |                                             |
| Potassium ferrocyanide / ferricyanide         |                                             |
| RNAse away                                    |                                             |
| Sodium carbonate / bicarbonate                |                                             |

**Table A.1 continued: List of compounds and reagents used in this study**

| <b>Material</b>                              | <b>Supplier</b>                             |
|----------------------------------------------|---------------------------------------------|
| Nonidet™ P-40                                | Sigma-Aldrich Ireland Ltd., Dublin, Ireland |
| Spam80                                       |                                             |
| Tris hydrochloride                           |                                             |
| Triton® X-100                                |                                             |
| Trypsin-EDTA                                 |                                             |
| EDTA                                         |                                             |
| Tris Base                                    |                                             |
| SDS-PAGE reagents                            |                                             |
| Tween 20                                     |                                             |
| MTT                                          |                                             |
| Xylene                                       |                                             |
| Proteinase K                                 |                                             |
| Paraformaldehyde                             |                                             |
| Glycerol                                     |                                             |
| DPX mountant                                 |                                             |
| TBE buffer                                   | Gentaur, Brussels                           |
| Polystyrene beads of 500, 1000 and 10,000 nm |                                             |
| Tetramethylethylenediamine                   | Biorad, USA                                 |
| Anti-CD31                                    | Abcam, UK                                   |
| Anti-CD80                                    |                                             |
| Quant-iT™ PicoGreen® dsDNA kit               | Invitrogen, Ireland                         |
| alamarBlue®                                  |                                             |
| 4',6-diamidino-2-phenylindole (DAPI)         |                                             |
| TO-PRO®-3 stain                              |                                             |
| Rhodamine phalloidin                         |                                             |
| Fluorescein isothiocyanate                   |                                             |
| Lysotracker® Blue DND-22                     |                                             |
| SimplyBlue™ SafeStain                        | Qiagen, West Sussex, UK                     |
| Giga prep plasmid kit                        |                                             |
| Rneasy® kit                                  |                                             |
| Deoxynucleotide solution mix                 |                                             |
| Reverse transcriptase                        |                                             |
| Nuclease-free water                          |                                             |
| Oligo (dT) primers                           |                                             |
| PCR core system I                            |                                             |
| Random primer (20µg)                         |                                             |
| Fast SYBR® green master mix                  |                                             |
| PCR array                                    | Qiagen, West Sussex, UK                     |
| TissueRuptor™                                |                                             |

**Table A.1 continued: List of compounds and reagents used in this study**

| <b>Material</b>                                      | <b>Supplier</b>                                     |
|------------------------------------------------------|-----------------------------------------------------|
| Label IT <sup>®</sup> Cy <sup>™</sup> 5 labeling kit | Mirus Bio, Madison, WI, USA                         |
| 6000 Nano LabChip <sup>®</sup> kit                   | Agilent Technologies, Dublin, Ireland               |
| XL1-Blue supercompetent cells                        |                                                     |
| Human umbilical artery smooth muscle cells (HUASMC)  |                                                     |
| Endothelial cell growth medium kit                   | R & D Systems, USA                                  |
| Human eNOS ELISA kit                                 |                                                     |
| Human IL-10 ELISA kit                                |                                                     |
| Mouse inflammatory cytokine multiplex array          | Meso Scale Discovery, Gaithersburg, MD, USA         |
| SECTOR <sup>®</sup> Imager 2400                      |                                                     |
| Gaussia princeps luciferase detection kits           |                                                     |
| Gaussia princeps luciferase plasmid DNA (Gluc)       | New England Biosciences, Ipswich, USA               |
| Bicinchoninic acid assay                             | Pierce, Rockford, USA                               |
| TNBSA kit                                            |                                                     |
| H & E staining kit                                   | Polysciences, Eppelheim, Germany                    |
| THP1 cells                                           | ATCC, USA                                           |
| Human IL-10 plasmid                                  | OriGene, USA                                        |
| Agar low viscous resin kit                           | Agar Scientific, UK                                 |
| SEM carbon tabs                                      |                                                     |
| Carbon coated copper grids                           |                                                     |
| Glass coverslips                                     | Thermonax <sup>™</sup> , Fisher Scientific, Ireland |
| Propylamine polyethylene glycol                      | Sunbright, Japan                                    |
| In Cell Analyzer 1000 <sup>™</sup>                   | GE, Healthcare, USA                                 |

**B. Chitosan/PGA Hollow Spheres***Sulfonation of Polystyrene Nanoparticles*

1. Take 1.7 gm of polystyrene (PS) nanoparticles in a round bottom flask.
2. Disperse in 60 ml of sulfuric acid
3. Sonicate to make the mixture well dispersed.
4. Raise the temperature of the flask to a constant of 40<sup>0</sup> C for a period of 18 hr.
5. Centrifuge at 6000 rpm it first and through the supernatant.
6. Again centrifuge it with ethanol for twice followed by water.
7. Lyophilize to get the particles.

*Preparation of Hollow Spheres*

1. Disperse the sulfonated nanoparticles in 100 ml of 1% acetic acid solution in water.

2. Prepare 0.5% wt of chitosan in 1% acetic acid solution at 0<sup>0</sup> C.
3. Mix 7 ml of the polymeric mixture with the sulfonated PS beads and agitate it in a mechanical shaker for 24 hr at 4<sup>0</sup> C.
4. In a separate round bottom flask , under stirring condition mix poly(glutamic acid) 77 mg in MES (20 ml), NHS (26 mg) and EDC (40  $\mu$ l) for 5 min at room temperature.
5. Add it to the suspension of sulfonated polystyrene beads coated with chitosan.
6. Crosslinking with EDC/NHS for 24 hr in a mechanical shaker.
7. Mix Tetrahydrofuran (THF) three times the mixture and centrifuge it at 4000 rpm several times to get the hollow spheres.
8. Wash the collected pellets for 3-4 times with THF and centrifuge.

### **C. Elastin-like Polypeptide (ELP) Hollow Sphere Fabrication**

#### *Purification of Microbial Transglutaminase*

1. Dissolve the mTGase sample in 20 mM sodium acetate buffer pH 5.8 at a concentration of 500 mg/ml.
2. Add the mTGase sample to a glass column (1.5 x 30 cm) containing CM52 cation exchange resin pre-equilibrated with the above buffer at a flow rate of 2 ml/min.
3. Wash the sample with two column volumes of the same buffer and elute by a gradient of 10 column volumes from 0 to 0.5 M sodium chloride.
4. Analyze the samples at 280 nm for protein.
5. Concentrate the pooled fractions, dialyze into PBS and analyze for enzyme activity using the transglutaminase colorimetric micro assay kit.

#### *ELP Hollow Sphere Fabrication using a Template Method*

1. ELP was kindly gifted by Elastin Specialties. Inc, Toronto, Canada.
2. PS beads of various sizes are available commercially from Sigma and Gentaur.
3. Sulfonate PS beads of various sizes.
4. Dissolve ELP and sulfonate PS beads in cold PBS at a ratio of 100 mg of PS beads to 5 mg of ELP. Keep the total amount of solution at 3 ml.
5. Mix it properly and incubate in a water bath at 37  $^{\circ}$ C for 5min.
6. Wash the mixture with deionized water for three times.
7. Re-suspend the ELP coated PS beads in 3 ml of deionized water.
8. Incubate with mTGase with 50U/mg of ELP at room temperature on shaker for overnight or for 1hr at 37  $^{\circ}$ C.

9. Wash the cross-linked ELP-PS beads three times with deionized water.
10. Spin the tube containing ELP-PS beads at 9000 rpm for 10 min.
11. Take out the supernatant and re-suspend the pellet with THF.
12. Repeat the process for three times.
13. Remove THF and re-suspend the pellet with water.
14. Keep the tube under the hood for overnight to evaporate the residual THF.
15. Wash the spheres in deionized water for three times and finally re-suspend with 70% ethanol to sterilize them.
16. Wash the spheres three times with PBS and keep them suspended for further use.

#### *Size and Charge Analysis of Hollow Spheres*

1. Switch on the zeta sizer (Malvern, Nano-ZS90) instrument and set the temperature to 25 °C. Give the laser at least 20 min to warm up.
2. Prepare the hollow spheres in PBS. Make sure that the samples are free of any free of unwanted dust/aggregates and bubbles.
3. Prepare the cuvette. Make sure that the cuvette is clean and free of dust. Rinse the cuvette three times with water followed by three times with absolute ethanol.
4. Transfer the hollow spheres sample to cuvette.
5. Close the cuvette to prevent dust.
6. Wipe the cuvette from outside with a lens paper.
7. Insert the cuvette into the sample holder of the zeta sizer.
8. Give the sample atleast 5 min to equilibrate before starting the software.
9. Start the software and analyze the samples for both size and charge.

#### **D. Dual Delivery Injectable ELP-Based System**

1. Dissolve ELP of 5mg in 50  $\mu$ l cold water (10% W/V of ELP).
2. Add mTGase (in powder) of 100U/g of ELP into the ELP solution, without changing the total volume.
3. Incubate the ELP and mTGase mixture at 37 °C for 10 min to get the scaffold
4. Prepare polyplexes using concentrated pDNA (10ug/ $\mu$ l).
5. To prepare polyplex add 3  $\mu$ l of SuperFect<sup>®</sup>/ $\mu$ g of pDNA.
6. In order to prepare the polyplex 10  $\mu$ g of DNA, add 30  $\mu$ l of SuperFect<sup>®</sup> to 1 $\mu$ l of pDNA containing 10  $\mu$ g of pDNA. And for 20  $\mu$ g of pDNA 60  $\mu$ l of SuperFect<sup>®</sup>.

7. To encapsulate 10  $\mu\text{g}$  of polyplexes (30  $\mu\text{l}$ ). Add ELP 6 mg, mTGase as needed (100U/g of ELP) and spheres loaded or 250  $\mu\text{g}$  unloaded pDNA.
8. Add extra 30  $\mu\text{l}$  of water and keep at 37  $^{\circ}\text{C}$  the mixture of solution to solidify as a scaffold.

### E. Trinitrobenzene Sulfonic Acid Assay

1. Prepare a standard curve with Glycine in sodium bicarbonate pH 8.5 (0.1M) (H<sub>2</sub>N-CH<sub>2</sub>-COOH) (100nm, 50nm, 25nmol, 10nm, 5nmol and 0nm).
2. Add 250 $\mu\text{L}$  of 0.01% TNBSA in 0.5mL of each sample. Mix well.

Stock solution at 5% w/v:  $C_1V_1=C_2V_2$

$$V_1 = 22\mu\text{l of the initial solution}$$

$\Rightarrow$  Dilution in sodium bicarbonate buffer

3. Incubate at 37  $^{\circ}\text{C}$  for 2 h.
4. Add 250 $\mu\text{l}$  of 10% SDS + 125 $\mu\text{l}$  of 1M HCl.
5. Measure the absorbance at 335nm.

$\Rightarrow$  Use glass cuvette

$\rightarrow$  Plate reader is working as well (new one)

In order to hydrolyse the ELP scaffold/sphere, the samples are incubated at 120 $^{\circ}\text{C}$  during 15min or can be autoclaved after reaction (add the HCl and after autoclave).

The absorbance is measured at 335nm as the standard curve.

#### ***Solution:***

*Sodium bicarbonate buffer pH8.5 0.1M*

*MW: 84g/mol*

$$m = CVM$$

$$m = 0.1 \times 250 \times 10^{-3} \times 84$$

$$m = 2.1\text{g}$$

*Adjust the pH at 8.5*

### F. Bicinchoninic Acid Assay

1. Mix reagent A and B in a ratio of 1:20 to prepare the working solution.
2. Pipette 100  $\mu\text{l}$ /well of working solution into 96 well microplate.
3. In order to prepare a standard curve add a gradient volume of standard BSA protein to each well followed by adding of ELP sample protein.

4. Mix wells thoroughly with pipet and incubate at 37 °C for 30 min- 1hr.
5. Measure the absorbance at 562 nm in a plate reader.
6. Calculate the amount of ELP from the standard curve.

## **G. Cell Culture**

### *Thawing Cells*

1. Wear protective gloves and face shield and remove tube containing cells from liquid nitrogen cylinder.
2. Thaw the contents of tube by rubbing in palm or in water bath at 37 °C.
3. Transfer the contents of the tube in 15 ml falcon tube containing 10 ml of appropriate media.
4. Centrifuge the tube at 1500 rpm for five minutes.
5. Remove the supernatant and discard.
6. Add 1 ml of pre-warmed media with gentle aspiration to homogeneously distribute cells.
7. Count cells using hemocytometer.
8. Transfer 1 ml of cells (of known cell density) to a new T75 flask or as appropriate.
9. Add 9 ml or appropriate amount of culture media.
10. Label the flask with name, date and cell type.
11. Place the flask in an incubator set at 37 °C and 5% CO<sub>2</sub>.
12. Refresh media every 2-3 days or as per requirement.

### *Culturing Cells*

1. Monitor cells using bright light microscope.
2. If cells are starting to float or media changes color, take off old media and rinse the cells using PBS.
3. Add fresh appropriate culture media.
4. Monitor cells for confluence.
5. When the cells are ready to split (70-80 % confluent), pipette out the media.
6. Rinse cells using 10ml PBS, and pour off PBS.
7. Add 5 ml of trypsin/EDTA and either incubate at 37°C or room temperature (for HUASMCs and HUVECs) for five minutes.

8. When trypsin starts to lift cells from the flask, tap the bottom of flask and bring cells to the corner.
9. Use cell scraper if needed.
10. Add 5 ml of serum containing media to halt the action of trypsin.
11. Rinse the bottom of the flask with this solution several times.
12. Transfer the contents in 15 ml tube and centrifuge the tube at 1500 rpm for five minutes.
13. Discard the supernatant and resuspend the cell pellet in 3 ml or appropriate amount of fresh culture media.
14. Count the cells using hemocytometer.
15. Plate the cells (with known density) in three new flasks with sufficient appropriate culture media.

#### *Counting Cells*

1. Trypsinize cells as above.
2. Add equal amount of serum containing media, aspirate several times and transfer the cell suspension to a new tube.
3. Ensure the hemocytometer is clean using 70% ethanol.
4. Take 10 $\mu$ l of cell suspension and add 10 $\mu$ l of trypan blue.
5. Take 20 $\mu$ l of this solution and add 10 $\mu$ l to each side of the hemocytometer under the cover slip.
6. Allow the sample to be drawn out of the pipette by capillary action, the fluid should run to the edges of the grooves.
7. Focus on the grid lines of the hemocytometer using the 10X objective of the microscope.
8. Focus on one set of 16 corner square as indicated by the circle in Figure G.1.
9. Count the number of cells in this area of 16 squares.
10. Count only healthy cells unstained by trypan blue.
11. Count cells that are within the square and any positioned on the right hand or bottom boundary line.
12. Dead cells stained blue with trypan blue can be counted separately for a viability count.

13. Move the hemocytometer to another set of 16 corner squares and carry on counting until all 4 sets of 16 corner squares are counted.
14. Get the average count and then multiply by two to adjust for the 1:2 dilution in trypan blue.
15. This is equivalent to number of cells  $\times 10^4$  /ml.
16. Finally total number of cells can be obtained by multiplying the above number by the volume of cell suspension.

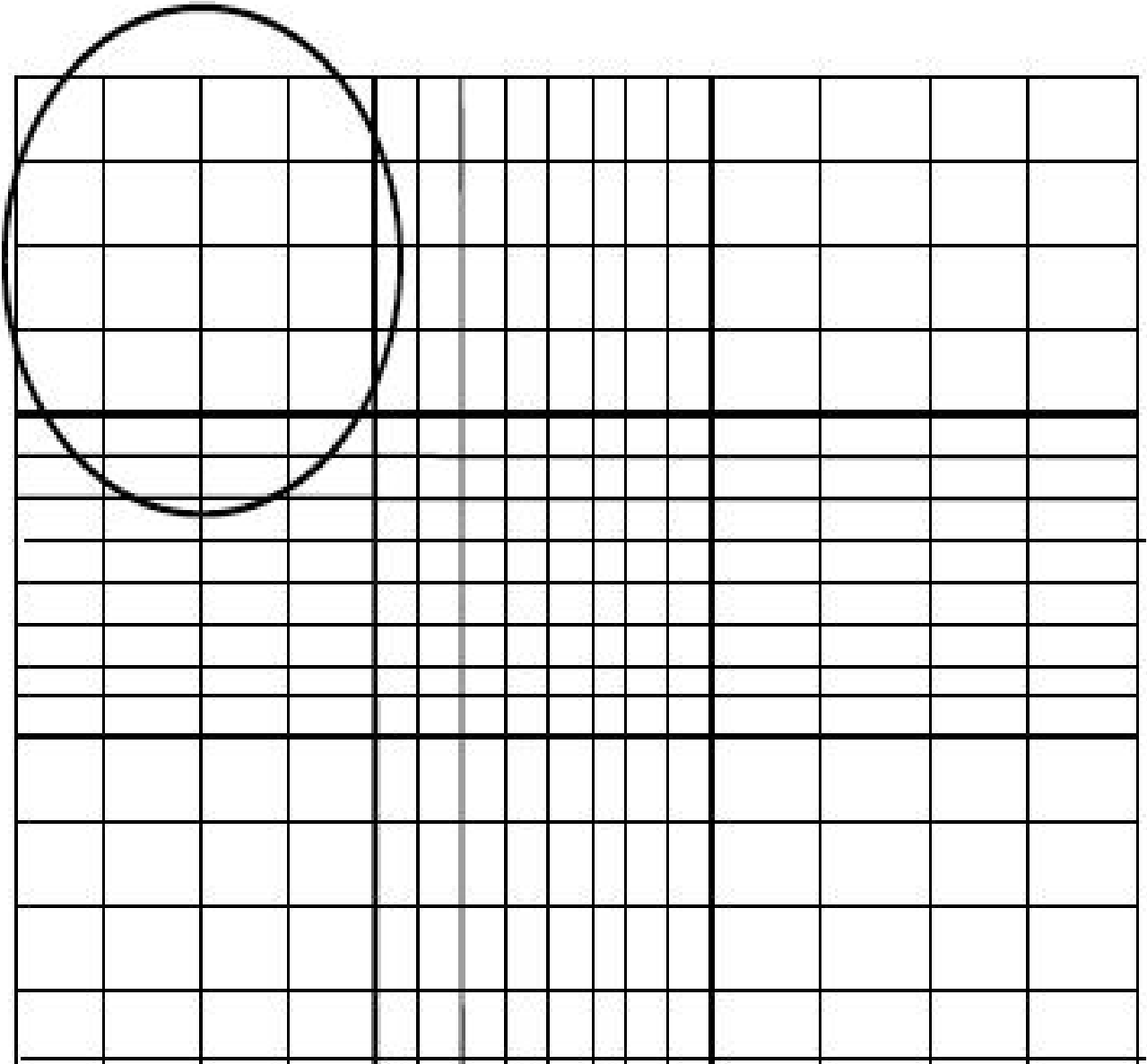


**Figure A.1: Gridlines on hemocytometer.**

*Freezing Cells*

1. Trypsinize cells as above and centrifuge to form cell pellet.
2. Resuspend the pellet in adequate amount of freezing medium (40% FBS + 10% DMSO + 50% media).
3. Pipette up and down several times gently to ensure homogenous suspension.
4. Transfer 1 ml of cell suspension to each freezing vial, giving the  $1 \times 10^6$  cells per vial.
5. Label each tube with date, cell line, passage number and initials.
6. Transfer the vials to  $-80^\circ\text{C}$  freezer overnight and then to liquid nitrogen.
7. Ensure that sufficient amount of liquid nitrogen is maintained in the tank.

**H. Cell Viability Assays***MTT Assay*

1. Prepare MTT solution of 5 mg/ml in PBS.
2. Remove tissue culture plate from incubator and add MTT solution in an amount equal culture volume in the laminar hood.
3. Incubate the tissue culture plate for 3 hr in the incubator.
4. Remove the medium without disturbing the cells.
5. Add 150  $\mu\text{l}$  DMSO.
6. Spin the tissue culture plate in a centrifuge at 4000 rpm for 15 min.
7. Measure the absorbance at 590 nm.

*Alamar Blue Assay*

1. Seed cells (HUVECS, ADSCs, HUASMCs) at a cell density of  $2 \times 10^4$  cell/well in a 48 well tissue culture plate.
2. Grow for 12 hr before incubating with hollow spheres.
3. Incubate the spheres for 48 hr before removing the medium.
4. Wash twice with HBSS and replace with 200  $\mu\text{L}$  of fresh HBSS with alamarBlue<sup>®</sup> (10% v/v).
5. Incubate for 3 hr at  $37^\circ\text{C}$  in 5%  $\text{CO}_2$ .
6. After the incubation transfer 200  $\mu\text{L}$  of assay to a 96 well plate.
7. Read the absorbance at 550 and 595 nm on a microplate reader and calculate the percentage reduction of the dye.

## **I. *In Vitro* Transfection Study**

### *Plating the Cells*

1. Pre-heat culture media for 30 minutes in a 37°C water bath.
2. One confluent T75 flask is needed for each 24 well plate.
3. Use a 24 well tissue culture plate.
4. Trypsinize cells as above.
5. Add 3ml of media and aspirate several times as above.
6. Transfer 500µl of cells suspension to each of the wells across the plate.
7. Overlay every well with 1ml of media, and incubate 37 °C overnight.
8. After 24 hours, cells should be 70-80% confluent and ready for transfection.

### *Transfecting Cells*

1. Prepare fresh samples of ELP hollow spheres/polyplex system and also defrost samples of collected elution samples from the ELP hollow spheres/polyplex at different time points.
2. Prepare polyplexes freshly with 1µg pDNA as a positive control.
3. Take 24 well plate cultured cells from incubator and remove media.
4. Rinse cells with PBS, and add 1ml of media.
5. Add the contents of one collected sample vial to each well, ensuring to label lid of plate adequately.
6. Incubate plates at 37 °C for 48 hr.
7. Cells and medium are ready for analysis by fluorescent microscopy and GLuc assay.

### *GLuc Analysis*

(As according to New England Biolabs recommended protocol)

1. Prepare 1x Gluc assay solution by dilution buffer 1 to 100.
2. Put 15-25µL into well plate or sample tube as appropriate to the plate reader (just be consistent). Dilute if necessary.
3. Add 50µL of the Gluc solution to each well (again, if initial experiments showed it was too bright, dilute).
4. Add PBS to dilute up to 150µL for the current plate reader.
5. If possible, read within 5-10 sec.

## **J. *In Vitro* Internalization Study**

### *Flow Cytometry Analysis*

1. Pre-heat culture media for 30 min in a 37 °C water bath.
2. One confluent T75 flask is needed for two T25 flasks.
3. Use a T25 flask to seed the cells (HUVECS, HUASMCs and THP1 cells).
4. Trypsinize cells as above.
5. Add 3ml of media and aspirate several times as above.
6. Transfer 1.5ml of cells suspension to each of the T25 flasks.
7. Overlay each flask with 5ml of media, and incubate 37 °C overnight.
8. After 24 hr, cells should be 70-80% confluent and ready for internalization study.
9. 1mg of FITC-labelled ELP hollow spheres were incubated for various time points and analyzed using flow cytometry.

### *High Content Analysis*

1. Precoat 96-well plates with 0.1% gelatin.
2. Seed cells (HUVECS and HUASMCs) at a density of ~16 000 cells/well in 100- $\mu$ l culture medium and culture it for 48 hr.
3. Seed FITC-Chitosan/PGA hollow spheres and incubate for 6, 12 and 24 and 48 hr.
4. Cells were fixed after desired incubation time and stained for nucleus with TO-PRO-3-iodide.
5. Switch on In Cell Analyzer 1000<sup>TM</sup>, GE Healthcare instrument.
6. Image on the IN Cell Analyzer 1000<sup>TM</sup>.
7. Analyze the images using the dual area object analysis module.

## **K. Plasmid DNA Expansion**

### *LB Agar Plates*

1. Add 7.5 g agar per 500 ml media in a 1 L flask.
2. Cover the flask with foil and sterilize by autoclaving.
3. When removed allow it to cool until it can be handled comfortably. Obviously, do not cool down too much or else it will start to solidify.
4. Prepare Bunsen burner and plates.
5. Remove the foil covering the flask with the LB agar.
6. Run the top across the Bunsen flame.

7. Add antibiotics. Mix well by swirling. Typical antibiotic final concentrations:
  - Kanamycin 30-50  $\mu\text{g/ml}$  or
  - Ampicillin 100  $\mu\text{g/ml}$
8. Pour into the plates in close vicinity to the flame.
9. Let plates set at room temperature.
10. Label the plates with date and antibiotic used and username, seal each plate with paraffin film and store in cold room (4 – 8<sup>o</sup>C).

#### *Transformation*

1. Turn on the water bath and set the temperature to 42<sup>o</sup>C.
2. Take out the plates for transformation and place at room temperature to warm up.
3. Fill ice in the ice box.
4. Take 1  $\mu\text{g}$  of plasmid DNA which is needs to be expanded in a tube. Label the tube.
5. Label another tube as control.
6. Take one tube of XL1Blue (bacteria) from box in -800C freezer and thaw on ice.
7. When thawed add 50  $\mu\text{l}$  bacteria to each tube.
8. Mix by flicking.
9. Leave on ice for 2 min.
10. Place the tubes in waterbath initially set to 42 <sup>o</sup>C for 45 sec.
11. Place the tubes on ice again for 2 min.
12. Repeat the process of heat shock for couple times more.
13. Add 1 ml autoclaved LB broth (without antibiotic) to each tube.
14. Tape up-right on shaker (200 rpm, 37 <sup>o</sup>C) for 1 hour.
15. Prepare plates, Bunsen burner, spreader, 70% ethanol.
16. The optical density of the LB broth will change indicating bacterial growth.
17. Add 100  $\mu\text{l}$  of inoculum in previously prepared LB agar plates containing appropriate antibiotics depending on the plasmid DNA.
18. Take out the spreader from 70% ethanol and burn off quickly in flame. Let it cool off. Touch off edge of LB agar before spreading.
19. Spread the inoculum over the plate.
20. Finish spreading all the plates and let them sit at room temperature for 10 min.

21. Put in incubator at 37 °C with upside down.
22. Take out of the incubator in 8 -10 hr when colonies of bacteria are obvious but still separate and not merged. These plates can be stored up to four weeks for further use.

#### *Plasmid Expansion by Giga Prep*

##### *Giga Prep (as per Instructions Given in Qiagen Plasmid Purification Handbook)*

1. Prepare sterilized lysogeny broth (LB) media (2L; 25g/L) by autoclaving. Add appropriate antibiotic.
2. Pick up a single colony from the agar plate with bacterial culture.
3. Inoculate a started culture using a 15 ml tube.
4. Pour 5 ml of the started culture in 2L of LB media.
5. Incubate the culture at 37 °C with continuous shaking at 200 rpm for 12-16 hrs.
6. Harvest the bacterial culture by spinning at 6000 x g for 15 min at 4°C.
7. Resuspend the bacterial pellet in 125 ml of resuspension buffer and add the same amount of lysis buffer. Mix thoroughly by shaking vigorously for 4–6 times, and incubate at room temperature for 5 min.
9. Add 125 ml of chilled neutralization buffer, mix immediately and thoroughly by vigorous inversion for 4–6 times, and incubate on ice for 30 min. A fluffy white material is formed and the lysate becomes less viscous.
10. Centrifuge at 20,000 x g for 30 min at 4°C and promptly remove supernatant containing plasmid DNA.
11. Centrifuge the supernatant again at 20,000 x g for 15 min at 4°C and promptly remove supernatant containing pDNA. At this stage, 75 µl of cleared lysate supernatant can be removed and saved for analysis.
12. Equilibrate a QIAGEN-tip 10000 by applying 75 ml equilibrium buffer, and allow the column to empty by gravity flow.
13. Apply the supernatant from step 11 to the QIAGEN-tip and allow it to enter the resin by gravity flow.
14. Wash the QIAGEN-tip with 2 x 30 ml wash buffer. Allow wash buffer to move through the QIAGEN-tip by gravity flow.
15. Elute DNA with 15 ml wash buffer. Collect the eluate in a 50 ml tube.

16. Precipitate DNA by adding 10.5 ml room-temperature isopropanol to the eluted DNA. Mix and centrifuge immediately at 15,000 x g for 30 min at 4°C. Carefully decant the supernatant.
17. Wash DNA pellet with 5 ml of room-temperature 70% ethanol, and centrifuge at 15,000 x g for 10 min. Carefully decant the supernatant without disturbing the pellet.
18. Air-dry the pellet for 5–10 min, and redissolve the DNA in a suitable volume of TE buffer. While redissolving, rinse the walls of the tube to collect all DNA.
19. Determine the yield by UV spectrophotometry at 260 nm.

### L. Plasmid Labelling

1. Warm vial containing reagent to room temperature.
2. Prepare labelling reaction.

**Table A.2: Protocol for preparation of DNA labelling reaction mixture**

| Component                   | Max. DNA Content | Lower DNA Content |
|-----------------------------|------------------|-------------------|
| Sterile, ddH <sub>2</sub> O | 25 µL            | 35 µL             |
| 10x labelling buffer A      | 5 µL             | 5 µL              |
| 1 µg/µL DNA sample          | 10 µL            | 5 µL              |
| LabelIT reagent             | 10 µL            | 5 µL              |
| Total volume                | 50 µL            | 50 µL             |

1. Incubate at 37 °C for 1 hr. Spin briefly midway to minimize effects of evaporation.
2. Purify by spinning through microspin column
  - a. Exactly 50µL per column.
  - b. 735 RCF (3000 rpm for 7.3 cm rotor like in small eppendorf centrifuges).
  - c. Vortex to suspend resin.
  - d. Loosen cap ¼ turn and pull out bottom plug.
  - e. Put column into a 1.5 mL centrifuge tube.

- f. Spin for 1 min at 735g.
  - g. Discard buffer, put column in a new tube.
  - h. Apply sample to top of resin.
  - i. Spin at 735g for 2 min.
3. Cap the support tube. Sample concentration is approximately 0.2 $\mu$ g/mL
4. Store protected from light.

#### **M. PicoGreen Assay**

The assay was performed according to the instructions supplied with the kit (Quant-iT™ PicoGreen® dsDNA kit, Invitrogen). The standard curve and experimental protocol are described below.

##### *Preparing the Assay Buffer*

1. Prepare a 1X TE working solution by diluting the concentrated buffer (supplied with the kit) 20-fold with sterile, distilled, DNase-free water.

##### *Preparing the Assay Reagent*

1. Prepare an aqueous working solution of the Quant-iT™ PicoGreen® reagent by making a 200-fold dilution of the concentrated solution in 1X TE buffer.
2. For best results, use this solution within few hours of its preparation and protect from light by covering with tin foil.
3. Handle with care as this reagent binds with DNA. Although there is no data available, still the reagent should be considered as mutagen and hence appropriate care should be taken.

##### *DNA Standard Curve*

Following points must be considered while preparing standard curves:

- For making standard curve, use same or similar dsDNA as in the experimental samples.
- Treat the dsDNA solution for standard curve in the same way as the experimental samples are treated.
- Prepare the dsDNA solution for standard curve with same level of compounds present in the experimental samples as these samples may have confounding effects on the fluorescence reading.

- To minimize photo bleaching effects, keep the time for fluorescence measurement constant for all samples.

Depending on the anticipated levels in the samples, either high range (1 ng/ml to 1 µg/ml) or low range (25 pg/ml to 25 ng/ml) standard curves or both must be prepared.

1. Follow the protocol in Table M1 for high range standard curve.
2. After making these dilutions, mix well and incubate for 2 to 5 min at room temperature. Make sure that the solutions are protected from light.
3. For microplate reader, use 200 µl from each dilution.
4. Measure the sample fluorescence using a fluorescence microplate reader and standard fluorescein wavelengths (excitation ~480 nm, emission ~520 nm).
5. Adjust the gain in the reader to accommodate highest fluorescence signals.
6. Subtract the fluorescence value of the reagent blank from that of each of the samples.
7. Use corrected data to generate a standard curve of fluorescence versus DNA concentration.
8. For low range standard curve from 25 pg/ml to 25 ng/ml, prepare a 40-fold dilution of the 2 µg/ml DNA solution to yield a 50 ng/ml DNA stock solution.
9. Follow protocol in Table M2 for the making the low range standard curve.
10. Continue as in steps 2 to 4.
11. Adjust the gain in the reader to accommodate the lowest fluorescence signals.
12. Continue with steps 6 and 7.

#### *Sample Analysis*

1. Dilute the experimental samples with known suitable dilution factor to a final volume of 100 µl.
2. Add 100 µl of the aqueous working solution of the Quant-iT™ PicoGreen® reagent to each sample.
3. Incubate for 2 to 5 minutes at room temperature, protected from light.
4. Measure the fluorescence of the sample using instrument parameters that correspond to those used when generating standard curve.
5. Subtract the fluorescence value of the reagent blank from that of each of the samples.

**Table A.3: Protocol for the preparation of high range standard curve**

| Volume of TE/Buffer in Experimental Samples (µl) | Volume of 2µg/ml pDNA Stock (µl) | Volume of Diluted Reagent (µl) | Final pDNA Concentration |
|--------------------------------------------------|----------------------------------|--------------------------------|--------------------------|
| 0                                                | 1000                             | 1000                           | 1 µg/ml                  |
| 900                                              | 100                              | 1000                           | 100 ng/ml                |
| 990                                              | 10                               | 1000                           | 10 ng/ml                 |
| 999                                              | 1                                | 1000                           | 1 ng/mL                  |
| 1000                                             | 0                                | 1000                           | blank                    |

**Table A.4: Protocol for preparing low range standard curve**

| Volume of TE/Buffer in Experimental Samples (µl) | Volume of 50 ng/ml pDNA Stock (µl) | Volume of Diluted Reagent (µl) | Final pDNA Concentration |
|--------------------------------------------------|------------------------------------|--------------------------------|--------------------------|
| 0                                                | 1000                               | 1000                           | 1 µg/ml                  |
| 900                                              | 100                                | 1000                           | 100 ng/ml                |
| 990                                              | 10                                 | 1000                           | 10 ng/ml                 |
| 999                                              | 1                                  | 1000                           | 1 ng/mL                  |
| 1000                                             | 0                                  | 1000                           | blank                    |

- Determine the DNA concentration of the sample from the standard curve generated in DNA standard curve. The assay may be repeated using a different dilutions of the sample to confirm the quantitative results.

## **N. Electrophoresis**

### *Agarose Gel Electrophoresis*

#### *Materials Needed*

- Agarose
- TAE buffer
- 6X sample loading buffer
- DNA ladder standard

- Electrophoresis chamber
- Power supply
- Gel casting tray and combs
- SYBR<sup>®</sup> Safe DNA gel stain
- Staining tray
- Gloves
- Pipette and tips

#### *Recipes*

- TAE Buffer
- 4.84 g Tris Base
- 1.14 ml Glacial Acetic Acid
- 2 ml 0.5M EDTA (pH 8.0)
- Bring the total volume up to 1L with water

#### *Preparing Agarose Gel*

1. Measure 0.7g of agarose powder and add it to 500 ml conical flask.
2. Add 100 ml of TAE buffer to the flask (depending on the number of samples and size of casting tray available, total volume of the gel may vary).
3. Melt the agarose in microwave until the solution becomes clear. Generally it takes around 1 min. Care should be taken not to over boil the solution as it may boil out of the flask.
4. Let the solution cool to about 50-55°C by swirling occasionally for even cooling.
5. Add 10 µl of SYBR<sup>®</sup> Safe DNA gel stain to the solution and mix by swirling.
6. Place appropriate combs in the casting tray at appropriate position.
7. Pour the solution in the gel casting tray. Make sure that the ends of the tray are sealed properly.
8. Allow the gel to cast in the tray until it is solid. It should generally take around 30 min.
9. Pull out the comb carefully.
10. Place the gel in the electrophoresis chamber and add enough TAE buffer so that the level of buffer is at least 2-3 mm over the gel.

*Loading Gel*

11. Note down the order in which samples will be loaded in the gel.
12. On a paraffin film, add 8  $\mu$ l of each DNA sample one beside the other in the sequence the samples will be loaded. Use separate pipette tip each time. Add 2  $\mu$ l of loading dye to each sample.
13. Using a fresh loading tip, mix each sample with the loading dye and load the sample in the appropriate well.
14. Pipette 10  $\mu$ l of the DNA ladder standard in at least one of the wells.
15. If there are empty wells load them with loading dye appropriately diluted in TE.

*Running Gel*

16. Place the lid on the gel box and connect the electrodes correctly (Red to positive and black to negative).
17. Turn on the power supply and set voltage to 100 volts.
18. Check to make sure that current is running through the buffer. This can be confirmed by presence bubbles forming on each electrode.
19. Check that the direction of the current is correct. This can be checked by observing the direction of movement of the blue loading dye after about couple of minutes of running the gel.
20. Let the gel run until the blue dye reaches the end of the gel. This generally would take 30-45 min.
21. Turn off the power supply and disconnect all the wires.
22. Remove the lid of electrophoresis chamber and using gloves carefully remove the gel with the tray.

*Examining the Gel*

23. Place the gel onto the transilluminator and ensure that the safety door of the darkroom cabinet is shut securely.
24. Select SYBR<sup>®</sup> safe filter. The transilluminator should turn on automatically.
25. Observe the image of gel on the computer screen. This image may be adjusted by opening or closing the aperture, or by increasing or decreasing the exposure time.

26. Once satisfied with the adjustments, click “capture” to capture image. At this stage, changes can be made such as cropping the image for new area of interest or enhance by adjusting brightness/contrast etc. Save the image/s.
27. Switch off the darkroom.
28. Remove the gel from the transilluminator, wrap in a tissue paper, discard in appropriate waste bin and wipe dry the transilluminator.

*Sodium Dodecyl Sulfate Polyacrylamide Gel Electrophoresis*

1. Prepare 5ml of stacking and 10 ml of 12% separating gels.
2. Take out the comb after complete gelation of the stacking gel.
3. Prepare the ELP samples by hydrolyzing them with 1N HCL.
4. Mix the ELP solution with sample/loading buffer.
5. Load the prepared ELP sample along with a protein marker.
6. Run the gel for 1 hr at 120V.

**O. Electron Microscopy**

*Fixation, Dehydration and Embedding of Cells for TEM*

*Chemicals and Reagents:*

1. Sodium cacodylate buffer 0.4M (stock solution) - 21.4g sodium cacodylate dissolved in 250 ml H<sub>2</sub>O. Store at 4°C.
2. Sodium cacodylate buffer 0.2M (working solution) - 50 ml 0.4M sodium cacodylate stock + 45 ml H<sub>2</sub>O. Add 1M HCL to adjust pH to 7.2. Bring up to 100 ml with H<sub>2</sub>O. (1M HCL – Add 0.86 ml conc HCL to 9.14 ml H<sub>2</sub>O).
3. Sodium cacodylate buffer 0.1M (50:50 0.2M:H<sub>2</sub>O)
4. Glutaraldehyde 25% EM grade. Store at 4°C.
5. Glutaraldehyde 3% in 0.2M sodium cacodylate buffer. Prepare just before using as follows:
  - 6 ml 25% gluteraldehyde
  - 25 ml 0.2M sodium cacodylate
  - Dilute to 45 ml with H<sub>2</sub>O and adjust to pH 7.3-7.4 with 1M HCl
  - Bring to 50 ml with H<sub>2</sub>O
6. 2% Osmium Tetroxide (HAZARD) = 1 glass vial + 12.5 ml H<sub>2</sub>O in a dark bottle. Allow to dissolve overnight.

7. 1% Osmium Tetroxide = 3 ml OsO<sub>4</sub> + 3 ml H<sub>2</sub>O
8. 30% Ethanol
  - 50% EtOH
  - 70% EtOH
  - 95% EtOH
  - 100% EtOH
9. 50: 50 resin: alcohol
10. 100% resin (1/4 batch of resin is enough for ~6 samples).

*Fixation*

1. Suspend cells in 3% gluteraldehyde in 0.2M cacodylate buffer for 1-2 h. Use 15 ml plastic centrifuge tubes (red caps).
2. Gently spin cells (1000 rpm for 5 min) to get a pellet.
3. Wash cells in 0.1 M cacodylate buffer (5 min x 2 washes).
4. Suspend cells in 1% OsO<sub>4</sub> for 1-2 h in the fume hood. Hazard – take care. Use the same 15 ml plastic centrifuge tube throughout.
5. After fixing in OsO<sub>4</sub>, gently spin cells to get a pellet. Remove OsO<sub>4</sub> and store safely for disposal. Then wash cells in 0.1M cacodylate buffer (5 min x 2 washes).

*Dehydration*

Dehydrate fixed cells in the following sequence:

30% EtOH for 15 min

50% EtOH for 15 min

70% EtOH for 15 min

95% EtOH for 15 min

100% EtOH for 30 min

100% EtOH for 30 min

50:50 EtOH: resin for 60 min or you can leave this to rotate overnight.

*Embedding*

1. Remove the 50:50 resin and replace with 100% resin which must be made fresh if the 50:50 resin has been rotating overnight. Rotate in the 100% resin for 2 h.
2. Embed cells in fresh 100% resin and polymerise for 2-3 days at 60°C in the fume hood.

3. When embedding half fill the moulds with resin, carefully place the specimen upright in the moulds, and then top up with resin. Fill the resin to the top of the mould but not over the top. Check orientation after 1 h. Adjust with a cocktail stick.
4. Polymerise any waste resin. This can then be disposed of in the bin.

#### *Scanning Electron Microscopy*

1. Fix and dehydrate the hollow spheres similarly protocol to those for the TEM.
2. Dry the hollow spheres in oven under vacuum.
3. Mount the hollow spheres samples on an aluminum stub using a carbon tape.
4. Coat the surface with gold using a sputter coater before observing under the microscope.

#### **P. Fluorescent Microscopy**

Fluorescent microscopy was used for *in vitro* transfection study. The cells were grown on glass coverslips (Thermanox™) in 24-well plate. This makes it easier to place the coverslip on glass slide for viewing under microscope.

1. At appropriate time point, remove the media from the cells.
2. Gently wash the coverslips with hank's balanced salt solution.
3. Add 500  $\mu$ l of 4% paraformaldehyde. Note that it takes time for paraformaldehyde to dissolve in PBS so stirring on magnetic hot plate is required. It is wise to prepare the solution a night before the actual experiment.
4. Incubate at room temperature for 15 min to allow fixation.
5. After fixation, remove paraformaldehyde solution and gently wash 2-3 times with PBS.
6. Place the coverslip on the glass slide with cell surface facing the slide. Place a drop of glycerol or DPX (A mixture of distyrene, a plasticizer, and xylene) in the center of glass slide before placing the coverslip.
7. Seal the edges of the glass coverslip with nail polish to prevent the samples from drying out.
8. Focus the cells under microscope and take bright field images.
9. With the same field of view, now change the filter to FITC (green) filter to see green fluorescence from GFP. The bright light should be turned off at this stage.

10. Presence of green fluorescence confirms transfection and comparison with the bright field images confirm that fluorescence is from cells. Internalization of hollow spheres were observed similarly.

#### **Q. Subcutaneous Study Protocol**

1. At time 0, weigh the mice.
2. Anaesthetized the mice using ketamine (80–100 mg/kg i.p.) and xylazine (10 mg/kg i.p.)
3. Shave the back of the mice and also the skin overlying scruff.
4. Swab the shaved area with 4% chlorhexidine or povidone iodine 10% to control bacterial contamination.
5. Inject the four different treatments (eNOS and IL-10 plasmids in injectable ELP system) subcutaneously.
6. After the implantation, place the mice on heating pads or in an incubator until they able to regulate their own temperature and are fully recovered from anaesthesia.
7. Antibiotics were administered for 3-4 days post-surgery in all animals to prevent infection.
8. Euthanize the mice after the set time pints by CO<sub>2</sub> asphyxiation.
9. Excise the injected scaffolds and process for histological and stereological analysis. Conduct standard H & E and immunohistochemical staining and analyse the results using stereology method (Image Pro Plus 5.0, Media Cybernetics).

#### **R. Induction of Unilateral Hind Limb Ischemia**

1. Sterilize surgical tools such as fine pointed forceps, surgical scissors and needle holder.
2. Anesthetize the mice with xylazine (10 mg/kg i.p.) and ketamine (80-100mg/kg i.p.).
3. Remove the hair from the hind limb.
4. Extend and secure the hind and fore limbs with pieces of tape.
5. Wipe the skin with betadine.
6. Use a dissection microscope for the surgery.
7. Make approximately 1 cm long incision of the skin from the knee towards the limb and remove the subcutaneous fat tissue to see femoral artery.

8. Pass a strand of 6-0 silk suture underneath the proximal end of the femoral artery and vein. Occlude the proximal femoral artery and vein using double knots. Then, pass a strand of 6-0 suture underneath the distal end of the femoral artery and vein. Occlude the vessel using double knots.
9. Excise the segment of femoral artery and vein between the distal and proximal knots.
10. Close the wound using 5-0 VICRYL™ sutures and place the animal for recovery on a heating pad.
11. After recovery, proceed with the laser doppler blood perfusion step in order to confirm the ischemia induction.

*Intramuscular Injection*

1. Inject the treatments via an intramuscular muscular injection after the ischemic surgery.
2. Restrain the mice by the scruff method.
3. Swab the muscle area (caudal thigh) to be injected with 70% ethanol.
4. Insert the needle and bevel up into the caudal thigh at a 45° angle so that it will not injure the sciatic nerve.
5. Use a 25 gauge needle for the injection and the total sample volume of 30 µl shouldn't exceed 50 µl.
6. No anesthesia is needed for this procedure.

*Laser Doppler Blood Perfusion*

1. To begin the laser doppler perfusion step, the mouse was put into anesthesia using xylazine (10mg/kg i.p.) and ketamine (80-100mg/kg i.p.).
2. Remove the hair and place the animal on a 37°C heated surface in the supine position on a green-colored cloth.
3. Next, turn on the laser doppler imager and the acquisition software and initialize the software.
4. Save and analyze the data after the acquisition is complete.
5. Repeat laser doppler every week for three weeks.

**S. Immunostaining**

1. Deparaffinise the paraffin embedded sections and rehydrate them by immersing in serial dilutions of ethanol (100%, 90%, 70% and 50%) and finally in PBS.
2. Rehydrate the frozen sections by immersing in PBS for at least 10 minutes.
3. Block by incubating sections with 20% new goat serum (NGS) in PBS containing 0.2% Triton-X for 20 minutes. Do not wash between these steps.
4. Dilute primary antibody (i.e. anti-mouse CD31 and CD68 grown in rabbit) 1:100 in PBS for 1.5 hours at room temperature (or overnight at 4°C). (Need about 200µL/slide).
5. Wash 3x in PBS.
6. Dilute secondary antibody (i.e. Alexa Fluor 488 anti-rabbit) 1:100 in PBS for 30 min at RT in dark (or overnight at 4°C).
7. Wash 3x in PBS.
8. Stain for 1 min in DAPI (2µL stock into 10mL PBS).
9. Rinse 2x in PBS.
10. Mount with Vectashield®.
11. Seal with nail polish.

**Notes:**

- All done in the dark (at least the incubations).
- Negative control – no PRIMARY antibody.
- Mounted and sealed slides stored at 4°C in the dark.

**T. Tissue Enzyme Linked Immunosorbent Assay**

1. Sample Preparation (tissue):
  - a. Take 20-50 mg tissue and added 1 mL/20mg tissue of Tissue Extraction Reagent (Sigma)
  - b. Homogenize using Qiagen TissueRuptor™
  - c. Spin samples at 4500 rpm for 1 min, removed 500 µL and put in eppendorf
  - d. Spin eppendorf at 1000g for 10 min
  - e. Prepare standard curves (standard is at 2000 pg/mL)
2. Prepare all reagents, working standards as directed as per R&D Systems protocol.

3. Remove excess microplate strips from the plate frame, return them to the foil pouch containing the desiccant pack, and reseal.
4. Add 100  $\mu$ l of assay diluent to each well.
5. Add 100  $\mu$ l of standard, control, or sample per well. Cover with the adhesive strip provided. Incubate for 2 hours at room temperature on a horizontal orbital microplate shaker (0.12" orbit) set at  $500 \pm 50$  rpm.
6. Aspirate each well and wash, repeating the process two times for a total of three washes. Wash by filling each well with wash buffer (400  $\mu$ l) using a squirt bottle, manifold dispenser, or auto washer. Complete removal of liquid at each step is essential to good performance. After the last wash, remove any remaining Wash Buffer by aspirating or decanting. Invert the plate and blot it against clean paper towels.
7. Add 200  $\mu$ l of eNOS/IL-10 conjugates to each well. Cover with a new adhesive strip. Incubate for 2 hours at room temperature on the shaker.
8. Repeat the aspiration/wash as in step 5.
9. Add 200  $\mu$ l of substrate solution to each well. Incubate for 30 min at room temperature on the benchtop. Protect from light.
10. Add 50  $\mu$ l of stop solution to each well. The color in the wells should change from blue to yellow. If the color in the wells is green or the color change does not appear uniform, gently tap the plate to ensure thorough mixing.
11. Determine the optical density of each well within 30 min, using a microplate reader set to 450 nm. If wavelength correction is available, set to 540 nm or 570 nm. If wavelength correction is not available, subtract readings at 540 nm or 570 nm from the readings at 450 nm. This subtraction will correct for optical imperfections in the plate. Readings made directly at 450 nm without correction may be higher and less accurate.

#### **U. Tissue PCR**

##### *Procedure:*

1. Prepare tubes (label, pre-chill on ice)
2. Add Master Mix to tubes (48.75 $\mu$ L/tube)
3. Add 1 $\mu$ L cDNA/tube
4. Add 0.25 $\mu$ L enzyme (Taq polymerase)/tube
5. Put tubes into PCR machine

**Table A.5: Master mix**

| <b>Step</b>          | <b>Temperature</b> | <b>Time</b> | <b>Number of Cycles</b> |
|----------------------|--------------------|-------------|-------------------------|
| Initial denaturation | 95°C               | 2 min       | 1                       |
| Denaturation         | 95°C               | 1 min       | 25                      |
| Annealing            | 56°C               | 30s         |                         |
| Extension            | 72°C               | 1.5 min     |                         |
| Final extension      | 72°C               | 5 min       | 1                       |
| Soak                 | 4°C                | Indefinite  | 1                       |

**A.6: Machine Protocol**

| <b>Component</b>               | <b>/Well</b> | <b>/12 Wells</b> | <b>/24 Wells</b> |
|--------------------------------|--------------|------------------|------------------|
| Nuclease-free H <sub>2</sub> O | 32.75        | 432              | 864.6            |
| 5x RT reaction buffer          | 10           | 132              | 264              |
| MgCl <sub>2</sub>              | 3            | 40               | 79.2             |
| dNTP mix                       | 1            | 13               | 26.4             |
| Forward primer                 | 1            | 13               | 26.4             |
| Reverse primer                 | 1            | 13               | 26.4             |
| Enzyme                         | 0.25         | 3                | 6.6              |

**V. Stereology**

1. Place stained slide under bright field light.
2. Capture an image at 1.25X objective.
3. Align the slide using 10X objective.
4. Identify implanted scaffold area.

- Capture six different images using the 40X objective.

#### *Volume Fraction of Inflammatory Cells*

- Open each image separately in Image Pro<sup>®</sup>.
- For each image, choose the 'grid mask' command.
- In the pop-up window, set the type of grid, grid size and margins to be used.
- To determine volume fraction, choose a line grid with 40X40 pixel spacing, and margins of 20 pixels.
- Make sure that the cell type or object of interest is not bigger than the area enclosed by four grid points.
- Click 'apply' and the grid will overlay the image.
- Use the 'measurements' command to count intersections between the cell type of interest (inflammatory cells) and the grid intersections.
- In an excel sheet, type in the number of intersections for each field of view.
- Also record the number of grid points which hit the tissue of interest.
- When the number of intersections and grid points has been counted for the six fields of view from one section, calculate the cumulative volume fraction, using the following equation:

$$V_V = \frac{\sum P_P}{\sum P_T}$$

Where  $\sum P_P$  is the total number of cell/ grid point intersections, and  $\sum P_T$  is the total number of grid points in the reference space for the six fields of view.

#### *Surface Density of Blood Vessels*

- Choose a 'cycloid' grid in the command box.
- Calibrate all images for this measurement. A microscope slide with markings of known dimensions has been captured in Image Pro<sup>®</sup> previously, with images at every objective and saved on the computer.
- Open the calibration folder.
- Select the appropriate objective lens folder, and open an image.
- Scroll down 'measurements' toolbar, and select 'calibration wizard'.
- In the pop-up menu, select 'set calibration'.

7. Choose the objective lens, and measure the size of the circle on the open image.
8. In the next command, enter the actual measurement of the circle (given in the name of the image).
9. Save this calibration, in your working folder.
10. When Image Pro<sup>®</sup> is re-opened, it is important to open this calibration file every time.
11. Go to ‘measurements,’ and ‘open.’ Open the calibration file.
12. Next, go to ‘measurements’ and ‘set system’.
13. To measure surface density, place a cycloid grid on the field of view of interest.
14. Choose a radius of 20 $\mu\text{m}$  and a spacing of 40 $\mu\text{m}$ .
15. Set margins at 20 $\mu\text{m}$ .
16. Overlay the grid, as described for volume fraction.
17. Ensure that the image is aligned, so that the cartilage layer is parallel to the major (x-axis) of the grid.
18. As the length of a cycloid arc is twice the height, each arc is 40 $\mu\text{m}$ .
19. Count the number of arcs on the reference space, and multiply by 40, to give the total length of test line.
20. Count the number of intersections between blood vessels and the test line, and calculate surface density according to the following equation.

$$S_v = 2 \times \frac{I}{L}$$

Where I is the number of intersections and  $L_T$  is the total length of test line. Again, a cumulative surface area for the six fields of view must be calculated.

#### *Length Density of Blood Vessels*

1. Rotate each image by 90 degrees, so that the cartilage lies along a y-axis.
2. Apply the same grid as in surface density.
3. The cartilage is now perpendicular to the major axis of the grid.
4. Count the intersections between blood vessels and cycloid arcs and use the following equation to calculate length density.

$$L_v = \frac{(2 \times I_L)}{T_s}$$

Where  $I_L$  is the number of intersections per unit of test line and  $T_s$  is the thickness of the section.

#### W. List of Journal Publications

1. Mahor, S., **Dash, B.C.**, O'Connor, S. and Pandit A. 'Mannosylated Polyethyleneimine-Hyaluronan Nanohybrids for Targeted Gene Delivery to Macrophage-like Cell Lines.' Bioconjugate Chemistry. 2012: 23(6): 1138-1148.
2. **Dash, B.C.**, Mahor, S., Carroll, O., Mathew, A., Wang, W., Woodhouse, K.A. and Pandit, A. 'Tunable Elastin-like Polypeptide Hollow Sphere as a High Payload and Controlled Delivery Gene Depot.' Journal of Controlled Release. 2011: 152: 382-392.
3. Mahor, S., Collin, E., **Dash, B.C.** and Pandit, A. 'Controlled Release of Plasmid DNA from Hyaluronan Nanoparticles.' Current Drug Delivery. 2011: 8(4): 354-362.
4. **Dash, B.C.**, Rethore, G., Monaghan, M., Fitzgerald, K., Gallagher, W. and Pandit, A. 'The Influence of Size and Charge of Chitosan/polyglutamic Acid Hollow Spheres on Cellular Internalization, Viability and Blood Compatibility.' Biomaterials. 2010: 31(32): 8188-8197.
5. **Dash B.C.**, Monaghan M., Thomas D., Carroll, O., Woodhouse K., Obrien, T., Pandit A. 'Delivery of Therapeutic eNOS and IL-10 genes using an ELP-based Injectable System to Induce Angiogenesis and Modulate Inflammation Level in the Mouse Hind Limb Ischemic Limb'. (Research Article in Preparation)
6. Recent Advances in Gene Delivery for Critical Limb Ischemia. (Review Article in Preparation)
7. Elastin-like Polypeptide Based Biomaterials for Drug Delivery and Tissue Engineering Applications. (Review Article in Preparation)

#### X. Book Chapter

Grad, S., Alini, M., Eglin, D., Sakai, D., Mochida, J., Mahor, S., Collin, E., **Dash, B.** and Pandit, A. 'Recent Advances in Biomaterials based Tissue Engineering for IVD Regeneration.' Synthesis Lectures on Tissue Engineering Eds. Athanasiou, K.A., Hasselmann, K.F. Morgan & Claypool Publishers. 2010: 2(1): 1-104.

#### Y. Conference Presentation (Podium)

1. Mahor, S., Newland, B., **Dash, B.**, Wang, W. and Pandit, A. 'Hyaluronic Acid based Nano Assemblies for Enhanced Gene Delivery to Nucleus Pulposus and Annulus Fibrosus Cells.' Podium presentation at the 24<sup>th</sup> European Conference on Biomaterials, Dublin, Ireland, 2011

2. **Dash, B.**, Holladay, C., Carroll, O., Mahor, S., Woodhouse, K. and Pandit, A. ‘A Bifunctional and Temporo-Spatial Delivery through an Injectable Elastin-like Polypeptide Scaffold.’ Podium presentation at the 24<sup>th</sup> European Conference on Biomaterials, Dublin, Ireland, 2011
3. **Dash, B.**, Mahor, S., Monaghan, M., Carroll, O., Woodhouse, K.A. and Pandit, A. ‘Tunable Elastin like Polypeptide Hollow Spheres as a High Payload and Controlled Gene Delivery Depot.’ Podium presentation at the 23<sup>rd</sup> European Conference on Biomaterials, Tampere, Finland, 2010.
4. **Dash, B.**, Mahor, S., Monaghan, M., Woodhouse K.A. and Pandit, A. ‘Tunable Elastin like Polypeptide Hollow Spheres as a High Payload and Controlled Gene Delivery Depot’ Podium presentation at the Tissue Engineering Regenerative Medicine International Society – EU Meeting, Galway, Ireland, 2010.
5. Mahor, S., Collin, E., **Dash, B.** and Pandit, A. ‘Hyaluronan Nanospheres for Sustained Gene Delivery.’ Podium presentation at the Tissue Engineering Regenerative Medicine International Society – EU Meeting, Galway, Ireland, 2010.
6. Fitzgerald, K., **Dash, B.**, Pandit, A. and Gallagher, W. ‘Neutrally Charged Nanospheres as Potential Candidates for Cardiovascular Targeting.’ Podium presentation at the Tissue Engineering Regenerative Medicine International Society – EU Meeting, Galway, Ireland, 2010.
7. Fitzgerald, K., **Dash, B.**, Pandit, A. and Gallagher, W.M ‘Neutrally Charged Nanospheres as Potential Candidates for Cardiovascular Targeting.’ Podium presentation at the Particles 2010 Conference, Florida, USA, 2010.
8. Réthoré, G., Monaghan, M., **Dash, B.** and Pandit, A. ‘Chitosan-PolyGlutamic Acid Biodegradable Nanospheres Show a Blood Compatibility Response that is Dictated by Size and Surface Charge.’ Podium presentation at the 2<sup>nd</sup> World Congress of the Tissue Engineering and Regenerative Medicine International Society, Seoul, Republic of Korea, 2009.
9. **Dash, B.**, Réthoré, G., Ceredig, R. and Pandit, A. ‘Chitosan/Polyglutamic Acid Nanospheres - A Model System to Study the Internalisation Behavior of Endothelial and Smooth Muscle Cells.’ Podium presentation at the 2<sup>nd</sup> World Congress of the Tissue Engineering and Regenerative Medicine International Society, Seoul, Republic of Korea, 2009.

10. Mathew, A., Réthoré, G., **Dash, B.**, Monaghan, M. and Pandit, A. ‘Chitosan/Polyglutamic Acid Nanospheres: DNA Encapsulation and Release, Cellular Uptake and Blood Interaction Studies.’ Podium presentation at the UK Society for Biomaterials Conference, Antrim, UK, 2009.
11. **Dash, B.**, Rethore, G., Mathew, A., Ceredig, R. and Pandit, A. ‘Model System to Study Plasmid Encapsulation Efficiency and Internalisation Behavior of Nanospheres in Endothelial and Smooth Muscle Cells.’ Podium presentation at the 22<sup>nd</sup> European Conference on Biomaterials, Lausanne, Switzerland, 2009.

#### **Z. Conference Presentation (Poster)**

8. **Dash, B.**, Carroll, O., Woodhouse, K. and Pandit, A. ‘An Injectable Elastin-like Polypeptide Based System for Spatio-Temporal Delivery of Dual Therapeutic Genes.’ Poster presentation at the Annual Meeting Royal Academy of Medicine in Ireland Biomedical Section, Galway, Ireland 2012.
9. Réthoré, G., Mathew, A., **Dash, B.** and Pandit, A. ‘Hollow Spheres: Encapsulation, Release and Uptake.’ Poster presentation at the 36<sup>th</sup> Annual Meeting and Exposition of the Controlled Release Society, Copenhagen, Denmark, 2009.